Investigations on the pulmonary toxicity of Saharan dust using advanced *in vitro* models

Inaugural-Dissertation

zur Erlangung des Doktorgrades
der Mathematisch-Naturwissenschaftlichen Fakultät
der Heinrich-Heine-Universität Düsseldorf

vorgelegt von

Gerrit Bredeck
aus Haltern

Düsseldorf, Dezember 2023

Aus dem IUF – Leibniz-Institut für umweltmedizinische Forschung.

Gedruckt mit Genehmigung der
Mathematisch-Naturwissenschaftlichen Fakultät der
Heinrich-Heine-Universität Düsseldorf.

Erstbetreuer: Univ.-Prof. Dr. med. Jean Krutmann, IUF
Mentor: Prof. Dr. rer. nat. Sebastian Fraune, HHU
Co-Supervisor: Dr. Roel Schins, IUF

Tag der mündlichen Prüfung: 23.04.2024

Table of Contents

Acknowledgments 3
Abbreviations 4
Summary 6
Zusammenfassung 7
1 General introduction 9
1.1 Characteristics of desert dusts 9
1.2 Desert dusts in the particle toxicology context 12
1.3 Models to assess the health hazards of aeolian particulate matter 16
1.4 Adverse health effects of desert dusts 18
1.5 Objectives of this thesis 20
1.6 References 21
2 Inhalable Saharan dust induces oxidative stress, NLRP3 inflammasome activation, and inflammatory cytokine release 35
2.1 Abstract 36
2.2 Introduction 36
2.3 Materials & methods 37
2.4 Results 40
2.5 Discussion 43
2.6 References 47
2.7 Supplemental material 50
3 Inflammatory properties of respirable and inhalable Saharan dusts in relation to dust events and composition: an in vitro study in human macrophages 57
3.1 Abstract 58
3.2 Introduction 58
3.3 Methods 61
3.4 Results 68
3.5 Discussion 78
3.6 Conclusions 83
3.7 References 83
3.8 Supplemental material 91
4 Saharan dust induces NLRP3-dependent inflammatory cytokines in an alveolar air-liquid interface co-culture model 115

4.1 Abstract ... 116
4.2 Background ... 117
4.3 Results ... 117
4.4 Discussion ... 121
4.5 Conclusion ... 126
4.6 Materials and methods ... 126
4.7 References ... 131
4.8 Supplemental material ... 135
5 Saharan dust induces the lung disease-related cytokines granulocyte-macrophage colony-stimulating factor and granulocyte colony-stimulating factor ... 149
5.1 Abstract ... 150
5.2 Introduction ... 150
5.3 Material and methods ... 152
5.4 Results and discussion ... 156
5.5 References ... 164
5.6 Supplemental material ... 173
6 General discussion ... 179
6.1 Overview of study outcomes ... 179
6.2 Identifying dust events that pose health risks ... 181
6.3 Mitigating the health risks of desert dust events ... 184
6.4 Conclusions ... 185
6.5 References ... 186
7 Publications beyond the scope of this thesis ... 195
Eidesstattliche Erklärung ... 203

Acknowledgments

First and foremost, I would like to thank my principal supervisor Univ.-Prof. Dr. Jean Krutmann for reviewing my dissertation, overseeing my work, and supporting my doctoral project, including the possibility of participating in the sampling campaign in Cape Verde. I would also like to thank my mentor and second supervisor Prof. Dr. Sebastian Fraune for his support during my doctorate and for reviewing this thesis.

Moreover, I express special gratitude to Dr. Roel Schins for promoting me and my doctorate project in any possible way. Thank you for always having an open door, for your invaluable feedback, for encouraging conference contributions, and for successfully publishing the work together. Thank you for being a humane and understanding supervisor, which only motivated me more in my work.

In addition, I am thankful to Dr. Tina Wahle, Dr. Angela Kämpfer, and Dr. Mathias Busch for helpful discussions and advice on both scientific and organizational topics. It was great to always find an open ear whenever there was an issue easier to solve after speaking it out loud.

Further, I appreciate the opportunity to share a workplace with Dr. Adriana Sofranko, Isabelle Masson, Lara Boßmann, Dr. Eleonora Scarcello, Dr. Catrin Albrecht, Veronica Büttner, Miriam Vieth, Andrea Boltendahl, Gözde Görmüş, Jessica Vossen, Max Trivonov, Janine Becht, and Noor Shuqair in the group “Particles, inflammation and genome integrity”. Thanks to all of you for a friendly and constructive working atmosphere.

I would also like to thank all the co-authors and cooperation partners, especially from the Dustrisk project, for the fruitful collaborations.

Last but not least, I would like to thank my partner Marina, my parents Ria and Gerd, and my sisters Anika and Theresa for their emotional and financial support during my doctorate and my entire academic education.

Abbreviations

ACTB	actin beta
AK	adenylate kinase
ALI	air-liquid interface
APE1/REF1	apurinic-apyrimidinic endonuclease 1/redox factor 1
ASC	apoptosis-associated speck-like protein
ASD	Asian sand dust
ATCC	American Type Culture Collection
BSA	bovine serum albumin
CASP	caspase
CC16	Club cell protein
CCL3L1	C-C motif chemokine ligand 3 like 1
CCM	cell culture medium
CD	cluster of differentiation
CMAM	culture medium for alveolar macrophages
COPD	chronic obstructive pulmonary disease
CVAO	Cape Verde Atmospheric Observatory
CXCL	C-X-C motif chemokine ligand
DAMP	danger-associated molecular pattern
DEG	differentially expressed gene
dH_2O	deionized H_2O
DMPO	5,5-dimethyl-1-pyrroline-N-oxide
DQ	Dörentrup Quartz
EC	elemental carbon
EDTA	ethylenediaminetetraacetic acid
EDX	energy dispersive x-ray analysis
ELISA	enzyme-linked immune-sorbent assay
EPA	Environmental Protection Agency
EPR	electron paramagnetic resonance
ESC	embryonic stem cell
EU	endotoxin units
FACS	fluorescence-activated cell sorting
FCS	fetal calf serum
GAPDH	glyceraldehyde 3-phosphate dehydrogenase
GCS	glutamylcysteine synthetase
G-CSF	granulocyte colony-stimulating factor
GM-CSF	granulocyte-macrophage colony-stimulating factor
GSEA	gene set enrichment analysis
HBSS	Hank's Balanced Salt Solution
HEPES	4-(2-hydroxyethyl)-1-piperazineethane sulfonic acid
HERC	HECT and RLD domain containing E3 ubiquitin protein ligase
HMOX	heme oxygenase
HRMA	High-Resolution Melt Analysis
IFN	interferon
IL	interleukin
iNOS	inducible nitric oxide synthase
iPSC	induced pluripotent stem cell
LAL	Limulus amebocyte lysate
LDH	lactate dehydrogenase

LOD	limit of detection
LPS	lipopolysaccharides
ME	mercaptoethanol
MSA	methane sulfonic acid
MyD	myeloid differentiation factor
NAD	Beta-Nicotinamide adenine dinucleotide
NDIR	non-dispersive infrared detector
NF-κB	nuclear factor κ-light chain enhancer of activated B-cells
NGS	normal goat serum
NLRP	NACHT, LRR, and PYD domains-containing protein
NP	nanoparticle
NQO	NAD(P)H quinone dehydrogenase
NRF2	nuclear factor erythroid 2-related factor
nRTc	no reverse transcriptase control
OC	organic carbon
PAMP	pathogen-associated molecular pattern
PBS	phosphate-buffered saline
PC	principal component
PCLS	precision cut lung-slices
PM	particulate matter
PMA	phorbol 12-myristate13-acetate
P/S	Penicillin/Streptomycin
qPCR	quantitative polymerase chain reaction
qRT-PCR	quantitative reverse transcription polymerase chain reaction
REACH	registration, evaluation, authorization and restriction of chemicals
ROS	reactive oxygen species
SAS	synthetic amorphous silica
SD	Saharan dust
SDS	sand and dust storms
SEM	scanning electron microscopy
SLC39A8	solute carrier family 39 member 8
SOD	superoxide dismutase
SP-C	surfactant protein C
sQCM	quartz crystal microbalance
St	sampling station
St. dev.	standard deviation
TC	total carbon
TEM	transmission electron microscopy
TGF	transforming growth factor
TLR	toll-like receptor
TNF	tumor necrosis factor
TNFRSF	TNF receptor superfamily member
TRIS	tris(hydroxymethyl)aminomethane
TSCA	Toxic Substances Control Act
TXRF	total reflection X-ray fluorescence
WHO	World Health Organization
WST	water soluble tetrazolium
WT	wild-type

Summary

Every year over one billion tons of desert dusts are aerosolized and transported around the globe causing respiratory morbidity and mortality. Studies on desert dusts from different sources have been shown to cause variable extents of oxidative stress and inflammation. In those studies, the largest of all desert dust sources, the Sahara, was largely neglected. Which constituents and molecular pathways mediate the toxicity of Saharan dust (SD) remains unclear.

The investigations underlying this thesis aimed to evaluate the toxicity of SD in relation to dust events, dust composition, and molecular mediators. Specifically, the NLRP3 inflammasome-caspase (CASP)-1 pathway was assessed because of its association with lung diseases.

Therefore, the oxidative and inflammatory potency of SD was examined in alveolar epithelial A549 cells, wild-type and *NLRP3*$^{-/-}$ THP-1 macrophages, as well as an advanced surfactant-producing air-liquid interface (ALI) co-culture model of A549 cells with either wild-type, *CASP1*$^{-/-}$, or *NLRP3*$^{-/-}$ THP-1 macrophages. Four studies were conducted.

In the first study, SD was shown to elicit the expressions of the oxidative stress marker gene heme oxygenase 1 (*HMOX1*) and the inflammatory cytokines interleukin 6 (*IL6*) and *IL8* in A549 cells. In THP-1 macrophages, SD induced IL-1β release which was exacerbated by endotoxins and depended on the NLRP3 inflammasome. In the second study, particulate matter $(PM)_{2.5}$ from two dust events and PM_{10} from one dust event had a higher inflammatory potency than PM from a reference period. For $PM_{2.5}$, variability in inflammatory potency was associated with the Fe content. For PM_{10}, the intra but not inter-event variability was associated with the endotoxin content. In the third study, using the ALI co-culture model, SD was found to cause stronger expression and release of *IL1B*/IL-1β, *IL6*/IL-6, *IL8*/IL-8, and tumor necrosis factor α (*TNFA*/TNFα) than quartz dust. The secretion of IL-1β depended on the NLRP3 inflammasome-CASP-1 pathway. NLRP3 and CASP-1 also boosted the releases of the other investigated cytokines. In the fourth study, SD-mediated upregulations of the cytokines granulocyte-macrophage colony-stimulating factor (*GMCSF*/GM-CSF) and granulocyte colony-stimulating factor (*GCSF*/G-CSF) in the ALI co-cultures were identified and validated. Other studies have related these cytokines to lung diseases such as allergies, asthma, and fibrosis.

Collectively, these findings emphasize the hazardousness of SD events. The contents of Fe and endotoxins can serve as indicators to identify hazardous dust events. The signaling pathways and cytokines involved suggest susceptibility to desert dust-mediated adverse health effects in people with allergies, asthma, and fibrosis. Additionally, individuals with gain of function polymorphisms in the *IL1B* gene may be vulnerable. The upregulated cytokines can also be considered potential drug targets. These outcomes provide a strong basis for further studies that bring the hazard assessment of desert dust events and the protection of human health closer together.

Zusammenfassung

Jedes Jahr werden über eine Milliarde Tonnen Wüstenstäube aerosoliert und um den Globus transportiert, was zu Atemwegserkrankungen und Mortalität führt. Studien über Wüstenstäube aus verschiedenen Regionen haben gezeigt, dass diese oxidativen Stress und Entzündungsreaktionen in unterschiedlichem Ausmaß auslösen. In diesen Studien wurde die größte aller Wüstenstaubquellen, die Sahara, weitgehend vernachlässigt. Welche Komponenten und Signalwege die Toxizität von Saharastaub (SD) vermitteln, ist nach wie vor unklar.

Ziel der im Rahmen dieser Thesis durchgeführten Untersuchungen war es, die Toxizität von SD in Abhängigkeit von Staubereignissen, Staubzusammensetzung und molekularer Mediatoren zu erforschen. Insbesondere wurde der NLRP3-Inflammasome-Caspase (CASP)-1-Signalweg untersucht, da er mit Lungenerkrankungen in Verbindung steht.

Zur Untersuchung der oxidativen und entzündlichen Potenz von SD wurden die folgenden Modelle genutzt: A549 Alveolarepithelzellen; wildtyp und *NLRP3*$^{-/-}$ THP-1 Makrophagen; ein Surfaktant-produzierendes Luft-Flüssigkeits-Interface (ALI) Co-Kulturmodell von A549 Zellen mit entweder wildtyp, *CASP1*$^{-/-}$ oder *NLRP3*$^{-/-}$ THP-1 Makrophagen. Es wurden vier Studien durchgeführt.

In der ersten Studie wurde gezeigt, dass SD die Expression des Markergens für oxidativen Stress, der Häm-Oxygenase 1 (*HMOX1*), und der entzündlichen Zytokine Interleukin 6 (*IL6*) und *IL8* in A549 Zellen auslöst. In THP 1-Makrophagen induzierte SD die Ausschüttung von IL-1β, die durch Endotoxine noch verstärkt wurde und vom NLRP3-Inflammasom abhing. In der zweiten Studie wiesen Feinstäube $(PM)_{2,5}$ aus zwei Staubereignissen und PM_{10} aus einem Staubereignis eine höhere Entzündungspotenz auf als PM aus einem Referenzzeitraum. Für $PM_{2,5}$ war die Variabilität der entzündlichen Potenz mit dem Fe-Gehalt assoziiert. Für PM_{10} war die Variabilität innerhalb der Ereignisse aber nicht zwischen den Ereignissen mit dem Endotoxingehalt assoziiert. In der dritten Studie wurde festgestellt, dass SD in den ALI Co-Kulturen eine stärkere Expression und Freisetzung von *IL1B*/IL-1β, *IL6*/IL-6, *IL8*/IL-8 und Tumor-Nekrose-Faktor α (*TNFA*/TNFα) verursacht als Quarzstaub. Die Sekretion von IL-1β hing vom NLRP3-Inflammasom-CASP-1-Signalweg ab. Außerdem verstärkten NLRP3 und CASP-1 die Freisetzung der anderen Zytokine. In der vierten Studie wurden SD-vermittelte Induktionen der Zytokine Granulozyten-Makrophagen-Kolonie-stimulierender Faktor (*GMCSF*/GM-CSF) und Granulozyten-Kolonie-stimulierender Faktor (*GCSF*/G-CSF) in den ALI-Co-Kulturen identifiziert und validiert. Andere Studien haben diese Zytokine mit Lungenerkrankungen wie Allergien, Asthma und Fibrose verknüpft.

Zusammengenommen unterstreichen diese Ergebnisse die Gefährlichkeit von SD-Ereignissen. Die Gehalte an Fe und Endotoxinen können als Indikatoren für die Identifizierung gefährlicher Staubereignisse dienen. Die beteiligten Signalwege und Zytokine deuten darauf hin, dass Menschen mit Allergien, Asthma und Fibrose sowie Personen mit Funktionsgewinn-Polymorphismen im *IL1B*-Gen anfällig für durch Wüstenstäube verursachte Gesundheitsschäden sind. Die Zytokine können auch als potenzielle Angriffspunkte für Medikamente betrachtet werden. Diese Ergebnisse bilden eine solide Grundlage für weitere Studien, die die Gefahrenbewertung von Wüstenstaubereignissen und den Schutz der menschlichen Gesundheit näher zusammenbringen.

1 General introduction

1.1 Characteristics of desert dusts

According to the United Nations Convention to Combat Desertification (2023), “sand and dust storms (SDS) have become increasingly frequent and severe having substantial transboundary impacts, affecting various aspects of the environment, climate, health, agriculture, livelihoods and the socioeconomic well-being of individuals.” These impacts manifest both near sources and far away from the origin. Due to the absorbance and scattering of light, desert dusts contributes to the temperature variability of the atmosphere and surface (Balkanski et al., 2007; Carlson and Benjamin, 1980; Tegen and Lacis, 1996). Desert dusts interfere with the precipitation of cloud water (Huang et al., 2014; Rosenfeld et al., 2001), decrease the albedo of snow, and, therefore, accelerate its melting (Painter et al., 2007). Furthermore, they provide micronutrients such as iron and phosphorous to marine and terrestrial ecosystems (Jickells et al., 2005; Martin et al., 1991; Swap et al., 1992). During desert dust events, concentrations become so elevated that they strongly impair visibility (Figure 1.1). Adverse health effects of such events have extensively been proven in epidemiological studies (Gutierrez et al., 2020; Johnston et al., 2011; Kwon et al., 2002; Lwin et al., 2023; Mallone et al., 2011; Stafoggia et al., 2016; Tam et al., 2012; Zauli Sajani et al., 2011; Zhang et al., 2016a).

Figure 1.1. Visibility on a clear day and a dust event day. The photos were taken by Gerrit Bredeck at the Cape Verde Atmospheric Observatory on February 7th and 18th, 2022 (left and right, respectively).

1.1.1 Sources and distribution of desert dusts

Cakmur et al. (2006) estimated global annual aerosolization of desert dusts in the range of one to three billion tons. The main sources are topographic depressions in semi-arid and arid regions that had been filled with alluvial deposits through intermittent inundations (Prospero et al., 2002). Examples of such sources can be found across North (Gillette et al., 1997) and South America (Troin et al., 2010), Asia (Abuduwaili et al., 2008), Australia (Bullard and McTainsh, 2016), and

especially Africa (Bryant, 2003; Bryant et al., 2007; Mahowald et al., 2003; Washington et al., 2006). Wind erodes these surfaces and thereby aerosolizes desert dusts (Knippertz et al., 2009; Washington et al., 2006). The eroded dust is not only a local phenomenon as it can be transported over thousands of kilometers to reach other continents (Chin et al., 2007; Swap et al., 1992). On the one hand, climate change has been predicted to decrease long-range transport of desert dusts because of lower temperature gradients between the Northern Tropic and the Arctic (Clifford et al., 2019). On the other hand, dust availability and dust event intensity will increase with droughts, aridity, and the removal of vegetation (Achakulwisut et al., 2019; Huang et al., 2015).

1.1.2 Composition of desert dusts

Desert dusts are complex mixtures of inorganic and organic constituents that can partly change in their properties during transport from the source region to the destination (Ryder et al., 2013a). Especially, the size distribution of desert dusts changes with transport. At source regions, even particles with a diameter > 100 µm can be aerosolized (Ryder et al., 2013b). However, due to the high ratio of gravitational force to friction with the air, large particles sediment relatively quickly. Ryder et al. (2013a) reported larger particles > 30 µm to have an aeolian half-life of < 12 h. According to Maring et al. (2003), dust particles > 7.3 µm are preferentially removed during transport over the ocean. Conversely, this means that the majority of desert dust particles with sizes relevant for inhalation, i.e. < 10 µm, are readily transported (ICRP, 1994) (see 1.2.1).

Differences in mineralogical and elemental composition between source regions and destinations are caused by the inhomogeneous distribution of these constituents throughout the size fractions of desert dusts (Chatenet et al., 1996; Formenti et al., 2014; Rahn, 1976). Within the same size fraction, the mineral and elemental composition of soil and aerosolized dust concur well (Claquin and Schulz, 1999; Jeong, 2008; Lafon et al., 2006). When identifying mineral contents, geologists distinguish the clay and silt fractions representing particle sizes < 2 µm and 2-50 µm, respectively. The clay fraction of desert dusts is dominated by phyllosilicates such as illite, kaolinite, and smectite, followed by quartz and calcite (Claquin and Schulz, 1999; Rodriguez-Navarro et al., 2018). In the silt fraction, quartz is more abundant than phyllosilicates. In addition, the silt fraction contains K-feldspar and plagioclase. Amongst further minor minerals, both clay and silt fractions contain the iron oxides goethite and hematite. The latter gives desert dusts their red color. Additionally, desert dusts contain amorphous constituents such as diatoms and ferrihydrite (Gasse et al., 2017; Rodriguez-Navarro et al., 2018; Shi et al., 2011). The presence of diatoms is not surprising considering that many erodible sediments stem from alluvial deposits. Amorphous iron species are particularly relevant because they are more readily soluble than crystalline goethite and hematite (Schwertmann, 1991).

In concordance with the aforementioned mineral composition, the most abundant elements in aerosolized desert dusts are oxygen, silicon, and aluminum, followed by iron, calcium, and magnesium (Goudie and Middleton, 2001). Desert dusts contain further minor and trace elements that include but are not limited to magnesium, titanium, manganese, carbon, and sulfur. While the listed minerals and elements can reliably be found in desert dusts, their relative abundances strongly vary between source regions (Claquin and Schulz, 1999; Goudie and Middleton, 2001; Lafon et al., 2006).

Moreover, desert dusts contain a multitude of biological components. Long-range transported desert dusts from Africa and Asia have been shown to increase the numbers of airborne viable bacteria and fungi (Favet et al., 2013; Griffin et al., 2001; Kellogg and Griffin, 2006; Lee et al., 2009; Yeo and Kim, 2002). Kellogg et al. (2004) described that the number of viable bacteria decreases during transatlantic transport. Yet, the remnants of dead microbes can stay attached to the dust. Microbial endotoxins and β-glucan have been detected in desert dust samples (He et al., 2010; Rodríguez-Cotto et al., 2013; Taylor et al., 2013; Yanagisawa et al., 2007). Furthermore, DNA sequencing is frequently applied to identify dust-associated microbes (An et al., 2014; Griffin et al., 2001; Kellogg et al., 2004; Lee et al., 2009; Stern et al., 2021). In this way, Griffin et al. (2001) and Stern et al. (2021) observed the presence of pathogenic species in desert dusts. While all size fractions contained microbes, Stern et al. (2021) reported increasing abundances associated with increasing particle sizes.

During transport, anthropogenic pollutants can mix with and adsorb to desert dusts (Erel et al., 2006). Alkaline species such as Ca^{2+} and Mg^{2+} in desert dusts can react with SO_2 and NO_2 from anthropogenic sources (Choi et al., 2001; Wang et al., 2016). Such reactions form SO_4^{2-} and NO_3^- which then adsorb to the surface of desert dust particles. When transported over urban or industrial areas, desert dusts could potentially pick up elemental carbon (EC) from combustion sources. Hussein et al. (2022) described elevated EC concentration during dust events in Amman (Jordan). Contrarily, Wang et al. (2016) found no increase in EC during Asian dust events, even though SO_4^{2-} concentrations related to anthropogenic contaminations were elevated. In addition, Gonçalves et al. (2014) reported low concentrations of EC in long-range transported Saharan dust (SD) which they attributed to the soil content of EC.

1.1.3 Desert dusts on Cape Verde

Due to the high seasonal concentration of long-range transported SD and the remote location, multiple studies have been conducted on the Cape Verde archipelago (Carpenter et al., 2011; Chiapello et al., 1997; Chiapello et al., 1995; Fomba et al., 2020; Fomba et al., 2013; Fomba et

al., 2014; Gonçalves et al., 2014). Cape Verde is located in the Northern Tropical Atlantic about 600-900 km off the African coast. The transport of SD to the archipelago is connected to the seasonal shift of the subtropical high-pressure center (Chiapello et al., 1997; Chiapello et al., 1995). The highest concentrations of desert dusts at ground level occur during the winter months. Applying back trajectory analyses, Chiapello et al. (1997) identified three Saharan source regions: the North/West Sahara, the Central/South Sahara, and the Sahel region. In the Sahel region lays the Bodélé depression which is considered the most intense single dust source worldwide (Goudie and Middleton, 2001; Prospero et al., 2002; Washington et al., 2006) and which contributes to SD on Cape Verde (Schepanski et al., 2009).

To investigate SD, the Cape Verde Atmospheric Observatory (CVAO) was founded in the north of the island São Vicente, situated 70 m from the coastline (Fomba et al., 2013; Fomba et al., 2014). Instruments at CVAO can be operated on the platform of a 30 m high tower to minimize the influence of sea spray (Fomba et al., 2013). A huge advantage of assessing long-range transported SD samples obtained at CVAO is the very low levels of local urban and industrial background pollution.

1.2 Desert dusts in the particle toxicology context

Insights into potentially toxic constituents of desert dusts and molecular pathways of desert dust toxicity can be gained from crystalline silica as well as ambient PM from urban and industrial sources. However, health protection against each of these contaminants necessitates different types of regulatory measures. Although sand pneumoconiosis has even been found in an Egyptian mummy (Tapp et al., 1975), substantial concerns about desert dusts emerged relatively recently, contrasting with well-established evidence of adverse health effects from crystalline silica dust and ambient urban/industrial PM, formerly also called smoke or suspended matter. The first study on silicosis, a form of pulmonary fibrosis caused by inhalation of crystalline silica dust, was published almost exactly 100 years ago (Elliott, 1923). Major concerns about the adverse health effects of ambient air pollutants, including urban/industrial PM arose a few decades later, spurred by events such as the Donora smog of 1948 and the London smog of 1952 (Doyle, 1953; Scott, 1953). Desert dusts exhibit parallels and differences with crystalline silica dust and urban/industrial PM in terms of size distribution, composition, and settings of exposure.

1.2.1 Particle size distribution

The size distribution is decisive for the potential toxicity of inhaled particles because it determines in which part of the lungs they deposit. The alveoli are mostly exposed to ultrafine and fine particles

with an effective aerodynamic diameter smaller than 0.1 µm and between 0.1 µm and 2.5 µm, respectively (ICRP, 1994). This is designated the respirable size fraction. As aerosol samples representing the respirable size fraction, particulate matter with a 50% mass cut-off at 2.5 µm ($PM_{2.5}$) is collected.

The trachea-bronchial airways are mainly exposed to coarse particles with an effective aerodynamic diameter between 2.5 µm and 10 µm (ICRP, 1994). $PM_{2.5-10}$ represents the coarse size fraction. Ultrafine, fine, and coarse size fractions together are sampled as PM_{10} and are designated the inhalable size fraction that can penetrate beyond the larynx. Notably, all particles of the inhalable size fraction can reach all parts of the lung. Merely the probabilities for deposition in specific regions differ.

The size distributions of desert dusts and crystalline silica are comparable and differ sharply from urban/industrial PM. Both desert dusts (reviewed by Mahowald et al. (2014)) and silica dust (Page, 2003; Verma and Shaw, 2001) contain fine and coarse particles. As crystalline silica for toxicological studies, usually reference quartz dusts such as DQ12, Min-U-Sil 5, and F600 are used that contain both fine and coarse particles and have median diameters between 1.6 µm and 3.2 µm (Verma and Shaw, 2001). Ultrafines are of minor importance for desert dusts and crystalline silica: The concentrations of ultrafine particles decrease during dust events (Jayaratne et al., 2011; Wehner et al., 2004) and ultrafines in crystalline silica dust are commonly not even assessed (Page, 2003; Verma and Shaw, 2001). Contrarily, ultrafines are very prominent in urban/industrial PM which to a high percentage is derived from fossil fuel combustion (Ban-Weiss et al., 2010; Winijkul et al., 2015). Coarse particles only play a minor role in urban/industrial PM (Kodros et al., 2018). Based on the size distributions, toxicity in both the alveolar and trachea-bronchial regions needs to be considered for desert and crystalline silica dusts. Because ultrafines can penetrate the air-blood barrier (Furuyama et al., 2009), primary effects on organs other than the lung are relevant to urban/industrial PM but not to desert dusts.

1.2.2 Composition

Overlapping components of desert dusts compared to crystalline silica and urban/industrial PM suggest potentially similar mechanisms of toxicity. The similarities in the composition of crystalline silica and desert dusts are evident. Quartz, the most-investigated polymorph of crystalline silica, is a component of desert dusts (see 1.1.2). Common constituents of desert dusts and urban/industrial PM are sulfates, nitrates, and trace metals such as iron, manganese, and nickel (Goudie and Middleton, 2001; Hsu et al., 2021; Rodríguez et al., 2011; Taylor et al., 2013). Moreover, when air masses travel over or into urban or industrial areas, PM from these sources

can mix with long-range transported desert dusts (Rodríguez et al., 2011). Based on these overlaps, these pollutants may trigger the same molecular mechanisms. An important molecular sensor that has been linked to the toxicity of both crystalline silica dust (Cassel et al., 2008; Dostert et al., 2008) and urban/industrial PM (Cao et al., 2022) is the NACHT, LRR, and PYD domains-containing protein 3 (NLRP3) inflammasome (see 1.2.4).

As evident as the similarities are compositional differences. Desert dusts encompass a much broader range of minerals and non-mineral compounds than crystalline silica. With exceptions such as the drilling industry, railways, and quarries, minerals are scarce in urban/industrial PM. Desert dusts have constituents that neither occur in crystalline silica nor urban/industrial PM. Moreover, the multiple constituents of desert dusts may act in antagonistic and synergistic ways (Wang et al., 2020b; Yu et al., 2018).

1.2.3 Exposure settings and regulation

Because the settings of exposure to crystalline silica dust, urban/industrial PM, and desert dusts are fundamentally different, regulatory measures need to be tailored for each specific case. Silica dust is associated with occupational exposure in industries such as mining and construction, leading to specific regulations to limit worker exposure (European Parliament and Council, 2017; United States Occupational Safety and Health Administration). In contrast, urban/industrial PM and desert dusts are ambient types of air pollution that affect broad populations. However, urban/industrial PM stems from anthropogenic sources that can be subjected to regulatory measures, while desert dust events occur naturally and cannot be controlled.

To foster public health, legislators can set air quality limit values of PM. For example, the newest proposal for a directive of the European Parliament and Council (European Commission, 2022) suggests maximum annual mean concentrations of $PM_{2.5}$ and PM_{10} of 10 µg/m³ and 20 µg/m³, respectively. In addition, daily concentrations of 25 µg/m³ and 45 µg/m³ not to be exceeded more than 18 times per year are suggested. In case of exceedance, authorities have to implement an air quality plan to ensure compliance with the aforementioned limit values.

However, in the European Union (European Commission, 2022; European Parliament and Council, 2008) and the United States (Environmental Protection Agency (EPA), 1971), authorities are exempt from taking measures if they can prove that exceedances were due to desert dusts. Considering the evident adverse health effects of desert dust exposure (see 1.4) and that daily PM_{10} concentrations can reach 600 µg/cm² during SD events (Fomba et al., 2014), risk mitigation strategies have been demanded (Fussell and Kelly, 2021) but not been incorporated into regulations, yet.

1.2.4 The NLRP3 inflammasome

NLRP3 inflammasome activation is a two-step process that can mediate particle and fiber-induced inflammation contributing to the development of lung fibrosis (Cassel et al., 2008; Dostert et al., 2008). The principal cytokines conveying the NLRP3-mediated signaling cascade are interleukin (IL)-1β and IL-18.

The first step, also called priming, is induced by danger-associated molecular patterns (DAMPs) or pathogen-associated molecular patterns (PAMPs), e.g., tumor necrosis factor α (TNFα) or lipopolysaccharides (LPS), respectively (Bauernfeind et al., 2009). PAMPs and DAMPs activate toll-like receptor 2 (TLR2), TLR3, TLR4, TLR7, or TNF receptors, which lead to the activation of nuclear factor κ-light chain enhancer of activated B-cells (NF-κB) and, finally, to the transcriptional upregulation of inactive NLRP3 and pro-IL-1β (Bauernfeind et al., 2009; Kahlenberg et al., 2005). Transcriptional priming of pro-IL-18 is cell type dependent. LPS-induced pro-IL-18 priming has been shown in macrophages (Lopategi et al., 2019; Zhu and Kanneganti, 2017) but not in monocytes in which pro-IL-18 is constitutively expressed (Ghonime et al., 2014; Mehta et al., 2001). Moreover, IL-1β can act in an autocrine fashion (Franchi et al., 2009; Warner et al., 1987).

The second step, also called activation, can be triggered by a variety of DAMPs. These DAMPs include small molecules like ATP and nigericin, as well as crystalline structures like silica (reviewed by Bryant and Fitzgerald (2009) and Rabolli et al. (2016)). DAMPs trigger cellular processes such as the efflux of K^+ ions (Kahlenberg and Dubyak, 2004; Petrilli et al., 2007), lysosomal rupture (Hornung et al., 2008), and cytosolic overload of reactive oxygen species (ROS) upon mitochondrial damage (Zhou et al., 2011). Subsequently, NLRP3 oligomerizes and recruits apoptosis-associated speck-like protein (ASC) (Manji et al., 2002). ASC recruits pro-caspase (CASP)-1 which cleaves to active CASP-1 (Martinon et al., 2002). CASP-1 in turn cleaves pro-IL-1β and pro-IL-18 to active IL-1β (Thornberry et al., 1992) and IL-18 (Ghayur et al., 1997). Once released, these cytokines stimulate further inflammatory cascades (Dinarello, 2002). Moreover, CASP-1 can cleave Gasdermin D, resulting in the formation of pores in cell membranes and inducing a form of cell death known as pyroptosis (Shi et al., 2015). While NLRP3 is the most-investigated family member, the NLRP1 (Martinon et al., 2002), NLRC4 (Poyet et al., 2001), AIM2 (Burckstummer et al., 2009), and NLRP6 (Grenier et al., 2002) inflammasomes can lead to CASP-1 activation as well.

Cassel et al. (2008) demonstrated that the NLRP3 inflammasome-CASP-1-pathway is essential for the development of silicosis. Besides crystalline silica, further types of particles including uric acid crystals (Martinon et al., 2006), TiO_2 nanoparticles (Baron et al., 2015; Kolling et al., 2020),

amorphous silica nanoparticles (Winter et al., 2011), and urban $PM_{2.5}$ (Cao et al., 2022) have been shown to activate the NLRP3 inflammasome. Apart from silicosis, no lung disease has yet been definitively causally linked to the NLRP3 inflammasome. Nevertheless, there are compelling indications that the NLRP3 inflammasome is also involved in acute lung injury, asthma, and chronic obstructive pulmonary disease (COPD) upon particle exposure (Sayan and Mossman, 2016).

1.3 Models to assess the health hazards of aeolian particulate matter

1.3.1 Epidemiology and controlled human exposures

Conclusions on the health effects of air pollution can be drawn from epidemiological studies and controlled human exposures. The advantage of studying humans is that no interspecies differences need to be considered. Additionally, in epidemiology, real-world exposure scenarios are studied.

Regarding desert dust events, exploring short-term effects on morbidity and mortality is well-achievable (see 1.4.1). However, it is difficult if not impossible to epidemiologically link such short irregular events to chronic diseases that manifest many years later and may also be caused by multiple other pollutants (Kim et al., 2013; Middleton, 2017) and influenced by inter-human variability (Varshavsky et al., 2023). Controlled human exposures are another valuable tool to explore health effects (Huang and Ghio, 2009). However, due to ethical concerns such studies are limited to low concentrations and easily accessible read-outs. Epidemiological and controlled human studies also have limited possibilities of interventions, such as targeted genetic modifications. Therefore, to gain a profound mechanistic understanding of severe and potentially chronic adverse health effects, *in vivo* and *in vitro* studies are required.

1.3.2 *In vivo* models

To assess the toxicity of particulate matter in whole organisms, typically rodents are exposed via inhalation or instillation. Advantages compared to *in vitro* methods (see 1.3.3) include the presence of all cell types and interactions between organs. Nose-only and whole-body inhalations offer relatively realistic ways of exposure whereas higher doses can be applied by intrapharyngeal or intratracheal instillations (Akhtar et al., 2010). Inhalation studies are also needed to fulfill regulatory requirements such as the European Registration, Evaluation, Authorization and Restriction of Chemicals (REACH) regulation (European Parliament and Council, 2006) or the U.S. Toxic Substances Control Act (TSCA) (EPA, 1998). A disadvantage of rodent studies is that

interspecies differences need to be extrapolated to humans, e.g., the anatomy of the respiratory tract (Crapo et al., 1983), particle deposition and retention (Yu, 1996), and genetics (Warren et al., 2015). Moreover, for ethical reasons reflected in the 3 Rs introduced by Russell and Burch (1959), animal experiments should be refined, reduced, and replaced whenever possible. This strive is emphasized by the directive 2010/63 of the European Parliament and Council (2010) aiming towards laboratory animal-free science and the self-commitment of the United States EPA (2019) to stop animal testing by 2035. Hence, alternative methods, especially advanced *in vitro* models, need to be established.

1.3.3 *In vitro* models

For alveoli and airways, *in vitro* models of increasing complexity exist, e.g., traditional submerged cultures, air-liquid interface (ALI) cultures, organ-on-a-chip models, organoids, and precision cut lung-slices (PCLS). For submerged cultures, a variety of immortalized cell lines is available. The most-used alveolar cell line is A549, representative of alveolar epithelial type II cells, whereas Calu-3, 16HBE14o$^-$, and BEAS-2B cells are mainly applied as models of bronchial epithelial cells (reviewed by Rothen-Rutishauser et al. (2008)). These cell lines can help unravel molecular mechanisms of particle toxicity and are apt for high-throughput testing (Rothen-Rutishauser et al., 2008). Further cell types that are of relevance in alveoli and airways are macrophages, fibroblasts, and endothelial cells which can be investigated using, for instance, THP-1 cells (Auwerx, 1991), MRC-5 cells (Jacobs et al., 1970), and EaHy926 cells (Suggs et al., 1986), respectively. Depending on the research question, epithelial cells can be co-cultured with one or more of these other cell types to cover their interactions (e.g., Alfaro-Moreno et al. (2008), Friesen et al. (2022), He et al. (2021)).

Morphological and functional properties of immortalized cell lines can vary from cells in original, healthy tissues. Thus, to properly interpret study results, characterization of the cell lines is critical (Rothen-Rutishauser et al., 2008). Primary cells are a more realistic alternative, which can even model diseased phenotypes (Essaidi-Laziosi et al., 2023). Drawback of primary cells are their limited availability and passage numbers as well as inter-donor variability (Li, 2019).

More realistic conditions can also be achieved by cultivation of the cells in contact with air at the ALI. ALI culture of A549 cells triggers the production of surfactant and a decrease in surface tension (Blank et al., 2006; Ohlinger et al., 2019; Wu et al., 2017). ALI culture of Calu-3 cells leads to the formation of tight junctions and secretion of mucus (Braakhuis et al., 2020; Grainger et al., 2006). Furthermore, in the last decade, major progress has been made on primary ALI cultures of

alveolar (Visigalli et al., 2022) and airway tissue (Huang et al., 2013). ALI cultures in combination with aerosol-generating devices enable a realistic way of exposure (Ding et al., 2020).

Organ-on-a-chip models are ALI cultures embedded in microfluidic systems. These systems can mimic the mechanical stress from cyclic breathing motion which influences permeability, metabolic activity, and cytokine secretion (Stucki et al., 2015). Both immortalized (Huh et al., 2012; Huh et al., 2010) and primary cells have been applied in such models (Benam et al., 2016; Blume et al., 2015; Stucki et al., 2015). Examples of particles tested in organ-on-a-chip models are silica nanoparticles (Huh et al., 2010) and pollen (Blume et al., 2015).

Beyond the *in vitro* models introduced so far, lung organoids and PCLS could be applied. Lung organoids are achieved by guided differentiation of embryonic stem cells (ESCs), induced pluripotent stem cells (iPSCs), or lung progenitor cells (Lancaster and Knoblich, 2014). PCLS are obtained from human lung tissue. The huge advantages of these models are that they contain multiple or all lung cell types and resemble or conserve natural organ structures. Yet, two critical issues with organoids are that the apical side which comes into contact with inhaled PM faces inside (Kastlmeier et al., 2022) and that ALI conditions have not yet been accomplished. The first issue may be overcome with apical-out organoids (Salahudeen et al., 2020) that, however, have not yet been applied in the field of particle toxicology. PCLS face limitations in terms of availability, varying viability durations of different cell types (Hiemstra et al., 2018), and notably, the lack of an apical side for PM exposure.

Although *in vitro* models are urgently needed to substitute animal testing, they are not yet ready for regulatory purposes. As Hiemstra et al. (2018) pointed out, “robustness, reproducibility and predictive value” still need to be validated.

1.4 Adverse health effects of desert dusts

Epidemiological, *in vivo*, and *in vitro* research has been applied to address the adverse health effects of desert dusts. Recently, Lwin et al. (2023) reviewed epidemiological studies on desert dusts, Fussell and Kelly (2021) reviewed toxicological *in vivo* and *in vitro* studies, and Zhang et al. (2016a) reviewed both.

1.4.1 Desert dusts in epidemiology

Epidemiological studies have shown that desert dust exposure affects respiratory and cardiovascular health, leads to allergic reactions, and carries infectious diseases. According to Lwin et al. (2023), each of the aforementioned health impacts has been covered by between 18

and 121 epidemiological studies on desert dust exposure of which about 80% reported adverse health effects. This implies that not all studies found adversities. Zhang et al. (2016a) suggested this to be related to differences between dust sources and trajectories. Typically, epidemiological studies analyzed mortality and morbidity of control days compared to the days during and after dust events (Gutierrez et al., 2020; Gyan et al., 2005; Johnston et al., 2011; Kwon et al., 2002; Mallone et al., 2011; Stafoggia et al., 2016; Tam et al., 2012; Thalib and Al-Taiar, 2012; Zauli Sajani et al., 2011; Zhang et al., 2016a). Thus, epidemiological studies could not link desert dust exposure to the etiology but to the manifestation or exacerbation of chronic diseases such as asthma (Bell et al., 2008; Gyan et al., 2005; Thalib and Al-Taiar, 2012), COPD (Gutierrez et al., 2020; Tam et al., 2012) or ischemic heart disease (Bell et al., 2008).

1.4.2 Desert dusts in toxicology studies

In vivo studies have mainly addressed the inflammatory effects and the exacerbation of allergic responses through desert dust exposure (Fussell and Kelly, 2021). An inflammatory effect frequently reported in instillation studies with Asian desert dusts (Ichinose et al., 2005; Lei et al., 2004; Naota et al., 2010; Rattanapinyopituk et al., 2013; Shimada et al., 2018; Yanagisawa et al., 2007), Arizona dust (Ghio et al., 2014) and Middle Eastern dust (Wilfong et al., 2011) was neutrophilic inflammation. Only two studies that generally described weak effects did not find neutrophilic inflammation. In one of these studies, relatively low doses were instilled (Taylor et al., 2013). The other was an inhalation study (Dorman et al., 2012). Increased numbers of macrophages, eosinophils, and lymphocytes as well as proliferation of goblet cells were also described in several of these investigations though not as consistently as neutrophilic inflammation. These analyses also revealed increases in a multitude of tissue damage markers in BAL, e.g., total protein, albumin, and LDH (Ghio et al., 2014; Lei et al., 2004; Naota et al., 2010), as well as chemokines and cytokines, e.g. C-X-C motif chemokine ligand 1 (CXCL1), CXCL2, CXCL10, interferon γ (IFNγ), IL-1β, IL-6, IL-12, and TNFα (Ghio et al., 2014; Ichinose et al., 2005; Yanagisawa et al., 2007) which varied between the tested dusts. Rattanapinyopituk et al. (2013) and Naota et al. (2010) also described elevated levels of Cu/Zn superoxide dismutase (SOD), and inducible nitric oxide synthase (iNOS) indicative of oxidative stress. Studies addressing the influence of desert dusts on allergic responses agree on its aggravating role, especially through enhanced recruitment of eosinophils and release of the cytokines IL-5 and IL-13 (He et al., 2010; He et al., 2019; Ichinose et al., 2008; Ren et al., 2014b). Both inflammation and allergic exacerbation have been related to the endotoxin and β-glucan content of desert dusts (He et al., 2019; Ichinose et al., 2005; Ren et al., 2014b; Ren et al., 2019). Applying both *in vivo* and *in vitro* methods, the inflammatory potency of desert dusts containing microbial components could be

linked to signaling via TLR4 and myeloid differentiation factor 88 (MyD88) (He et al., 2013; He et al., 2016). He et al. (2010) also suggested an involvement of the NLRP3 inflammasome due to increased expression of *NLRP3*, *ASC*, and *IL1B* in Asian sand dust-exposed mouse RAW264.7 macrophages. Generally, the results from *in vitro* and *in vivo* studies agreed with each other (Fussell and Kelly, 2021).

1.5 Objectives of this thesis

Globally millions of people inhale aerosolized desert dusts. It is well-established that desert dust exposure causes adverse health effects and pulmonary inflammation while the extent varies between source regions and samples (see 1.4). While SD significantly contributes to global desert dust emissions, accounting for approximately 50% (Ginoux et al., 2012; Middleton, 2017; Washington et al., 2003), its toxicity remains largely understudied when compared to dust from other desert sources (Middleton, 2017; Zhang et al., 2016a). Moreover, it is debated whether desert dust events reduce or increase the intrinsic inflammatory potency of the local air pollution cocktail (Rodriguez-Cotto et al., 2015; Val et al., 2013). Yet, for regulatory purposes, it is essential to understand the variability in desert dust toxicity and which constituents it depends on. From a mechanistic perspective, the NLRP3 inflammasome-CASP-1 pathway has insufficiently been studied for desert dusts although it is recognized as crucial for the toxicity of quartz dust and lung disease (Sayan and Mossman, 2016). Furthermore, holistic approaches to identify yet unknown mediators of toxicity have merely been applied to mice and BEAS-2B cells exposed to Asian sand dust (Yanagisawa et al., 2007) and particulate matter from Saudi Arabia (Sun et al., 2012), respectively. For SD and advanced human *in vitro* models exposed to desert dusts, a holistic approach such as RNA sequencing has not been applied so far.

The hypothesis underlying this thesis was that SD poses health hazards through the induction of oxidative stress and inflammation in the lung. Therefore, this thesis aimed to achieve six **objectives**. The first objective was to assess the oxidative and inflammatory potency of SD compared to quartz dusts. The second objective was to associate SD's oxidative and inflammatory potency with its constituents. The third objective was to evaluate the inflammatory potency of PM from dust events compared to background PM. The fourth objective was to investigate the role of the NLRP3 inflammasome in SD's inflammatory potency. The fifth objective was to identify other potential molecular pathways of adverse health effects of SD. Finally, the sixth objective was to address the first five objectives using pulmonary *in vitro* models in adherence to the 3 R principles (Russell and Burch, 1959).

Chapter 2 offers insights into the physicochemical properties of SD and its oxidative and inflammatory potency. The effects of SD on traditional submerged mono-cultures of alveolar epithelial A549 cells and THP-1 macrophages were assessed in comparison to well-investigated quartz dusts. The role of the NLRP3 inflammasome was examined using wild-type and *NLRP3*$^{-/-}$ THP-1 cells. **Chapter 3** provides a comparison of a panel of 63 $PM_{2.5}$ and PM_{10} samples from a reference period and two dust events screened on THP-1 cells. The intrinsic inflammatory potency of desert dust event PM compared to reference period PM was assessed and related to the contents of water-soluble ions, elements, organic and elemental carbon, and endotoxins. In **Chapter 4**, the characteristics of an ALI co-culture of A549 and THP-1 cells are described. The inflammatory potency of SD compared to DQ12 quartz dust in this more realistic model was evaluated. The hypothesis that the NLRP3 inflammasome-CASP-1 pathway was involved in SD's inflammatory potency was tested by incorporating wild-type, *CASP1*$^{-/-}$, and *NLRP3*$^{-/-}$ THP-1 cells. In **Chapter 5**, the application of RNA sequencing arrays to SD and DQ12 quartz-exposed ALI co-cultures is presented. This procedure was used to identify further mediators of the toxicity of SD. **Chapter 6** provides a common discussion of the study outcomes, offering insights into their applicability and relevance to protecting human health.

1.6 References

Abuduwaili, J., Gabchenko, M.V., Junrong, X., 2008. Eolian transport of salts—A case study in the area of Lake Ebinur (Xinjiang, Northwest China). J Arid Environ 72, 1843-1852. https://doi.org/10.1016/j.jaridenv.2008.05.006

Achakulwisut, P., Anenberg, S.C., Neumann, J.E., Penn, S.L., Weiss, N., Crimmins, A., Fann, N., Martinich, J., Roman, H., Mickley, L.J., 2019. Effects of Increasing Aridity on Ambient Dust and Public Health in the U.S. Southwest Under Climate Change. Geohealth 3, 127-144. https://doi.org/10.1029/2019GH000187

Akhtar, U.S., Scott, J.A., Chu, A., Evans, G.J. In vivo and In vitro Assessment of Particulate Matter Toxicology. Urban Airborne Particulate Matter; 2010

Alfaro-Moreno, E., Nawrot, T.S., Vanaudenaerde, B.M., Hoylaerts, M.F., Vanoirbeek, J.A., Nemery, B., Hoet, P.H., 2008. Co-cultures of multiple cell types mimic pulmonary cell communication in response to urban PM10. Eur Respir J 32, 1184-1194. https://doi.org/10.1183/09031936.00044008

An, S., Sin, H.H., DuBow, M.S., 2014. Modification of atmospheric sand-associated bacterial communities during Asian sandstorms in China and South Korea. Heredity 114, 460-467. https://doi.org/10.1038/hdy.2014.102

Auwerx, J., 1991. The human leukemia cell line, THP-1: a multifacetted model for the study of monocyte-macrophage differentiation. Experientia 47, 22-31. https://doi.org/10.1007/BF02041244

Balkanski, Y., Schulz, M., Claquin, T., Guibert, S., 2007. Reevaluation of Mineral aerosol radiative forcings suggests a better agreement with satellite and AERONET data. Atmos Chem Phys 7, 81-95. https://doi.org/10.5194/acp-7-81-2007

Ban-Weiss, G.A., Lunden, M.M., Kirchstetter, T.W., Harley, R.A., 2010. Size-resolved particle number and volume emission factors for on-road gasoline and diesel motor vehicles. J Aerosol Sci 41, 5-12. https://doi.org/10.1016/j.jaerosci.2009.08.001

Baron, L., Gombault, A., Fanny, M., Villeret, B., Savigny, F., Guillou, N., Panek, C., Le Bert, M., Lagente, V., Rassendren, F., Riteau, N., Couillin, I., 2015. The NLRP3 inflammasome is activated by nanoparticles through ATP, ADP and adenosine. Cell Death Dis 6, e1629. https://doi.org/10.1038/cddis.2014.576

Bauernfeind, F.G., Horvath, G., Stutz, A., Alnemri, E.S., MacDonald, K., Speert, D., Fernandes-Alnemri, T., Wu, J., Monks, B.G., Fitzgerald, K.A., Hornung, V., Latz, E., 2009. Cutting edge: NF-kappaB activating pattern recognition and cytokine receptors license NLRP3 inflammasome activation by regulating NLRP3 expression. J Immunol 183, 787-791. https://doi.org/10.4049/jimmunol.0901363

Bell, M.L., Levy, J.K., Lin, Z., 2008. The effect of sandstorms and air pollution on cause-specific hospital admissions in Taipei, Taiwan. Occup Environ Med 65, 104-111. https://doi.org/10.1136/oem.2006.031500

Benam, K.H., Villenave, R., Lucchesi, C., Varone, A., Hubeau, C., Lee, H.H., Alves, S.E., Salmon, M., Ferrante, T.C., Weaver, J.C., Bahinski, A., Hamilton, G.A., Ingber, D.E., 2016. Small airway-on-a-chip enables analysis of human lung inflammation and drug responses in vitro. Nat Methods 13, 151-157. https://doi.org/10.1038/nmeth.3697

Blank, F., Rothen-Rutishauser, B.M., Schurch, S., Gehr, P., 2006. An optimized in vitro model of the respiratory tract wall to study particle cell interactions. J Aerosol Med 19, 392-405. https://doi.org/10.1089/jam.2006.19.392

Blume, C., Reale, R., Held, M., Millar, T.M., Collins, J.E., Davies, D.E., Morgan, H., Swindle, E.J., 2015. Temporal Monitoring of Differentiated Human Airway Epithelial Cells Using Microfluidics. PLoS One 10, e0139872. https://doi.org/10.1371/journal.pone.0139872

Braakhuis, H.M., He, R., Vandebriel, R.J., Gremmer, E.R., Zwart, E., Vermeulen, J.P., Fokkens, P., Boere, J., Gosens, I., Cassee, F.R., 2020. An Air-liquid Interface Bronchial Epithelial Model for Realistic, Repeated Inhalation Exposure to Airborne Particles for Toxicity Testing. J Vis Exp, https://doi.org/10.3791/61210

Bryant, C., Fitzgerald, K.A., 2009. Molecular mechanisms involved in inflammasome activation. Trends Cell Biol 19, 455-464. https://doi.org/10.1016/j.tcb.2009.06.002

Bryant, R.G., 2003. Monitoring hydrological controls on dust emissions: preliminary observations from Etosha Pan, Namibia. Geogr J 169, 131-141. https://doi.org/10.1111/1475-4959.04977

Bryant, R.G., Bigg, G.R., Mahowald, N.M., Eckardt, F.D., Ross, S.G., 2007. Dust emission response to climate in southern Africa. J Geophys Res-Atmos 112, https://doi.org/10.1029/2005jd007025

Bullard, J.E., McTainsh, G.H., 2016. Aeolian-fluvial interactions in dryland environments: examples, concepts and Australia case study. Prog Phys Geog 27, 471-501. https://doi.org/10.1191/0309133303pp386ra

Burckstummer, T., Baumann, C., Bluml, S., Dixit, E., Durnberger, G., Jahn, H., Planyavsky, M., Bilban, M., Colinge, J., Bennett, K.L., Superti-Furga, G., 2009. An orthogonal proteomic-genomic screen identifies AIM2 as a cytoplasmic DNA sensor for the inflammasome. Nat Immunol 10, 266-272. https://doi.org/10.1038/ni.1702

Cakmur, R.V., Miller, R.L., Perlwitz, J., Geogdzhayev, I.V., Ginoux, P., Koch, D., Kohfeld, K.E., Tegen, I., Zender, C.S., 2006. Constraining the magnitude of the global dust cycle by minimizing the difference between a model and observations. J Geophy Res-Atmos 111, https://doi.org/10.1029/2005jd005791

Cao, W., Wang, X., Li, J., Yan, M., Chang, C.H., Kim, J., Jiang, J., Liao, Y.P., Tseng, S., Kusumoputro, S., Lau, C., Huang, M., Han, P., Lu, P., Xia, T., 2022. NLRP3 inflammasome activation determines the fibrogenic potential of PM2.5 air pollution particles in the lung. J Environ Sci-China 111, 429-441. https://doi.org/10.1016/j.jes.2021.04.021

Carlson, T.N., Benjamin, S.G., 1980. Radiative Heating Rates for Saharan Dust. J Atmos Sci 37, 193-213. https://doi.org/10.1175/1520-0469(1980)037<0193:Rhrfsd>2.0.Co;2

Carpenter, L.J., Fleming, Z.L., Read, K.A., Lee, J.D., Moller, S.J., Hopkins, J.R., Purvis, R.M., Lewis, A.C., Müller, K., Heinold, B., Herrmann, H., Fomba, K.W., van Pinxteren, D., Müller, C., Tegen, I., Wiedensohler, A., Müller, T., Niedermeier, N., Achterberg, E.P., Patey, M.D., Kozlova, E.A., Heimann, M., Heard, D.E., Plane, J.M.C., Mahajan, A., Oetjen, H., Ingham, T., Stone, D., Whalley, L.K., Evans, M.J., Pilling, M.J., Leigh, R.J., Monks, P.S., Karunaharan, A., Vaughan, S., Arnold, S.R., Tschritter, J., Pöhler, D., Frieß, U., Holla, R., Mendes, L.M., Lopez, H., Faria, B., Manning, A.J., Wallace, D.W.R., 2011. Seasonal characteristics of tropical marine boundary layer air measured at the Cape Verde Atmospheric Observatory. J Atmos Chem 67, 87-140. https://doi.org/10.1007/s10874-011-9206-1

Cassel, S.L., Eisenbarth, S.C., Iyer, S.S., Sadler, J.J., Colegio, O.R., Tephly, L.A., Carter, A.B., Rothman, P.B., Flavell, R.A., Sutterwala, F.S., 2008. The Nalp3 inflammasome is essential for the development of silicosis. Proc Natl Acad Sci U S A 105, 9035-9040. https://doi.org/10.1073/pnas.0803933105

Chatenet, B., Marticorena, B., Gomes, L., Bergametti, G., 1996. Assessing the microped size distributions of desert soils erodible by wind. Sedimentology 43, 901-911. https://doi.org/10.1111/j.1365-3091.1996.tb01509.x

Chiapello, I., Bergametti, G., Chatenet, B., Bousquet, P., Dulac, F., Soares, E.S., 1997. Origins of African dust transported over the northeastern tropical Atlantic. J Geophy Res-Atmos 102, 13701-13709. https://doi.org/10.1029/97jd00259

Chiapello, I., Bergametti, G., Gomes, L., Chatenet, B., Dulac, F., Pimenta, J., Suares, E.S., 1995. An additional low layer transport of Sahelian and Saharan dust over the north-eastern Tropical Atlantic. Geophy Res Lett 22, 3191-3194. https://doi.org/10.1029/95gl03313

Chin, M., Diehl, T., Ginoux, P., Malm, W., 2007. Intercontinental transport of pollution and dust aerosols: implications for regional air quality. Atmos Chem Phys 7, 5501-5517. https://doi.org/10.5194/acp-7-5501-2007

Choi, J.C., Lee, M., Chun, Y., Kim, J., Oh, S., 2001. Chemical composition and source signature of spring aerosol in Seoul, Korea. J Geophys Res-Atmos 106, 18067-18074. https://doi.org/10.1029/2001jd900090

Claquin, T., Schulz, M., 1999. Modeling the mineralogy of atmospheric dust sources. J Geophys Res-Atmos 104, 22243-22256. https://doi.org/10.1029/1999jd900416

Clifford, H.M., Spaulding, N.E., Kurbatov, A.V., More, A., Korotkikh, E.V., Sneed, S.B., Handley, M., Maasch, K.A., Loveluck, C.P., Chaplin, J., McCormick, M., Mayewski, P.A., 2019. A 2000 Year Saharan Dust Event Proxy Record from an Ice Core in the European Alps. J Geophys Res-Atmos 124, 12882-12900. https://doi.org/10.1029/2019jd030725

Crapo, J.D., Young, S.L., Fram, E.K., Pinkerton, K.E., Barry, B.E., Crapo, R.O., 1983. Morphometric characteristics of cells in the alveolar region of mammalian lungs. Am Rev Respir Dis 128, S42-46. https://doi.org/10.1164/arrd.1983.128.2P2.S42

Dinarello, C.A., 2002. The IL-1 family and inflammatory diseases. Clin Exp Rheumatol 5, S1-13.

Ding, Y., Weindl, P., Lenz, A.G., Mayer, P., Krebs, T., Schmid, O., 2020. Quartz crystal microbalances (QCM) are suitable for real-time dosimetry in nanotoxicological studies using VITROCELL®Cloud cell exposure systems. Part Fibre Toxicol 17, 44. https://doi.org/10.1186/s12989-020-00376-w

Dorman, D.C., Mokashi, V., Wagner, D.J., Olabisi, A.O., Wong, B.A., Moss, O.R., Centeno, J.A., Guandalini, G., Jackson, D.A., Dennis, W.E., Lewis, J.A., Thomas, R.S., Chapman, G.D., 2012. Biological responses in rats exposed to cigarette smoke and Middle East sand (dust). Inhal Toxicol 24, 109-124. https://doi.org/10.3109/08958378.2011.647413

Dostert, C., Petrilli, V., Van Bruggen, R., Steele, C., Mossman, B.T., Tschopp, J., 2008. Innate immune activation through Nalp3 inflammasome sensing of asbestos and silica. Science 320, 674-677. https://doi.org/10.1126/science.1156995

Doyle, H.N., 1953. Polluted air, a growing community problem. Public Health Rep (1896) 68, 858-867.

Elliott, J.H., 1923. Silicosis in Ontario Gold Miners. Trans Am Climatol Clin Assoc 39, 24-43.

Environmental Protection Agency (EPA), 1971. Code of Federal Regulations Title 40 Part 50 National primary and secondary ambient air quality standards. https://www.ecfr.gov/current/title-40/chapter-I/subchapter-C/part-50. Accessed: 03/10/2023

EPA, 1998. Health Effects Test Guidelines OPPTS 870.3465 90-Day Inhalation Toxicity. https://www.regulations.gov/document/EPA-HQ-OPPT-2009-0156-0014. Accessed: 14/11/2023

EPA, 2019. Directive to Prioritize Efforts to Reduce Animal testing. https://www.epa.gov/sites/default/files/2019-09/documents/image2019-09-09-231249.pdf. Accessed: 14/11/2023

Erel, Y., Dayan, U., Rabi, R., Rudich, Y., Stein, M., 2006. Trans boundary transport of pollutants by atmospheric mineral dust. Environ Sci Technol 40, 2996-3005. https://doi.org/10.1021/es051502l

Essaidi-Laziosi, M., Royston, L., Boda, B., Perez-Rodriguez, F.J., Piuz, I., Hulo, N., Kaiser, L., Clement, S., Huang, S., Constant, S., Tapparel, C., 2023. Altered cell function and increased replication of rhinoviruses and EV-D68 in airway epithelia of asthma patients. Front Microbiol 14, 1106945. https://doi.org/10.3389/fmicb.2023.1106945

European Commission, 2022. Proposal for a directive of the European Parliament and of the council on ambient air quality and cleaner air for Europe (recast). https://eur-lex.europa.eu/legal-content/EN/TXT/?uri=CELEX%3A52022PC0542&qid=1696327827017. Accessed: 03/10/2023

European Parliament and Council, 2006. REGULATION (EC) No 1907/2006 OF THE EUROPEAN PARLIAMENT AND OF THE COUNCIL of 18 December 2006 concerning the Registration, Evaluation, Authorisation and Restriction of Chemicals (REACH), establishing a European Chemicals Agency, amending Directive 1999/45/EC and repealing Council Regulation (EEC) No 793/93 and Commission Regulation (EC) No 1488/94 as well as Council Directive 76/769/EEC and Commission Directives 91/155/EEC, 93/67/EEC, 93/105/EC and 2000/21/EC. https://eur-lex.europa.eu/legal-content/EN/TXT/?uri=CELEX%3A02006R1907-20221217. Accessed: 14/11/2023

European Parliament and Council, 2008. Directive 2008/50/EC of the European Parliament and of the Council of 21 May 2008 on ambient air quality and cleaner air for Europe. Official Journal of the European Union. https://eur-lex.europa.eu/legal-content/EN/TXT/?uri=celex%3A32008L0050. Accessed: 03/10/2023

European Parliament and Council, 2010. Directive 2010/63/EU of the European Parliament and of the Council of 22 September 2010 on the protection of animals used for scientific purposes. Official Journal of the European Union. https://eur-lex.europa.eu/LexUriServ/LexUriServ.do?uri=OJ:L:2010:276:0033:0079:en:PDF. Accessed: 16/11/2023

European Parliament and Council, 2017. Directive (EU) 2017/2398 of the European Parliament and of the Council of 12 December 2017 amending Directive 2004/37/EC on the protection of workers from the risks related to exposure to carcinogens or mutagens at work (Text with EEA relevance). Official Journal of the European Union. https://eur-lex.europa.eu/eli/dir/2017/2398/oj. Accessed: 12/04/2023

Favet, J., Lapanje, A., Giongo, A., Kennedy, S., Aung, Y.Y., Cattaneo, A., Davis-Richardson, A.G., Brown, C.T., Kort, R., Brumsack, H.J., Schnetger, B., Chappell, A., Kroijenga, J., Beck, A., Schwibbert, K., Mohamed, A.H., Kirchner, T., de Quadros, P.D., Triplett, E.W., Broughton, W.J., Gorbushina, A.A., 2013. Microbial hitchhikers on intercontinental dust: catching a lift in Chad. ISME J 7, 850-867. https://doi.org/10.1038/ismej.2012.152

Fomba, K.W., Deabji, N., Barcha, S.E.I., Ouchen, I., Elbaramoussi, E.M., El Moursli, R.C., Harnafi, M., El Hajjaji, S., Mellouki, A., Herrmann, H., 2020. Application of TXRF in monitoring trace metals in particulate matter and cloud water. Atmos Meas Tech 13, 4773-4790. https://doi.org/10.5194/amt-13-4773-2020

Fomba, K.W., Müller, K., van Pinxteren, D., Herrmann, H., 2013. Aerosol size-resolved trace metal composition in remote northern tropical Atlantic marine environment: case study Cape Verde islands. Atmos Chem Phys 13, 4801-4814. https://doi.org/10.5194/acp-13-4801-2013

Fomba, K.W., Müller, K., van Pinxteren, D., Poulain, L., van Pinxteren, M., Herrmann, H., 2014. Long-term chemical characterization of tropical and marine aerosols at the Cape Verde Atmospheric Observatory (CVAO) from 2007 to 2011. Atmos Chem Phys 14, 8883-8904. https://doi.org/10.5194/acp-14-8883-2014

Formenti, P., Caquineau, S., Desboeufs, K., Klaver, A., Chevaillier, S., Journet, E., Rajot, J.L., 2014. Mapping the physico-chemical properties of mineral dust in western Africa: mineralogical composition. Atmos Chem Phys 14, 10663-10686. https://doi.org/10.5194/acp-14-10663-2014

Franchi, L., Eigenbrod, T., Nunez, G., 2009. Cutting edge: TNF-alpha mediates sensitization to ATP and silica via the NLRP3 inflammasome in the absence of microbial stimulation. J Immunol 183, 792-796. https://doi.org/10.4049/jimmunol.0900173

Friesen, A., Fritsch-Decker, S., Hufnagel, M., Mulhopt, S., Stapf, D., Hartwig, A., Weiss, C., 2022. Comparing alpha-Quartz-Induced Cytotoxicity and Interleukin-8 Release in Pulmonary Mono- and Co-Cultures Exposed under Submerged and Air-Liquid Interface Conditions. Int J Mol Sci 23, https://doi.org/10.3390/ijms23126412

Furuyama, A., Kanno, S., Kobayashi, T., Hirano, S., 2009. Extrapulmonary translocation of intratracheally instilled fine and ultrafine particles via direct and alveolar macrophage-associated routes. Arch Toxicol 83, 429-437. https://doi.org/10.1007/s00204-008-0371-1

Fussell, J.C., Kelly, F.J., 2021. Mechanisms underlying the health effects of desert sand dust. Environ Int 157, 106790. https://doi.org/10.1016/j.envint.2021.106790

Gasse, F., Stabell, B., Fourtanier, E., van Iperen, Y., 2017. Freshwater Diatom Influx in Intertropical Atlantic: Relationships with Continental Records from Africa. Quaternary Res. 32, 229-243. https://doi.org/10.1016/0033-5894(89)90079-3

Ghayur, T., Banerjee, S., Hugunin, M., Butler, D., Herzog, L., Carter, A., Quintal, L., Sekut, L., Talanian, R., Paskind, M., Wong, W., Kamen, R., Tracey, D., Allen, H., 1997. Caspase-1 processes IFN-gamma-inducing factor and regulates LPS-induced IFN-gamma production. Nature 386, 619-623. https://doi.org/10.1038/386619a0

Ghio, A.J., Kummarapurugu, S.T., Tong, H., Soukup, J.M., Dailey, L.A., Boykin, E., Gilmour, I.M., Ingram, P., Roggli, V.L., Goldstein, H.L., Reynolds, R.L., 2014. Biological effects of desert dust in respiratory epithelial cells and a murine model. Inhal Toxicol 26, 299-309. https://doi.org/10.3109/08958378.2014.888109

Ghonime, M.G., Shamaa, O.R., Das, S., Eldomany, R.A., Fernandes-Alnemri, T., Alnemri, E.S., Gavrilin, M.A., Wewers, M.D., 2014. Inflammasome priming by lipopolysaccharide is dependent upon ERK signaling and proteasome function. J Immunol 192, 3881-3888. https://doi.org/10.4049/jimmunol.1301974

Gillette, D.A., Fryrear, D.W., Gill, T.E., Ley, T., Cahill, T.A., Gearhart, E.A., 1997. Relation of vertical flux of particles smaller than 10 µm to total aeolian horizontal mass flux at Owens Lake. J Geophys Res-Atmos 102, 26009-26015. https://doi.org/10.1029/97jd02252

Ginoux, P., Prospero, J.M., Gill, T.E., Hsu, N.C., Zhao, M., 2012. Global-scale attribution of anthropogenic and natural dust sources and their emission rates based on MODIS Deep Blue aerosol products. Rev Geophys 50, https://doi.org/10.1029/2012rg000388

Gonçalves, C., Alves, C., Nunes, T., Rocha, S., Cardoso, J., Cerqueira, M., Pio, C., Almeida, S.M., Hillamo, R., Teinilä, K., 2014. Organic characterisation of PM10 in Cape Verde under Saharan dust influxes. Atmos Envir 89, 425-432. https://doi.org/10.1016/j.atmosenv.2014.02.025

Goudie, A.S., Middleton, N.J., 2001. Saharan dust storms: nature and consequences. Earth-Sci Rev 56, 179-204. https://doi.org/10.1016/s0012-8252(01)00067-8

Grainger, C.I., Greenwell, L.L., Lockley, D.J., Martin, G.P., Forbes, B., 2006. Culture of Calu-3 cells at the air interface provides a representative model of the airway epithelial barrier. Pharm Res 23, 1482-1490. https://doi.org/10.1007/s11095-006-0255-0

Grenier, J.M., Wang, L., Manji, G.A., Huang, W.J., Al-Garawi, A., Kelly, R., Carlson, A., Merriam, S., Lora, J.M., Briskin, M., DiStefano, P.S., Bertin, J., 2002. Functional screening of five PYPAF family members identifies PYPAF5 as a novel regulator of NF-kappaB and caspase-1. FEBS Lett 530, 73-78. https://doi.org/10.1016/s0014-5793(02)03416-6

Griffin, D.W., Garrison, V.H., Herman, J.R., Shinn, E.A., 2001. African desert dust in the Caribbean atmosphere: Microbiology and public health. Aerobiologia 17, 203-213. https://doi.org/10.1023/a:1011868218901

Gutierrez, M.P., Zuidema, P., Mirsaeidi, M., Campos, M., Kumar, N., 2020. Association between African Dust Transport and Acute Exacerbations of COPD in Miami. J Clin Med 9, 2496. https://doi.org/10.3390/jcm9082496

Gyan, K., Henry, W., Lacaille, S., Laloo, A., Lamsee-Ebanks, C., McKay, S., Antoine, R.M., Monteil, M.A., 2005. African dust clouds are associated with increased paediatric asthma accident and emergency admissions on the Caribbean island of Trinidad. Int J Biometeorol 49, 371-376. https://doi.org/10.1007/s00484-005-0257-3

He, M., Ichinose, T., Song, Y., Yoshida, Y., Arashidani, K., Yoshida, S., Liu, B., Nishikawa, M., Takano, H., Sun, G., 2013. Effects of two Asian sand dusts transported from the dust source regions of Inner Mongolia and northeast China on murine lung eosinophilia. Toxicol Appl Pharmacol 272, 647-655. https://doi.org/10.1016/j.taap.2013.07.010

He, M., Ichinose, T., Song, Y., Yoshida, Y., Bekki, K., Arashidani, K., Yoshida, S., Nishikawa, M., Takano, H., Shibamoto, T., Sun, G., 2016. Desert dust induces TLR signaling to trigger Th2-dominant lung allergic inflammation via a MyD88-dependent signaling pathway. Toxicol Appl Pharmacol 296, 61-72. https://doi.org/10.1016/j.taap.2016.02.011

He, M., Ichinose, T., Yoshida, S., Nishikawa, M., Mori, I., Yanagisawa, R., Takano, H., Inoue, K., Sun, G., Shibamoto, T., 2010. Airborne Asian sand dust enhances murine lung eosinophilia. Inhal Toxicol 22, 1012-1025. https://doi.org/10.3109/08958378.2010.510151

He, M., Ichinose, T., Yoshida, S., Nishikawa, M., Sun, G., Shibamoto, T., 2019. Role of iron and oxidative stress in the exacerbation of allergic inflammation in murine lungs caused by urban particulate matter <2.5 μm and desert dust. J Appl Toxicol 39, 855-867. https://doi.org/10.1002/jat.3773

He, R.W., Braakhuis, H.M., Vandebriel, R.J., Staal, Y.C.M., Gremmer, E.R., Fokkens, P.H.B., Kemp, C., Vermeulen, J., Westerink, R.H.S., Cassee, F.R., 2021. Optimization of an air-liquid interface in vitro cell co-culture model to estimate the hazard of aerosol exposures. J Aerosol Sci 153, 105703. https://doi.org/10.1016/j.jaerosci.2020.105703

Hiemstra, P.S., Grootaers, G., van der Does, A.M., Krul, C.A.M., Kooter, I.M., 2018. Human lung epithelial cell cultures for analysis of inhaled toxicants: Lessons learned and future directions. Toxicol In Vitro 47, 137-146. https://doi.org/10.1016/j.tiv.2017.11.005

Hornung, V., Bauernfeind, F., Halle, A., Samstad, E.O., Kono, H., Rock, K.L., Fitzgerald, K.A., Latz, E., 2008. Silica crystals and aluminum salts activate the NALP3 inflammasome through phagosomal destabilization. Nat Immunol 9, 847-856. https://doi.org/10.1038/ni.1631

Hsu, C.Y., Chi, K.H., Wu, C.D., Lin, S.L., Hsu, W.C., Tseng, C.C., Chen, M.J., Chen, Y.C., 2021. Integrated analysis of source-specific risks for PM(2.5)-bound metals in urban, suburban, rural, and industrial areas. Environ Pollut 275, 116652. https://doi.org/10.1016/j.envpol.2021.116652

Huang, J., Wang, T., Wang, W., Li, Z., Yan, H., 2014. Climate effects of dust aerosols over East Asian arid and semiarid regions. J Geophys Res-Atmos 119, https://doi.org/10.1002/2014jd021796

Huang, J., Yu, H., Guan, X., Wang, G., Guo, R., 2015. Accelerated dryland expansion under climate change. Nat Clim Change 6, 166-171. https://doi.org/10.1038/nclimate2837

Huang, S., Wiszniewski, L., Constant, S., Roggen, E., 2013. Potential of in vitro reconstituted 3D human airway epithelia (MucilAir) to assess respiratory sensitizers. Toxicol In Vitro 27, 1151-1156. https://doi.org/10.1016/j.tiv.2012.10.010

Huang, Y.C., Ghio, A.J., 2009. Controlled human exposures to ambient pollutant particles in susceptible populations. Environ Health 8, 33. https://doi.org/10.1186/1476-069X-8-33

Huh, D., Leslie, D.C., Matthews, B.D., Fraser, J.P., Jurek, S., Hamilton, G.A., Thorneloe, K.S., McAlexander, M.A., Ingber, D.E., 2012. A human disease model of drug toxicity-induced pulmonary edema in a lung-on-a-chip microdevice. Sci Transl Med 4, 159ra147. https://doi.org/10.1126/scitranslmed.3004249

Huh, D., Matthews, B.D., Mammoto, A., Montoya-Zavala, M., Hsin, H.Y., Ingber, D.E., 2010. Reconstituting organ-level lung functions on a chip. Science 328, 1662-1668. https://doi.org/10.1126/science.1188302

Hussein, T., Li, X., Bakri, Z., Alastuey, A., Arar, S., Al-Hunaiti, A., Viana, M., Petäjä, T., 2022. Organic and Elemental Carbon in the Urban Background in an Eastern Mediterranean City. Atmosphere-Basel 13, https://doi.org/10.3390/atmos13020197

Ichinose, T., Nishikawa, M., Takano, H., Sera, N., Sadakane, K., Mori, I., Yanagisawa, R., Oda, T., Tamura, H., Hiyoshi, K., Quan, H., Tomura, S., Shibamoto, T., 2005. Pulmonary toxicity induced by intratracheal instillation of Asian yellow dust (Kosa) in mice. Environ Toxicol Pharmacol 20, 48-56. https://doi.org/10.1016/j.etap.2004.10.009

Ichinose, T., Yoshida, S., Sadakane, K., Takano, H., Yanagisawa, R., Inoue, K., Nishikawa, M., Mori, I., Kawazato, H., Yasuda, A., Shibamoto, T., 2008. Effects of asian sand dust, Arizona sand dust, amorphous silica and aluminum oxide on allergic inflammation in the murine lung. Inhal Toxicol 20, 685-694. https://doi.org/10.1080/08958370801935133

ICRP, 1994. Human Respiratory Tract Model for Radiological Protection. ICRP Publication 66. Ann ICRP 24, 1-482.

Jacobs, J.P., Jones, C.M., Baille, J.P., 1970. Characteristics of a human diploid cell designated MRC-5. Nature 227, 168-170. https://doi.org/10.1038/227168a0

Jayaratne, E.R., Johnson, G.R., McGarry, P., Cheung, H.C., Morawska, L., 2011. Characteristics of airborne ultrafine and coarse particles during the Australian dust storm of 23 September 2009. Atmos Environ 45, 3996-4001. https://doi.org/10.1016/j.atmosenv.2011.04.059

Jeong, G.Y., 2008. Bulk and single-particle mineralogy of Asian dust and a comparison with its source soils. J Geophy Res-Atmos 113, https://doi.org/10.1029/2007jd008606

Jickells, T.D., An, Z.S., Andersen, K.K., Baker, A.R., Bergametti, G., Brooks, N., Cao, J.J., Boyd, P.W., Duce, R.A., Hunter, K.A., Kawahata, H., Kubilay, N., laRoche, J., Liss, P.S., Mahowald, N., Prospero, J.M., Ridgwell, A.J., Tegen, I., Torres, R., 2005. Global iron connections between desert dust, ocean biogeochemistry, and climate. Science 308, 67-71. https://doi.org/10.1126/science.1105959

Johnston, F., Hanigan, I., Henderson, S., Morgan, G., Bowman, D., 2011. Extreme air pollution events from bushfires and dust storms and their association with mortality in Sydney, Australia 1994-2007. Environ Res 111, 811-816. https://doi.org/10.1016/j.envres.2011.05.007

Kahlenberg, J.M., Dubyak, G.R., 2004. Mechanisms of caspase-1 activation by P2X7 receptor-mediated K+ release. Am J Physiol Cell Physiol 286, C1100-1108. https://doi.org/10.1152/ajpcell.00494.2003

Kahlenberg, J.M., Lundberg, K.C., Kertesy, S.B., Qu, Y., Dubyak, G.R., 2005. Potentiation of caspase-1 activation by the P2X7 receptor is dependent on TLR signals and requires NF-kappaB-driven protein synthesis. J Immunol 175, 7611-7622. https://doi.org/10.4049/jimmunol.175.11.7611

Kastlmeier, M.T., Guenther, E.M., Stoeger, T., Voss, C., 2022. Lung Organoids for Hazard Assessment of Nanomaterials. Int J Mol Sci 23, https://doi.org/10.3390/ijms232415666

Kellogg, C.A., Griffin, D.W., 2006. Aerobiology and the global transport of desert dust. Trends Ecol Evol 21, 638-644. https://doi.org/10.1016/j.tree.2006.07.004

Kellogg, C.A., Griffin, D.W., Garrison, V.H., Peak, K.K., Royall, N., Smith, R.R., Shinn, E.A., 2004. Characterization of Aerosolized Bacteria and Fungi From Desert Dust Events in Mali, West Africa. Aerobiologia 20, 99-110. https://doi.org/10.1023/B:AERO.0000032947.88335.bb

Kim, K.H., Jahan, S.A., Kabir, E., 2013. A review on human health perspective of air pollution with respect to allergies and asthma. Environ Int 59, 41-52. https://doi.org/10.1016/j.envint.2013.05.007

Knippertz, P., Ansmann, A., Althausen, D., Müller, D., Tesche, M., Bierwirth, E., Dinter, T., Müller, T., Von Hoyningen-Huene, W., Schepanski, K., Wendisch, M., Heinold, B., Kandler, K., Petzold, A., Schütz, L., Tegen, I., 2009. Dust mobilization and transport in the northern Sahara during SAMUM 2006 – a meteorological overview. Tellus B 61, https://doi.org/10.1111/j.1600-0889.2008.00380.x

Kodros, J.K., Volckens, J., Jathar, S.H., Pierce, J.R., 2018. Ambient Particulate Matter Size Distributions Drive Regional and Global Variability in Particle Deposition in the Respiratory Tract. Geohealth 2, 298-312. https://doi.org/10.1029/2018GH000145

Kolling, J., Tigges, J., Hellack, B., Albrecht, C., Schins, R.P.F., 2020. Evaluation of the NLRP3 Inflammasome Activating Effects of a Large Panel of TiO2 Nanomaterials in Macrophages. Nanomaterials (Basel) 10, 1876. https://doi.org/10.3390/nano10091876

Kwon, H.J., Cho, S.H., Chun, Y., Lagarde, F., Pershagen, G., 2002. Effects of the Asian dust events on daily mortality in Seoul, Korea. Environ Res 90, 1-5. https://doi.org/10.1006/enrs.2002.4377

Lafon, S., Sokolik, I.N., Rajot, J.L., Caquineau, S., Gaudichet, A., 2006. Characterization of iron oxides in mineral dust aerosols: Implications for light absorption. J Geophys Res-Atmos 111, https://doi.org/10.1029/2005jd007016

Lancaster, M.A., Knoblich, J.A., 2014. Organogenesis in a dish: modeling development and disease using organoid technologies. Science 345, 1247125. https://doi.org/10.1126/science.1247125

Lee, S., Choi, B., Yi, S.M., Ko, G., 2009. Characterization of microbial community during Asian dust events in Korea. Sci Total Environ 407, 5308-5314. https://doi.org/10.1016/j.scitotenv.2009.06.052

Lei, Y.C., Chan, C.C., Wang, P.Y., Lee, C.T., Cheng, T.J., 2004. Effects of Asian dust event particles on inflammation markers in peripheral blood and bronchoalveolar lavage in pulmonary hypertensive rats. Environ Res 95, 71-76. https://doi.org/10.1016/S0013-9351(03)00136-1

Li, Z. In Vitro Micro Tissue and Organ Models for Toxicity Testing. Comprehensive Biotechnology; 2019

Lopategi, A., Flores-Costa, R., Rius, B., Lopez-Vicario, C., Alcaraz-Quiles, J., Titos, E., Claria, J., 2019. Frontline Science: Specialized proresolving lipid mediators inhibit the priming and activation of the macrophage NLRP3 inflammasome. J Leukoc Biol 105, 25-36. https://doi.org/10.1002/JLB.3HI0517-206RR

Lwin, K.S., Tobias, A., Chua, P.L., Yuan, L., Thawonmas, R., Ith, S., Htay, Z.W., Yu, L.S., Yamasaki, L., Roque, M., Querol, X., Fussell, J.C., Nadeau, K.C., Stafoggia, M., Saliba, N.A., Sheng Ng, C.F., Hashizume, M., 2023. Effects of Desert Dust and Sandstorms on Human Health: A Scoping Review. Geohealth 7, e2022GH000728. https://doi.org/10.1029/2022GH000728

Mahowald, N., Albani, S., Kok, J.F., Engelstaeder, S., Scanza, R., Ward, D.S., Flanner, M.G., 2014. The size distribution of desert dust aerosols and its impact on the Earth system. Aeolian Research 15, 53-71. https://doi.org/10.1016/j.aeolia.2013.09.002

Mahowald, N.M., Bryant, R.G., del Corral, J., Steinberger, L., 2003. Ephemeral lakes and desert dust sources. Geophys Res Lett 30, https://doi.org/10.1029/2002gl016041

Mallone, S., Stafoggia, M., Faustini, A., Gobbi, G.P., Marconi, A., Forastiere, F., 2011. Saharan dust and associations between particulate matter and daily mortality in Rome, Italy. Environ Health Perspect 119, 1409-1414. https://doi.org/10.1289/ehp.1003026

Manji, G.A., Wang, L., Geddes, B.J., Brown, M., Merriam, S., Al-Garawi, A., Mak, S., Lora, J.M., Briskin, M., Jurman, M., Cao, J., DiStefano, P.S., Bertin, J., 2002. PYPAF1, a PYRIN-containing Apaf1-like protein that assembles with ASC and regulates activation of NF-kappa B. J Biol Chem 277, 11570-11575. https://doi.org/10.1074/jbc.M112208200

Maring, H., Savoie, D.L., Izaguirre, M.A., Custals, L., Reid, J.S., 2003. Mineral dust aerosol size distribution change during atmospheric transport. J Geophys Res-Atmos 108, https://doi.org/10.1029/2002jd002536

Martin, J.H., Gordon, M., Fitzwater, S.E., 1991. The case for iron. Limnol Oceanogr 36, 1793-1802. https://doi.org/10.4319/lo.1991.36.8.1793

Martinon, F., Burns, K., Tschopp, J., 2002. The inflammasome: a molecular platform triggering activation of inflammatory caspases and processing of proIL-beta. Mol Cell 10, 417-426. https://doi.org/10.1016/s1097-2765(02)00599-3

Martinon, F., Petrilli, V., Mayor, A., Tardivel, A., Tschopp, J., 2006. Gout-associated uric acid crystals activate the NALP3 inflammasome. Nature 440, 237-241. https://doi.org/10.1038/nature04516

Mehta, V.B., Hart, J., Wewers, M.D., 2001. ATP-stimulated release of interleukin (IL)-1beta and IL-18 requires priming by lipopolysaccharide and is independent of caspase-1 cleavage. J Biol Chem 276, 3820-3826. https://doi.org/10.1074/jbc.M006814200

Middleton, N.J., 2017. Desert dust hazards: A global review. Aeolian Res 24, 53-63. https://doi.org/10.1016/j.aeolia.2016.12.001

Naota, M., Mukaiyama, T., Shimada, A., Yoshida, A., Okajima, M., Morita, T., Inoue, K., Takano, H., 2010. Pathological study of acute pulmonary toxicity induced by intratracheally instilled Asian sand dust (kosa). Toxicol Pathol 38, 1099-1110. https://doi.org/10.1177/0192623310385143

Ohlinger, K., Kolesnik, T., Meindl, C., Galle, B., Absenger-Novak, M., Kolb-Lenz, D., Frohlich, E., 2019. Air-liquid interface culture changes surface properties of A549 cells. Toxicol In Vitro 60, 369-382. https://doi.org/10.1016/j.tiv.2019.06.014

Page, S.J., 2003. Comparison of coal mine dust size distributions and calibration standards for crystalline silica analysis. AIHA J 64, 30-39. https://doi.org/10.1080/15428110308984781

Painter, T.H., Barrett, A.P., Landry, C.C., Neff, J.C., Cassidy, M.P., Lawrence, C.R., McBride, K.E., Farmer, G.L., 2007. Impact of disturbed desert soils on duration of mountain snow cover. Geophys Res Lett 34, https://doi.org/10.1029/2007gl030284

Petrilli, V., Papin, S., Dostert, C., Mayor, A., Martinon, F., Tschopp, J., 2007. Activation of the NALP3 inflammasome is triggered by low intracellular potassium concentration. Cell Death Differ 14, 1583-1589. https://doi.org/10.1038/sj.cdd.4402195

Poyet, J.L., Srinivasula, S.M., Tnani, M., Razmara, M., Fernandes-Alnemri, T., Alnemri, E.S., 2001. Identification of Ipaf, a human caspase-1-activating protein related to Apaf-1. J Biol Chem 276, 28309-28313. https://doi.org/10.1074/jbc.C100250200

Prospero, J.M., Ginoux, P., Torres, O., Nicholson, S.E., Gill, T.E., 2002. Environmental Characterization of Global Sources of Atmospheric Soil Dust Identified with the Nimbus 7 Total Ozone Mapping Spectrometer (Toms) Absorbing Aerosol Product. Rev Geophys 40, https://doi.org/10.1029/2000rg000095

Rabolli, V., Lison, D., Huaux, F., 2016. The complex cascade of cellular events governing inflammasome activation and IL-1beta processing in response to inhaled particles. Part Fibre Toxicol 13, 40. https://doi.org/10.1186/s12989-016-0150-8

Rahn, K.A., 1976. Silicon and aluminum in atmospheric aerosols: Crust-air fractionation? Atmos Environ 10, 597-601. https://doi.org/10.1016/0004-6981(76)90044-5

Rattanapinyopituk, K., Shimada, A., Morita, T., Togawa, M., Hasegawa, T., Seko, Y., Inoue, K., Takano, H., 2013. Ultrastructural changes in the air-blood barrier in mice after intratracheal instillations of Asian sand dust and gold nanoparticles. Exp Toxicol Pathol 65, 1043-1051. https://doi.org/10.1016/j.etp.2013.03.003

Ren, Y., Ichinose, T., He, M., Song, Y., Yoshida, Y., Yoshida, S., Nishikawa, M., Takano, H., Sun, G., Shibamoto, T., 2014b. Enhancement of OVA-induced murine lung eosinophilia by co-exposure to contamination levels of LPS in Asian sand dust and heated dust. Allergy Asthma Cl Im 10, 30. https://doi.org/10.1186/1710-1492-10-30

Ren, Y., Ichinose, T., He, M., Youshida, S., Nishikawa, M., Sun, G., 2019. Co-exposure to lipopolysaccharide and desert dust causes exacerbation of ovalbumin-induced allergic lung inflammation in mice via TLR4/MyD88-dependent and -independent pathways. Allergy Asthma Clin Immunol 15, 82. https://doi.org/10.1186/s13223-019-0396-4

Rodriguez-Cotto, R.I., Ortiz-Martinez, M.G., Jimenez-Velez, B.D., 2015. Organic extracts from African dust storms stimulate oxidative stress and induce inflammatory responses in human lung cells through Nrf2 but not NF-kappaB. Environ Toxicol Pharmacol 39, 845-856. https://doi.org/10.1016/j.etap.2015.02.015

Rodríguez-Cotto, R.I., Ortiz-Martínez, M.G., Rivera-Ramírez, E., Méndez, L.B., Dávila, J.C., Jiménez-Vélez, B.D., 2013. African Dust Storms Reaching Puerto Rican Coast Stimulate the Secretion of IL-6 and IL-8 and Cause Cytotoxicity to Human Bronchial Epithelial Cells (BEAS-2B). Health 5, 14-28. https://doi.org/10.4236/health.2013.510A2003

Rodriguez-Navarro, C., di Lorenzo, F., Elert, K., 2018. Mineralogy and physicochemical features of Saharan dust wet deposited in the Iberian Peninsula during an extreme red rain event. Atmos Chem Phys 18, 10089-10122. https://doi.org/10.5194/acp-18-10089-2018

Rodríguez, S., Alastuey, A., Alonso-Pérez, S., Querol, X., Cuevas, E., Abreu-Afonso, J., Viana, M., Pérez, N., Pandolfi, M., de la Rosa, J., 2011. Transport of desert dust mixed with North African industrial pollutants in the subtropical Saharan Air Layer. Atmos Chem Phys 11, 6663-6685. https://doi.org/10.5194/acp-11-6663-2011

Rosenfeld, D., Rudich, Y., Lahav, R., 2001. Desert dust suppressing precipitation: a possible desertification feedback loop. Proc Natl Acad Sci U S A 98, 5975-5980. https://doi.org/10.1073/pnas.101122798

Rothen-Rutishauser, B., Blank, F., Muhlfeld, C., Gehr, P., 2008. In vitro models of the human epithelial airway barrier to study the toxic potential of particulate matter. Expert Opin Drug Metab Toxicol 4, 1075-1089. https://doi.org/10.1517/17425255.4.8.1075

Russell, W.M.S., Burch, R.L. The Principles of Humane Experimental Technique. Methuen; 1959

Ryder, C.L., Highwood, E.J., Lai, T.M., Sodemann, H., Marsham, J.H., 2013a. Impact of atmospheric transport on the evolution of microphysical and optical properties of Saharan dust. Geophys Res Lett 40, 2433-2438. https://doi.org/10.1002/grl.50482

Ryder, C.L., Highwood, E.J., Rosenberg, P.D., Trembath, J., Brooke, J.K., Bart, M., Dean, A., Crosier, J., Dorsey, J., Brindley, H., Banks, J., Marsham, J.H., McQuaid, J.B., Sodemann, H., Washington, R., 2013b. Optical properties of Saharan dust aerosol and contribution from the coarse mode as measured during the Fennec 2011 aircraft campaign. Atmos Chem Phys 13, 303-325. https://doi.org/10.5194/acp-13-303-2013

Salahudeen, A.A., Choi, S.S., Rustagi, A., Zhu, J., van Unen, V., de la, O.S., Flynn, R.A., Margalef-Catala, M., Santos, A.J.M., Ju, J., Batish, A., Usui, T., Zheng, G.X.Y., Edwards, C.E., Wagar, L.E., Luca, V., Anchang, B., Nagendran, M., Nguyen, K., Hart, D.J., Terry, J.M., Belgrader, P., Ziraldo, S.B., Mikkelsen, T.S., Harbury, P.B., Glenn, J.S., Garcia, K.C., Davis, M.M., Baric, R.S., Sabatti, C., Amieva, M.R., Blish, C.A., Desai, T.J., Kuo, C.J., 2020. Progenitor identification and SARS-CoV-2 infection in human distal lung organoids. Nature 588, 670-675. https://doi.org/10.1038/s41586-020-3014-1

Sayan, M., Mossman, B.T., 2016. The NLRP3 inflammasome in pathogenic particle and fibre-associated lung inflammation and diseases. Part Fibre Toxicol 13, 51. https://doi.org/10.1186/s12989-016-0162-4

Schepanski, K., Tegen, I., Macke, A., 2009. Saharan dust transport and deposition towards the tropical northern Atlantic. Atmos Chem Phys 9, 1173-1189. https://doi.org/10.5194/acp-9-1173-2009

Schwertmann, U., 1991. Solubility and dissolution of iron oxides. Plant Soil 130, 1-25.

Scott, J.A., 1953. Fog and deaths in London, December 1952. Public Health Rep (1896) 68, 474-479.

Shi, J., Zhao, Y., Wang, K., Shi, X., Wang, Y., Huang, H., Zhuang, Y., Cai, T., Wang, F., Shao, F., 2015. Cleavage of GSDMD by inflammatory caspases determines pyroptotic cell death. Nature 526, 660-665. https://doi.org/10.1038/nature15514

Shi, Z., Krom, M.D., Bonneville, S., Baker, A.R., Bristow, C., Drake, N., Mann, G., Carslaw, K., McQuaid, J.B., Jickells, T., Benning, L.G., 2011. Influence of chemical weathering and aging of iron oxides on the potential iron solubility of Saharan dust during simulated atmospheric processing. Global Biogeochem Cy 25, https://doi.org/10.1029/2010gb003837

Shimada, A., Miyake, K., Kenmotsu, Y., Ogihara, K., Naya, Y., Naota, M., Morita, T., Inoue, K., Takano, H., 2018. Pathological study of pulmonary toxicity induced by intratracheally instilled Asian sand dust (Kosa): effects of lowered serum zinc level on the toxicity. Folia Histochem Cytobiol 56, 38-48. https://doi.org/10.5603/FHC.a2018.0006

Stafoggia, M., Zauli-Sajani, S., Pey, J., Samoli, E., Alessandrini, E., Basagana, X., Cernigliaro, A., Chiusolo, M., Demaria, M., Diaz, J., Faustini, A., Katsouyanni, K., Kelessis, A.G., Linares, C., Marchesi, S., Medina, S., Pandolfi, P., Perez, N., Querol, X., Randi, G., Ranzi, A., Tobias, A., Forastiere, F., Group, M.-P.S., 2016. Desert Dust Outbreaks in Southern Europe: Contribution to Daily PM(1)(0) Concentrations and Short-Term Associations with Mortality and Hospital Admissions. Environ Health Perspect 124, 413-419. https://doi.org/10.1289/ehp.1409164

Stern, R.A., Mahmoudi, N., Buckee, C.O., Schartup, A.T., Koutrakis, P., Ferguson, S.T., Wolfson, J.M., Wofsy, S.C., Daube, B.C., Sunderland, E.M., 2021. The Microbiome of Size-Fractionated Airborne Particles from the Sahara Region. Environ Sci Technol 55, 1487-1496. https://doi.org/10.1021/acs.est.0c06332

Stucki, A.O., Stucki, J.D., Hall, S.R., Felder, M., Mermoud, Y., Schmid, R.A., Geiser, T., Guenat, O.T., 2015. A lung-on-a-chip array with an integrated bio-inspired respiration mechanism. Lab Chip 15, 1302-1310. https://doi.org/10.1039/c4lc01252f

Suggs, J.E., Madden, M.C., Friedman, M., Edgell, C.J., 1986. Prostacyclin expression by a continuous human cell line derived from vascular endothelium. Blood 68, 825-829. https://doi.org/10.1182/blood.V68.4.825.825

Sun, H., Shamy, M., Kluz, T., Munoz, A.B., Zhong, M., Laulicht, F., Alghamdi, M.A., Khoder, M.I., Chen, L.C., Costa, M., 2012. Gene expression profiling and pathway analysis of human bronchial epithelial cells exposed to airborne particulate matter collected from Saudi Arabia. Toxicol Appl Pharmacol 265, 147-157. https://doi.org/10.1016/j.taap.2012.10.008

Swap, R., Garstang, M., Greco, S., Talbot, R., Kallberg, P., 1992. Saharan dust in the Amazon Basin. Tellus B 44, 133-149. https://doi.org/10.1034/j.1600-0889.1992.t01-1-00005.x

Tam, W.W., Wong, T.W., Wong, A.H., Hui, D.S., 2012. Effect of dust storm events on daily emergency admissions for respiratory diseases. Respirology 17, 143-148. https://doi.org/10.1111/j.1440-1843.2011.02056.x

Tapp, E., Curry, A., Anfield, C., 1975. Letter: Sand pneumoconiosis in an egyptian mummy. Br Med J 2, 276. https://doi.org/10.1136/bmj.2.5965.276-b

Taylor, K., Foster, M.L., Law, J.M., Centeno, J.A., Fornero, E., Henderson, M.S., Trager, S.A., Stockelman, M.G., Dorman, D.C., 2013. Assessment of geographical variation in the respiratory toxicity of desert dust particles. Inhal Toxicol 25, 405-416. https://doi.org/10.3109/08958378.2013.797524

Tegen, I., Lacis, A.A., 1996. Modeling of particle size distribution and its influence on the radiative properties of mineral dust aerosol. J Geophys Res-Atmos 101, 19237-19244. https://doi.org/10.1029/95jd03610

Thalib, L., Al-Taiar, A., 2012. Dust storms and the risk of asthma admissions to hospitals in Kuwait. Sci Total Environ 433, 347-351. https://doi.org/10.1016/j.scitotenv.2012.06.082

Thornberry, N.A., Bull, H.G., Calaycay, J.R., Chapman, K.T., Howard, A.D., Kostura, M.J., Miller, D.K., Molineaux, S.M., Weidner, J.R., Aunins, J., et al., 1992. A novel heterodimeric cysteine protease

is required for interleukin-1 beta processing in monocytes. Nature 356, 768-774. https://doi.org/10.1038/356768a0

Troin, M., Vallet-Coulomb, C., Sylvestre, F., Piovano, E., 2010. Hydrological modelling of a closed lake (Laguna Mar Chiquita, Argentina) in the context of 20th century climatic changes. J Hydrol 393, 233-244. https://doi.org/10.1016/j.jhydrol.2010.08.019

United Nations Convention to Combat Desertification, 2023. Sand and dust storm frequency increasing in many world regions, UN warns. https://www.unccd.int/news-stories/press-releases/sand-and-dust-storm-frequency-increasing-many-world-regions-un-warns. Accessed: 16/11/2023

United States Occupational Safety and Health Administration. 1910.1053 - Respirable crystalline silica. https://www.osha.gov/laws-regs/regulations/standardnumber/1910/1910.1053. Accessed: 10/04/2023

Val, S., Liousse, C., Doumbia el, H.T., Galy-Lacaux, C., Cachier, H., Marchand, N., Badel, A., Gardrat, E., Sylvestre, A., Baeza-Squiban, A., 2013. Physico-chemical characterization of African urban aerosols (Bamako in Mali and Dakar in Senegal) and their toxic effects in human bronchial epithelial cells: description of a worrying situation. Part Fibre Toxicol 10, 10. https://doi.org/10.1186/1743-8977-10-10

Varshavsky, J.R., Rayasam, S.D.G., Sass, J.B., Axelrad, D.A., Cranor, C.F., Hattis, D., Hauser, R., Koman, P.D., Marquez, E.C., Morello-Frosch, R., Oksas, C., Patton, S., Robinson, J.F., Sathyanarayana, S., Shepard, P.M., Woodruff, T.J., 2023. Current practice and recommendations for advancing how human variability and susceptibility are considered in chemical risk assessment. Environ Health 21, 133. https://doi.org/10.1186/s12940-022-00940-1

Verma, D.K., Shaw, D.S., 2001. A comparison of international silica (α-quartz) calibration standards by Fourier transform–infrared spectrophotometry. Ann Occup Hyg 45, 429-435. https://doi.org/10.1093/annhyg/45.6.429

Visigalli, R., Rotoli, B.M., Ferrari, F., Di Lascia, M., Riccardi, B., Puccini, P., Dall'Asta, V., Barilli, A., 2022. Expression and Function of ABC Transporters in Human Alveolar Epithelial Cells. Biomolecules 12, https://doi.org/10.3390/biom12091260

Wang, Q., Zhuang, G., Huang, K., Liu, T., Lin, Y., Deng, C., Fu, Q., Fu, J.S., Chen, J., Zhang, W., Yiming, M., 2016. Evolution of particulate sulfate and nitrate along the Asian dust pathway: Secondary transformation and primary pollutants via long-range transport. Atmos Res 169, 86-95. https://doi.org/10.1016/j.atmosres.2015.09.013

Wang, Y., Puthussery, J.V., Yu, H., Verma, V., 2020b. Synergistic and antagonistic interactions among organic and metallic components of the ambient particulate matter (PM) for the cytotoxicity measured by Chinese hamster ovary cells. Sci Total Environ 736, 139511. https://doi.org/10.1016/j.scitotenv.2020.139511

Warner, S.J., Auger, K.R., Libby, P., 1987. Interleukin 1 induces interleukin 1. II. Recombinant human interleukin 1 induces interleukin 1 production by adult human vascular endothelial cells. J Immunol 139, 1911-1917. https://doi.org/10.4049/jimmunol.139.6.1911

Warren, H.S., Tompkins, R.G., Moldawer, L.L., Seok, J., Xu, W., Mindrinos, M.N., Maier, R.V., Xiao, W., Davis, R.W., 2015. Mice are not men. Proc Natl Acad Sci U S A 112, E345. https://doi.org/10.1073/pnas.1414857111

Washington, R., Todd, M., Middleton, N.J., Goudie, A.S., 2003. Dust-Storm Source Areas Determined by the Total Ozone Monitoring Spectrometer and Surface Observations. Ann Assoc Am Geogr 93, 297-313. https://doi.org/10.1111/1467-8306.9302003

Washington, R., Todd, M.C., Engelstaedter, S., Mbainayel, S., Mitchell, F., 2006. Dust and the low-level circulation over the Bodélé Depression, Chad: Observations from BoDEx 2005. J Geophys Res-Atmos 111, https://doi.org/10.1029/2005jd006502

Wehner, B., Wiedensohler, A., Tuch, T.M., Wu, Z.J., Hu, M., Slanina, J., Kiang, C.S., 2004. Variability of the aerosol number size distribution in Beijing, China: New particle formation, dust storms, and high continental background. Geophys Res Lett 31, https://doi.org/10.1029/2004gl021596

Wilfong, E.R., Lyles, M., Rietcheck, R.L., Arfsten, D.P., Boeckman, H.J., Johnson, E.W., Doyle, T.L., Chapman, G.D., 2011. The acute and long-term effects of Middle East sand particles on the rat airway following a single intratracheal instillation. J Toxicol Env Heal A 74, 1351-1365. https://doi.org/10.1080/15287394.2010.516239

Winijkul, E., Yan, F., Lu, Z., Streets, D.G., Bond, T.C., Zhao, Y., 2015. Size-resolved global emission inventory of primary particulate matter from energy-related combustion sources. Atmos Environ 107, 137-147. https://doi.org/10.1016/j.atmosenv.2015.02.037

Winter, M., Beer, H.D., Hornung, V., Kramer, U., Schins, R.P., Forster, I., 2011. Activation of the inflammasome by amorphous silica and TiO2 nanoparticles in murine dendritic cells. Nanotoxicology 5, 326-340. https://doi.org/10.3109/17435390.2010.506957

Wu, J., Wang, Y., Liu, G., Jia, Y., Yang, J., Shi, J., Dong, J., Wei, J., Liu, X., 2017. Characterization of air-liquid interface culture of A549 alveolar epithelial cells. Braz J Med Biol Res 51, e6950. https://doi.org/10.1590/1414-431X20176950

Yanagisawa, R., Takano, H., Ichinose, T., Mizushima, K., Nishikawa, M., Mori, I., Inoue, K., Sadakane, K., Yoshikawa, T., 2007. Gene expression analysis of murine lungs following pulmonary exposure to Asian sand dust particles. Exp Biol Med 232, 1109-1118. https://doi.org/10.3181/0612-RM-311

Yeo, H.-G., Kim, J.-H., 2002. SPM and fungal spores in the ambient air of west Korea during the Asian dust (Yellow sand) period. Atmos Environ 36, 5437-5442. https://doi.org/10.1016/s1352-2310(02)00672-6

Yu, C.P., 1996. Extrapolation Modeling of Particle Deposition and Retention from Rats to Humans. Particul Sci Technol 14, 1-13. https://doi.org/10.1080/02726359608906682

Yu, H., Wei, J., Cheng, Y., Subedi, K., Verma, V., 2018. Synergistic and Antagonistic Interactions among the Particulate Matter Components in Generating Reactive Oxygen Species Based on the Dithiothreitol Assay. Environ Sci Technol 52, 2261-2270. https://doi.org/10.1021/acs.est.7b04261

Zauli Sajani, S., Miglio, R., Bonasoni, P., Cristofanelli, P., Marinoni, A., Sartini, C., Goldoni, C.A., De Girolamo, G., Lauriola, P., 2011. Saharan dust and daily mortality in Emilia-Romagna (Italy). Occup Environ Med 68, 446-451. https://doi.org/10.1136/oem.2010.058156

Zhang, X., Zhao, L., Tong, D., Wu, G., Dan, M., Teng, B., 2016a. A Systematic Review of Global Desert Dust and Associated Human Health Effects. Atmosphere-Basel 7, 158. https://doi.org/10.3390/atmos7120158

Zhou, R., Yazdi, A.S., Menu, P., Tschopp, J., 2011. A role for mitochondria in NLRP3 inflammasome activation. Nature 469, 221-225. https://doi.org/10.1038/nature09663

Zhu, Q., Kanneganti, T.D., 2017. Cutting Edge: Distinct Regulatory Mechanisms Control Proinflammatory Cytokines IL-18 and IL-1beta. J Immunol 198, 4210-4215. https://doi.org/10.4049/jimmunol.1700352

2 Inhalable Saharan dust induces oxidative stress, NLRP3 inflammasome activation, and inflammatory cytokine release

Gerrit Bredeck,[a] Mathias Busch,[a] Andrea Rossi,[a] Burkhard Stahlmecke,[b] Khanneh Wadinga Fomba,[c] Hartmut Herrmann,[c] Roel P. F. Schins[a]

[a]*IUF – Leibniz Research Institute for Environmental Medicine, Düsseldorf, Germany*

[b]*Institut für Umwelt & Energie, Technik & Analytik e.V. (IUTA), formerly: Institute for Energy and Environmental Technology e.V., Duisburg, Germany*

[c]*Atmospheric Chemistry Department (ACD), Leibniz-Institute for Tropospheric Research (TROPOS), Leipzig, Germany*

Environment International 172 (2023) 107732

Doi: 10.1016/j.envint.2023.107732

Author contribution: The author of this thesis planned and performed the characterization for hydroxyl radical formation and endotoxin content as well as *in vitro* experiments, prepared the graphs, interpreted and discussed the results, and wrote the manuscript. Relative contribution: about 75%.

Environment International 172 (2023) 107732

Contents lists available at ScienceDirect

Environment International

journal homepage: www.elsevier.com/locate/envint

Full length article

Inhalable Saharan dust induces oxidative stress, NLRP3 inflammasome activation, and inflammatory cytokine release

Gerrit Bredeck [a], Mathias Busch [a], Andrea Rossi [a], Burkhard Stahlmecke [b], Khanneh Wadinga Fomba [c], Hartmut Herrmann [c], Roel P.F. Schins [a,*]

[a] IUF – Leibniz Research Institute for Environmental Medicine, Düsseldorf, Germany
[b] Institute for Energy and Environmental Technology e.V. (IUTA), Duisburg, Germany
[c] Atmospheric Chemistry Department (ACD), Leibniz-Institute for Tropospheric Research (TROPOS), Leipzig, Germany

ARTICLE INFO

Handling Editor: Adrian Covaci

Keywords:
African dust
Hazard
Lung inflammation
Alveolar epithelium
Lung disease
Crystalline silica

ABSTRACT

Desert dust is increasingly recognized as a major air pollutant affecting respiratory health. Since desert dust exposure cannot be regulated, the hazardousness of its components must be understood to enable health risk mitigation strategies. Saharan dust (SD) comprises about half of the global desert dust and contains quartz, a toxic mineral dust that is known to cause severe lung diseases via oxidative stress and activation of the NLRP3 inflammasome-interleukin-1β pathway. We aimed to assess the physicochemical and microbial characteristics of SD responsible for toxic effects. Also, we studied the oxidative and pro-inflammatory potential of SD in alveolar epithelial cells and the activation of the NLRP3 inflammasome in macrophage-like cells in comparison to quartz dusts and synthetic amorphous silica (SAS).

Characterization revealed that SD contained Fe, Al, trace metals, sulfate, diatomaceous earth, and endotoxin and had the capacity to generate hydroxyl radicals. We exposed A549 lung epithelial cells and wild-type and *NLRP3*$^{-/-}$ THP-1 macrophage-like cells to SD, three well-investigated quartz dusts, and SAS. SD induced oxidative stress in A549 cells after 24 h more potently than the quartz dusts. The quartz dusts and SAS upregulated *interleukin 8* expression after 4 h and 24 h while SD only caused a transient upregulation. SD, the quartz dusts, and SAS induced interleukin-1β release from wild-type THP-1 cells>20-fold stronger than from *NLRP3*$^{-/-}$ THP-1 cells. Interleukin-1β release was lower for SD, in which microbial components including endotoxin were heat-destructed.

In conclusion, microbial components in SD are pivotal for its toxicity. In the epithelium, the effects of SD contrasted with crystalline and amorphous silica in terms of potency and persistence. In macrophages, the strong involvement of the NLRP3 inflammasome emphasizes the acute and chronic health risks associated with desert dust exposure.

1. Introduction

As desert dust is increasingly considered a major global air pollutant, understanding its health hazards is crucial for risk assessment and mitigation. Desert dust exposure is not only relevant for people living in arid regions, but also for those living where the dust is transported by the wind, even on different continents (Chen et al., 2017). The hazardousness of desert dust exposure has been reported in numerous epidemiological studies that associated dust episodes with elevated mortalities on the next days (Diaz et al., 2012; Johnston et al., 2011; Kashima et al., 2016; Zhang et al., 2016a). As reviewed by Fussell and Kelly (2021), desert dust concentrations can obviously not be regulated, but instead, the consequential risk can be mitigated by avoiding exposure, especially considering susceptible individuals. In order to understand when exposure needs to be avoided, information is required on which components of desert dust are critical determinants of its toxicity, on when the concentration of these components is highest, and on the toxicological mechanisms that dust exposure triggers.

Desert dust has been reported to cause inflammation and oxidative stress in relation to biological components (He et al., 2010; Ichinose et al., 2005) and trace metals (He et al., 2019; Rodriguez-Cotto et al., 2013). He et al. (2010) suggested that the NACHT, LRR, and PYD

* Corresponding author at: IUF - Leibniz Research Institute for Environmental Medicine, Auf'm Hennekamp 50, 40225 Düsseldorf, Germany.
E-mail address: roel.schins@iuf-duesseldorf.de (R.P.F. Schins).

https://doi.org/10.1016/j.envint.2023.107732
Received 24 June 2022; Received in revised form 7 December 2022; Accepted 2 January 2023
Available online 11 January 2023

domains-containing protein 3 (NLRP3) inflammasome pathway might be involved in Asian dust-mediated lung eosinophilia.

Before the NLRP3 inflammasome is activated, the expression of NLRP3 and pro-interleukin (IL)-1β is increased in a first priming step (Bauernfeind et al., 2009). The priming step can be mediated by microbial danger signals such as lipopolysaccharide (LPS), the endotoxin from Gram-negative bacteria (Schroder et al., 2012). In a second step, the NLRP3 inflammasome is activated. Activation of the NLRP3 inflammasome in alveolar macrophages and the resulting persistent overproduction of the early pro-inflammatory cytokine interleukin (IL)-1β is a pivotal step in the quartz mediated induction of lung inflammation and fibrosis, i.e. silicosis (Cao et al., 2022; Cassel et al., 2008; Davis et al., 1998; Dostert et al., 2008). As extensively reviewed by Rabolli et al. (2016), quartz has been suggested to mediate inflammasome activation in several ways including oxidative stress and rupture of phagolysosomes following endocytosis. Upon assembly and activation of the NLRP3 inflammasome, pro-caspase-1 is cleaved to active caspase-1 which in turn cleaves pro-IL-1β to mature IL-1β (Agostini et al., 2004; Martinon et al., 2002). IL-1β is a potent acute inflammatory cytokine, that amongst others stimulates the transcription factor NF-κB leading to the expression of other pro-inflammatory cytokines, such as IL-6 and IL-8 (Bonizzi et al., 1997; Jobin et al., 1997; Parikh et al., 1997).

To date, only few studies have been conducted on the toxicity of Saharan dust (SD) (Middleton, 2017), although >50 % of worldwide desert dust is derived from Sahara. Val et al. (2013) tested dust collected in Bamako, Mali, on a dust storm day. However, their samples still contained an important background of urban pollutants. Studies with organic extracts from SD sampled in Puerto Rico have shown that toxicity was driven by trace metals, including Fe (Rodriguez-Cotto et al., 2013), and endotoxin (Ortiz-Martinez et al., 2015) as well as other not yet identified components (Rodriguez-Cotto et al., 2015). From these studies, it remains unclear how endotoxin and trace metals behave in combination with the insoluble SD particles and to what extent the insoluble SD particles *per se* contribute to toxicity. Inferring SD toxicity from samples from other deserts is of limited reliability because different potencies have been reported depending on the source region (Ghio et al., 2014; He et al., 2013; Taylor et al., 2013).

In this study, we investigated the pulmonary toxicity of SD collected on the Cape Verde islands. We performed physicochemical and biological characterization of SD and compared the effects of SD to three well-studied quartz dusts as well as to synthetic amorphous silica (SAS) in order to find out which components and properties can contribute to its toxic effects. Relevant mechanisms of toxicity in the alveolar epithelium are the induction of oxidative stress and the expression and secretion of pro-inflammatory cytokines (Becker et al., 2005; Lag et al., 2018; Wessels et al., 2010). To investigate these mechanisms, we used the by far most widely applied *in vitro* model for the alveolar epithelium, the A549 cell line (Papazian et al., 2016) (Fig. 1). A549 cells represent the surfactant-producing alveolar type II cells (Lieber et al., 1976). Additionally, as introduced above, the activation of the NLRP3 inflammasome in alveolar macrophages is of high clinical relevance. A widely utilized *in vitro* model for human macrophages are phorbol 12-myristate-13-acetate (PMA)-differentiated THP-1 cells (Cappellini et al., 2020; Kampfer et al., 2017; Meldrum et al., 2022). Using differentiated THP-1 cells, we sought to assess the involvement of the NLRP3 inflammasome activation in SD-mediated pro-inflammatory capacity (Fig. 1). Therefore, in addition to wild-type (WT) THP-1 cells, we generated *NLRP3*$^{-/-}$ THP-1 cells via CRISPR/Cas9 gene editing.

2. Materials & methods

2.1. Investigated Saharan dust, quartz dusts, and synthetic amorphous silica nanoparticles

The Saharan dust sample was collected on the top of the Cape Verde Atmospheric Observatory's 30 m high tower, to reduce the influence of local coastal sea salt, using a stainless steel PM_{10} Hurricane Cyclone (Advanced Cyclone Systems, Portugal). The sampling period lasted for the entire period of a Saharan dust event from December 29th, 2016 to January 6th, 2017. The cyclone was operated at a flow rate of 200 m^3/h at 25 °C with a median volume diameter of the particles of<5 μm. The dust was deposited into a Teflon hopper at the bottom of the cyclone, transferred into glass bottles, preserved, and transported at −20 °C for

Table 1
Origin and particle size characterization of reference silica samples.

Reference sample	Originally obtained from	Reference for particle size analysis
DQ12	Dörentrup Quarz, Germany	Verma and Shaw (2001)
Min-U-Sil 5	US Silica, Berkely Springs, WV, USA	Verma and Shaw (2001)
Sikron F600	Quarzwerke Frechen, Germany	Verma and Shaw (2001)
SAS	Sigma-Aldrich	Bredeck et al. (2021)

SAS: synthetic amorphous silica.

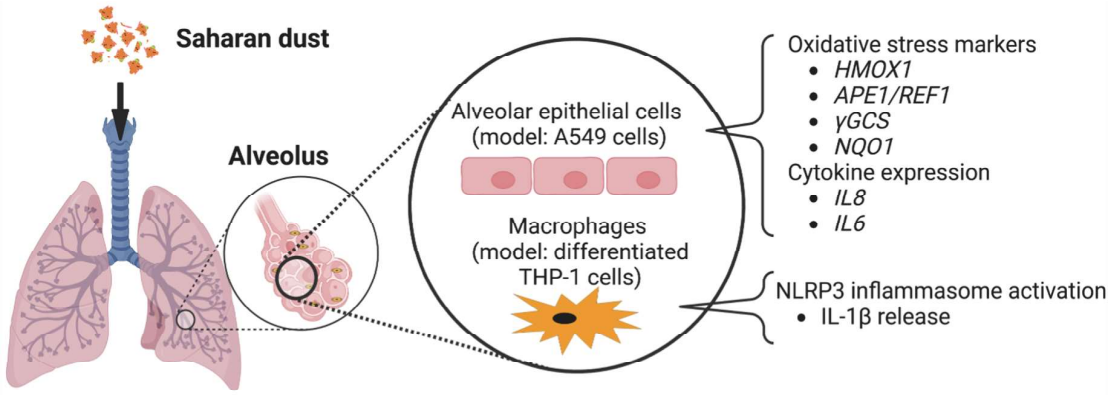

Fig. 1. Overview of the study. Upon inhalation, Saharan dust can be transported deep into the lung, into the alveoli. In the alveoli, inhaled Saharan dust can get into contact with alveolar epithelial cells and macrophages. As a model for alveolar epithelial cells, A549 cells were used. Using A549 cells, the induction of the oxidative stress marker genes *heme-oxygenase 1 (HMOX1)*, *apurinic-apyrimidinic endonuclease 1/redox factor 1 (APE1/REF1)*, *γ-glutamylcysteine synthetase (γGCS)*, and *NAD(P)H quinone dehydrogenase 1 (NQO1)* as well as the cytokines interleukin (*IL*) *6* and *IL8* were measured. As a model for macrophages, differentiated THP-1 cells were used. Using differentiated THP-1 cells, the activation of the NLRP3 inflammasome and the secretion of its major downstream cytokine IL-1β was assessed. Created with BioRender.com.

further analysis.

The three quartz dusts, i.e. DQ12, Min-U-Sil 5, and F600, and SAS nanoparticles (NPs) listed in Table 1 were used as reference silica samples. The different quartz samples were included to cover three quartz dusts typically used in particle toxicology studies and thus to facilitate comparisons. From size distribution analyses it is known that > 45 vol% of each quartz dust's particles are smaller than 2.5 μm and > 90 vol% are smaller than 10 μm with particle sizes F600 > DQ12 > Min-U-Sil 5 (Verma and Shaw, 2001). To assess the influence of biological components such as endotoxin, SD and DQ12 quartz were heat-inactivated at 220 °C overnight, hereinafter referred to as baked SD and baked DQ12. SAS was purchased from Sigma-Aldrich (#S5130).

2.2. Characterization of dusts and particle samples

2.2.1. Scanning electron microscopy

To analyze the composition, including agglomerate size distribution (including single particles, if present) and elemental composition of SD, high resolution scanning electron microscopy (SEM, Tescan CLARA RISE, Tescan GmbH, Dortmund, Germany) in conjunction with energy dispersive x-ray analysis (EDX, EDAX Octane Elect detector, AMETEK GmbH, Wiesbaden, Germany) was applied. For the analysis of the microscopic composition, dry SD was transferred onto a stub with a conductive carbon tap. Images were obtained at nominal magnifications of 0.1–10 kx. Droplets of sonicated SD suspensions were dried on single-crystalline Si or GaAs wafer pieces for size distribution or EDX analysis, respectively. To account for the broad range of agglomerate sizes, the images for size distribution analysis were obtained at a nominal magnification of 1.0 kx with a resolution of 4048 × 3790 pixels (pixel size: 31.0 nm) allowing an unbiased assessment of particles with highly differing sizes. The area equivalent diameter, based on $Feret_{max}$ and $Feret_{min}$ diameters obtained on single particles present in the suspension, was manually assessed for 500 particles using ImageJ (version 1.51f, https://imagej.nih.gov/ij). A particle within the suspension can consist of smaller (primary) particles that agglomerated to a bigger compact particle which is considered to be relevant for exposure. Thus, not the primary particle size distribution was assessed but the agglomerate size distribution. The chemical composition of SD was qualitatively assessed by EDX mappings of particle agglomerates.

2.2.2. Total reflection X-ray fluorescence

The elemental composition of SD was analyzed using the Total reflection X-Ray Fluorescence (TXRF) technique operated with a molybdenum X-ray source (S2-PICOFOX, Bruker Germany). For the analysis, 17.4 mg SD were transferred to a 10 mL digestion bomb. A volume of 1.5 mL of concentrated HCl and HNO_3 (1:3) was added. The mixture was microwave digested (MARS 6, CEM GmbH, Kamp-Lintfort, Germany) at 180 °C and high pressure for 2 h to provide a homogenous solution. After cooling to room temperature, 10 μL of the solution was placed on a TXRF quartz carrier, spiked with a Ga/Y internal standard, allowed to evaporate on a heating plate for 10 min at 80 °C, and measured. Due to low sensitivity, elements of the first two periods in the periodic table of elements could not be analyzed. Al and Si could not be analyzed because the concentrated HCl and HNO_3 (1:3) was unable to digest the aluminosilicate content of samples. Further details about the method can be found in the literature (Fomba et al., 2020).

2.2.3. Ion chromatography

Water-soluble ions were analyzed using ion chromatography technique (ICS3000, Dionex, USA) equipped with automatic eluent generation (KOH for anions and methane sulfonic acid (MSA) for cations) and a micro-membrane removal unit. For these analyses, 60 mg of SD was added to 50 mL of deionized H_2O (dH_2O) and shaken for 2 h. The extract was filtered through a 0.45 μm unidirectional syringe filter to remove insoluble particulate matter, and thereafter aliquots of 50 μL of the filtrate was analyzed. Further details can be found in the literature (Fomba et al., 2014; van Pinxteren et al., 2016).

2.2.4. Quantification of organic and elemental carbon

Organic carbon (OC) and elemental carbon (EC) were analyzed using a two-step thermo-optical method with the help of a C-Mat 5500 carbon analyzer (Ströhlein, Germany) according to the VDI 2465 part 2 protocol. A total of 68 mg of the SD sample was thermally desorbed at 650 °C in an N_2 atmosphere for the quantification of OC. Subsequently, it was heated at 850 °C in an oxidizing O_2 atmosphere for the quantification of EC. All the desorbed carbonaceous compounds were oxidized to CO_2 that was measured by a non-dispersive infrared detector (NDIR). More details can be found in the literature (Spindler et al., 2013).

2.2.5. Electron paramagnetic resonance spectroscopy

The objective of electron paramagnetic resonance (EPR) spectroscopy was to measure the ability of SD, the quartz dusts, and SAS to generate hydroxyl radicals (·OH) in the presence of hydrogen peroxide. The samples were suspended in dH_2O and sonicated for 10 min using a Branson Sonifier 450 at a duty cycle of 0.2 s and an output of 240 W. The suspension (final concentration 2.5 mg/mL) was mixed with hydrogen peroxide (125 mM) (Sigma-Aldrich/Merck) and the spin trap 5,5-Dimethyl-1-Pyrroline-N-Oxide (DMPO) (25 mM) (Cayman Chemical). As a negative control, dH_2O was used. The mixture was shaken at 37 °C in the dark for 15 min and was subsequently passed through a 0.1 μm PES syringe filter (Neolab, Germany). The filtrate was drawn into a 50 μL capillary and transferred to a Miniscope MS 200 EPR spectrometer (Magnettech, Germany). The following measurement settings were applied: Sweep: 100 G, Sweep time: 30 s, number of scans: 3. For quantification, the mean amplitude of the DMPO-OH quartet was calculated.

2.2.6. Endotoxin quantification assay

To determine the concentration of endotoxin in SD, the quartz dusts, and SAS, the Limulus amebocyte lysate (LAL) test based Pierce™ Chromogenic Endotoxin Quant Kit (Thermo Fisher Scientific) was used according to the manufacturer's instructions. For the assay, samples were suspended to 4 mg/mL and sonicated as described above. The concentration was adjusted to 50 μg/mL with endotoxin-free H_2O. An endotoxin standard curve ranging from 0.01 to 0.1 endotoxin units (EU)/mL was performed. For validation purposes, suspensions spiked with endotoxin were tested in parallel.

2.3. Generation of *NLRP3*$^{-/-}$ THP-1 cells

NLRP3$^{-/-}$ THP-1 cells were generated as previously described (Ramachandran et al., 2021). Briefly, gRNAs were designed using the CRISPR design tool CHOPCHOP (https://chopchop.cbu.uib.no/) and cloned into a modified PX458 plasmid (Addgene #48138). The resulting bicistronic vector encoded the respective gRNA, Cas9 nuclease, and a GFP selection marker. gRNA efficiency was assessed using High-Resolution Melt Analysis (HRMA). An efficient gRNA targeting *NLRP3* exon 2 (5′-GCTAATGATCGACTTCAATG-3′) was chosen for further experiments (HRMA primers: forward 5′-CAGACCATGTGGATCTAGCC-3′, reverse 5′-TGTTGATCGCAGCGAAGAT-3′). THP-1 cells were electroporated using a Neon transfection system (Thermo Fisher Scientific) according to the manufacturer's instructions. After 48 h, cells were FACS sorted and plated as single cells into 96-well plates. Cells were duplicated into maintenance and lysis plates after a week. Clones were then lysed with proteinase K and genotyped by PCR followed by deep sequencing using a miSeq Illumina sequencer and a V2 Nano cassette. Generating our own THP-1 *NLRP3*$^{-/-}$ cells enabled us to better control this model cell line and offers us the opportunity to further modify the cell line. We validated the model in a previous study (Busch et al., 2022).

2.4. Cell culture procedures

A549 (American Type Culture Collection) cells were cultured in RPMI-1640 (containing L-glutamine) (Thermo Fisher Scientific) substituted with 10 % fetal calf serum (FCS) (Sigma-Aldrich/Merck) and 1 % Penicillin/Streptomycin (P/S) (Sigma-Aldrich/Merck). Cells were regularly detached with trypsin (Sigma-Aldrich/Merck) and sub-cultured upon reaching about 80 % confluence every three to four days. THP-1 (ATCC, TIB-202) cells were cultured in RPMI-1640 (containing L-glutamine and 25 mM HEPES) (Thermo Fisher Scientific) substituted with 10 % FCS, 1 % P/S, 1 mM sodium pyruvate (Thermo Fisher Scientific), 0.7 % D-glucose (Sigma-Aldrich/Merck) and 50 nM 2-mercaptoethanol (ME) (Thermo Fisher Scientific). THP-1 cells were maintained at densities between $2*10^5$ and $8*10^5$ cells/mL.

2.5. Analysis of in vitro toxicity of dust and particle samples

2.5.1. Exposure procedure

A549 cells were used at passages 2–20 after thawing. A total of $2*10^4$ cells in 0.1 mL or $1.2*10^5$ cells in 1.0 mL per well were seeded in 96-well plates or 24-well plates, respectively. After 24 h, the medium was changed to RPMI-1640 (containing L-glutamine) substituted with 1 % FCS and 1 % P/S, hereinafter A549 exposure medium. Again 24 h later, exposure was started.

A total of $3*10^6$ THP-1 cells at passages 5–15 after thawing were differentiated with 100 nM PMA (Sigma-Aldrich/Merck) in 25 cm^2 flasks for 24 h. Subsequently, the differentiated cells were detached with accutase (Sigma-Aldrich/Merck) and $1.2*10^5$ cells in 1.0 mL per well were seeded in 24-well plates using THP-1 cell culture medium without ME. Following reattachment for 1 h, exposure was started using RPMI-1640 (containing L-glutamine and 25 mM HEPES) substituted with 1 % FCS, 1 % P/S, 1 mM sodium pyruvate, and 0.7 % D-glucose, hereinafter THP-1 exposure medium.

Dust and particle samples were suspended in A549 or THP-1 exposure medium to 4 mg/mL. The suspensions were sonicated as described above (see 2.2.5) and diluted in exposure medium to the desired concentrations. For controls, the amount of sonicated exposure medium was adjusted to correspond to the highest exposure concentration. A549 cells were exposed for 4 h or 24 h. THP-1 cells were exposed for 24 h. To minimize interferences of SD with RNA isolation, LDH assay, and ELISAs caused by the binding of biomolecules to the surface of SD, bovine serum albumin (BSA) (Sigma-Aldrich/Merck) was added 30 min before the end of incubation time. We used 47 % BSA in Hank's Balanced Salt Solution containing $MgCl_2$ and $CaCl_2$ (HBSS) (Thermo Fisher Scientific). Per well that contained 1000 µL of cell culture medium, 333 µL of 47 % BSA was added resulting in 12 % BSA. When LDH assay, gene expression analyses, or ELISAs were performed, two controls were used: one control with adding BSA for SD and bSD and one control without adding BSA for the other exposure groups. For the measurement of cytokine expression and release, LPS (Sigma-Aldrich/Merck) was used as positive control.

2.5.2. WST-1 cell viability assay

In A549 cells, viability was assessed via the water soluble tetrazolium (WST)-1 assay after 24 h of exposure to SD or DQ12 at concentrations between 0 and 200 µg/cm^2 using a 96-well-plate format. The assay was performed as described by Kolling et al. (2020) and based on the nanOxiMet project's SOP "Cellular viability – WST-1 assay" (https://nanopartikel.info/data/projekte/nanOxiMet/SOP/nanOxiMet_SOP_WST-1-assay_V2.pdf). WST-1 reagent (Sigma-Aldrich/Merck) was added to the cells at a dilution of 1:5 in exposure medium and the absorbances at 450 nm and 630 nm were measured after incubation for 1 h.

2.5.3. LDH cytotoxicity assay

In parallel to the gene expression or cytokine secretion experiments in A549 and THP-1 cells, cytotoxicity was assessed via LDH assay after 4 h and 24 h of exposure. Following exposure, 50 µL of supernatant was transferred to 96-well plates and the assay was performed as described previously (Busch et al., 2021). The LDH reaction was stopped with H_2SO_4 (Roth) after 16 min or 10 min for A549 cells or THP-1 cells, respectively. β-nicotinamide adenine dinucleotide sodium salt, lithium L-lactate, phenazine methosulfate, and iodonitrotetrazolium chloride were purchased from Sigma-Aldrich/Merck.

2.5.4. Gene expression analysis

The expressions of *IL6*, *IL8*, *heme oxygenase (HMOX) 1*, *apurinic-apyrimidinic endonuclease 1/redox factor 1 (APE1/REF1)*, *γ-glutamylcysteine synthetase (γGCS)*, and *NAD(P)H quinone dehydrogenase 1 (NQO1)* in A549 cells were assessed using a 24–well plate format. Following exposure, A549 cells were washed with phosphate-buffered saline (PBS) (Sigma-Aldrich/Merck) twice. PBS was discarded, 0.5 mL TRIzol reagent (Thermo Fisher Scientific) was added and the mixture was frozen at −80 °C until further processing. For complete homogenization, the mixture was vigorously shaken for 10 min. A volume of 100 µL ice-cold $CHCl_3$ (Sigma-Aldrich/Merck) was added, the mixture was vortexed, incubated at room temperature for 10 min, and centrifuged at 4 °C and 12,000 g for 15 min. Approximately 200 µL of the upper aqueous phase was transferred to a fresh vial and 250 µL 2-propanol (Sigma-Aldrich/Merck) was added. The mixture was vortexed, incubated at room temperature for 10 min, and centrifuged at 4 °C and 12,000 g for 15 min. The supernatant was discarded, 1.0 mL 75 % ethanol (Roth) in nuclease-free H_2O (Qiagen) was added, and the vial was vortexed and centrifuged at 4 °C and 12,000 g for 5 min. The supernatant was discarded and after drying, the pellet was resuspended in 30 µL nuclease-free H_2O.

Besides the adaptions mentioned below, RNA quantification, DNase I digestion, reverse transcription, and quantitative PCR (qPCR) were performed as described previously (Kampfer et al., 2021). Briefly, the optical density of RNA was measured at 260 nm and 280 nm to determine the concentration. A total of 0.75 µg RNA per sample was treated with amplification grade DNase I (Sigma-Aldrich/Merck). Of this RNA, 0.5 µg was reversely transcribed using the iScript™ cDNA synthesis kit (Bio-Rad). A no reverse transcriptase control (nRTc) with 0.25 µg RNA was performed in parallel to control for residual DNA. The cDNA and nRTc were diluted in nuclease-free H_2O by factors 15 and 7.5, respectively. When less RNA was available, the amount of RNA and the dilution factors were decreased proportionally. The primers (Eurofins) listed in Table S1 and the iQ™ SYBR® Green Supermix (Bio-Rad) were used. *β-ACTIN* was analyzed as reference gene. The qPCR was run for 40 cycles on a MyiQ™ cycler (Bio-Rad) or a QuantStudio™ 3 device (Thermo Fisher Scientific). C_T values were determined using the Bio-Rad iQ5 software (v2.1) or QuantStudio™ Design & Analysis Software and corrected for primer efficiencies. Exposure-dependent changes in the gene expression were calculated using the $\Delta\Delta C_T$ method (Livak and Schmittgen, 2001).

2.5.5. Cytokine quantification by enzyme-linked immune-sorbent assay (ELISA)

The releases of IL-6 and IL-8 from A549 cells and the releases of IL-1β and IL-8 from THP-1 cells into the supernatant were analyzed using R&D systems DuoSet ELISA kits as described previously (Busch et al., 2021). Briefly, high-protein-binding 96-well plates were coated with primary antibody, blocked with BSA, and incubated with 100 µL sample. Consecutively, detection antibody, horseradish peroxidase, and Bio-Rad TMP Peroxidase EIA Substrate were incubated. The color reaction was stopped with H_2SO_4 and absorbance was measured at 450 nm and 540 nm. The standard curve was plotted using a four-parameter log fit. In case the measured concentrations were below the limit of detection (LOD), half the LODs, i.e. 1.95 pg/mL for IL-1β and 15.63 pg/mL for IL-8, were used for calculations and statistics (Hornung and Reed, 1990).

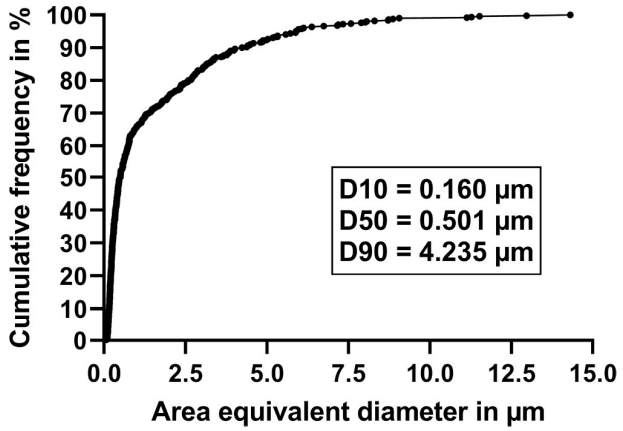

Fig. 2. Cumulative agglomerate size distribution of Saharan dust. A Saharan dust suspension in dH_2O was sonicated and pipetted onto a single-crystalline silicon wafer. After drying, images were obtained at a nominal magnification of 1 kx (pixel size: 31 nm). For 500 agglomerates, the area equivalent diameter was determined based on $Feret_{max}$ and $Ferret_{min}$ diameters.

2.6. Statistical analysis

Microsoft Excel was used to calculate ΔC_T values, $\Delta\Delta C_T$ values, fold changes, mean values, and standard deviations from at least three independent experiments. For the gene expression analyses, ΔC_T values were used for statistics. Mean values and standard deviations were calculated from $\Delta\Delta C_T$ values and subsequently converted into fold changes. GraphPad Prism version 9 was used for visualization of means ± standard deviation. To test statistical significance for EPR spectroscopy data, a one-way ANOVA with Tukey's post hoc test was calculated using GraphPad Prism. To test correlation, GraphPad Prism was used. To test the statistical significance of cytotoxicity analyses in A549 cells, mixed effect models with Dunnett's post hoc test were applied in R version 4. For gene expression analyses, ELISA experiments, and LDH release, mixed effect models with Šídák's post hoc test were applied in R. In the mixed effect models, exposure and, where applicable, genotype were applied as fixed factors. The experimental run was applied as random factor. To address a potential synergistic effect, the interaction factor in a mixed effects model was tested. *p*-values of < 0.05 were considered statistically significant.

3. Results

3.1. Characterization of Saharan dust

3.1.1. Size distribution

To analyze the size distribution and aspect ratio of SD, we applied scanning electron microscopy (SEM). The agglomerate size within the applied suspension was log-normally distributed with a mode diameter of approximately 200 nm and a variance of $\sigma = 1.93$. Based on the area equivalent diameter, 50 % of the agglomerates were smaller than 0.5 µm and over 90 % were smaller than 5 µm (Fig. 2, Fig. S1A,B). In addition, the number of agglomerates with a size < 100 nm is expected to be even higher as such small agglomerates could not reliably be identified. A mean aspect ratio of smaller than 2 indicated a rather compact shape of the agglomerates.

3.1.2. Composition

The composition of SD was analyzed by SEM, SEM coupled to EDX, TXRF, ion chromatography, and thermal desorption techniques. Using SEM, SD was found as diverse in its shape and structure (Fig. S1C-H). The depicted images must cautiously be considered only as exemplary because no image can be representative of SD as a complex mixture. Further, using SEM, diatomaceous earth was identified as a composite (Figure S2). According to SEM coupled to EDX, O, Si, and Al were the most abundant elements found in all agglomerates (Fig. 3). C was also found to be abundant but could not be mapped to the particles and may be a residue from sample preparation may have been deposited on the samples during SEM observation. Fe, Ca, S, and Ti were found in isolated particles. Using TXRF and ion chromatography, we could confirm the content of Fe, Ca, and S, the latter in the form of sulfate (Table 2). Al and Si could not be reliably analyzed by TXRF because of poor solubility of aluminosilicates during sample preparation. Additionally, we found traces of many other metals (Table S2). Applying thermal desorption, we found that carbon was only present in low amounts of < 1 % and mainly in the form of organic compounds (Table 2).

3.1.3. Hydroxyl radical formation

To assess SD in comparison to the investigated quartz dusts and SAS regarding the capacity to generate hydroxyl radicals, EPR spectroscopy was performed with DMPO as spin trap. For SD and all quartz dusts, the characteristic spectrum for hydroxyl radical-DMPO adducts of amplitudes in the ratio 1:2:2:1 was obtained (Fig. 4A). The hydroxyl radical formation of SD was higher than of DQ12 and Min-U-Sil 5 but lower than of F600 (Fig. 4B). Baking of SD had little impact on its capacity to generate hydroxyl radicals, whereas baked DQ12 generated more hydroxyl radicals than pristine DQ12. SAS showed no capacity to generate hydroxyl radicals.

3.1.4. Endotoxin content

We analyzed the endotoxin content of SD, the quartz dusts, and SAS using the LAL test. Only SD but none of the quartz dusts or SAS contained a detectable amount of endotoxin (Table 3). No endotoxin was detected in baked SD either.

3.1.5. Interferences with LDH and ELISA assays

The interferences of SD, quartz dusts, and SAS with the LDH assay, IL-1β ELISA, and IL-8 ELISA through adsorption of the analyzed proteins on the particles' surfaces were tested in spiking experiments (Figure S3). For SD, we had already been aware of the interferences from preliminary experiments. To minimize the interferences, 33 % BSA solution (47 % in HBSS) was added to SD samples and to additional control samples 30 min before collecting supernatants. For the LDH assay, merely a slight decrease in recovery was observed for SAS. For the IL-1β ELISA, the recovery was decreased for SD only. At the tested concentration of 50 µg/cm^2, the interference was still low. For the IL-8 ELISA, we observed a 20-fold decreased recovery when spiking with 50 µg/cm^2 SD. Spiking with 50 µg/cm^2 SAS reduced the recovery of IL-8 less strongly by about 30 %.

3.2. Cytotoxicity

SD but not DQ12 was identified as cytotoxic towards A549 cells using the WST-1 assay (Fig. 5). While there was no effect at 12.5 µg/cm^2, exposure to 50 µg/cm^2 SD slightly decreased the viability by approximately 10 %. Exposure to 200 µg/cm^2 SD reduced the viability by approximately 40 %. There was no difference between pristine and baked SD. Based on the low cytotoxicity and the quartz concentrations used by us and others in previous *in vitro* studies (Cassel et al., 2008; Schins et al., 2002; Skuland et al., 2020; van Berlo et al., 2010), the following experiments were performed at 50 µg/cm^2.

3.3. Oxidative stress in A549 cells

To analyze oxidative stress, the mRNA expression of the marker genes *HMOX1*, *APE1/REF1*, *γGCS*, and *NQO1* was assessed in A549 cells following 4 h and 24 h of exposure to SD, quartz dusts, or SAS at concentrations of 50 µg/cm^2 (Fig. 6). After 4 h, the only significant effect was the weak upregulation of *NQO1* upon exposure to SAS. After 24 h,

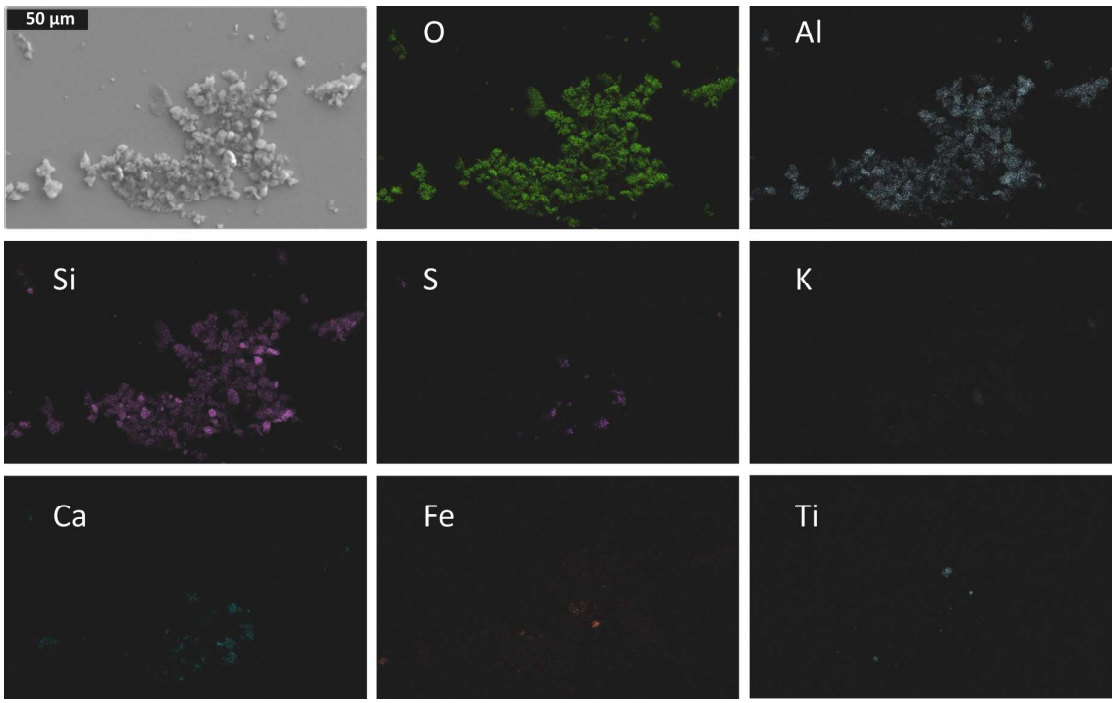

Fig. 3. Elemental composition of Saharan dust. The elemental composition of Saharan dust was analyzed by scanning electron microscopy coupled with energy dispersive X-ray analysis (EDX). A Saharan dust suspension in dH_2O was sonicated and pipetted onto a single crystalline GaAs wafer piece. After drying, an EDX mapping analysis was conducted on the frame shown in the top left panel (size: 512 × 340 pixel, approximate pixel size: 445 nm). The distribution of each of the nine most abundant elements, except C, is shown in the other eight panels. C was disregarded as it may be a residue from sample preparation or may have been deposited on the samples during SEM observation.

SD significantly upregulated *HMOX1* about 1.5- to 2-fold. The quartz dusts were weaker in their effects. Pristine DQ12 quartz did not influence *HMOX1* expression and for baked DQ12, the upregulation did not reach significance ($p = 0.080$), whereas Min-U-Sil 5 slightly but significantly augmented *HMOX1* expression 1.3-fold. The expression of *γGCS* was slightly downregulated upon exposure to pristine DQ12. SAS did not affect the oxidative stress marker genes. Thus, amongst the assessed samples, SD was the strongest inducer of oxidative stress at the 24 h time point. The effect of each dust and particle sample on the expression of *HMOX1* after 24 h was plotted against the amplitude in the EPR measurement (Fig. 6J). Only a weak non-significant correlation was found.

3.4. Expression and secretion of pro-inflammatory cytokines in A549 cells

To determine the pro-inflammatory effects of SD, quartz dusts, and SAS on A549 cells after 4 h and 24 h, the gene expressions and cytokine releases of IL-8 and IL-6 were analyzed in the same experiments performed for the oxidative stress assessment.

Only SD and baked SD upregulated the expressions of *IL8* and *IL6* after 4 h but not after 24 h (Fig. 7). The effects of SD were slightly stronger than of baked SD. The quartz dusts significantly upregulated *IL8*, but not *IL6* at both time points. At the 4 h time point, the potency of the quartz dusts was weaker than of SD. With fold changes > 30, SAS was the strongest inducer of *IL8* at both time points and of *IL6* after 24 h. After 4 h, SAS upregulated *IL6* expression 3.7-fold, less than SD.

Because of the assay interference described in 3.1.5, we refrained from interpreting IL-8 release for SD. For the quartz dusts and SAS, the extents of IL-8 release corresponded to the upregulations of *IL8* expression (Fig. S4A). All quartz dusts upregulated IL-8 release in a range between 5- and 13-fold in the order DQ12 > Min-U-Sil 5 > F600. SAS increased IL-8 release even more potently by about 100-fold, despite the interference with the assay. None of the exposures lifted IL-8 cytokine concentrations after 4 h and IL-6 cytokine concentrations above the limits of detection, i.e. 31.3 and 9.4 pg/mL, respectively (data not shown), which might be due to interferences with the ELISA.

In parallel, we assessed LDH release as a marker of cytotoxicity and cell membrane rupture (Fig. S4B,C). We found a 2-fold increase in LDH release upon 24 h exposure to SAS. Still, the correspondence between IL-8 release and *IL8* expression indicates that SAS-induced IL-8 release was not primarily a secondary effect of cytotoxicity-associated membrane rupture.

In summary, in the A549 cell model, SD and the quartz dusts did not cause oxidative stress at the early 4 h time point but at the later 24 h time point (Table 4). Conversely, SD induced pro-inflammatory cytokine expression only at the early time point. In contrast, the pro-inflammatory effects of the quartz dusts and SAS were persistent. After 24 h, conversely to the results from oxidative stress assessment, not SD but quartz and even more potently SAS induced pro-inflammatory

Table 2
Content of metals and ions > 1 mg/g and content of organic and elemental carbon in Saharan dust analyzed by total reflection X-ray fluorescence, ion chromatography, and thermographic thermal desorption techniques, respectively.

	Compound	Content in mg/g
Metals	K	7.8
	Ca	14.2
	Fe	37.2
Ions	Cl^-	44.4
	NO_3^-	6.8
	SO_4^{2-}	16.1
	Na^+	26.6
	K^+	1.5
	Mg^{2+}	2.1
	Ca^{2+}	8.0
Carbon	Organic Carbon	7.6
	Elemental Carbon	0.8

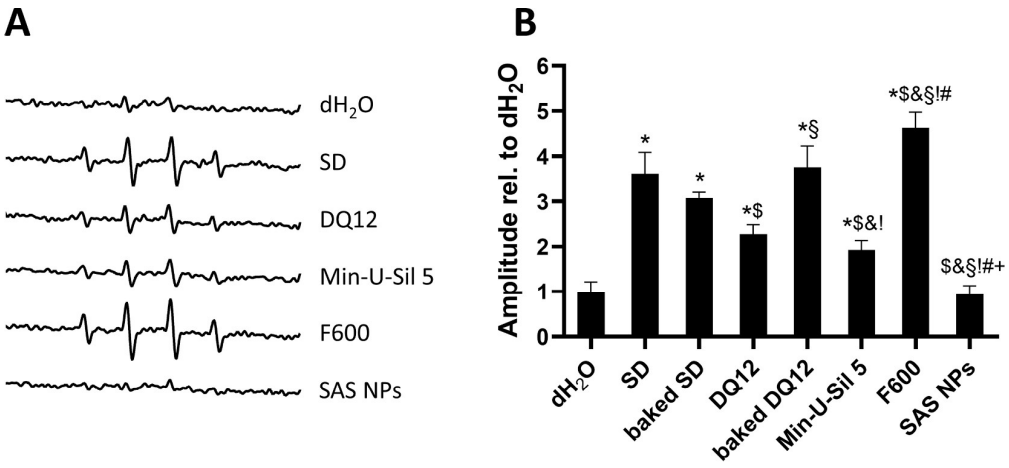

Fig. 4. Hydroxyl radical formation capacity. SD, quartz dusts, or SAS were mixed with hydrogen peroxide and the spin-trap DMPO. Electron paramagnetic resonance spectra were measured in three independent experiments. Representative spectra of pristine samples are shown in **A**. Amplitudes in the ratio 1:2:2:1 indicate hydroxyl radical formation. The amplitudes of pristine and baked samples relative to dH_2O were assessed as a measure of hydroxyl radical formation capacity (**B**). A one-way ANOVA with Tukey's post-hoc test was calculated (*$p \leq 0.05$ vs. dH_2O; $^{\$}p \leq 0.05$ vs. SD; $^{\&}p \leq 0.05$ vs. baked SD; $^{\S}p \leq 0.05$ vs. DQ12; $^{!}p \leq 0.05$ vs. baked DQ12; $^{\#}p \leq 0.05$ vs. Min-U-Sil 5; $^{+}p \leq 0.05$ vs. SAS NPs).

signals in A549 cells.

3.5. NLRP3 inflammasome activation in THP-1 cells

As a model for macrophages, we used PMA-differentiated THP-1 WT and *NLRP3*$^{-/-}$ cells. During initial model development (also published previously in Busch et al. (2022)) we assessed IL-1β and IL-8 concentrations in unexposed cells versus cells exposed to 10 ng/mL LPS to test the functionality of the model. Only WT but not *NLRP3*$^{-/-}$ cells constitutively released IL-1β and IL-8 (Figure S5). Exposure to LPS strongly induced IL-8 release from both WT and *NLRP3*$^{-/-}$ cells, showing the capability of *NLRP3*$^{-/-}$ cells to release cytokines not directly associated with the NLRP3 inflammasome pathway.

Table 3
Endotoxin content of pristine and baked SD and DQ12 and of Min-U-Sil 5, F600, and SAS.

Sample	EU/mg
SD	0.46
Baked SD	n.d.
DQ12	n.d.
Baked DQ12	n.d.
Min-U-Sil 5	n.d.
F600	n.d.
SAS	n.d.

n.d.: not detected.

We used the WT and *NLRP3*$^{-/-}$ THP-1 cells to address the pro-inflammatory potential of SD in comparison to the quartz dusts and SAS. Simultaneously, we evaluated the dependence of the pro-inflammatory potential on microbial components and the NLRP3 inflammasome. Therefore, we studied IL-1β and IL-8 release after 24 h of exposure to 50 μg/cm^2 of pristine and baked samples as well as IL-1β release after 24 h of exposure to 50 μg/cm^2 baked SD in co-exposure with LPS.

Pristine DQ12 and pristine SD similarly increased IL-1β release about 8-fold (Fig. 8A). Again, the potencies of the quartz dusts followed the order DQ12 > Min-U-Sil 5 > F600. SAS upregulated IL-1β release more strongly by almost 10-fold. Baked SD increased IL-1β release 4-fold less than pristine SD while for DQ12, baking made no difference. SD-mediated release of IL-1β from *NLRP3*$^{-/-}$ cells was 20-fold lower than from WT cells. For the quartz dusts and SAS, the difference in IL-1β release between WT and *NLRP3*$^{-/-}$ cells was even bigger because the absolute IL-1β concentrations released from *NLRP3*$^{-/-}$ cells were even lower.

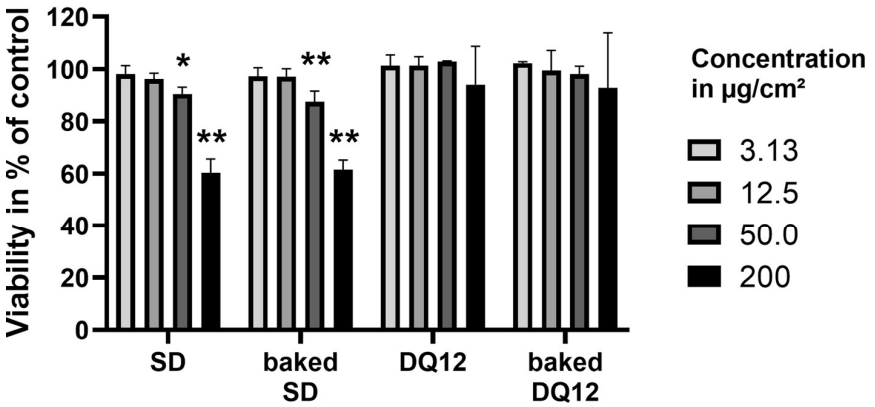

Fig. 5. Cytotoxicity of Saharan dust and DQ12 quartz. A549 cells were exposed to pristine and baked SD and DQ12 quartz at concentrations in the range of 0–200 μg/cm^2 for 24 h. The cell viability examined with the WST-1 assay was normalized to the negative control. The values are plotted as mean ± standard deviation of $N = 3$ independent experiments. A mixed-effects model with Dunnett's post hoc test was calculated (*$p \leq 0.05$; **$p \leq 0.01$).

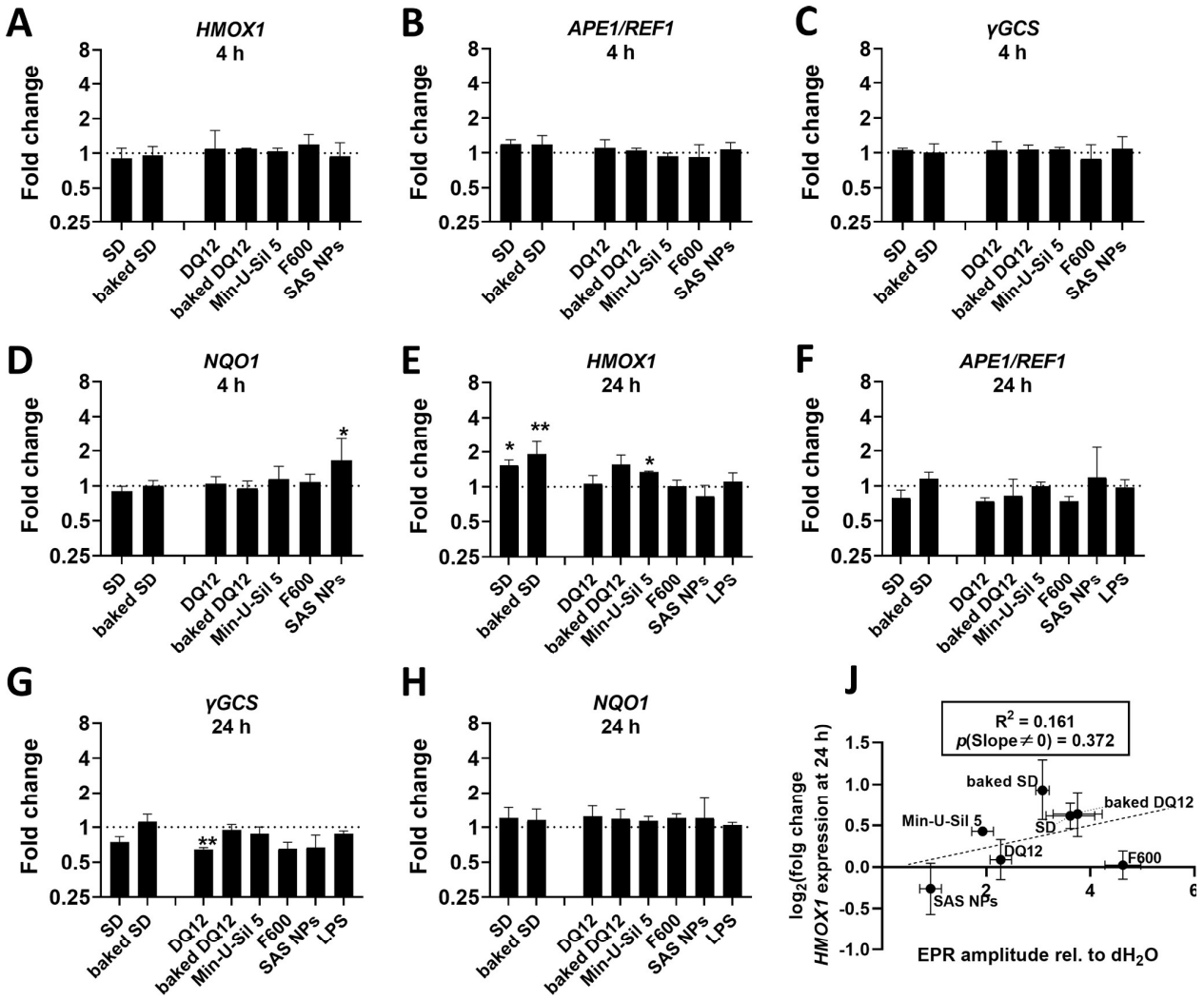

Fig. 6. Oxidative stress marker gene expression in A549 cells. A549 cells were exposed to SD, quartz dusts, or SAS at concentrations of 50 μg/cm^2 for 4 h (**A-D**) and 24 h (**E-J**) or to 10 μg/mL LPS for 24 h. To minimize interference, bovine serum albumin was added to SD samples and to an additional control sample 30 min before the end of incubation time. The relative gene expression of *HMOX1* (**A, E, J**), *APE1/REF1* (**B, F**), *γGCS* (**C, G**), and *NQO1* (**D, H**) was assessed by qRT-PCR. The results were normalized to control cells and to *β-ACTIN* as reference gene. The depicted fold changes with standard deviation were derived from the means and standard deviations of the $\Delta\Delta C_T$-values of $N = 3$–4 independent experiments. A mixed-effects model with Šídák's post hoc test was calculated based on the ΔC_T-values (*$p \leq 0.05$; **$p \leq 0.01$). The correlation of the amplitudes of pristine and baked samples in EPR relative to dH_2O as a measure of hydroxyl radical formation capacity (shown in Fig. 4A) and the fold change of expression of *HMOX1* after 24 h was assessed (**J**).

Again, considering the strong interference with the ELISA, it is challenging to evaluate the effect of SD on IL-8 secretion. Still, despite the interference, IL-8 release from *NLRP3*$^{-/-}$ cells was induced by SD while baked SD had no effect (Fig. S6A). All quartz dusts and SAS increased IL-8 release from WT cells 2- to 3-fold. *NLRP3*$^{-/-}$ cells exposed to any of the investigated dust and particle samples released substantially lower concentrations of IL-8 than WT cells. For IL-8, the potencies of the quartz dusts also followed the order DQ12 > Min-U-Sil 5 > F600.

To confirm the potential of endotoxin to exacerbate the inflammatory effects of SD, we exposed WT cells to SD and baked SD, as well as to LPS at concentrations between 0.08 and 10 ng/mL with or without co-exposure to baked SD (Fig. 8B). With increasing LPS concentrations we observed increasing enhancements of IL-1β release through co-exposure to baked SD. In combination with the statistically significant interaction factor between LPS concentration and the co-exposure to baked SD, this suggests a synergistic effect of SD and endotoxin. The LPS concentration of 0.08 ng/mL corresponds to the amount of endotoxin that is present when exposing to 50 μg/cm^2 pristine SD. Notably, adding 0.08 ng/mL LPS to baked SD increased the IL-1β release while it did not lead to full recovery of the effect of pristine SD (Fig. 8B).

To exclude the possibility that cytokine releases were influenced by cytotoxicity, we performed the LDH assay in parallel. Merely exposure to the quartz dusts slightly increased LDH release by about 1.3-fold (Fig. S6B,C).

Taken together, the pro-inflammatory potencies of SD, the quartz dusts, and SAS on macrophage-like cells were similar and strongly dependent on the functionality of NLRP3. Baking of SD, which destroyed the contained endotoxin, substantially decreased its pro-inflammatory potency.

4. Discussion

Here, we report that microbial components including endotoxins potently contribute to the pro-inflammatory potency of Saharan dust (SD). Besides microbial components, SD's content of other constituents including sulfate, diatomaceous earth, trace metals, Fe, or Al may be

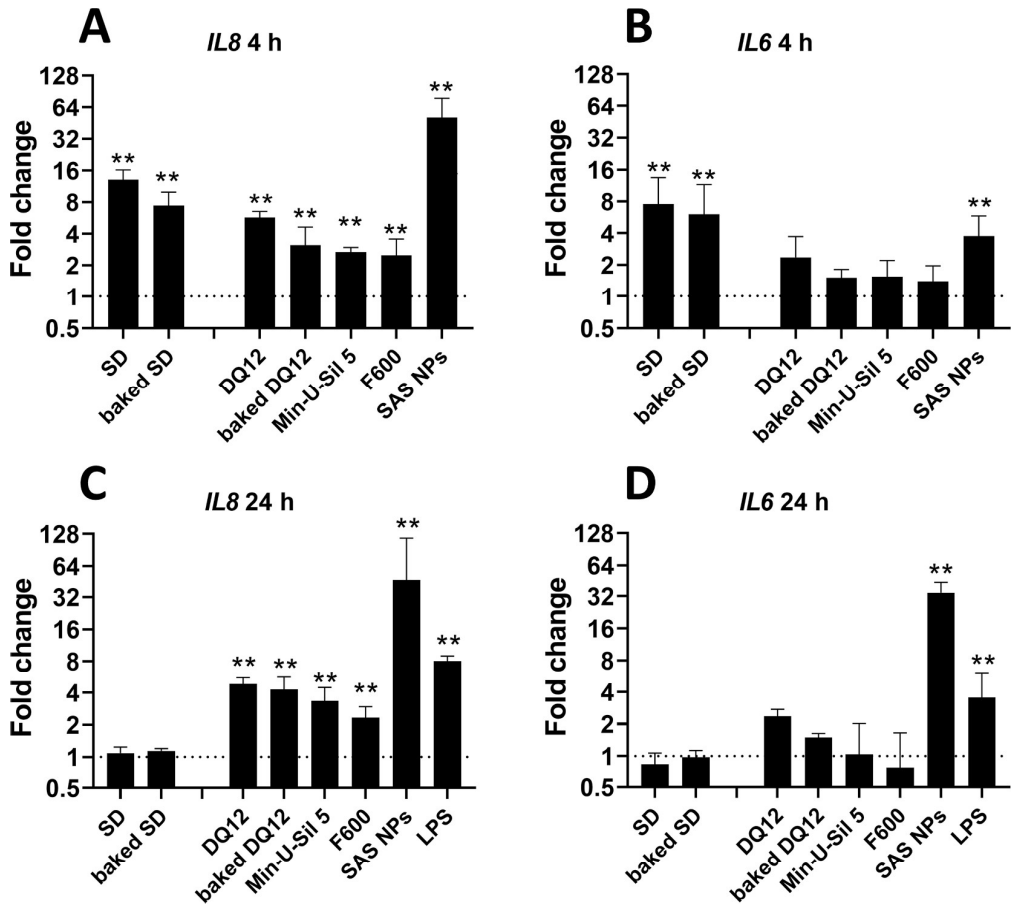

Fig. 7. *IL8* and *IL6* expression in A549 cells. A549 cells were exposed to SD, quartz dusts, or SAS at a concentration of 50 μg/cm^2 for 4 h (**A, B**) and 24 h (**C, D**) or to the positive control 10 μg/mL LPS for 24 h. The relative gene expression of *IL8* (**B**) and *IL6* (**C**) was assessed by qRT-PCR. The results were normalized to control cells and to *β-ACTIN* as reference gene. The depicted fold changes with standard deviation were derived from the means and standard deviations of the $\Delta\Delta C_T$-values of $N = 3$–4 independent experiments. Mixed-effects models with Šídák's post hoc test were calculated based on the ΔC_T-values (**$p \leq 0.01$).

involved in its toxicity. In alveolar epithelial A549 cells, SD exerted oxidative stress and pro-inflammation with different potency and *in vitro* persistence when compared to quartz dusts and synthetic amorphous silica (SAS). Moreover, the pro-inflammatory potential of pristine SD on the THP-1 macrophage-like cells was similar to that of the quartz dusts and SAS. Finally, we could confirm that the NLRP3 inflammasome in macrophages plays an important role in SD-induced IL-1β secretion. This underlines the risks of acute and chronic adverse effects associated with desert dust exposure.

Table 4
Overview of the effects of SD, quartz dusts, and SAS NPs on the gene expressions of *APE1/REF1*, *γGCS, NQO1, HMOX1, IL8,* and *IL6* in A549 cells after 4 h and 24 h.

	4 h			24 h		
	SD	Quartz dusts	SAS NPs	SD	Quartz dusts	SAS NPs
APE1/REF1	o	o	o	o	o	o
γGCS	o	o	o	o	-*	o
NQO1	o	o	+	o	o	o
HMOX1	o	o	o	+	+**	o
IL8	++	+	++	o	+	++
IL6	+	o	+	o	o	++

Significantly downregulated (-), no significant effect (o), significantly $< 2^3$ fold upregulated (+), significantly $> 2^3$ fold upregulated (++), *statistically significant only for DQ12, **statistically significant only for Min-U-Sil 5.

Characterization of our SD sample indicated that the investigated sample was a good representative of desert dust and of SD in particular. Val et al. (2013) and Rodriguez-Navarro et al. (2018) also found high shares of submicron-sized particles in SD. Furthermore, the presence of diatomaceous earth (Gasse et al., 2017; Rodriguez-Navarro et al., 2018), the distribution of O, Al, Si, Ca, and Fe (Rodriguez-Navarro et al., 2018), the Fe content (Linke et al., 2006), the presence of sulfate and nitrate (Savoie et al., 1989), the low contents of organic and elemental carbon (Eglinton et al., 2002; Gonçalves et al., 2014), and the presence of endotoxin (He et al., 2010; Honda et al., 2014; Rodriguez-Cotto et al., 2013; Taylor et al., 2013) were in agreement with former studies.

4.1. Compounds potentially driving Saharan dust toxicity

The identified characteristics of SD provide information on which components and properties are implicated in its toxicity. Toxic effects may be related to the content of biological components, sulfate, diatomaceous earth, trace metals or iron. While the hydroxyl radical generating capacity did not correlate to toxic effects in A549 cells (see Fig. 6J), the agglomerate size and the contents of Al may have played a role.

Remarkably, removing biological components such as endotoxin from SD decreased its potential to induce *IL8* expression in the alveolar epithelial cell model and strongly mitigated its potential to trigger IL-1β release from macrophage-like cells which agrees with studies from Ortiz-Martinez et al. (2015), Honda et al. (2014), and He et al. (2010). At

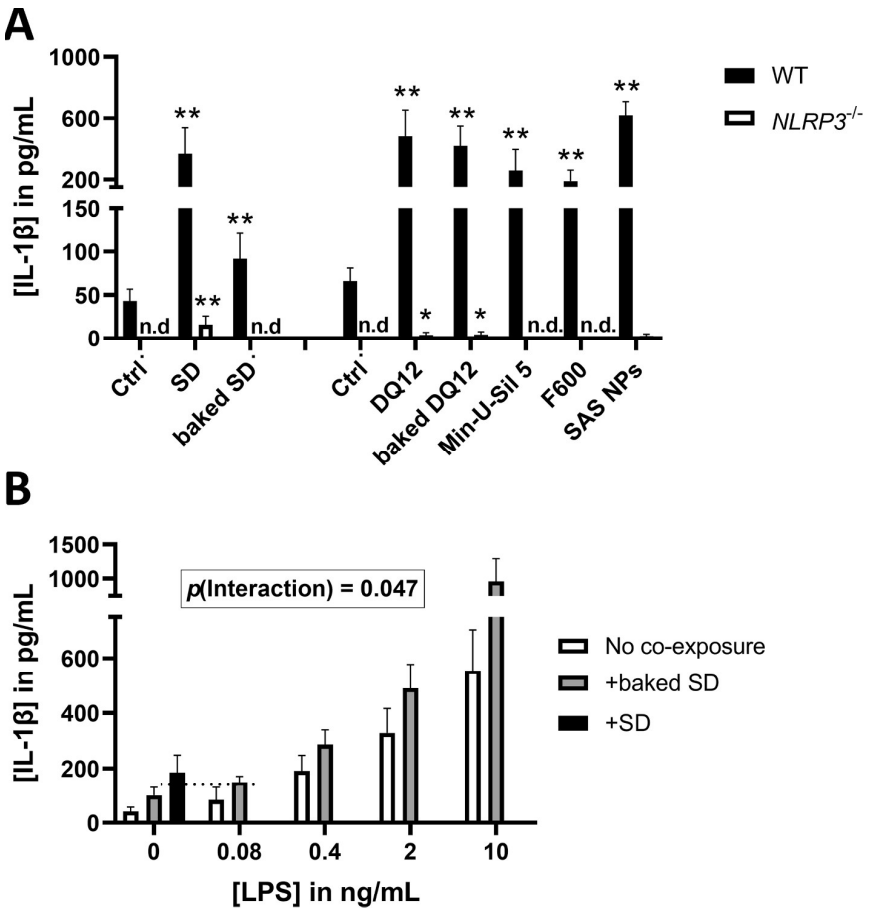

Fig. 8. NLRP3 dependent IL-1β release from THP-1 cells and combination effect of baked SD and LPS. Wild type (WT) and *NLRP3*$^{-/-}$ THP-1 cells were exposed to SD, quartz dusts, or SAS at a concentration of 50 μg/cm^2 or to the positive control 10 ng/mL LPS for 24 h (**A**). Additionally, WT THP-1 cells were exposed to LPS concentrations between 0 and 10 ng/mL without co-exposure or co-exposed to 50 μg/cm^2 SD or baked SD (**B**). To minimize interference, bovine serum albumin was added to all samples exposed to SD and baked SD (**A, B**), to an additional control sample (**A**), and to the corresponding LPS exposed samples (**B**) 30 min before the end of incubation time. The concentrations of IL-1β in the supernatants were assessed via ELISA and are plotted as mean ± standard deviation of $N \geq 3$ independent experiments. A dotted line was added to mark the release of IL-1β in response 0.08 ng/mL LPS + baked SD in comparison to pristine SD (**B**). The concentration of 0.08 ng/mL corresponds to the amount of endotoxin found in pristine SD. A mixed-effects model with Šídák's post hoc test was calculated together with the data from LPS exposure (Fig. S5B-C) ($^*p \leq 0.05$; $^{**}p \leq 0.01$) (**A**). The interaction effect between LPS concentration and co-exposure to baked SD was calculated from a mixed-effects model (**B**). n.d.: not detected.

the same time, adding endotoxin to baked SD could not fully recover the potential of pristine SD to induce IL-1β release suggesting the contribution of other biological components, as well. Bacterial peptidoglycans and fungal β-glucans have been proposed as further relevant components of desert dust (Fussell and Kelly, 2021; He et al., 2010; Ortiz-Martinez et al., 2015). They may also play a role in the strong exacerbation of the pro-inflammatory effects of SD.

It has also been argued that the toxicity of SD might be related to its sulfate content. Ichinose et al. (2005) described that adding sulfate to desert dust increased lung inflammation in mice whereas Hiyoshi et al. (2005) reported the opposite. Similarly inconclusive were epidemiological studies on the influence of the sulfate content on ambient air adverse effects (Schlesinger, 2007). Moreover, we found diatomaceous earth as a constituent of SD. Considering its hematolytic activity (Adamis et al., 2000; Nattrass et al., 2015), diatomaceous earth may contribute to the pro-inflammatory potential of SD. Furthermore, we found traces of several metals. Earlier studies suggested that trace metals might be involved in the toxicity of desert dust (Rodriguez-Cotto et al., 2013; Taylor et al., 2013). Yet, it remains to be investigated in future studies whether trace metals contribute to the toxicity of SD and, if they do so, which ones. A metal we found in isolated particles was Fe. Previous studies, one of which was conducted at the same sampling site, described that in SD, Fe could especially be found in smaller particles (Carpenter et al., 2011; Rodriguez-Navarro et al., 2018). Because of its Fenton reactivity, Fe might contribute to the oxidative stress induction. The important role of Fe content in dust-induced *HMOX1* upregulation was shown by Napierska et al. (2012). It must be considered that in this study Fe-ion release may be artificially increased due to the sonication of SD before exposure.

Interestingly, we found that the upregulation of *HMOX1* gene expression in A549 cells did not correlate with the capacity of the different samples to generate hydroxyl radicals. This may be explained by differences in particle size and the content of Fe and Al. Although F600 had the highest capacity to generate hydroxyl radicals, it did not induce oxidative stress. F600 was also the quartz dust with the biggest particle size, meaning that uptake may have been lower (dos Santos et al., 2011) so that fewer intracellular particles could generate radicals. In contrast, SD contained a high number of sub-micron agglomerates. As elucidated above, Fe might also contribute to oxidative stress induced by SD. Moreover, traces of Al might explain the absence of *HMOX1* upregulation in response to F600 (Albrecht et al., 2007; Albrecht et al., 2004; Drosselmeyer et al., 1988; Ghiazza et al., 2011; Nattrass et al., 2017; Nolan et al., 1987; Schins et al., 2002). Despite its relatively high Al content, SD more potently upregulated *HMOX1* than the quartz dusts. At the same time, quartz particles might be less relevant for the toxicity of SD because of the high Al content (Albrecht et al., 2007; Albrecht et al., 2004; Nattrass et al., 2017; Nolan et al., 1987).

Still, we consider it important to test the whole dust sample and not just extracts in order to cover potential synergistic effects. When using either organic or aqueous extracts, which both are potentially toxic (Naimabadi et al., 2016), their mixture effect is neglected. Moreover, synergistic effects between particles and Fe (Zhou et al., 2003) and between particles and endotoxin (Ning et al., 2000) have been suggested. The results from our co-exposure experiment strongly support a synergistic effect of Saharan dust and endotoxin.

4.2. Mechanisms of toxicity in epithelial cells

By causing oxidative stress and the expression of pro-inflammatory cytokines, SD triggered two main mechanisms of toxicity in alveolar epithelial cells. SD triggered these mechanisms with different potency and *in vitro* persistence than quartz dusts and SAS. Surprisingly, at the early time point of 4 h, only SAS induced oxidative stress. The upregulation of *NQO1* through SAS was transient. To the best of our knowledge, a transient upregulation of *NQO1* by SAS in the absence of *HMOX1*, *APE1/REF1*, and *γGCS* induction has not been reported before and the upstream mechanisms remain shrouded.

After 24 h, SD and quartz dusts upregulated *HMOX1* expression. In concordance with our results, the upregulation of *HMOX1* has also been reported for dust sampled in Arizona (Ghio et al., 2014) and on the Arabian Peninsula (Sun et al., 2012) as well as for extracts from SD which also had the capacity to generate ROS (Rodriguez-Cotto et al., 2015). However, unlike in our study, Ghio et al. (2014) observed a stronger induction by Min-U-Sil 5 quartz than Arizona dust. The reason may be differences in dust properties such as the size distribution or Al content (see 4.1). Moreover, Ghio et al. (2014) collected surface dust in Arizona while we sampled SD from the air. Therefore, SD but not Arizona dust might have been mechanically activated during transport with the wind (Fenoglio et al., 2000). Furthermore, Ghio et al. (2014) used BEAS-2B cells while we tested in A549 cells. Rodriguez-Cotto et al. (2015), in contrast to our study, found a peak of *HMOX1* upregulation at 3–4 h. The faster response may be explained by the fact that they tested SD extracts and thus the components inducing oxidative stress did not have to be released from the dust first.

While SD exposure caused oxidative stress at the late 24 h time point, it only caused a transient upregulation of pro-inflammatory cytokines at the earlier 4 h time point. This finding contrasts with Ghio et al. (2014) who discussed that particles from diverse sources including desert dusts share the common mechanism of oxidative stress induction, leading to the expression of pro-inflammatory genes and finally to pulmonary inflammation. Our findings rather suggest SD-induced pro-inflammation independent of oxidative stress (Barrett et al., 1999).

Unlike the quartz dusts and SAS, SD only caused a transient upregulation of pro-inflammatory cytokine expression. The transient nature of this effect is in line with the results from Rodriguez-Cotto et al. (2015) and Ghio et al. (2014) who observed transient increases of pro-inflammatory cytokine expression in BEAS-2B cells and cytokine release in murine lung lavages, respectively. Other studies found increased secretions of pro-inflammatory cytokines from BEAS-2B cells following exposure to Asian dust (Honda et al., 2014; Shin et al., 2013), Arizona dust (Ghio et al., 2014) or SD extracts (Ortiz-Martinez et al., 2015; Rodriguez-Cotto et al., 2013), suggesting antecedently increased gene expressions. The transient pro-inflammation through SD and baked SD versus the *in vitro* persistent pro-inflammation through the quartz dusts and SAS suggests that the components responsible for the pro-inflammatory effect differ. In the case of SD, microbial components may cause the pro-inflammation after 4 h whereas they may be degraded after 24 h (Sharma et al., 2020).

4.3. SD effects on macrophage-like cells, NLRP3 inflammasome activation and associated health risks

In macrophage-like THP-1 cells, we observed increased IL-1β and IL-8 release upon SD exposure. This is in line with studies performed in rats (Wilfong et al., 2011), mice (Ghio et al., 2014; He et al., 2010; Ren et al., 2014), murine bone marrow-derived macrophages (He et al., 2013), and murine RAW264.7 cells (He et al., 2010).

The potency of SD but not of baked SD to induce IL-1β release was similar to that of the crystalline and amorphous silica reference samples. As discussed in 4.1, the higher potency of SD compared to baked SD can be explained by the presence of microbial components including endotoxins. Comparing SD to the silica reference samples this means that SD may additionally trigger priming of the NLRP3 inflammasome upstream of the activation of the NLRP3 inflammasome (Bauernfeind et al., 2009).

We found that the extent to which the quartz dusts upregulated pro-inflammatory cytokines consistently followed the order DQ12 > Min-U-Sil 5 > F600. This order agrees with the hemolytic potencies of the three quartz dusts (Hadnagy et al., 2003; Nolan et al., 1987). The hemolysis generating properties of particles have long been recognized a marker of their fibrogenic potencies (Hefner and Gehring, 1975). Moreover, the hemolytic and pro-inflammatory activities of dusts are known to be well-correlated (Pavan et al., 2014) which underpins the validity of the THP-1 cell model.

Importantly, in our study, we confirm the decisive role of the NLRP3 inflammasome pathway for desert dust-mediated pro-inflammation. When He et al. (2010) observed the upregulation of *NLRP3* and *IL1β* in RAW264.7 cells, they advocated for the testing of desert dust in *NLRP3*$^{-/-}$ mice to confirm the meaning of the NLRP3 inflammasome pathway. Using differentiated THP-1 cells as a well-established *in vitro* model, we have achieved this without further *in vivo* experiments.

For asbestos, quartz dust, and ambient PM10, the induction of adverse respiratory health effects is well-established (Cassel et al., 2008; Donaldson et al., 2010; Elliott, 1923; Ghio and Devlin, 2001; Hnizdo and Vallyathan, 2003). Adverse respiratory health effects such as chronic obstructive pulmonary disease (COPD), neutrophilic asthma, pneumoconiosis, fibrosis, and acute lung injury have been shown to be critically linked to the NLRP3 inflammasome pathway (Fukumoto et al., 2013; Grailer et al., 2014; Kim et al., 2015; Sayan and Mossman, 2016; Yang et al., 2020; Zhang et al., 2016b). With the identification of SD as potent activator of the NLRP3 inflammasome, our results suggest a relevant environmental hazard of developing acute and chronic lung disease from SD exposure. In line with this, epidemiological studies have already related desert dust exposure to COPD and asthma (Meo et al., 2013; Rutherford et al., 1999; Tam et al., 2012). Detailed future studies must address to what extent desert dust exposure can cause or exacerbate various lung diseases. Specifically, these studies need to unravel the exact mechanisms upstream and downstream of NLRP3 inflammasome activation that link desert dust exposure and adverse health outcomes. In our hands, SD showed surprisingly strong induction of oxidative stress and IL-1β release which was even stronger or comparable to quartz dusts as a well-known toxicant. Thus, SD must be considered as a further main component of concern in the particle air pollution mixture.

4.4. Conclusion

Our results point out the multitude of biological and inorganic components of SD possibly involved in its toxic effects. Future studies should investigate which bacteria or fungi on desert dust are responsible for the pro-inflammatory effects. Future studies should also address the importance of Fe compared to other trace metals as well as the role of sulfate, diatomaceous earth, and Al. This could be achieved through spiking experiments or by means of correlating the toxicity of several desert dust samples to their composition. This information on the toxicity of the specific components in combination with information on their current or predicted exposure is required for accurate risk assessment and risk mitigation. The aforementioned multitude of components of SD probably explains that the potency and *in vitro* persistence of oxidative stress and pro-inflammation in alveolar epithelial cells differ upon exposure to SD compared to quartz dusts and SAS. It remains uncertain which upstream signaling pathways SD, quartz dusts, and SAS induce differently. Considering the oxidative stress induction, the nuclear factor erythroid 2-related factor (NRF2) pathway appears especially relevant to study (Ahmed et al., 2017). Particularly in view of the transient pro-inflammatory effect of SD, it will also be interesting to follow up on the roles of soluble versus insoluble components. The important role of biological components for SD effects in macrophages warrants studying toll-like receptor signaling (He et al., 2013; Ren et al., 2014). Finally, we prove that SD activates the NLRP3 inflammasome,

emphasizing its hazardousness in acute and chronic exposure scenarios. To understand the impact of NLRP3 activation through SD more precisely, further studies should also be performed on more realistic co-cultures of epithelial cells and macrophages that include the cross-talk of both cell types.

Funding

This work has received funding from the Leibniz Association in the framework of the Leibniz Collaborative Excellence Programme project DUSTRISK under the grant agreement number K225/2019.

CRediT authorship contribution statement

Gerrit Bredeck: Conceptualization, Methodology, Formal analysis, Investigation, Data curation, Writing – original draft. **Mathias Busch:** Methodology, Formal analysis, Data curation, Writing – review & editing. **Andrea Rossi:** Methodology. **Burkhard Stahlmecke:** Methodology, Formal analysis, Investigation, Data curation. **Khanneh Wadinga Fomba:** Methodology, Resources, Writing – review & editing, Funding acquisition. **Hartmut Herrmann:** Resources, Writing – review & editing, Funding acquisition. **Roel P.F. Schins:** Conceptualization, Methodology, Resources, Writing – review & editing, Supervision, Project administration, Funding acquisition.

Declaration of Competing Interest

The authors declare that they have no known competing financial interests or personal relationships that could have appeared to influence the work reported in this paper.

Data availability

Data will be made available on request.

Acknowledgments

We would like to thank Dr. Tamara Schikowski, Dr. Claudia Wigmann, and Sara Kress for their support with the statistical analysis. Moreover, we are thankful to Dr. Haribaskar Ramachandran for establishing the NLRP3-deficient THP-1 cells. Also, we would like to thank Isabelle Masson for her support with the *in vitro* toxicology experiments.

Appendix A. Supplementary material

Supplementary data to this article can be found online at https://doi.org/10.1016/j.envint.2023.107732.

References

Adamis, Z., Tatrai, E., Honma, K., Six, E., Ungvary, G., 2000. In vitro and in vivo tests for determination of the pathogenicity of quartz, diatomaceous earth, mordenite and clinoptilolite. Ann. Occup. Hyg. 44, 67–74. https://doi.org/10.1093/annhyg/44.1.67.

Agostini, L., Martinon, F., Burns, K., McDermott, M.F., Hawkins, P.N., Tschopp, J., 2004. NALP3 Forms an IL-1β-Processing Inflammasome with Increased Activity in Muckle-Wells Autoinflammatory Disorder. Immunity 20, 319–325. https://doi.org/10.1016/s1074-7613(04)00046-9.

Ahmed, S.M., Luo, L., Namani, A., Wang, X.J., Tang, X., 2017. Nrf2 signaling pathway: Pivotal roles in inflammation. Biochim. Biophys. Acta Mol. basis Dis. 1863, 585–597. https://doi.org/10.1016/j.bbadis.2016.11.005.

Albrecht, C., Schins, R.P., Hohr, D., Becker, A., Shi, T., Knaapen, A.M., Borm, P.J., 2004. Inflammatory time course after quartz instillation: role of tumor necrosis factor-alpha and particle surface. Am. J. Respir. Cell Mol. Biol. 31, 292–301. https://doi.org/10.1165/rcmb.2003-0300OC.

Albrecht, C., Hohr, D., Haberzettl, P., Becker, A., Borm, P.J., Schins, R.P., 2007. Surface-dependent quartz uptake by macrophages: potential role in pulmonary inflammation and lung clearance. Inhal. Toxicol. 19, 39–48. https://doi.org/10.1080/08958370701492979.

Barrett, E.G., Johnston, C., Oberdorster, G., Finkelstein, J.N., 1999. Silica-induced chemokine expression in alveolar type II cells is mediated by TNF-alpha-induced oxidant stress. Am. J. Phys. Anthropol. 276, L979–L988. https://doi.org/10.1152/ajplung.1999.276.6.L979.

Bauernfeind, F.G., Horvath, G., Stutz, A., Alnemri, E.S., MacDonald, K., Speert, D., Fernandes-Alnemri, T., Wu, J., Monks, B.G., Fitzgerald, K.A., Hornung, V., Latz, E., 2009. Cutting edge: NF-kappaB activating pattern recognition and cytokine receptors license NLRP3 inflammasome activation by regulating NLRP3 expression. J. Immunol. 183, 787–791. https://doi.org/10.4049/jimmunol.0901363.

Becker, S., Mundandhara, S., Devlin, R., Madden, M., 2005. Regulation of cytokine production in human alveolar macrophages and airway epithelial cells in response to ambient air pollution particles: Further mechanistic studies. Toxicol. Appl. Pharmacol. 207, 269–275. https://doi.org/10.1016/j.taap.2005.01.023.

Bonizzi, G., Piette, J., Merville, M.P., Bours, V., 1997. Distinct signal transduction pathways mediate nuclear factor-kappaB induction by IL-1beta in epithelial and lymphoid cells. J. Immunol. 159, 5264–5272. https://doi.org/10.4049/jimmunol.159.11.5264.

Bredeck, G., Kampfer, A.A.M., Sofranko, A., Wahle, T., Lison, D., Ambroise, J., Stahlmecke, B., Albrecht, C., Schins, R.P.F., 2021. Effects of dietary exposure to the engineered nanomaterials CeO_2, SiO_2, Ag, and TiO_2 on the murine gut microbiome. Nanotoxicology 15, 934–950. https://doi.org/10.1080/17435390.2021.1940339.

Busch, M., Bredeck, G., Kampfer, A.A.M., Schins, R.P.F., 2021. Investigations of acute effects of polystyrene and polyvinyl chloride micro- and nanoplastics in an advanced in vitro triple culture model of the healthy and inflamed intestine. Environ. Res. 193, 110536 https://doi.org/10.1016/j.envres.2020.110536.

Busch, M., Bredeck, G., Waag, F., Rahimi, K., Ramachandran, H., Bessel, T., Barcikowski, S., Herrmann, A., Rossi, A., Schins, R.P.F., 2022. Assessing the NLRP3 Inflammasome Activating Potential of a Large Panel of Micro- and Nanoplastics in THP-1 Cells. Biomolecules 12. https://doi.org/10.3390/biom12081095.

Cao, W., Wang, X., Li, J., Yan, M., Chang, C.H., Kim, J., Jiang, J., Liao, Y.P., Tseng, S., Kusumoputro, S., Lau, C., Huang, M., Han, P., Lu, P., Xia, T., 2022. NLRP3 inflammasome activation determines the fibrogenic potential of $PM_{2.5}$ air pollution particles in the lung. J. Environ. Sci. (China) 111, 429–441. https://doi.org/10.1016/j.jes.2021.04.021.

Cappellini, F., Di Bucchianico, S., Karri, V., Latvala, S., Malmlof, M., Kippler, M., Elihn, K., Hedberg, J., Odnevall Wallinder, I., Gerde, P., Karlsson, H.L., 2020. Dry Generation of CeO_2 Nanoparticles and Deposition onto a Co-Culture of A549 and THP-1 Cells in Air-Liquid Interface-Dosimetry Considerations and Comparison to Submerged Exposure. Nanomaterials (Basel) 10, 618. https://doi.org/10.3390/nano10040618.

Carpenter, L.J., Fleming, Z.L., Read, K.A., Lee, J.D., Moller, S.J., Hopkins, J.R., Purvis, R. M., Lewis, A.C., Müller, K., Heinold, B., Herrmann, H., Fomba, K.W., van Pinxteren, D., Müller, C., Tegen, I., Wiedensohler, A., Müller, T., Niedermeier, N., Achterberg, E.P., Patey, M.D., Kozlova, E.A., Heimann, M., Heard, D.E., Plane, J.M. C., Mahajan, A., Oetjen, H., Ingham, T., Stone, D., Whalley, L.K., Evans, M.J., Pilling, M.J., Leigh, R.J., Monks, P.S., Karunaharan, A., Vaughan, S., Arnold, S.R., Tschritter, J., Pöhler, D., Frieß, U., Holla, R., Mendes, L.M., Lopez, H., Faria, B., Manning, A.J., Wallace, D.W.R., 2011. Seasonal characteristics of tropical marine boundary layer air measured at the Cape Verde Atmospheric Observatory. J. Atmos. Chem. 67, 87–140. https://doi.org/10.1007/s10874-011-9206-1.

Cassel, S.L., Eisenbarth, S.C., Iyer, S.S., Sadler, J.J., Colegio, O.R., Tephly, L.A., Carter, A. B., Rothman, P.B., Flavell, R.A., Sutterwala, F.S., 2008. The Nalp3 inflammasome is essential for the development of silicosis. PNAS 105, 9035–9040. https://doi.org/10.1073/pnas.0803933105.

Chen, S., Huang, J., Li, J., Jia, R., Jiang, N., Kang, L., Ma, X., Xie, T., 2017. Comparison of dust emissions, transport, and deposition between the Taklimakan Desert and Gobi Desert from 2007 to 2011. Sci. China Earth Sci. 60, 1338–1355. https://doi.org/10.1007/s11430-016-9051-0.

Davis, G.S., Pfeiffer, L.M., Hemenway, D.R., 1998. Persistent overexpression of interleukin-1beta and tumor necrosis factor-alpha in murine silicosis. J. Environ. Pathol. Toxicol. Oncol. 17, 99–114.

Diaz, J., Tobias, A., Linares, C., 2012. Saharan dust and association between particulate matter and case-specific mortality: a case-crossover analysis in Madrid (Spain). Environ. Health 11, 11. https://doi.org/10.1186/1476-069X-11-11.

Donaldson, K., Murphy, F.A., Duffin, R., Poland, C.A., 2010. Asbestos, carbon nanotubes and the pleural mesothelium: a review of the hypothesis regarding the role of long fibre retention in the parietal pleura, inflammation and mesothelioma. Part. Fibre Toxicol. 7, 5. https://doi.org/10.1186/1743-8977-7-5.

dos Santos, T., Varela, J., Lynch, I., Salvati, A., Dawson, K.A., 2011. Quantitative assessment of the comparative nanoparticle-uptake efficiency of a range of cell lines. Small 7, 3341–3349. https://doi.org/10.1002/smll.201101076.

Dostert, C., Petrilli, V., Van Bruggen, R., Steele, C., Mossman, B.T., Tschopp, J., 2008. Innate immune activation through Nalp3 inflammasome sensing of asbestos and silica. Science 320, 674–677. https://doi.org/10.1126/science.1156995.

Drosselmeyer, E., Hofheinz, V., Pätzold, S., Polzer, G., Schimmelpfeng, J., Seidel, A., 1988. Parameters influencing the effects of quartz on alveolar macrophages. J. Aerosol Sci 19, 1157–1160. https://doi.org/10.1016/0021-8502(88)90125-5.

Eglinton, T.I., Eglinton, G., Dupont, L., Sholkovitz, E.R., Montluçon, D., Reddy, C.M., 2002. Composition, age, and provenance of organic matter in NW African dust over the Atlantic Ocean. Geochem. Geophy. Geosy. 3, 1–27. https://doi.org/10.1029/2001gc000269.

Elliott, J.H., 1923. Silicosis in Ontario Gold Miners. Trans. Am. Climatol. Clin. Assoc. 39, 24–43.

Fenoglio, I., Martra, G., Prandi, L., Tomatis, M., Coluccia, S., Fubini, B., 2000. The Role of Mechanochemistry in the Pulmonary Toxicity Caused by Particulate Minerals. J. Mater. Synth. Process. 8, 145–153. https://doi.org/10.1023/a:1011303924468.

Fomba, K.W., Müller, K., van Pinxteren, D., Poulain, L., van Pinxteren, M., Herrmann, H., 2014. Long-term chemical characterization of tropical and marine aerosols at the

Cape Verde Atmospheric Observatory (CVAO) from 2007 to 2011. Atmos. Chem. Phys. 14, 8883–8904. https://doi.org/10.5194/acp-14-8883-2014.

Fomba, K.W., Deabji, N., Barcha, S.E.I., Ouchen, I., Elbaramoussi, E.M., El Moursli, R.C., Harnafi, M., El Hajjaji, S., Mellouki, A., Herrmann, H., 2020. Application of TXRF in monitoring trace metals in particulate matter and cloud water. Atmos. Meas. Tech. 13, 4773–4790. https://doi.org/10.5194/amt-13-4773-2020.

Fukumoto, J., Fukumoto, I., Parthasarathy, P.T., Cox, R., Huynh, B., Ramanathan, G.K., Venugopal, R.B., Allen-Gipson, D.S., Lockey, R.F., Kolliputi, N., 2013. NLRP3 deletion protects from hyperoxia-induced acute lung injury. Am. J. Physiol. Cell Physiol. 305, C182–C189. https://doi.org/10.1152/ajpcell.00086.2013.

Fussell, J.C., Kelly, F.J., 2021. Mechanisms underlying the health effects of desert sand dust. Environ. Int. 157, 106790 https://doi.org/10.1016/j.envint.2021.106790.

Gasse, F., Stabell, B., Fourtanier, E., van Iperen, Y., 2017. Freshwater Diatom Influx in Intertropical Atlantic: Relationships with Continental Records from Africa. Quaternary Res. 32, 229–243. https://doi.org/10.1016/0033-5894(89)90079-3.

Ghiazza, M., Scherbart, A.M., Fenoglio, I., Grendene, F., Turci, F., Martra, G., Albrecht, C., Schins, R.P., Fubini, B., 2011. Surface iron inhibits quartz-induced cytotoxic and inflammatory responses in alveolar macrophages. Chem. Res. Toxicol. 24, 99–110. https://doi.org/10.1021/tx1003003.

Ghio, A.J., Devlin, R.B., 2001. Inflammatory lung injury after bronchial instillation of air pollution particles. Am. J. Respir. Crit. Care Med. 164, 704–708. https://doi.org/10.1164/ajrccm.164.4.2011089.

Ghio, A.J., Kummarapurugu, S.T., Tong, H., Soukup, J.M., Dailey, L.A., Boykin, E., Ian Gilmour, M., Ingram, P., Roggli, V.L., Goldstein, H.L., Reynolds, R.L., 2014. Biological effects of desert dust in respiratory epithelial cells and a murine model. Inhal. Toxicol. 26, 299–309. https://doi.org/10.3109/08958378.2014.888109.

Gonçalves, C., Alves, C., Nunes, T., Rocha, S., Cardoso, J., Cerqueira, M., Pio, C., Almeida, S.M., Hillamo, R., Teinilä, K., 2014. Organic characterisation of PM10 in Cape Verde under Saharan dust influxes. Atmos. Envir. 89, 425–432. https://doi.org/10.1016/j.atmosenv.2014.02.025.

Grailer, J.J., Canning, B.A., Kalbitz, M., Haggadone, M.D., Dhond, R.M., Andjelkovic, A. V., Zetoune, F.S., Ward, P.A., 2014. Critical role for the NLRP3 inflammasome during acute lung injury. J. Immunol. 192, 5974–5983. https://doi.org/10.4049/jimmunol.1400368.

Hadnagy, W., Marsetz, B., Idel, H., 2003. Hemolytic activity of crystalline silica–separated erythrocytes versus whole blood. Int. J. Hyg. Environ. Health 206, 103–107. https://doi.org/10.1078/1438-4639-00200.

He, M., Ichinose, T., Yoshida, S., Nishikawa, M., Mori, I., Yanagisawa, R., Takano, H., Inoue, K., Sun, G., Shibamoto, T., 2010. Airborne Asian sand dust enhances murine lung eosinophilia. Inhal. Toxicol. 22, 1012–1025. https://doi.org/10.3109/08958378.2010.510151.

He, M., Ichinose, T., Song, Y., Yoshida, Y., Arashidani, K., Yoshida, S., Liu, B., Nishikawa, M., Takano, H., Sun, G., 2013. Effects of two Asian sand dusts transported from the dust source regions of Inner Mongolia and northeast China on murine lung eosinophilia. Toxicol. Appl. Pharmacol. 272, 647–655. https://doi.org/10.1016/j.taap.2013.07.010.

He, M., Ichinose, T., Yoshida, S., Nishikawa, M., Sun, G., Shibamoto, T., 2019. Role of iron and oxidative stress in the exacerbation of allergic inflammation in murine lungs caused by urban particulate matter <2.5 mum and desert dust. J. Appl. Toxicol. 39, 855–867. https://doi.org/10.1002/jat.3773.

Hefner Jr., R.E., Gehring, P.J., 1975. A comparison of the relative rates of hemolysis induced by various fibrogenic and non-fibrogenic particles with washed rat erythrocytes in vitro. Am. Ind. Hyg. Assoc. J. 36, 734–740. https://doi.org/10.1080/0002889758507332.

Hiyoshi, K., Ichinose, T., Sadakane, K., Takano, H., Nishikawa, M., Mori, I., Yanagisawa, R., Yoshida, S., Kumagai, Y., Tomura, S., Shibamoto, T., 2005. Asian sand dust enhances ovalbumin-induced eosinophil recruitment in the alveoli and airway of mice. Environ. Res. 99, 361–368. https://doi.org/10.1016/j.envres.2005.03.008.

Hnizdo, E., Vallyathan, V., 2003. Chronic obstructive pulmonary disease due to occupational exposure to silica dust: a review of epidemiological and pathological evidence. Occup. Environ. Med. 60, 237–243. https://doi.org/10.1136/oem.60.4.237.

Honda, A., Matsuda, Y., Murayama, R., Tsuji, K., Nishikawa, M., Koike, E., Yoshida, S., Ichinose, T., Takano, H., 2014. Effects of Asian sand dust particles on the respiratory and immune system. J. Appl. Toxicol. 34, 250–257. https://doi.org/10.1002/jat.2871.

Hornung, R.W., Reed, L.D., 1990. Estimation of Average Concentration in the Presence of Nondetectable Values. Appl. Occup. Environ. Hyg. 5, 46–51. https://doi.org/10.1080/1047322x.1990.10389587.

Ichinose, T., Nishikawa, M., Takano, H., Sera, N., Sadakane, K., Mori, I., Yanagisawa, R., Oda, T., Tamura, H., Hiyoshi, K., Quan, H., Tomura, S., Shibamoto, T., 2005. Pulmonary toxicity induced by intratracheal instillation of Asian yellow dust (Kosa) in mice. Environ. Toxicol. Pharmacol. 20, 48–56. https://doi.org/10.1016/j.etap.2004.10.009.

Jobin, C., Haskill, S., Mayer, L., Panja, A., Sartor, R.B., 1997. Evidence for altered regulation of I kappa B alpha degradation in human colonic epithelial cells. J. Immunol. 158, 226–234. https://doi.org/10.4049/jimmunol.158.1.226.

Johnston, F., Hanigan, I., Henderson, S., Morgan, G., Bowman, D., 2011. Extreme air pollution events from bushfires and dust storms and their association with mortality in Sydney, Australia 1994–2007. Environ. Res. 111, 811–816. https://doi.org/10.1016/j.envres.2011.05.007.

Kampfer, A.A.M., Urban, P., Gioria, S., Kanase, N., Stone, V., Kinsner-Ovaskainen, A., 2017. Development of an in vitro co-culture model to mimic the human intestine in healthy and diseased state. Toxicol. In Vitro 45, 31–43. https://doi.org/10.1016/j.tiv.2017.08.011.

Kampfer, A.A.M., Busch, M., Buttner, V., Bredeck, G., Stahlmecke, B., Hellack, B., Masson, I., Sofranko, A., Albrecht, C., Schins, R.P.F., 2021. Model Complexity as Determining Factor for In Vitro Nanosafety Studies: Effects of Silver and Titanium Dioxide Nanomaterials in Intestinal Models. Small 17, e2004223. https://doi.org/10.1002/smll.202004223.

Kashima, S., Yorifuji, T., Bae, S., Honda, Y., Lim, Y.-H., Hong, Y.-C., 2016. Asian dust effect on cause-specific mortality in five cities across South Korea and Japan. Atmos. Enviro. 128, 20–27. https://doi.org/10.1016/j.atmosenv.2015.12.063.

Kim, R.Y., Pinkerton, J.W., Gibson, P.G., Cooper, M.A., Horvat, J.C., Hansbro, P.M., 2015. Inflammasomes in COPD and neutrophilic asthma. Thorax 70, 1199–1201. https://doi.org/10.1136/thoraxjnl-2014-206736.

Kolling, J., Tigges, J., Hellack, B., Albrecht, C., Schins, R.P.F., 2020. Evaluation of the NLRP3 Inflammasome Activating Effects of a Large Panel of TiO2 Nanomaterials in Macrophages. Nanomaterials (Basel) 10, 1876. https://doi.org/10.3390/nano10091876.

Lag, M., Skuland, T., Godymchuk, A., Nguyen, T.H.T., Pham, H.L.T., Refsnes, M., 2018. Silica Nanoparticle-induced Cytokine Responses in BEAS-2B and HBEC3-KT Cells: Significance of Particle Size and Signalling Pathways in Different Lung Cell Cultures. Basic Clin. Paharmacol. Toxicol. 122, 620–632. https://doi.org/10.1111/bcpt.12963.

Lieber, M., Smith, B., Szakal, A., Nelson-Rees, W., Todaro, G., 1976. A continuous tumor-cell line from a human lung carcinoma with properties of type II alveolar epithelial cells. Int. J. Cancer 17, 62–70. https://doi.org/10.1002/ijc.2910170110.

Linke, C., Möhler, O., Veres, A., Mohácsi, Á., Bozóki, Z., Szabó, G., Schnaiter, M., 2006. Optical properties and mineralogical composition of different Saharan mineral dust samples: a laboratory study. Atmos. Chem. Phys. 6, 3315–3323. https://doi.org/10.5194/acp-6-3315-2006.

Livak, K.J., Schmittgen, T.D., 2001. Analysis of Relative Gene Expression Data Using Real-Time Quantitative PCR and the ΔΔCT Method. Methods 25, 402–408. https://doi.org/10.1006/meth.2001.1262.

Martinon, F., Burns, K., Tschopp, J., 2002. The Inflammasome. Mol. Cell 10, 417–426. https://doi.org/10.1016/s1097-2765(02)00599-3.

Meldrum, K., Evans, S.J., Vogel, U., Tran, L., Doak, S.H., Clift, M.J.D., 2022. The influence of exposure approaches to in vitro lung epithelial barrier models to assess engineered nanomaterial hazard. Nanotoxicology AHEAD-OF-PRINT 1–21. https://doi.org/10.1080/17435390.2022.2051627.

Meo, S.A., Al-Kheraiji, M.F., Alfaraj, Z.F., Alwehaibi, N.A., Aldereihim, A.A., 2013. Respiratory and general health complaints in subjects exposed to sandstorm at Riyadh, Saudi Arabia. Pak. J. Med. Sci. 29, 642–646. https://doi.org/10.12669/pjms.292.3065.

Middleton, N.J., 2017. Desert dust hazards: A global review. Aeolian Res. 24, 53–63. https://doi.org/10.1016/j.aeolia.2016.12.001.

Naimabadi, A., Ghadiri, A., Idani, E., Babaei, A.A., Alavi, N., Shirmardi, M., Khodadadi, A., Marzouni, M.B., Ankali, K.A., Rouhizadeh, A., Goudarzi, G., 2016. Chemical composition of PM10 and its in vitro toxicological impacts on lung cells during the Middle Eastern Dust (MED) storms in Ahvaz, Iran. Environ. Pollut. 211, 316–324. https://doi.org/10.1016/j.envpol.2016.01.006.

Napierska, D., Rabolli, V., Thomassen, L.C., Dinsdale, D., Princen, C., Gonzalez, L., Poels, K.L., Kirsch-Volders, M., Lison, D., Martens, J.A., Hoet, P.H., 2012. Oxidative stress induced by pure and iron-doped amorphous silica nanoparticles in subtoxic conditions. Chem. Res. Toxicol. 25, 828–837. https://doi.org/10.1021/tx200361v.

Nattrass, C., Horwell, C.J., Damby, D.E., Kermanizadeh, A., Brown, D.M., Stone, V., 2015. The global variability of diatomaceous earth toxicity: a physicochemical and in vitro investigation. J. Occup. Med. Toxicol. 10, 23. https://doi.org/10.1186/s12995-015-0064-7.

Nattrass, C., Horwell, C.J., Damby, D.E., Brown, D., Stone, V., 2017. The effect of aluminium and sodium impurities on the in vitro toxicity and pro-inflammatory potential of cristobalite. Environ. Res. 159, 164–175. https://doi.org/10.1016/j.envres.2017.07.054.

Ning, Y., Imrich, A., Goldsmith, C.A., Qin, G., Kobzik, L., 2000. Alveolar macrophage cytokine production in response to air particles in vitro: role of endotoxin. J. Toxicol. Env. Heal. A 59, 165–180. https://doi.org/10.1080/009841000156952.

Nolan, R.P., Langer, A.M., Eskenazi, R.A., Herson, G.B., Foster, K.W., 1987. Membranolytic activities of quartz standards. Toxicol. In Vitro 1, 239–245. https://doi.org/10.1016/0887-2333(87)90026-9.

Ortiz-Martinez, M.G., Rodriguez-Cotto, R.I., Ortiz-Rivera, M.A., Pluguez-Turull, C.W., Jimenez-Velez, B.D., 2015. Linking Endotoxins, African Dust PM10 and Asthma in an Urban and Rural Environment of Puerto Rico. Mediators Inflamm. 2015, 784212 https://doi.org/10.1155/2015/784212.

Papazian, D., Wurtzen, P.A., Hansen, S.W., 2016. Polarized Airway Epithelial Models for Immunological Co-Culture Studies. Int. Arch. Allergy Immunol. 170, 1–21. https://doi.org/10.1159/000445833.

Parikh, A.A., Salzman, A.L., Kane, C.D., Fischer, J.E., Hasselgren, P.O., 1997. IL-6 production in human intestinal epithelial cells following stimulation with IL-1 beta is associated with activation of the transcription factor NF-kappa B. J. Surg. Res. 69, 139–144. https://doi.org/10.1006/jsre.1997.5061.

Pavan, C., Rabolli, V., Tomatis, M., Fubini, B., Lison, D., 2014. Why does the hemolytic activity of silica predict its pro-inflammatory activity? Part. Fibre Toxicol. 11, 76. https://doi.org/10.1186/s12989-014-0076-y.

Rabolli, V., Lison, D., Huaux, F., 2016. The complex cascade of cellular events governing inflammasome activation and IL-1beta processing in response to inhaled particles. Part. Fibre Toxicol. 13, 40. https://doi.org/10.1186/s12989-016-0150-8.

Ramachandran, H., Martins, S., Kontarakis, Z., Krutmann, J., Rossi, A., 2021. Fast but not furious: a streamlined selection method for genome-edited cells. Life Sci. Alliance 4, e202101051. https://doi.org/10.26508/lsa.202101051.

Ren, Y., Ichinose, T., He, M., Song, Y., Yoshida, Y., Yoshida, S., Nishikawa, M., Takano, H., Sun, G., Shibamoto, T., 2014. Enhancement of OVA-induced murine lung eosinophilia by co-exposure to contamination levels of LPS in Asian sand dust and heated dust. Allergy Asthma Cl. Im. 10, 30. https://doi.org/10.1186/1710-1492-10-30.

Rodriguez-Cotto, R.I., Ortiz-Martinez, M.G., Rivera-Ramirez, E., Mendez, L.B., Davila, J. C., Jimenez-Velez, B.D., 2013. African Dust Storms Reaching Puerto Rican Coast Stimulate the Secretion of IL-6 and IL-8 and Cause Cytotoxicity to Human Bronchial Epithelial Cells (BEAS-2B). Health (Irvine Calif) 5, 14–28. https://doi.org/10.4236/health.2013.510A2003.

Rodriguez-Cotto, R.I., Ortiz-Martinez, M.G., Jimenez-Velez, B.D., 2015. Organic extracts from African dust storms stimulate oxidative stress and induce inflammatory responses in human lung cells through Nrf2 but not NF-kappaB. Environ. Toxicol. Pharmacol. 39, 845–856. https://doi.org/10.1016/j.etap.2015.02.015.

Rodriguez-Navarro, C., di Lorenzo, F., Elert, K., 2018. Mineralogy and physicochemical features of Saharan dust wet deposited in the Iberian Peninsula during an extreme red rain event. Atmos. Chem. Phys. 18, 10089–10122. https://doi.org/10.5194/acp-18-10089-2018.

Rutherford, S., Clark, E., McTainsh, G., Simpson, R., Mitchell, C., 1999. Characteristics of rural dust events shown to impact on asthma severity in Brisbane, Australia. Int. J. Biometeorol. 42, 217–225. https://doi.org/10.1007/s004840050108.

Savoie, D.L., Prospero, J.M., Saltzman, E.S., 1989. Non-sea-salt sulfate and nitrate in trade wind aerosols at Barbados: Evidence for long-range transport. J. Geophys. Res. 94, 5069–5080. https://doi.org/10.1029/JD094iD04p05069.

Sayan, M., Mossman, B.T., 2016. The NLRP3 inflammasome in pathogenic particle and fibre-associated lung inflammation and diseases. Part. Fibre Toxicol. 13, 51. https://doi.org/10.1186/s12989-016-0162-4.

Schins, R.P., Duffin, R., Hohr, D., Knaapen, A.M., Shi, T., Weishaupt, C., Stone, V., Donaldson, K., Borm, P.J., 2002. Surface modification of quartz inhibits toxicity, particle uptake, and oxidative DNA damage in human lung epithelial cells. Chem. Res. Toxicol. 15, 1166–1173. https://doi.org/10.1021/tx025558u.

Schlesinger, R.B., 2007. The health impact of common inorganic components of fine particulate matter (PM2.5) in ambient air: a critical review. Inhal. Toxicol. 19, 811–832. https://doi.org/10.1080/08958370701402382.

Schroder, K., Sagulenko, V., Zamoshnikova, A., Richards, A.A., Cridland, J.A., Irvine, K. M., Stacey, K.J., Sweet, M.J., 2012. Acute lipopolysaccharide priming boosts inflammasome activation independently of inflammasome sensor induction. Immunobiology 217, 1325–1329. https://doi.org/10.1016/j.imbio.2012.07.020.

Sharma, L., Feng, J., Britto, C.J., Dela Cruz, C.S., 2020. Mechanisms of Epithelial Immunity Evasion by Respiratory Bacterial Pathogens. Front. Immunol. 11, 91. https://doi.org/10.3389/fimmu.2020.00091.

Shin, S.H., Ye, M.K., Hwang, Y.J., Kim, S.T., 2013. The effect of Asian sand dust-activated respiratory epithelial cells on activation and migration of eosinophils. Inhal. Toxicol. 25, 633–639. https://doi.org/10.3109/08958378.2013.826755.

Skuland, T., Lag, M., Gutleb, A.C., Brinchmann, B.C., Serchi, T., Ovrevik, J., Holme, J.A., Refsnes, M., 2020. Pro-inflammatory effects of crystalline- and nano-sized non-crystalline silica particles in a 3D alveolar model. Part. Fibre Toxicol. 17, 13. https://doi.org/10.1186/s12989-020-00345-3.

Spindler, G., Grüner, A., Müller, K., Schlimper, S., Herrmann, H., 2013. Long-term size-segregated particle (PM10, PM2.5, PM1) characterization study at Melpitz – influence of air mass inflow, weather conditions and season. J. Atmos. Chem. 70, 165–195. https://doi.org/10.1007/s10874-013-9263-8.

Sun, H., Shamy, M., Kluz, T., Munoz, A.B., Zhong, M., Laulicht, F., Alghamdi, M.A., Khoder, M.I., Chen, L.C., Costa, M., 2012. Gene expression profiling and pathway analysis of human bronchial epithelial cells exposed to airborne particulate matter collected from Saudi Arabia. Toxicol. Appl. Pharmacol. 265, 147–157. https://doi.org/10.1016/j.taap.2012.10.008.

Tam, W.W., Wong, T.W., Wong, A.H., Hui, D.S., 2012. Effect of dust storm events on daily emergency admissions for respiratory diseases. Respirology 17, 143–148. https://doi.org/10.1111/j.1440-1843.2011.02056.x.

Taylor, K., Foster, M.L., Law, J.M., Centeno, J.A., Fornero, E., Henderson, M.S., Trager, S. A., Stockelman, M.G., Dorman, D.C., 2013. Assessment of geographical variation in the respiratory toxicity of desert dust particles. Inhal. Toxicol. 25, 405–416. https://doi.org/10.3109/08958378.2013.797524.

Val, S., Liousse, C., Doumbia el, H.T., Galy-Lacaux, C., Cachier, H., Marchand, N., Badel, A., Gardrat, E., Sylvestre, A., Baeza-Squiban, A., 2013. Physico-chemical characterization of African urban aerosols (Bamako in Mali and Dakar in Senegal) and their toxic effects in human bronchial epithelial cells: description of a worrying situation. Part. Fibre Toxicol. 10, 10. https://doi.org/10.1186/1743-8977-10-10.

van Berlo, D., Knaapen, A.M., van Schooten, F.J., Schins, R.P., Albrecht, C., 2010. NF-kappaB dependent and independent mechanisms of quartz-induced proinflammatory activation of lung epithelial cells. Part. Fibre Toxicol. 7, 13. https://doi.org/10.1186/1743-8977-7-13.

van Pinxteren, D., Fomba, K.W., Spindler, G., Muller, K., Poulain, L., Iinuma, Y., Loschau, G., Hausmann, A., Herrmann, H., 2016. Regional air quality in Leipzig, Germany: detailed source apportionment of size-resolved aerosol particles and comparison with the year 2000. Faraday Discuss. 189, 291–315. https://doi.org/10.1039/c5fd00228a.

Verma, D.K., Shaw, D.S., 2001. A comparison of international silica (α-quartz) calibration standards by Fourier transform–infrared spectrophotometry. Ann. Occup. Hyg. 45, 429–435. https://doi.org/10.1093/annhyg/45.6.429.

Wessels, A., Birmili, W., Albrecht, C., Hellack, B., Jermann, E., Wick, G., Harrison, R.M., Schins, R.P., 2010. Oxidant generation and toxicity of size-fractionated ambient particles in human lung epithelial cells. Environ. Sci. Tech. 44, 3539–3545. https://doi.org/10.1021/es9036226.

Wilfong, E.R., Lyles, M., Rietcheck, R.L., Arfsten, D.P., Boeckman, H.J., Johnson, E.W., Doyle, T.L., Chapman, G.D., 2011. The acute and long-term effects of Middle East sand particles on the rat airway following a single intratracheal instillation. J. Toxicol. Env. Heal. A 74, 1351–1365. https://doi.org/10.1080/15287394.2010.516239.

Yang, H.H., Duan, J.X., Liu, S.K., Xiong, J.B., Guan, X.X., Zhong, W.J., Sun, C.C., Zhang, C.Y., Luo, X.Q., Zhang, Y.F., Chen, P., Hammock, B.D., Hwang, S.H., Jiang, J. X., Zhou, Y., Guan, C.X., 2020. A COX-2/sEH dual inhibitor PTUPB alleviates lipopolysaccharide-induced acute lung injury in mice by inhibiting NLRP3 inflammasome activation. Theranostics 10, 4749–4761. https://doi.org/10.7150/thno.43108.

Zhang, Y., Li, X., Grailer, J.J., Wang, N., Wang, M., Yao, J., Zhong, R., Gao, G.F., Ward, P. A., Tan, D.X., Li, X., 2016b. Melatonin alleviates acute lung injury through inhibiting the NLRP3 inflammasome. J. Pineal Res. 60, 405–414. https://doi.org/10.1111/jpi.12322.

Zhang, X., Zhao, L., Tong, D., Wu, G., Dan, M., Teng, B., 2016a. A Systematic Review of Global Desert Dust and Associated Human Health Effects. Atmos. 7, 158. https://doi.org/10.3390/atmos7120158.

Zhou, Y.-M., Zhong, C.-Y., Kennedy, I.M., Leppert, V.J., Pinkerton, K.E., 2003. Oxidative stress and NFκB activation in the lungs of rats: a synergistic interaction between soot and iron particles. Toxicol. Appl. Pharm. 190, 157–169. https://doi.org/10.1016/S0041-008X(03)00157-1.

2.7 Supplemental material

Table S1. Primers for qPCR

Gene		Sequence (5′ → 3′)	Working conc. (nM)		Amplicon length (bp)	Primer efficiency (%)	
			MyiQ	QS3		MyiQ	QS3
βACTIN	fw	CCTGGCACCCAGCACAAT	60	200	70	90.3	81.2
	rv	GCCGATCCACACGGAGTACT	60	200			
IL6	fw	TCATCACTGGTCTTTTGGAG	200	200	161	92.3	80.2
	rv	GTCAGGGGTGGTTATTGC	200	200			
IL8	fw	ACTCCAAACCTTTCCACCC	60	200	168	91.2	83.7
	rv	CCCTCTTCAAAAACTTCTCCAC	60	200			
HMOX1	fw	ATGACACCAAGGACCAGAGCC	200	200	151	91.6	86.9
	rv	GTAAGGACCCATCGGAGAAGC	200	200			
APE1/REF1	fw	CTGCCTGGACTCTCTCATCAATAC	200	200	118	92.3	94.6
	rv	CCTCATCGCCTATGCCGTAAG	200	200			
γGCS	fw	TTGCAGGAAGGCATTGATCA	200	200	101	103.0	89.3
	rv	GCATCATCCAGGTGTATTTTCTCTT	200	200			
NQO1	fw	AACCACGAGCCCAGCCAAT		200	177		96.3
	rv	TGGCATAGAGGTCCGACTCC		200			

MyiQ: MyiQ™ cycler (Bio-Rad), QS3™: QuantoStudio 3 device (Thermo Fisher Scientific)

Table S2. Content of metals in Saharan dust analyzed by total reflection X-ray fluorescence.

Compound	Content in µg/g
K	7755.9
Ca	14171.9
Sc	10.3
Ti	847.9
V	47.3
Cr	336.4
Mn	536.7
Fe	37238.2
Co	72.9
Ni	250.7
Cu	6.9
Zn	89.9
As	0.0
Se	0.9
Br	0.9
Rb	79.8
Sr	228.2
Mo	132.0
Ru	61.7
In	13.5
Sb	455.3
Ba	263.4
La	204.1
Ce	147.3
Pb	54.1

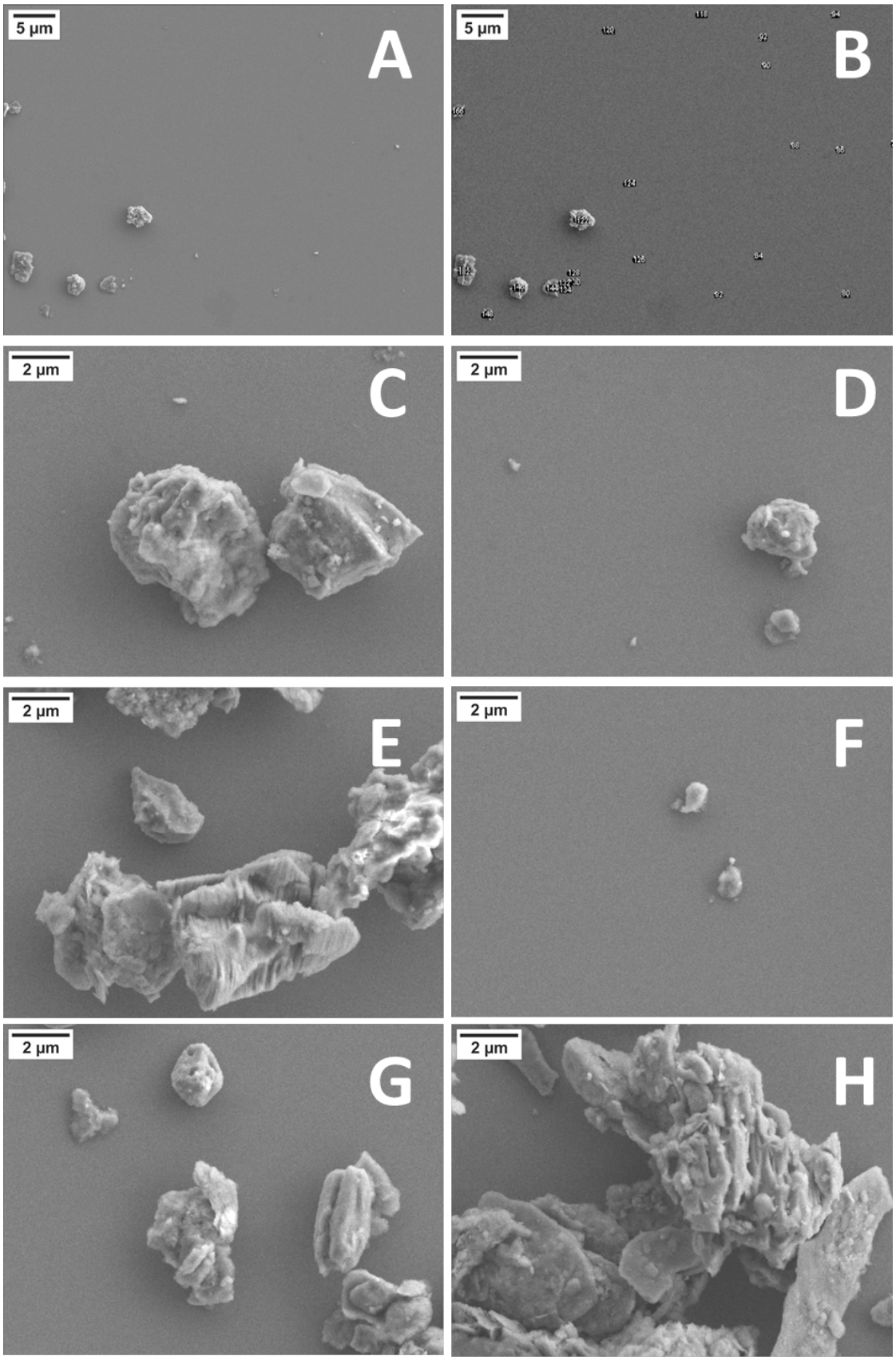

Caption of Figure S1 on the next page.

Figure S1. Exemplary scanning electron microscope images of Saharan dust. A Saharan dust suspension in dH_2O was sonicated and an amount of 15 µL was pipetted onto a single-crystalline Si wafer. After drying, images were obtained at 1 kx nominal magnification (images with 4048 x 3790 pixel, pixel size: 31.0 nm). Image **A** shows an excerpt from an image used for size determination. Image **B** shows the same area after size determination using ImageJ. To visualize the shape and structure of SD, further images with increased zoom are provided (**C-H**).

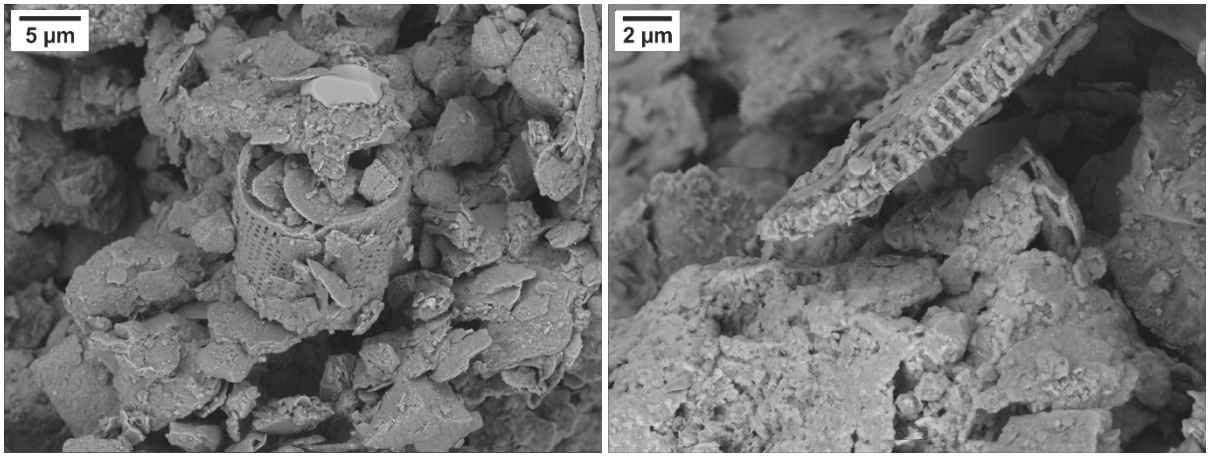

Figure S2. Scanning electron microscope images of diatomaceous earth in Saharan dust. Saharan dust was transferred onto a stub with conductive carbon tape. Images were obtained at a nominal magnification of 2.5 kx (left panel, images with 2024 x 1894 pixel, pixel size: 24.8 nm) and 5 kx (right panel, images with 2024 x 1894 pixel, pixel size 12.4 nm).

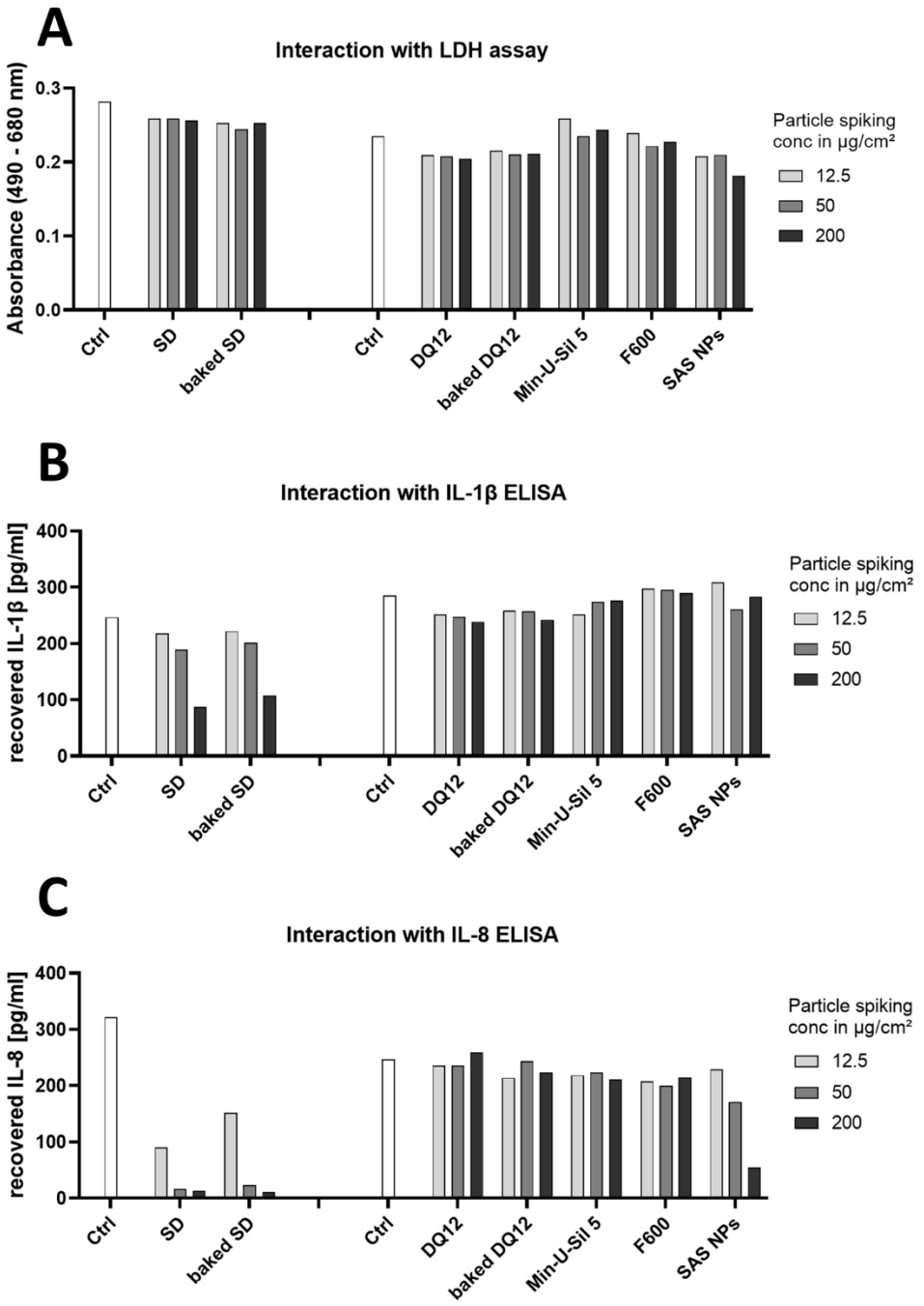

Figure S3. Interferences with the LDH assay, interleukin-1β ELISA, and interleukin-8 ELISA. Diluted lysate of A549 cells, as well as a mixture of 1000 pg/mL recombinant IL-1β and 1000 pg/mL recombinant IL-8, were spiked with 12.5, 50, and 200 µg/cm² of SD, quartz dusts, or SAS NPs. Bovine serum albumin was added to SD samples and additional control samples 30 min before the end of incubation time. The LDH assay was performed on the lysates after 24 h of incubation (**A**). The cytokine solutions were collected after 24 h of incubation and the recoveries of IL-1β (**B**) and IL-8 (**C**) were assessed via ELISA.

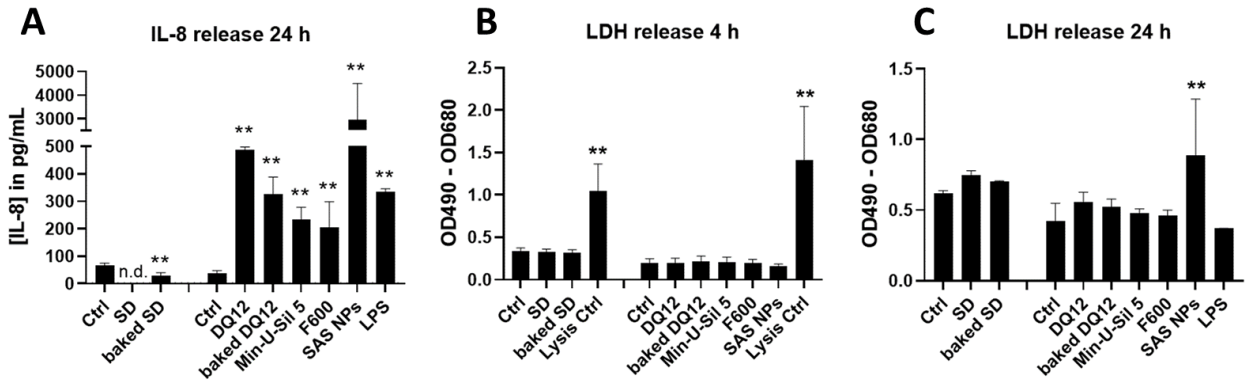

Figure S4. IL-8 and LDH releases from A549 cells. A549 cells were exposed to SD, quartz dusts, or SAS NPs at a concentration of 50 µg/cm² for 4 h (**B**) and 24 h (**A, C)** or to 10 µg/mL LPS for 24 h. To minimize interference, bovine serum albumin was added to SD samples and to an additional control sample 30 min before the end of incubation time. For lysis controls, 0.5% Triton-X 100 was used. The LDH assay was performed on the supernatants (**B, C**). Simultaneously, the IL-8 concentrations in supernatants (**A**) were assessed via ELISA. The values are plotted as means ± standard deviation of N=3-4 independent experiments. Mixed-effects models with Šídák's post hoc test were calculated (**p≤0.01). n.d.: not detected.

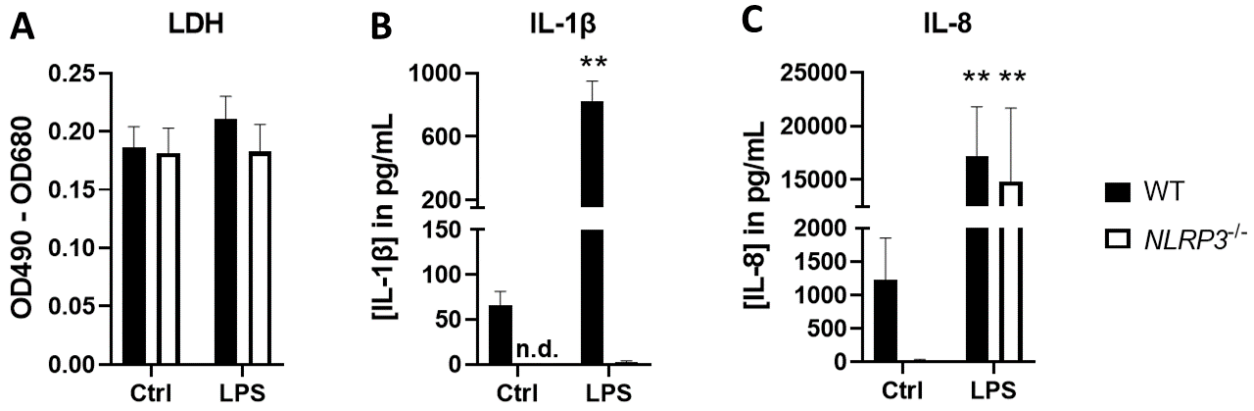

Figure S5. LPS effects on wild type and *NLRP3*$^{-/-}$ THP-1 cells as in Busch et al. (2022)[i]. Wild type (WT) and *NLRP3*$^{-/-}$ THP-1 cells were exposed to 10 ng/mL LPS for 24 h. The supernatants were collected to perform the LDH assay (**A**) and to measure the concentrations of IL-1β (**B**) and IL-8 (**C**) The values are plotted as means ± standard deviation of N=5 independent experiments. A mixed-effects model with Šídák's post hoc test was calculated together with the data from particle exposure (Figure 7) (**p≤0.01). n.d.: not detected.

[i] Busch, M., Bredeck, G., Waag, F., Rahimi, K., Ramachandran, H., Bessel, T., Barcikowski, S., Herrmann, A., Rossi, A., Schins, R.P.F., 2022. Assessing the NLRP3 Inflammasome Activating Potential of a Large Panel of Micro- and Nanoplastics in THP-1 Cells. Biomolecules 12, https://doi.org/10.3390/biom12081095

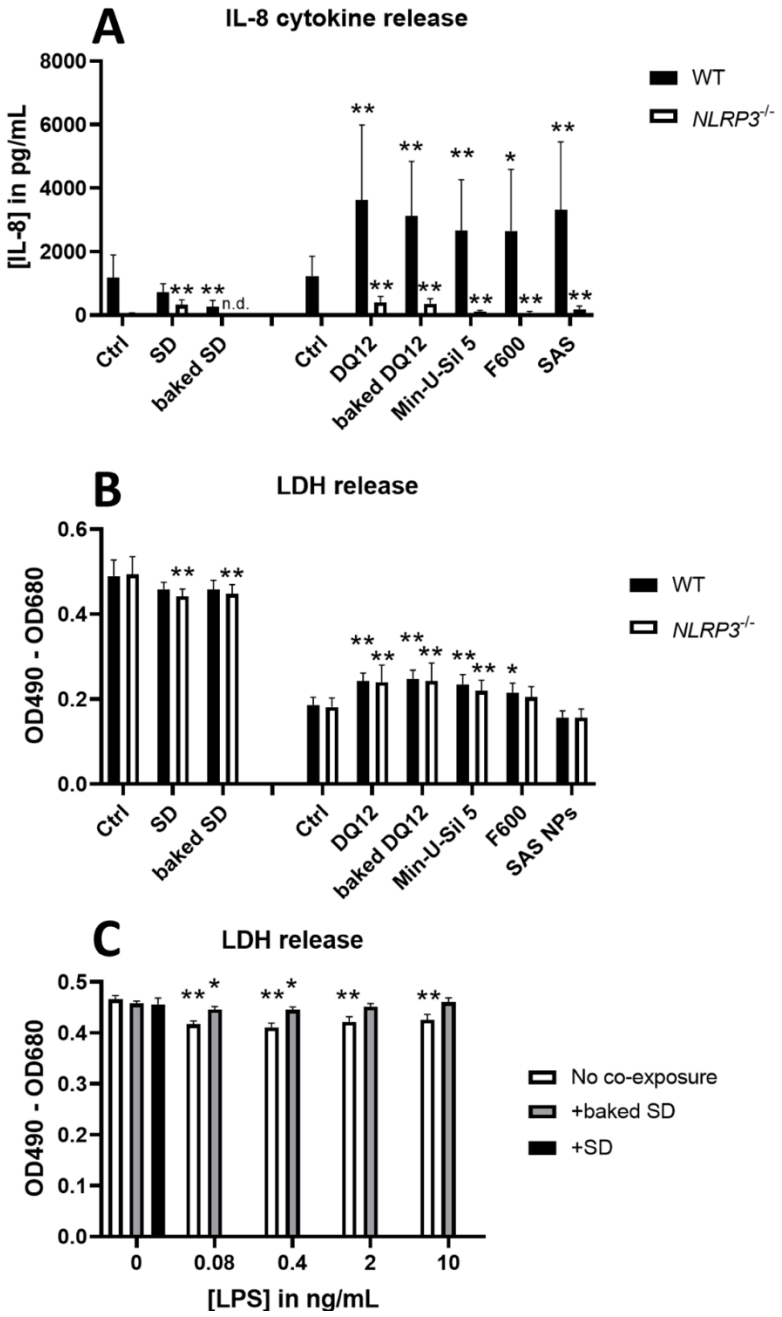

Figure S6. IL-8 and LDH releases from THP-1 cells. Wild type (WT) and *NLRP3*$^{-/-}$ THP-1 cells were exposed to SD, quartz dusts, or SAS at a concentration of 50 µg/cm² for 24 h (**A**, **B**). Additionally, WT THP-1 cells were exposed to LPS concentrations between 0 and 10 ng/mL without co-exposure or co-exposed to 50 µg/cm² SD or baked SD (**C**). To minimize interference, bovine serum albumin was added to all samples exposed to SD and baked SD (**A-C**), to an additional control sample (**A, B**), and to the corresponding LPS exposed samples (**C**) 30 min before the end of incubation time. The LDH assay was performed on the supernatants (**B, C**). The concentrations of IL-8 in the supernatants (**A**) were assessed via ELISA. The values are plotted as means ± standard deviation of N≥3 independent experiments. Mixed-effects models with Šídák's post hoc test were calculated together with the data from LPS exposure (Figure S5A) (*p≤0.05; **p≤0.01) (**A, B**). A mixed-effects model with Dunnett's post hoc test was calculated using unexposed cells as control for all other conditions (*p≤0.05; **p≤0.01) (**C**).

3 Inflammatory properties of respirable and inhalable Saharan dusts in relation to dust events and composition: an in vitro study in human macrophages

Gerrit Bredeck,[a] Eduardo J. dos Santos Souza,[b] Claudia Wigmann,[a] Khanneh Wadinga Fomba,[b] Hartmut Herrmann,[b] Roel P. F. Schins[a]

[a]*IUF – Leibniz Research Institute for Environmental Medicine, Düsseldorf, Germany*

[b]*Atmospheric Chemistry Department (ACD), Leibniz-Institute for Tropospheric Research (TROPOS), Leipzig, Germany*

Manuscript submitted to Environmental Health Perspectives

Author contribution: The author of this thesis planned and performed the extraction of dust samples, quantification of endotoxin contents, as well as *in vitro* experiments, prepared the graphs, interpreted and discussed the results, and wrote the manuscript. Relative contribution: about 70%.

3.1 Abstract

Background: Although desert dusts are major air pollutants promoting morbidity and mortality, it is exempt from regulations. The health effects of desert dusts have been related to their inflammatory properties, which vary between source regions. It remains unclear which constituents cause this variability. Moreover, whether long-range transported desert dusts potentiate the hazardousness of local particulate matter (PM) is still unresolved.

Objectives: We assessed the influence of long-range transported desert dusts on the inflammatory potency of $PM_{2.5}$ and PM_{10} collected in Cabe Verde and examined the associated constituents.

Methods: During a reference period and two Saharan dust events, 63 $PM_{2.5}$ and PM_{10} samples were collected. The contents of water-soluble ions, elements, and organic and elemental carbon were measured in all samples and endotoxins in selected PM_{10} samples. PM-induced inflammatory cytokine releases from differentiated THP-1 macrophages were evaluated. The association of interleukin (IL)-1β release with PM composition was assessed using principal component regressions.

Results: We observed similar trends of IL-1β, IL-8, and tumor necrosis factor α (TNFα) inductions. Due to the interference of dusts with IL-8 detection and because of low constitutive TNFα release, only normalized IL-1β releases were well-reproducible. $PM_{2.5}$ from both dust events and PM_{10} from one dust event caused higher IL-1β release than $PM_{2.5}$ and PM_{10} from the reference period. The transition metal iron in $PM_{2.5}$ was positively associated with IL-1β release. Endotoxins in PM_{10} were associated with the intra but not inter-event variability in IL-1β release.

Discussion: Our results indicate considerable variability in the inflammatory potency of desert dusts in association with the iron content of $PM_{2.5}$ and endotoxins in PM_{10}. Our study also suggests that long-range transported desert dusts can amplify the hazardousness of local air pollution. The increasing inflammatory potency of respirable and inhalable PM from desert dust events warrants regulatory measures and risk mitigation strategies.

3.2 Introduction

According to the World Health Organization (WHO) (2022) 99% of people worldwide are exposed to pollution above air quality limit values. The estimated toll is 6.7 million premature deaths annually. One source of air pollution is aerosolized desert dust, of which globally over 50% can be attributed to emissions from the Saharan desert (Ginoux et al., 2012; Middleton, 2017; Washington et al., 2003). Due to long-range transport, Saharan dust (SD) can be transported as

far as the eastern parts of the U.S. where it exacerbates respiratory morbidities as has been shown in an epidemiological study on subjects with chronic obstructive pulmonary disease (COPD) (Gutierrez et al., 2020).

The difficulty in protecting people from the adverse health effects caused by desert dust exposure is that it can obviously not be regulated like anthropogenic pollutants. In addition, regulations in the U.S. and the European Union exempt authorities from taking action on exceeded particulate matter (PM) threshold concentrations if exceedances are attributable to desert dusts (Environmental Protection Agency (EPA), 1971; European Commission, 2022; European Parliament and Council, 2008), although epidemiological studies have proven that desert dust exposure increases respiratory morbidity and mortality (Achakulwisut et al., 2019; Gutierrez et al., 2020; Kashima et al., 2016; Lwin et al., 2023; Mallone et al., 2011; Stafoggia et al., 2016). Instead of regulatory exemptions, risk mitigation strategies are required to alert affected populations of hazardous desert dust events and prevent exposure (Fussell and Kelly, 2021), for instance by advising against outdoor activities. In order to enable risk mitigation strategies, hazardous desert dust events need to be identified.

However, it is uncertain which physicochemical properties render desert dusts toxic and, thus, hazardous. Former studies on particulate matter (PM) revealed that not only mass but especially composition and size determine toxicity. For instance, endobronchial instillation studies in humans demonstrated that metal-rich PM caused greater lung damage, oxidant radical generation, and inflammatory cytokine release (Ghio and Devlin, 2001; Schaumann et al., 2004). Two *in vitro* studies on human bronchial epithelial BEAS-2B cells have also associated the potency of desert dust to induce oxidative stress and inflammatory cytokines with metals (Rodriguez-Cotto et al., 2015; Rodríguez-Cotto et al., 2013). However, Pardo et al. (2017) and Val et al. (2013) argued that there was no metal-mediated induction of oxidative stress upon desert dust exposure of rat alveolar NR8383 macrophages and human bronchial epithelial 16HBE14o$^-$ cells, respectively. Further examples of potentially harmful desert dust constituents are sulfate (Hiyoshi et al., 2005; Ichinose et al., 2005) and elemental carbon (EC) (Bredeck et al., 2023a; Lei et al., 2004). The involvement of sulfate in the inflammatory potency of desert dusts was assessed in mouse instillation studies that came to contradictory results (Hiyoshi et al., 2005; Ichinose et al., 2005). EC can stem from anthropogenic sources such as diesel exhaust which is well-known to cause pulmonary inflammation (Abe et al., 2000; Miyabara et al., 1998; Nordenhäll et al., 2000).

While several studies have shown that desert dusts from different sources vary in their toxicity (Ghio et al., 2014; Ichinose et al., 2005; Ichinose et al., 2008; Taylor et al., 2013), the literature is inconclusive on whether desert dust events increase the intrinsic toxicity of the ambient air

pollution cocktail. Val et al. (2013) reported that SD events weakened the potency of ultrafine, fine, and coarse urban dust from Bamako (Mali) to induce oxidative stress markers and inflammatory cytokines in 16HBE14o$^-$ cells. Contrarily, Rodríguez-Cotto et al. (2013, 2015) compared organic extracts of $PM_{2.5}$ and PM_{10} collected in Puerto Rico during episodes with and without SD. These authors found higher induction of oxidative stress markers and cytokines in BEAS-2B cells for extracts of samples with SD.

Here, we assessed the release of the inflammatory cytokines interleukin (IL)-1β, tumor necrosis factor α (TNFα), and IL-8. We chose these cytokines based on our previous studies on SD (Bredeck et al., 2023a; Bredeck et al., 2023b) and consensus on the implications of these cytokines in particulate air pollution induced lung diseases. IL-1β release depends on the NLRP3 inflammasome-caspase-1 pathway (Martinon et al., 2002; Thornberry et al., 1992), which participates in mediating the inflammatory potency of SD (Bredeck et al., 2023a; Bredeck et al., 2023b). Mouse studies have proven that IL-1β conveys silica dust-induced lung fibrosis (Cassel et al., 2008; Dostert et al., 2008). IL-1β has also been associated with acute lung injury (Grailer et al., 2014; Zhang et al., 2016b), asthma (Hosoki et al., 2015; Jarjour and Busse, 1995; Okada et al., 1995), and COPD (Lappalainen et al., 2005; Zou et al., 2017). TNFα is the other early cytokine connected to silica dust-induced lung fibrosis (Piguet et al., 1990). TNFα has also been associated with acute lung injury (Stephens et al., 1988), dust storm-mediated asthma (Ghozikali et al., 2022), and air pollution-related COPD (Chen et al., 2022; Yang et al., 2014). Like IL-1β, TNFα levels have been shown to be elevated upon desert dust exposure (Bredeck et al., 2023b; Ghio et al., 2014; Ichinose et al., 2005). IL-8 is an early chemokine that others (Honda et al., 2014; Kim et al., 2021; Shin et al., 2013) and ourselves (Bredeck et al., 2023a; Bredeck et al., 2023b) demonstrated to be induced by desert dusts. IL-8 mediates neutrophil recruitment and activation (Peveri et al., 1988; Schröder et al., 1987) and has been associated with respiratory distress syndrome (Ikuta et al., 1996), asthma (Hosoki et al., 2015; Kikuchi et al., 2009), and COPD (Aaron et al., 2001; Pease and Sabroe, 2002). We used THP-1 macrophages to assess the releases of these cytokines in response to a wide panel of dust samples. In a sub-study, we used primary human alveolar macrophages. Application of primary cells for the whole panel would not have been feasible due to the limited number of cells available from a single donor.

The first aim of our study was to determine how much the intrinsic inflammatory potency of $PM_{2.5}$ and PM_{10} varied depending on the influence of long-distance transported SD from two dust events. We further aimed to determine how much the intrinsic inflammatory potency of dust varied locally, i.e. comparing four sampling stations. Finally, we sought to identify dust constituents that contributed to inflammatory potency. For these purposes, we assessed 63 $PM_{2.5}$ and PM_{10}

samples, collected either during a reference period without SD or during dust events with high SD concentrations. We handled $PM_{2.5}$ and PM_{10} in parallel but analyzed them separately to gain information on both respirable and inhalable dust.

3.3 Methods

The used reagents and resources are listed in Table S3.1.

3.3.1 Dust samples

$PM_{2.5}$ and PM_{10} samples were collected at four stations on the Cape Verde islands. On each of the islands Praia (stations 1 and 2) and São Vicente (stations 3 and 4), there were a non-urban station (1 and 3) and an urban station (2 and 4) (see Figure 3.1). The stations were located at the following coordinates: 14.990° N, 23.471° W (station 1), 14.909° N, 23.515° W (station 2), 16.864° N, 24.867° W (station 3), 16.874° N, 24.984° W (station 4). At each station, a $PM_{2.5}$ and a PM_{10} Digitel DHA 80 high-volume sampler were operated. On both islands, dust samples were collected during a reference period with low dust concentrations (January 26 to 30, 2022) and a dust event (February 10 to 13, 2022), hereinafter dust event 1. On São Vicente, further dust samples were collected during another dust event (February 17 to 19, 2022), hereinafter dust event 2. Each sampling day lasted from noon to noon (UTC-1). Each sample was collected on one, two, or three Ahlstrom micro-quartz fiber filters MK 360 for a duration of 20-24 h. After sampling, filters were partitioned, protected from light, frozen at -20°C, shipped at -80°C, and stored at -20°C. For physicochemical analysis, pieces of filters belonging to the same sample were analyzed separately, and mean values were calculated subsequently. For *in vitro* toxicology, pieces of filters belonging to the same sample were pooled during preparation.

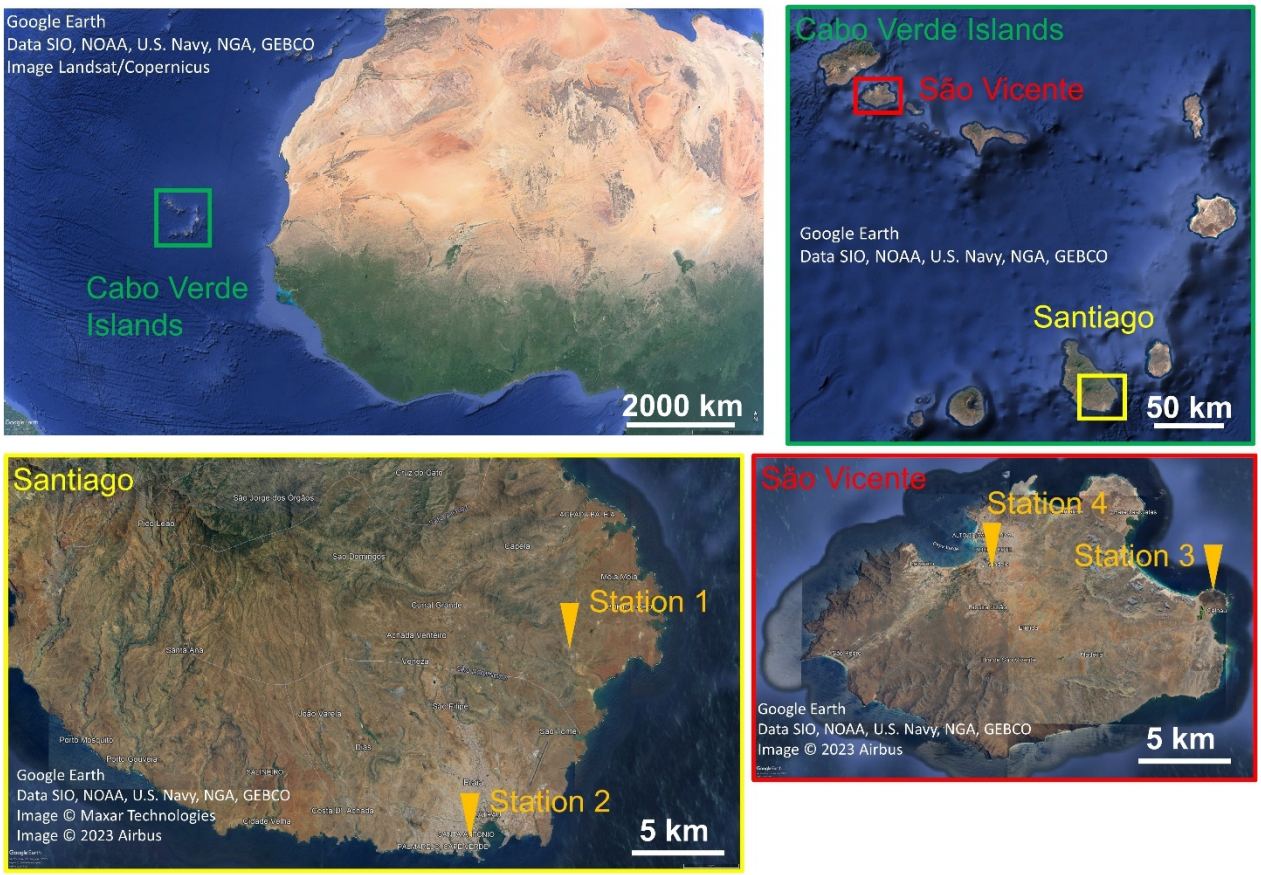

Figure 3.1. Sampling stations on the Cape Verde islands. Desert dust samples were collected on the Cape Verdean islands of Santiago and São Vicente. On each of these two islands, two sampling stations were operated. Maps were downloaded from Google Earth Pro (v7.3.6.9345).

The collected PM mass was gravimetrically determined using a Mettler Toledo AT261 Delta Range balance with an accuracy of 0.01 mg. To determine mass concentrations, PM masses were divided by the sampled volume. At each sampling station, the PM concentrations during the dust events were at least 2.5-fold higher than during the reference period (Figure 3.2). During the reference period, $PM_{2.5}$ and PM_{10} concentrations were 5-23 µg/m³ and 18-59 µg/m³, respectively, while during dust events, the concentrations reached 28-144 µg/m³ and 114-347 µg/m³, respectively. During the reference period and dust event 1, $PM_{2.5}$ and PM_{10} concentrations on the island of Santiago were higher than on São Vicente.

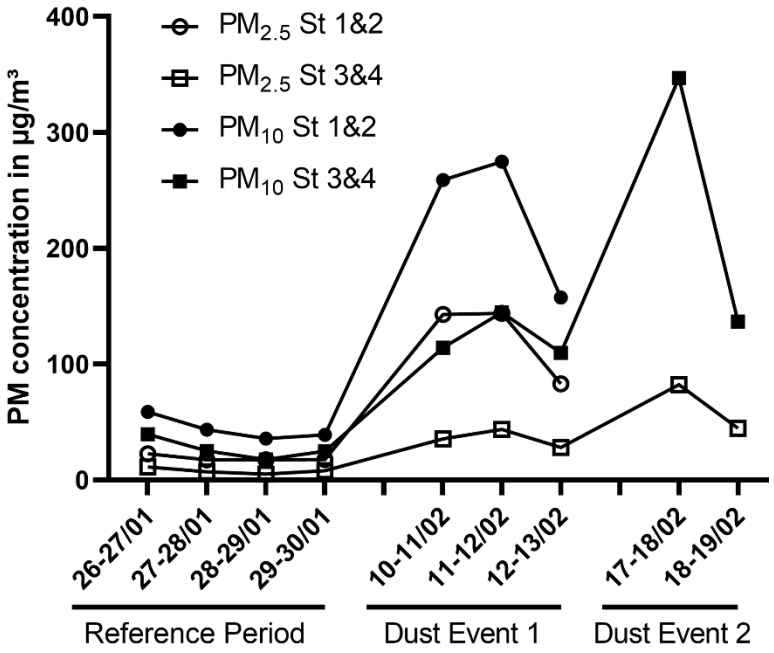

Figure 3.2. Atmospheric $PM_{2.5}$ and PM_{10} concentrations. $PM_{2.5}$ and PM_{10} were collected during a reference period without Saharan dust (January 26 to 30, 2022) and two dust events with Saharan dust influence (February 10 to 13, 2022 and February 17 to 19, 2022). Two sampling stations (St) each were operated on the Cape Verdean islands of Santiago (St 1&2) and São Vicente (St 3&4). PM concentrations were derived from the sampled mass divided by the sampled volume of air. Thus, the determined concentrations were averages over 20-24 h. Each point represents the mean value of the two stations from the same island. Abbreviations: St, sampling stations. Dates: DD/MM/YYYY.

As a reference, an SD sample with 99% of particles < 10 µm was used that had been collected with a cyclone sampler at station 3 during a dust event from December 29, 2016 to January 6, 2017. The sample was collected and characterized as previously described in detail (Bredeck et al., 2023a). It was tested on primary human alveolar macrophages in pristine conditions as well as after heat-destruction of microbial constituents at 220°C overnight, hereinafter referred to as “baked” sample.

3.3.2 Quantification of water-soluble ions

To quantify water-soluble ions, three PM-loaded filter pieces with an area of 3.1 cm² were extracted with deionized water by shaking for two hours. A 0.45 µm unidirectional syringe filter was used to remove insoluble matter from the extract, and the filtrate was analyzed. The Dionex ICS-3000 ion chromatography system was used. The system was equipped with automatic KOH and methane sulfonic acid (MSA^-) eluent generators for anions and cations, respectively, as well as a micro-membrane removal system. Blank field filters were assessed using the same methodology, and the values were discounted from those of PM samples (Iinuma et al., 2009).

3.3.3 Quantification of elements

Total reflection X-ray fluorescence (TXRF) was used to quantify elements as previously described in detail (Dos Santos Souza et al., 2021; Fomba et al., 2020). Briefly, PM-loaded and field blank filter pieces with an area of 1.5 cm² were digested in a mixture of 0.375 mL HCl and 1.125 mL HNO_3 using a CEM Mars 6 microwave. Internal standards containing Ga/Co were added to 10 µL of the digested solution before its application on siliconized quartz carriers (Fomba et al., 2013). A Bruker S4 T-STAR instrument was used to measure the PM and blank filter samples. Due to the high values of Al and Si in the field blank filters, these elements were not considered in the further interpretation of the results.

3.3.4 Quantification of organic and elemental carbon

To determine organic carbon (OC) and elemental carbon (EC), we applied a thermal-optical method using the Sunset Laboratory Dual-Optical Carbonaceous Analyzer OCEC – Model 5L. In preparation, PM-loaded filter pieces with an area of 1.5 cm² were preheated at 105°C for 24 h. In the first step of thermal desorption, the samples were gradually heated to 850 °C in an inert He atmosphere. Then samples were gradually heated to 850 °C in an oxidizing He/O_2 atmosphere. After the catalytic methanation of CO_2, a flame ionization detector was used to quantify methane. A charring correction was applied using the EUSAAR2 temperature protocol (Cavalli et al., 2009).

3.3.5 Preparation of desert dust samples for in vitro toxicity testing

Using a scalpel, a filter piece of 10-40 cm² was cut. To determine the size area of the filter and the area covered with dust, the filter was placed on a black square of 15.0x15.0 cm which was placed on a white sheet of paper of 21.0x29.7 cm. To control the lighting, a box of 36x58x32 cm (height x width x depth) having a hole in the upper side was placed over the filter. A photo was acquired with an iPhone XR or iPhone X with flash, and the sizes of the filter piece and the dust covered area were calculated using a self-programmed macro in ImageJ (v1.53r). Subsequently, the part of the filter not covered with dust was removed according to visual inspection. The filter was cut into smaller pieces of about 5 cm². Per 10 cm² filter area, 2.55 mL endotoxin-free H_2O was advanced into a 50 mL Falcon tube. Every second piece was immersed in endotoxin-free H_2O and sonicated in a Bandelin RK 52 water bath for 5 min. The filter pieces were removed, the residual filter pieces immersed, the sonication repeated and again the filter pieces removed. The extracts were pressed through a 40 µm cell strainer to remove filter material. The filtered extracts were divided into five aliquots and transferred into baked (220°C, overnight) and tared glass vials, frozen at -20°C, and lyophilized at 0.4-0.8 mbar using a Leybold Heraeus LyoVac GT2 set to -30°C. After lyophilization, the extracted dust mass was weighed using a Mettler Toledo XS205

DualRange balance with an accuracy of 0.01 mg. The vials were closed with a butyl injection stopper, crimped, and stored at -20°C. Field blank filters were subjected to the same procedure. Half of the blank filter extract was passed through 40 µm cell strainers, and the other half through 20 µm cell strainers to compare their efficiency in removing filter material.

3.3.6 Cell culture procedure

As described previously (Bredeck et al., 2023a), RPMI-1640 containing L-glutamine and 25 mM 4-(2-hydroxyethyl)-1-piperazineethanesulfonic acid (HEPES) and substituted with 10% fetal calf serum, 1% Penicillin-Streptomycin, 1% Na-pyruvate, 0.7% D-glucose, and 0.1% 2-mercaptoethanol (ME) was used as cell culture medium (CCM) for THP-1 cells. Cells were maintained between $2x10^5$ and $8x10^5$ cells/mL. For experiments, $3x10^6$ cells in 5 mL were differentiated with 100 nM phorbol 12-myristate-13-acetate in 25 cm² flasks for 24 h. Differentiated THP-1 cells were washed with PBS, detached with accutase, collected and diluted in CCM without ME, and seeded into 48-well plates at $5x10^4$ cells in 0.5 mL per well. Cells were used at passages 5 to 15 after thawing.

Primary human alveolar macrophages were purchased from Epithelix Sárl (Geneva, Switzerland). The donor was a 62 years old Caucasian male non-smoker with no reported pathology. Macrophages were thawed, suspended in MucilAir culture medium (Epithelix Sárl), and seeded in 48-well plates at $5x10^4$ cells in 0.5 mL per well. After attachment, the medium was changed to culture medium for alveolar macrophages (CMAM) (Epithelix Sárl).

3.3.7 Exposure procedure

THP-1 cells were exposed within 4 h after seeding. For exposure, CCM without ME containing only 1% FCS, hereinafter exposure medium, was used. To expose THP-1 cells, one aliquot of lyophilized dust was used per independent experiment. The dusts were suspended to 1 mg/mL in exposure medium and sonicated using the Cup Horn configuration of the Branson Sonifier 450 at an output of 240 W and a duty cycle of 0.2 s for 10 min. Exposure medium for controls was sonicated in the same way. The suspensions were diluted to concentrations corresponding to 5 µg/cm². Samples from stations 3 and 4 collected during the reference period and dust event 2 were also diluted to concentrations corresponding to 100 L sampled air/cm². The PM mass corresponding to 100 L of air was derived from the sampled volume of air and the collected PM mass. Cells were exposed for 24 h. To minimize the interference of dusts with the enzyme-linked immuno-sorbent assay (ELISA), 30 min before the end of exposure time, bovine serum albumin (BSA) in Hank's Balanced Salt Solution containing $MgCl_2$ and $CaCl_2$ (HBSS) was added. Per well, 150 µL 47% BSA was added and mixed with the exposure medium resulting in 11% BSA. As

positive control for the lactate dehydrogenase (LDH) assay, 25 µL 10% Triton X-100 in H_2O was added 30 min before the end of exposure. As a positive control for cytokine release, cells were exposed to 10 ng/mL lipopolysaccharides (LPS) for 24 h. Per 48-well plate, the four $PM_{2.5}$ and four PM_{10} samples from one sampling day were tested at 5 µg/cm² and, if applicable, 100 L/cm² as well as a negative control, 10 ng/mL LPS, and optionally the SD sample from 2016-17 at 5 µg/cm². For dust event 2, per 48-well plate, the $PM_{2.5}$ and PM_{10} samples from two sampling days were tested. For each PM sample from 2022, per concentration *N* = 3-4 independent experiments, each with two technical replicates, were performed. The SD sample from 2016-17 was tested in *N* = 8 independent experiments with 2-6 technical replicates. The concentration of 5 µg/cm² was chosen as a relatively low *in vitro* concentration still high enough to potentially trigger cytokine release. Val et al. (2013) assessed desert dust-containing urban PM at 1 µg/cm², 5 µg/cm², and 10 µg/cm² and reported that mostly from 5 µg/cm² significant effects on cytokine expression and release were obtained. Further previous *in vitro* studies, by others (Choi et al., 2015; Ghio et al., 2014; He et al., 2016; Ho et al., 2019; Sun et al., 2012) and ourselves (Bredeck et al., 2023a) used concentrations of at least 10-50 µg/cm², assuming that cells were covered by a layer of at least 3 mm of exposure medium to convert concentrations from µg/mL into µg/cm². The concentration of 100 L/cm² was chosen because it corresponds to concentrations around 5 µg/cm².

Primary human alveolar macrophages were exposed 24 h after changing the medium to CMAM. Baked and pristine SD from 2016-17 was suspended in CMAM to 4 mg/mL. SD suspensions and CMAM for controls were sonicated as described above. SD samples were diluted in CMAM to concentrations corresponding to 10 µg/cm², 30 µg/cm², and 50 µg/cm² and macrophages were exposed for 24 h. The addition of BSA and Triton X-100 and the collection of supernatants were performed as described above. The concentration of 50 µg/cm² corresponded to a former study in which the same pristine and baked sample was tested on THP-1 macrophages (Bredeck et al., 2023a).

3.3.8 LDH cytotoxicity assay

Cytotoxicity was tested via LDH assay. After exposure, 50 µL of supernatants were transferred to 96-well plates. The procedure was as previously described (Busch et al., 2021). Briefly, a mixture of tris(hydroxymethyl)aminomethane (TRIS) buffer (pH 8), β-nicotinamide adenine dinucleotide sodium salt, lithium L-lactate, phenazine methosulfate, and iodonitrotetrazolium chloride was added to the samples. After 16 min at 37°C, the reaction was stopped using 1 M H_2SO_4.

3.3.9 Cytokine quantification by ELISA

The releases of IL-1β, IL-8, and TNFα were determined using DuoSet ELISA kits as previously described (Busch et al., 2021). Briefly, 96-well immuno-plates were coated with primary antibodies in 0.1 M $NaHCO_3$ buffer (pH 8.2). Consecutively, 3% BSA, test samples and standards, secondary antibody, streptavidin-horseradish peroxidase, and TMB Peroxidase EIA Substrate were added. Between the steps, plates were washed with 0.05% Tween-20 in PBS. The color reaction was stopped using 1 M H_2SO_4. Concentrations were interpolated from standard curves using a four-parameter logistic regression in GraphPad Prism (v9.1.0). When the determined concentrations of IL-1β and TNFα were lower than the limit of detection (LOD), half the LODs were used, i.e. 1.95 pg/mL and 7.8 pg/mL, respectively. The determined concentrations were divided by the recovery rates (Table S3.2) to correct for interference with the ELISAs (Bredeck et al., 2023a). To determine recovery rates, recombinant IL-1β, IL-8, and TNFα from the DuoSet ELISA kits were mixed with dust in parallel to cell exposure. The mixtures were incubated, collected, and analyzed in parallel to cells and supernatants.

3.3.10 Quantification of endotoxins

To determine endotoxin contents, the Limulus amebocyte lysate (LAL)-based Pierce Chromogenic Endotoxin Quant Kit was used according to the manufacturer's instructions as described previously (Bredeck et al., 2023a). Briefly, dust samples were suspended to 1 mg/mL, sonicated as described above and diluted to 50 µg/mL. This corresponded to 0.012 – 1.364 cm²/mL filter area. A field blank filter extract concentration of 1.364 cm²/mL was tested in parallel. A standard curve with a range spanning from 0.01 – 0.1 endotoxin units (EU)/mL was generated. To validate the procedure, spiked samples were concurrently examined.

3.3.11 Statistical analysis

PM concentrations and bar charts were plotted using GraphPad Prism (v9.1.0). Statistical analyses were carried out using R (v4.3.0) (R Core Team, 2023). The natural logarithm of cytokine concentrations and normalized cytokine releases was used for all computations. The effect of blank filter exposure on cytokine release was analyzed after stratification of data for cell strainer pore size. Mixed-effects models were applied using the package lmerTest (v3.1.3) and Dunnett's post hoc tests using the package emmeans (v.1.8.6). Exposure was applied as fixed factor and the independent experiment number as random factor. Assessments of dusts were all stratified for $PM_{2.5}$ and PM_{10}. Differences between the dust events were analyzed applying linear models and Holm's post hoc tests using the package emmeans. The linear models were applied to the means of normalized IL-1β releases per sampling day and sampling station with event as predictor

and adjusted for the sampling station. Graphs were created using the packages ggplot2 (v.3.4.3) and ggpubr (v.0.6.0). The analyses of differences between sampling stations were stratified for the reference period and dust event 1. Linear models and Holm's post hoc tests were applied to the means of normalized IL-1β releases per sampling day and sampling station with sampling station as predictor using the package emmeans. Spearman correlation matrices were calculated using the means of normalized IL-1β releases per sampling day and sampling station and depicted using the package ggcorrplot (v0.1.4). Principal component regression was applied separately for water-soluble ion contents and contents of carbonaceous constituents and elements. Principal components accounting for at least 10% of variance were tested for association with the means of normalized IL-1β releases per sampling day and sampling station using linear models. For one PM_{10} reference period sample, the Ni content could not be determined because of contamination during sample preparation. Therefore, the mean value of the other PM_{10} reference period samples was allocated for principal component regressions.

The data belonging to the $PM_{2.5}$ sample collected at Station 1 on 26-27/02/2022 were removed from the analysis of dust composition, comparisons of the reference period and dust events, comparisons of sampling stations, Spearman correlation analyses, and principal component regressions. We considered this sample an artifact causing extraordinarily high cytokine releases because the corresponding PM_{10} sample did not trigger strong cytokine release and no constituent was conspicuously sparse or abundant.

3.4 Results

3.4.1 Dust composition

Each $PM_{2.5}$ and PM_{10} dust sample was analyzed for its content of water-soluble ions, elements, and organic and elemental carbon by ion chromatography, TXRF, and thermal desorption techniques, respectively. For each sampling period, the mean contents are presented in Table 3.1 and Table S3.3. $PM_{2.5}$ from the reference period contained at least 2-fold more Cl^-, SO_4^{2-}, Na^+, NH_4^+, oxalate, K, Zn, P, Ba, Cr, Cu, and V, than $PM_{2.5}$ from dust events. The contents of Fe, OC, and EC were particularly high in $PM_{2.5}$ from dust event 1. The Ca^{2+} and K^+ contents in $PM_{2.5}$ from dust events were about 5-fold higher than in $PM_{2.5}$ from the reference period. PM_{10} from the reference period had relatively high contents of Na^+, Mg^{2+}, Zn, Ba, Ni, and Cl^- whereas dust event samples were more abundant in Fe, Rb, and OC. PM_{10} from dust event 1 was especially rich in Mn, Sr, and Ca^{2+} and PM_{10} from dust event 2 in NH_4^+. SO_4^{2-}, NO_3^- and PO_4^{3-} were most abundant in PM_{10} from the reference period and least in PM_{10} from dust event 2.

Table 3.1. Contents of elements and ions > 10 mg/g and contents of carbonaceous constituents.

		$PM_{2.5}$			PM_{10}		
		RP	**DE1**	**DE2**	**RP**	**DE1**	**DE2**
Elements	K	82.7	22.3	13.3	15.7	16.5	9.7
	Ca	74.2	55.1	41.9	36.8	43.4	25.3
	Zn	53.4	7.5	8.1	7.5	1.6	1.0
	Fe	17.6	34.4	13.7	13.2	36.8	25.9
	P	11.8	2.2	1.4	1.9	1.3	0.74
	Mg	8.7	8.7	10.7	11.1	8.5	6.1
Ions	Cl^-	70.8	23.8	24.3	145.6	45.5	46.2
	SO_4^{2-}	54.5	21.1	23.2	39.8	24.1	18.7
	Na^+	51.1	14.7	16.8	87.2	27.2	27.3
	NO_3^-	19.3	11.5	9.5	24.7	13.6	9.5
	NH_4^+	10.7	3.4	7.2	3.4	3.3	6.1
	Ca^{2+}	3.6	15.5	18.5	12.6	22.7	12.3
Carbon	TC	0.75	1.93	0.96	1.07	3.47	3.09
	OC	0.53	1.59	0.83	0.86	3.11	2.94
	EC	0.22	0.34	0.13	0.21	0.37	0.16

The elemental composition was analyzed by total reflection X-ray fluorescence (TXRF). Water-soluble ions were analyzed by ion chromatography. The carbonaceous constituents were analyzed by thermal desorption techniques. Table S3.3 also contains elements and ions < 10 mg/g.

3.4.2 Blank filter toxicity

To test whether the filter material was cytotoxicity or caused cytokine release, THP-1 cells were exposed to field blank filter extracts that had been passed through cell strainers of 20 µm and 40 µm pore size. None of the tested concentrations of blank filter material induced the cytotoxicity marker LDH release (Figure S3.1). The releases of IL-1β and IL-8 were not affected up to concentrations of 0.512 cm^2/cm^2. The released TNFα concentrations were below the limit of detection for all concentrations of blank filter extracts. Blank filter extracts passed through cell strainers with a pore size of 20 µm tended to trigger higher IL-1β and IL-8 releases than extracts passed through 40 µm cell strainers. Therefore, all dusts extracted from filters were passed through 40 µm cell strainers to remove filter material. When testing extracted PM, the maximum corresponding filter concentration was 0.36 cm^2/cm^2.

3.4.3 Cytotoxicity

To assess if the applied dust concentrations were cytotoxic to THP-1 cells we performed the LDH assay (Figure S3.2). For all tested dust samples as well as for 10 ng/mL LPS, the LDH release was at the level of the negative control.

3.4.4 Cytokine release

Next, we assessed the releases of IL-1β, IL-8, and TNFα upon dust exposure. For dust event 1, the released cytokine concentrations after exposure to 5 µg/cm² $PM_{2.5}$ and PM_{10} are presented in Figure 3.3 and Figure 3.4, respectively. The same data, complemented with the reference period and dust event 2 are presented in Figure S3.3. We additionally assessed dusts collected at stations 3 and 4 during the reference period and dust event 2 at 100 L/cm² (Figure S3.3). The $PM_{2.5}$ and PM_{10} samples that induced IL-1β strongest also had the strongest effects on IL-8 and TNFα.

We used the dust samples of which two different concentrations (i.e. 5 µg/cm² and 100 L/cm²) were tested to confirm the relationship between dust concentration and cytokine release (Figure S3.4). For most $PM_{2.5}$ and PM_{10} samples, the releases of IL-1β increased with increasing concentration. We only observed slightly negative concentration-response relationships for samples of low potency that elevated cytokine releases by less than 1.3-fold compared to the negative control. The same applied to IL-8 releases with the exceptions of the $PM_{2.5}$ and PM_{10} samples collected at station 3 during day 2 of the reference period. For the samples leading to detectable TNFα concentrations, all concentration-response relationships were positive. Yet, due to its constitutively low release levels, TNFα was only detectable for one of eight $PM_{2.5}$ and four of eight PM_{10} samples.

For more accurate comparisons between sampling periods and stations, we normalized IL-1β and IL-8 releases to the corresponding negative controls. This was necessary because we observed a relatively large variability in constitutive cytokine releases when comparing the independent experiments. For IL-1β, these constitutive deviations applied similarly to the controls and dust exposures. In contrast, for IL-8, the normalized releases varied strongly. For example, for the PM_{10} sample collected at station 2 during day 2 of dust event 1 and tested at 5 µg/cm², we determined increases of 2.7, 10.2, and 18.8-fold for the three independent experiments. This high variation may be due to the particularly strong interference of desert dusts with IL-8 ELISAs we reported previously (Bredeck et al., 2023a) and which we also found for the present dust samples (Table S3.2). The interference factor could differ depending on the IL-8 concentration. Since assessing the interference factors of each PM sample for multiple cytokine concentrations was not feasible, we decided not to include normalized IL-8 releases in further analyses. We did not include TNFα, either, because the non-detectable TNFα concentrations of negative controls did not permit normalization. We considered the $PM_{2.5}$ sample collected at Station 1 on 26-27/01/2022 an artifact and excluded it from further analyses (see subsection Statistical analysis).

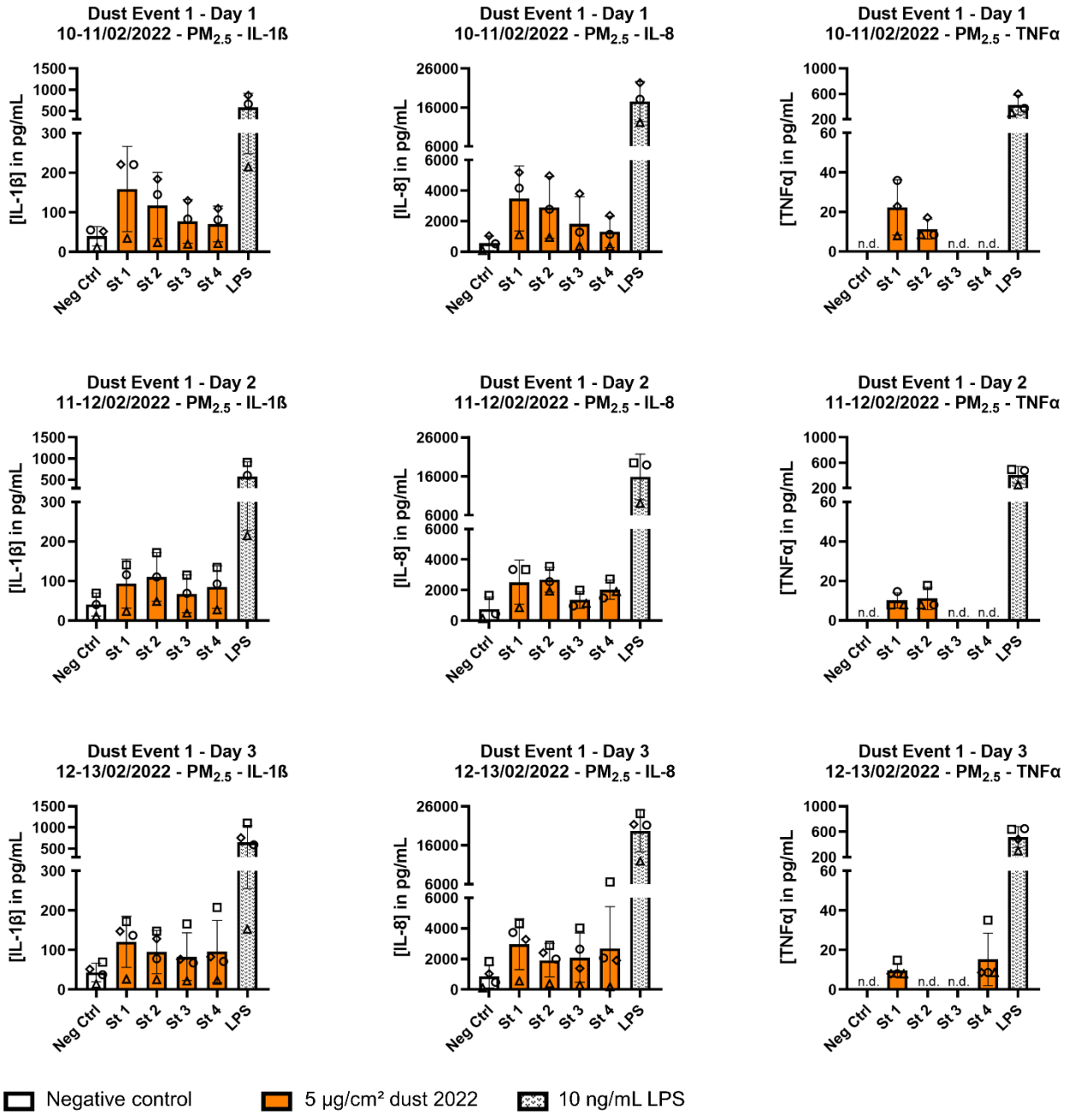

Figure 3.3. IL-1β, IL-8, and TNFα release in response to $PM_{2.5}$ dust exposure. THP-1 cells were exposed to exposure medium as negative control (Neg Ctrl), 10 ng/mL LPS as positive control, and 5 µg/cm² of $PM_{2.5}$ collected in 2022 for 24 h. IL-1β, IL-8, and TNFα concentrations in the supernatants were measured by ELISA. Plotted are mean values with standard deviations of *N* = 3-4 independent experiments. Within each plot, points with the same shape belong to the same independent experiment. Abbreviations: IL, interleukin; LPS, lipopolysaccharides; n.d., not detected; Neg Ctrl, negative control; St, sampling station; TNF, tumor necrosis factor. Dates: DD/MM/YYYY.

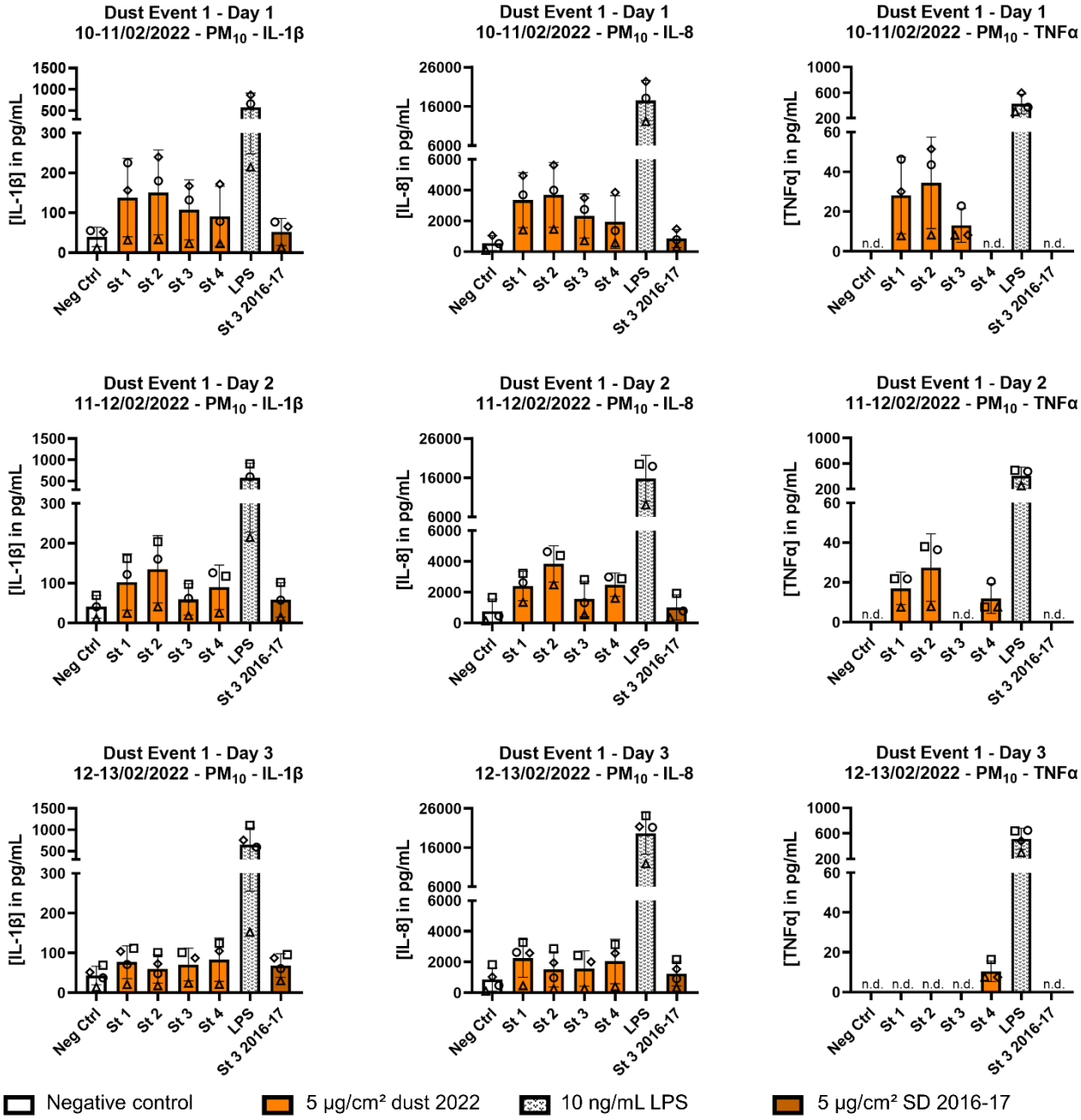

Figure 3.4. IL-1β, IL-8, and TNFα release in response to PM_{10} dust exposure. THP-1 cells were exposed to exposure medium as negative control, 10 ng/mL LPS as positive control, 5 µg/cm² of PM_{10} collected in 2022, and 5 µg/cm² reference Saharan dust (SD) sample collected in 2016-17 for 24 h. IL-1β, IL-8, and TNFα concentrations in the supernatants were measured by ELISA. Plotted are mean values with standard deviations of *N* = 3-4 independent experiments. Within each plot, points with the same shape belong to the same independent experiment. Abbreviations: IL, interleukin; LPS, lipopolysaccharides; n.d., not detected; Neg Ctrl, negative control; SD, Saharan dust; St, sampling station; TNF, tumor necrosis factor. Dates: DD/MM/YYYY.

3.4.5 Comparing reference period and dust events

To assess the intrinsic inflammatory potency of $PM_{2.5}$ and PM_{10} from desert dust events we compared IL-1β releases upon exposure to 5 µg/cm² dust from the reference period, with $PM_{2.5}$ and PM_{10} from dust events (Figure 3.5). $PM_{2.5}$ from both dust events had a higher intrinsic potency to induce IL-1β than $PM_{2.5}$ from the reference period while there was no difference between the two dust events. For PM_{10}, the intrinsic potency to induce IL-1β followed the order reference period < dust event 1 < dust event 2, whereas only the difference between the reference period and dust event 2 reached statistical significance.

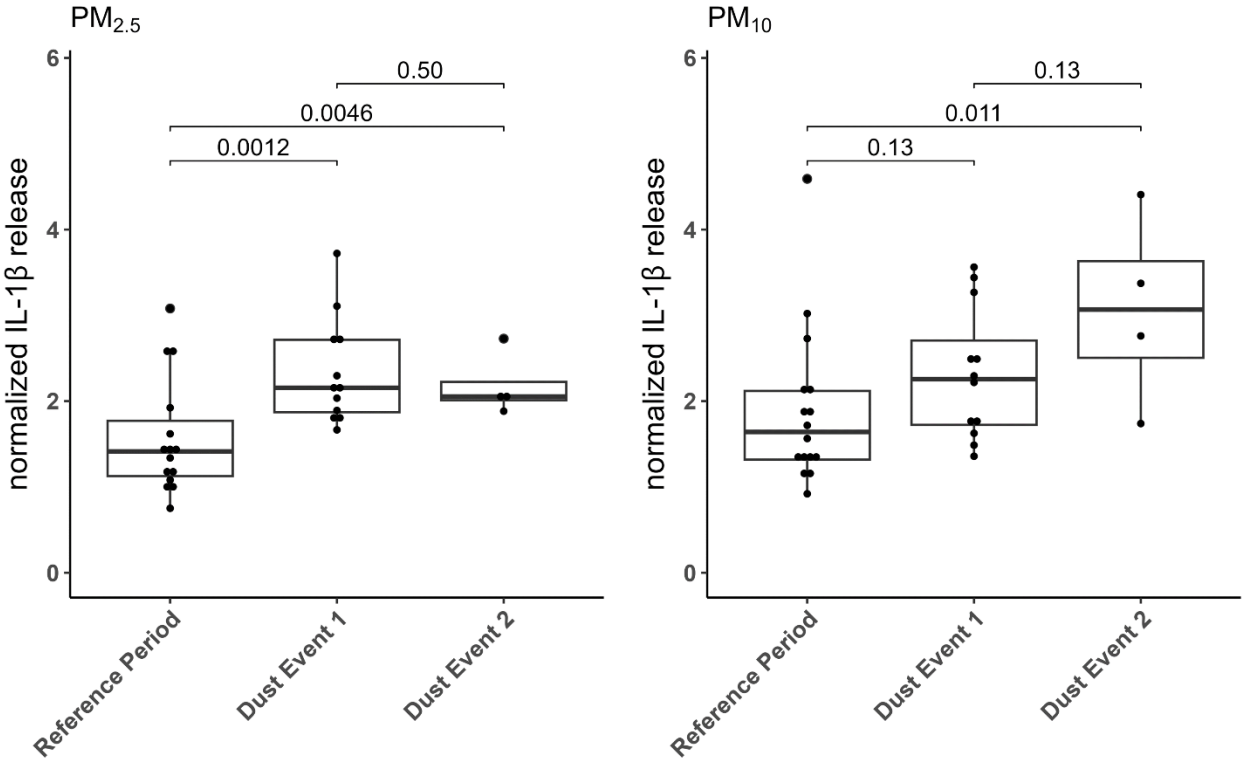

Figure 3.5. Dust event dependent IL-1β release. THP-1 cells were exposed to 5 µg/cm² $PM_{2.5}$ and PM_{10} for 24 h. IL-1β concentrations in the supernatants were measured by ELISA and normalized to unexposed negative controls. Each point represents the mean normalized IL-1β releases of N = 3-4 independent experiments per sampling day and sampling station. *p*-values for the differences between the reference period, dust event 1, and dust event 2 are indicated in the graphs and were calculated by applying a linear model with Holm's post hoc test to the natural logarithm of the mean normalized IL-1β releases. The linear models with event as predictor were adjusted for the sampling station. $PM_{2.5}$ and PM_{10} were analyzed separately. Data was extracted from Figures 3.3, 3.4, and S3.3 and subjected to further analyses to obtain the results presented in this figure. Abbreviations: IL, interleukin.

To confirm that the higher air-borne PM concentrations during dust events were also associated with higher inflammatory potencies, we additionally compared effects at $PM_{2.5}$ and PM_{10} concentrations corresponding to 100 L/cm². At this volume-based concentration, both $PM_{2.5}$ and

PM_{10} from dust event 2 caused substantially higher IL-1β releases than samples from the reference period (Figure S3.5).

3.4.6 Comparison of the sampling stations

To estimate whether the inflammatory potency of $PM_{2.5}$ and PM_{10} within the same dust event varied locally, we compared the dusts from the different sampling stations regarding IL-1β induction (Figure 3.6). While $PM_{2.5}$ collected during dust event 1 on the island Santiago (stations 1 and 2) tended to cause stronger IL-1β release than $PM_{2.5}$ from São Vicente (stations 3 and 4), this effect was not statistically significant. For PM_{10} from dust event 1, the inflammatory potency was similar for all stations while for the reference period, the inflammatory potency was higher for PM_{10} from stations 1 and 4. For neither $PM_{2.5}$ nor PM_{10}, dusts from the urban stations 2 and 4 had a consistently higher inflammatory potency. Dust event 2 was excluded from this analysis because only two days and two stations had been assessed.

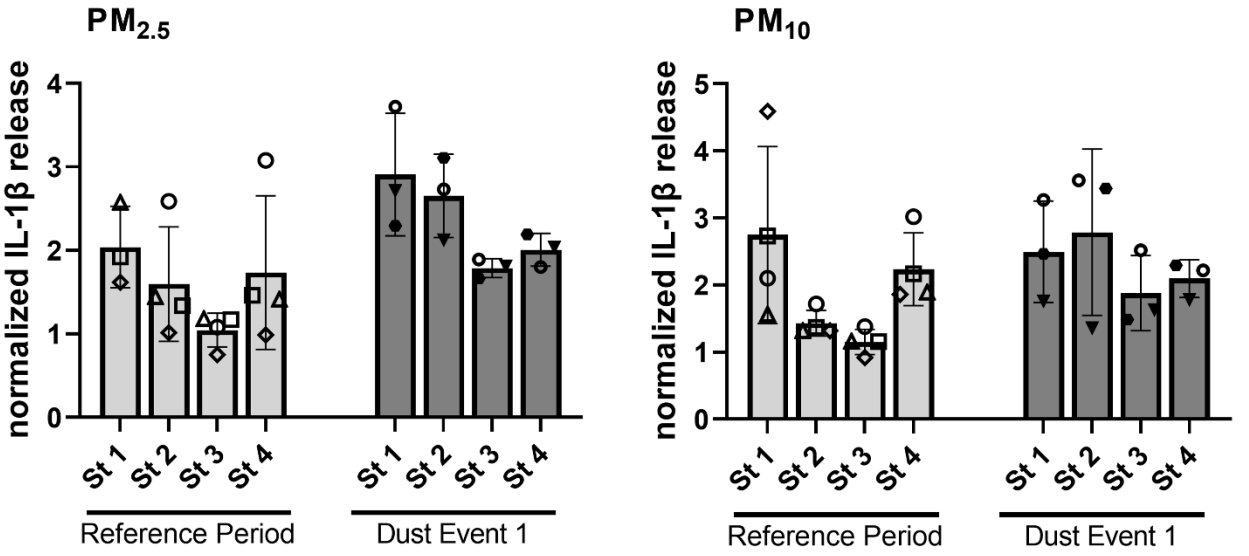

	St 2	St 3	St 4	St 2	St 3	St 4
St 1	0.94	0.20	0.94	0.85	0.054	0.13
St 2		0.65	0.94		0.11	0.25
St 3			0.58			0.85

	St 2	St 3	St 4	St 2	St 3	St 4
St 1	0.047	0.0089	0.56	1	1	1
St 2		0.56	0.14		1	1
St 3			0.029			1

Figure 3.6. Sampling station dependent IL-1β release. THP-1 cells were exposed to 5 µg/cm² of $PM_{2.5}$ and PM_{10} for 24 h. IL-1β concentrations in the supernatants were measured by ELISA and normalized to unexposed negative controls. Each point represents the mean normalized IL-1β releases from N = 3-4 independent experiments per sampling day and sampling station. Points with the same shape belong to the same sampling day. Points are plotted with mean values and standard deviations. p-values for the differences between the sampling stations were calculated by applying linear models with Holm's post hoc test to the natural logarithm of the mean normalized IL-1β releases with sampling station as predictor. $PM_{2.5}$ and PM_{10} were analyzed separately. p-values are shown in the tables underneath the graphs. Data was extracted from Figures 3.3, 3.4, and S3.3 and subjected to further analyses to obtain the results presented in this figure. Abbreviations: IL, interleukin; St, sampling station.

3.4.7 Comparing to a well-studied Saharan dust sample

To put the intrinsic inflammatory potency of the PM_{10} samples from the dust events in 2022 into perspective, we compared them to an SD sample with 99% of particles < 10 µm which we assessed in previous studies (Bredeck et al., 2023a; Bredeck et al., 2023b). This SD sample was collected at sampling station 3 during a strong dust event in December 2016 and January 2017. Overall, the upregulations of IL-1β release after exposure to 5 µg/cm² PM_{10} ranged from 1.5 to 4.4-fold (Figure S3.6). SD from 2016-17 was the second-weakest, inducing IL-1β release by only 1.6-fold.

3.4.8 Dust constituents that potentially contribute to the inflammatory potency

To obtain an overview of dust constituents that may contribute to the inflammatory potency of $PM_{2.5}$ and PM_{10} desert dust, we calculated Spearman correlation matrices (Figure S3.7). For these calculations, we included the normalized IL-1β release after exposure to 5 µg/cm² and the contents of water-soluble ions, elements, OC and EC. The Spearman matrices revealed that the IL-1β releases after $PM_{2.5}$ and PM_{10} exposure correlated with 15 and 13 of the assessed constituents, respectively. However, non-surprisingly, many constituents also correlated amongst each other, rendering the assessment of single constituents impossible.

Therefore, we performed principal component regressions to identify clusters of constituents associated with each other and with inflammatory potency. We performed principal component regressions separately for $PM_{2.5}$ and PM_{10} and separately for water-soluble ion contents and contents of elements, OC and EC. For each PC that contributed to variance by at least 10%, we tested the statistical significance of the association with normalized IL-1β release. For the water-soluble ion contents of both $PM_{2.5}$ and PM_{10}, PC1 contained a cluster of SO_4^{2-}, Na^+, Cl^-, oxalate, NO_3^-, and Mg^{2+}, which was associated with low IL-1β release (Table 3.2). This cluster was complemented by NH_4^+ and K^+ for $PM_{2.5}$ and PM_{10}, respectively.

Table 3.2. Principal components regressions on the association of water-soluble ions with normalized IL-1β release.

Parameter		$PM_{2.5}$		PM_{10}		
		PC1	**PC2**	**PC1**	**PC2**	**PC3**
PC % var.		60%	19%	56%	21%	11%
PC loading	SO_4^{2-}	-0.37	0.09	-0.38	0.04	-0.08
	Na^+	-0.37	0.06	-0.37	-0.15	-0.03
	Cl^-	-0.36	0.04	-0.37	-0.15	-0.02
	Oxalate	-0.36	0.08	-0.34	0.02	0.32
	NO_3^-	-0.35	0.19	-0.36	0.13	-0.06
	Mg^{2+}	-0.33	0.21	-0.37	-0.13	-0.10
	NH_4^+	-0.32	0.00	-0.16	0.26	-0.54
	F^-	0.20	0.49	0.06	0.59	-0.07
	Ca^{2+}	0.21	0.44	0.06	0.56	-0.07
	MSA^-	-0.02	0.49	-0.21	0.37	0.12
	K^+	0.14	0.47	-0.35	0.08	0.01
	PO_4^{3-}	0.19	-0.06	-0.07	0.22	0.75
Coef. of linear model	Reg. coef.	0.075	0.055	0.073	0.039	0.070
	SE	0.022	0.039	0.025	0.041	0.057
	p-value	0.0016	0.17	0.0069	0.34	0.23

Separate principal component analyses were performed for $PM_{2.5}$ and PM_{10}. Principal components (PCs) contributing to variance by at least 10% were statistically tested for association with normalized IL-1β release using a linear model. For PCs that were significantly associated with normalized IL-1β release ($p \leq 0.05$), loadings with absolute values ≥ 0.20 are highlighted with a frame. For all PCs with a negative regression coefficient, the plus/minus signs of the loadings and the regression coefficient were reversed so that higher contents of the constituent with a positive loading are associated with higher normalized IL-1β release and vice versa. Abbreviations: Coef., coefficients; MSA^-, methanesulfonic acid; PC, principal component; PM, particulate matter; Reg. coef., regression coefficient; SE, standard error; var., variance.

Analyzing the contents of elements, OC, and EC of $PM_{2.5}$, the cluster of Ni, Rb, Ca, Sr, Mn, Cr, Ti, Zn, Fe, and V in PC1 was associated with low IL-1β releases (Table 3.3). In contrast, according to PC2 the cluster of Fe, Mn, and Sr was positively and OC, EC, K, and P inversely associated with IL-1β release. Considering the higher regression coefficient of PC2 than PC1 and the loadings of the elements, Fe showed the strongest association with IL-1β release.

Table 3.3. Principal components regressions on the association of elements and carbonaceous constituents with normalized IL-1β release.

Parameter		$PM_{2.5}$				PM_{10}		
		PC1	**PC2**	**PC3**	**PC4**	**PC1**	**PC2**	**PC3**
PC % var.		30%	19%	16%	13%	40%	17%	14%
PC loadings	Ni	-0.39	-0.02	-0.03	0.10	0.00	-0.22	0.12
	Rb	-0.34	0.09	0.01	-0.26	0.35	0.10	-0.11
	Ca	-0.34	-0.02	0.23	0.19	0.30	-0.22	0.18
	Sr	-0.34	0.24	0.16	-0.19	0.36	-0.02	-0.09
	Mn	-0.32	0.29	0.10	-0.18	0.37	0.02	-0.07
	Cr	-0.30	-0.17	0.15	0.34	0.20	-0.07	-0.08
	Ti	-0.30	-0.11	-0.38	-0.06	0.31	-0.03	0.27
	Zn	-0.26	-0.18	0.11	0.44	-0.06	-0.22	0.10
	Fe	-0.22	0.36	0.10	-0.20	0.36	0.08	-0.04
	V	-0.20	-0.17	-0.49	-0.09	0.34	0.14	-0.02
	Ba	-0.19	-0.17	-0.49	-0.07	0.26	0.34	-0.05
	OC	-0.12	-0.38	0.27	0.11	0.07	-0.35	0.44
	EC	-0.05	-0.42	0.25	-0.12	0.01	-0.17	0.50
	K	-0.07	-0.35	0.10	-0.47	0.18	-0.30	-0.31
	P	0.04	-0.34	0.19	-0.42	0.07	-0.50	-0.22
	Cu	0.02	-0.02	-0.06	0.11	0.15	0.06	0.41
	Mg	-0.03	0.15	0.24	-0.13	0.03	-0.45	-0.28
Coef. of linear model	Reg. coef.	0.060	0.12	0.021	0.036	0.048	0.075	0.009
	SE	0.024	0.030	0.032	0.036	0.026	0.040	0.043
	p-value	0.018	0.00042	0.52	0.33	0.075	0.067	0.85

Separate principal component analyses were performed for $PM_{2.5}$ and PM_{10}. Principal components (PCs) contributing to variance by at least 10% were statistically tested for association with normalized IL-1β release using a linear model. For PCs that were significantly associated with normalized IL-1β release ($p \leq 0.05$), loadings with absolute values ≥ 0.20 are highlighted with a frame. For all PCs with a negative regression coefficient, the plus/minus signs of the loadings and the regression coefficient were reversed so that higher contents of the constituent with a positive loading are associated with higher normalized IL-1β release and vice versa. Abbreviations: Coef., coefficients; EC, elemental carbon; OC, organic carbon; PC, principal component; PM, particulate matter; Reg. coef., regression coefficient; SE, standard error; var., variance.

3.4.9 The role of endotoxins

To understand whether the variability in inflammatory potency of PM_{10} and potential differences between dust events (see Figure 3.5) might have been related to endotoxins, we performed a LAL assay. We focused on PM_{10} because former studies demonstrated that endotoxins were mainly responsible for the inflammatory potency of the coarse fraction of PM (Manzano-León et al., 2016; Monn and Becker, 1999; Rodríguez-Cotto et al., 2013; Schins et al., 2004). We selected the two most and least potent amongst the still available samples from the reference period and each dust

event for endotoxin quantification. Except one sample from dust event 2, within the reference period and each dust event, increasing endotoxin contents were associated with increasing IL-1β releases (Table 3.4). Endotoxins were more abundant in PM_{10} samples from dust event 1 than dust event 2. The endotoxin content of field blank filters was not detectable (< 0.0073 EU/cm² filter area).

Table 3.4. Endotoxin contents of selected PM_{10} samples.

Period/Event	Day	Sampling station	EU/mg	Normalized IL-1β release
Reference Period	D4	St 3	< 0.2[a]	0.92
	D2	St 3	< 0.2[a]	1.15
	D1	St 4	1.83	3.02
	D4	St 1	> 2.0[b]	4.59
Dust Event 1	D2	St 3	0.77	1.49
	D1	St 4	0.77	2.22
	D2	St 2	0.93	3.44
	D1	St 2	1.08	3.56
Dust Event 2	D2	St 3	0.29	1.74
	D1	St 3	0.36	3.37
	D1	St 4	0.46	4.41
	D2	St 4	0.61	2.76

[a]below the concentration of the lowest standard
[b]above the concentration of the highest standard

Endotoxin contents were determined applying a Limulus amebocyte lysate (LAL)-based assay. THP-1 cells were exposed to 5 µg/cm² of PM_{10} dusts for 24 h. IL-1β concentrations in the supernatants were measured by ELISA and normalized to unexposed negative controls. *N* = 3-4 independent experiments per sampling day and sampling station were performed. Abbreviations: D, day; EU, endotoxin units; IL, interleukin; St, sampling station.

To confirm the association of endotoxins with inflammatory potency we used primary human alveolar macrophages. We exposed these macrophages to the pristine and baked SD sample from 2016-17 containing 0.46 EU/mg and < 0.2 EU/mg, respectively (Bredeck et al., 2023a). Only the pristine but not the baked sample caused concentration-dependent release of IL-1β at minimal cytotoxicity (Figure S3.8).

3.5 Discussion

In this study, we assessed the inflammatory potency of 63 $PM_{2.5}$ and PM_{10} samples from a reference period and two SD events *in vitro* on THP-1 macrophages. While dust exposure induced the releases of IL-1β, IL-8, and TNFα, after normalization to negative controls only IL-1β release was well-reproducible. At the relatively low and non-cytotoxic concentration of 5 µg/cm², $PM_{2.5}$ from both dust events and PM_{10} from one dust event had a higher intrinsic inflammatory potency

than $PM_{2.5}$ and PM_{10} from the reference period. Dust event PM from the different sampling stations did not differ in inflammatory potency. Moreover, dust event PM_{10} samples of this study were even more potent than a relatively potent SD sample that we had assessed in former studies (Bredeck et al., 2023a; Bredeck et al., 2023b). Using principal component regressions, we could identify a cluster of sea spray ions and a cluster of trace metals in $PM_{2.5}$ associated with lower inflammatory potency whereas Fe in $PM_{2.5}$ was associated with higher inflammatory potency. The endotoxin contents of PM_{10} could not explain different inflammatory potencies of dust events but aligned with the inflammatory potency within the events.

We used differentiated THP-1 macrophages to assess both $PM_{2.5}$ and PM_{10}. Despite the higher deposition of $PM_{2.5}$ in the alveoli and PM_{10} in the airways (ICRP, 1994), it is common to test $PM_{2.5}$ and PM_{10} in the same way and the same model (Manzano-León et al., 2016; Rodríguez-Cotto et al., 2013; Schins et al., 2004; Skuland et al., 2022; Steerenberg et al., 2006). Because macrophages are present in both alveoli and airways and because both $PM_{2.5}$ and PM_{10} increased the intrinsic inflammatory potency, our results indicate that the whole lung may be affected by desert dust exposure.

The higher intrinsic and volume-based inflammatory potency of dust event than reference period PM emphasizes the health hazards and risks associated with dust storms. The increase in intrinsic inflammatory potency agrees with two studies from Puerto Rico using BEAS-2B cells to assess the effect of dust events on the oxidative and inflammatory potency of organic extracts of dusts sampled at a rural site and over the ocean (Rodriguez-Cotto et al., 2015; Rodríguez-Cotto et al., 2013). Contrarily, a study from Bamako (Mali) using 16HBE14o$^-$ cells reported that desert dust decreased the intrinsic oxidative and inflammatory potency of urban dust (Val et al., 2013). These different study outcomes may be explained by the different potencies of the reference period dusts. While in Puerto Rico, the reference period dust may be composed of high shares of sea spray with a rather low inflammatory potency (see below) and few urban pollutants, in Bamako the background is dominated by rather toxic urban pollutants such as elemental carbon (Abe et al., 2000; Miyabara et al., 1998; Nordenhäll et al., 2000; Val et al., 2013). Yet, also on Cape Verde we operated two urban and two non-urban sampling station and even during the reference period, $PM_{2.5}$ and PM_{10} from the urban sampling stations was not consistently more potent. Here, it needs to be considered that Bamako has over 20 times more inhabitants and, therefore, a much higher expected urban pollution than cities on Cape Verde.

For risk estimation, it is very important to take into account that desert dusts are not inhaled instead of but in addition to the local background dust. Therefore, even though desert dusts' hazardousness may be lower than that of an urban background, our results indicate that

additionally inhaling desert dust increases health risks. This is stressed by the high $PM_{2.5}$ and PM_{10} concentrations measured on the island of Santiago which exceeded 65 µg/cm² and 150 µg/cm² on all three assessed dust event days, respectively. U.S. regulation allows these concentrations to be exceeded no more than once per year (Environmental Protection Agency (EPA), 1971). The hazardousness is also underlined by the higher inflammatory potency of the desert dust event PM_{10} from this study compared to the reference SD sample from 2016-17. In previous studies (Martinon et al., 2002; Thornberry et al., 1992), we demonstrated that the SD sample from 2016-17 triggered inflammatory cytokine release through the lung disease-related NLRP3 inflammasome-caspase-1 pathway.

Different potencies of PM_{10} from dust events 1 and 2 might be explained by the desert dusts originating from different source regions within the Saharan as desert sediment dusts from different sources have been shown to vary in their toxicity: Taylor et al. (2013) administered Middle Eastern desert dusts from three different locations to rats and observed differences in the acute releases of the inflammatory cytokines interleukin IL-6 and TNFα as well as acute lung lesions. Ichinose et al. (2005, 2008) reported varying potencies to elevate inflammatory cell numbers and cytokine concentrations in bronchioalveolar lavages in mice when testing three Asian yellow dust samples and Asian sand dust compared to Arizona sand dust. Ghio et al. (2014) exposed bronchial epithelial BEAS-2B cells and mice to two different surface sediment samples from Arizona. While in BEAS-2B cells the samples triggered releases of IL-1β and IL-6 to different extents, in mice both samples had similar inflammatory potencies. To associate the toxicity of long-range transported desert dusts with source regions, more than two dust events need to be examined. Therefore, future studies on a higher number dust events and including back trajectory analyses should combine information on dust source regions and dust event-specific hazardousness. In a next step, forecasts covering dust concentrations and source regions could aid dust-event-resolved risk assessment.

According to principal component regressions for both $PM_{2.5}$ and PM_{10}, a cluster of the sea spray ions SO_4^{2-}, Cl^-, Na^+, and Mg^{2+} with higher contents during dust events than the reference period was associated with low inflammatory potency. This agreed with the lower inflammatory potency of PM from the reference period. This also aligns well with a maritime PM sample that in contrast to urban PM samples did not induce oxidative damage or IL-8 release in A549 cells (Wessels et al., 2010). However, Steerenberg et al. (2006) reported increased IL-6 release from primary rat alveolar macrophages *in vitro* and increased levels of the bronchiolar epithelium damage marker Club cell protein (CC16) in bronchioalveolar lavage fluid of rats instilled with sea spray PM. Moreover, Jalava et al. (2008) described a positive correlation between TNFα release from

RAW 264.7 macrophages and sea salt in fine and coarse PM. These contrasts to our results may be explained by the over 100-fold and about 20-fold higher PM concentrations used in the aforementioned studies. Although Ca^{2+} is a constituent of sea spray, its content in $PM_{2.5}$ was higher during dust events and it was associated with higher inflammatory potency. However, it is very unlikely that the Ca^{2+} from desert dusts conveyed the inflammatory potency in our study since it elevated the Ca^{2+} concentration of the cell culture medium by 1% at most.

Surprisingly, principal component regressions also indicated that amongst transition metals in $PM_{2.5}$, only Fe and Mn were associated with inflammatory potency. Studies assessing urban or industrial PM in rat alveolar macrophages rat alveolar type II cells, instilled rats (Steerenberg et al., 2006), murine RAW 264.7 macrophages (Guastadisegni et al., 2010), A549 cells (Wessels et al., 2010), and instilled humans (Ghio and Devlin, 2001; Schaumann et al., 2004) connected inflammatory potency to the contents of transition metals including Fe and Mn and to their capacity to induce oxidative stress (Ayres et al., 2008). Mn has been shown to induce oxidative stress and inflammatory cytokine release in lung epithelial cells *in vitro* but to our knowledge has not specifically been addressed in the context of desert dusts (Frick et al., 2011; Pascal and Tessier, 2004). He et al. (2019) assessed desert dust and urban $PM_{2.5}$ in a mouse instillation model of allergy. In agreement with our results and with the contrast between desert dusts and urban PM, they reported that eosinophilia and inflammatory cytokine release in response to Asian desert dust $PM_{2.5}$ depended especially on Fe whereas they suggested that the inflammatory effect of urban $PM_{2.5}$ was rather related to other trace metals such as Pb, Cu, Ni, Cr, Co, and Cd. Furthermore, transition metals including Fe have been shown to mediate oxidative stress and inflammatory cytokines in BEAS-2B cells upon exposure to organic extracts of SD (Rodriguez-Cotto et al., 2015; Rodríguez-Cotto et al., 2013). Contrarily, metal concentrations in aqueous extracts of desert dust from Israel were so low that the authors argued metals were not responsible for the oxidative stress induced in rat alveolar NR8383 macrophages (Pardo et al., 2017). This contrast can probably be explained by the enrichment of the metal contents in the organic extract and low contents in aqueous extracts described in the aforementioned studies. Moreover, Val et al. (2013) argued that metals including Fe and Mn played a minor role in oxidative stress and inflammatory cytokine induction through SD-containing urban PM because the coarse fraction with higher metal contents was less potent than the fine and ultrafine fractions. However, Fe speciation may differ between size fractions and Fe from finer PM may have a higher surface-to-volume ratio, especially considering that Fe in SD has been reported to be also present in smaller particles (Fomba et al., 2020; Rodriguez-Navarro et al., 2018). Considering the redox activity of Fe (Ghio et al., 1992; Gilmour et al., 1996; HaMai and Bondy, 2004) and Mn (HaMai and Bondy, 2004), their contribution

to the inflammatory potency of desert dust event $PM_{2.5}$ is plausible. At the same time our results indicate that apart from Fe and Mn in $PM_{2.5}$, transition metals and elemental carbon in desert dusts do not drive inflammatory potency. Noteworthy, Mn in $PM_{2.5}$ was not significantly associated with inflammatory potency according to Spearman correlation.

The alignment of endotoxin content with intra but not inter-event variability of inflammatory potency indicates that endotoxins can explain part but not all the inflammatory potency of PM_{10} from desert dust events. The contribution of endotoxins to the inflammatory potency of desert dusts agrees with former *in vitro* (Bredeck et al., 2023a; He et al., 2010; Rodríguez-Cotto et al., 2013) and *in vivo* (He et al., 2016; He et al., 2010; Yanagisawa et al., 2007) studies. The IL-1β release from primary human alveolar macrophages in response to pristine but not endotoxin-free baked SD, that we report here, further strengthens the importance of endotoxins in desert dusts. That endotoxins only explain part of the inflammatory potency agrees with our previous study (Bredeck et al., 2023a) in which heat-destruction of endotoxins reduced but not completely abolished the ability of SD to induce IL-1β release from THP-1 macrophages. Moreover, reconstitution with LPS did not completely restore IL-1β secretion levels. Therefore, endotoxin contents should be considered for hazard assessment of desert dust events but need to be complemented with further yet to identify dust properties. Such a property could be microbial constituents other than endotoxins. Stern et al. (2021) described a high microbial variability and potential pathogens in SD. Additionally, microbial β-glucan was found in Asian sand dust (He et al., 2010; Yanagisawa et al., 2007). Furthermore, variations in mineralogical composition may influence inflammatory potency. SD was shown to contain, amongst others, quartz, albite, and K-feldspar (Rodriguez-Navarro et al., 2018) which can also trigger cytokine release from THP-1 macrophages (Grytting et al., 2022).

Limitations of our study were that we did not assess the mineralogical composition and microbial constituents other than endotoxins. Another limitation was that the extraction procedures for the quantification of water-soluble ions, elements, OC and EC and for *in vitro* toxicology differed. Because for *in vitro* toxicology experiments not all insoluble PM could be extracted from filters, the ratio of water-soluble ions to elements, OC and EC in the extracts that were applied to cells was by an unknown factor higher than the concentrations in Table 3.1 and Table S3.3 indicate. Thus, we performed principal component regressions separately for water-soluble ions and elements, OC and EC. A limitation of the principal component regression-based analysis was that constituents associated with IL-1β release negatively or positively do not necessarily exert anti or pro-inflammatory effects, respectively, but can just as well correlate with inflammatory constituents. Being a disadvantage for mechanistic investigations, this can also be considered a

strength in a regulatory context because even substances and clusters of substances that do not exert effects can serve as markers.

3.6 Conclusions

Our results suggest that long-range transported desert dusts potentiate the inflammatory potency of local PM. Our study also indicates that the Fe content of $PM_{2.5}$ and the endotoxin content of PM_{10} contribute to the observed variability in inflammatory potency. Using dust forecasts and back trajectories, future studies should aim to connect the composition of desert dusts at source regions to the hazardousness at the destinations of long-range transport. In such studies, further desert dust properties like the contents of microbial compounds other than endotoxins and the mineralogical composition should be included. Overall, the observed intrinsic inflammatory potency of dust event PM together with the high $PM_{2.5}$ and PM_{10} concentrations during dust events warrants authorities to take regulatory actions and implement risk mitigation strategies.

Funding

This work has received funding from the Leibniz Association in the framework of the Leibniz Collaborative Excellence Programme project DUSTRISK under grant agreement number K225/2019. The IUF is funded by the federal and state governments - the Ministry of Culture and Science of North Rhine-Westphalia (MKW) and the Federal Ministry of Education and Research (BMBF).

Acknowledgments

We would like to thank Sandra Freire and João Cardoso from the University of Cape Verde (UniCV), René Rabe and Sofía Gómez Maqueo Anaya from TROPOS, Luis Neves and Anedito da Costa from the National Institute of Meteorology of Cape Verde (INMG), and Christian Nehls from Leibniz Lung Center Borstel (FZB) for their support with dust sampling and the preparation of the sampling campaign. Furthermore, we are grateful to Isabelle Masson from IUF for supporting with the extraction of dust samples for in vitro exposure and Miriam Vieth for supporting with the THP-1 exposures.

3.7 References

Aaron, S.D., Angel, J.B., Lunau, M., Wright, K., Fex, C., Le Saux, N., Dales, R.E., 2001. Granulocyte inflammatory markers and airway infection during acute exacerbation of chronic obstructive pulmonary disease. Am J Respir Crit Care Med 163, 349-355. https://doi.org/10.1164/ajrccm.163.2.2003122

Abe, S., Takizawa, H., Sugawara, I., Kudoh, S., 2000. Diesel exhaust (DE)-induced cytokine expression in human bronchial epithelial cells: a study with a new cell exposure system to freshly generated DE in vitro. Am J Respir Cell Mol Biol 22, 296-303. https://doi.org/10.1165/ajrcmb.22.3.3711

Achakulwisut, P., Anenberg, S.C., Neumann, J.E., Penn, S.L., Weiss, N., Crimmins, A., Fann, N., Martinich, J., Roman, H., Mickley, L.J., 2019. Effects of Increasing Aridity on Ambient Dust and Public Health in the U.S. Southwest Under Climate Change. Geohealth 3, 127-144. https://doi.org/10.1029/2019GH000187

Ayres, J.G., Borm, P., Cassee, F.R., Castranova, V., Donaldson, K., Ghio, A., Harrison, R.M., Hider, R., Kelly, F., Kooter, I.M., Marano, F., Maynard, R.L., Mudway, I., Nel, A., Sioutas, C., Smith, S., Baeza-Squiban, A., Cho, A., Duggan, S., Froines, J., 2008. Evaluating the toxicity of airborne particulate matter and nanoparticles by measuring oxidative stress potential--a workshop report and consensus statement. Inhal Toxicol 20, 75-99. https://doi.org/10.1080/08958370701665517

Bredeck, G., Busch, M., Rossi, A., Stahlmecke, B., Fomba, K.W., Herrmann, H., Schins, R.P.F., 2023a. Inhalable Saharan dust induces oxidative stress, NLRP3 inflammasome activation, and inflammatory cytokine release. Environ Int 172, 107732. https://doi.org/10.1016/j.envint.2023.107732

Bredeck, G., Dobner, J., Stahlmecke, B., Fomba, K.W., Herrmann, H., Rossi, A., Schins, R.P.F., 2023b. Saharan dust induces NLRP3-dependent inflammatory cytokines in an alveolar air-liquid interface co-culture model. Part Fibre Toxicol 20, https://doi.org/10.1186/s12989-023-00550-w

Busch, M., Bredeck, G., Kampfer, A.A.M., Schins, R.P.F., 2021. Investigations of acute effects of polystyrene and polyvinyl chloride micro- and nanoplastics in an advanced in vitro triple culture model of the healthy and inflamed intestine. Environ Res 193, 110536. https://doi.org/10.1016/j.envres.2020.110536

Cassel, S.L., Eisenbarth, S.C., Iyer, S.S., Sadler, J.J., Colegio, O.R., Tephly, L.A., Carter, A.B., Rothman, P.B., Flavell, R.A., Sutterwala, F.S., 2008. The Nalp3 inflammasome is essential for the development of silicosis. Proc Natl Acad Sci U S A 105, 9035-9040. https://doi.org/10.1073/pnas.0803933105

Cavalli, F., Viana, M., Yttri, K.E., Genberg, J., Putaud, J.-P., 2009. Toward a standardised thermal-optical protocol for measuring atmospheric organic and elemental carbon: the EUSAAR protocol. Atmos Meas Tech Niscuss 2, 2321-2345. https://doi.org/10.2788/87062

Chen, X., Luan, M., Liu, J., Yao, Y., Li, X., Wang, T., Zhang, H., Han, Y., Lu, X., Chen, W., Hu, X., Zheng, M., Qiu, X., Zhu, T., 2022. Risk factors in air pollution exposome contributing to higher levels of TNFalpha in COPD patients. Environ Int 159, 107034. https://doi.org/10.1016/j.envint.2021.107034

Choi, Y.S., Bae, C.H., Song, S.Y., Kim, Y.D., 2015. Asian sand dust increases MUC8 and MUC5B expressions via TLR4-dependent ERK2 and p38 MAPK in human airway epithelial cells. Am J Rhinol Allergy 29, 161-165. https://doi.org/10.2500/ajra.2015.29.4162

Dos Santos Souza, E.J., Zapata Mora, C., Aristizabal Zuluaga, B.H., Britto do Amaral, C.D., Grassi, M.T., 2021. Multi-elemental analysis of particulate matter PM(2.5) and PM(10) by ICP OES. Talanta 221, 121457. https://doi.org/10.1016/j.talanta.2020.121457

Dostert, C., Petrilli, V., Van Bruggen, R., Steele, C., Mossman, B.T., Tschopp, J., 2008. Innate immune activation through Nalp3 inflammasome sensing of asbestos and silica. Science 320, 674-677. https://doi.org/10.1126/science.1156995

Environmental Protection Agency (EPA), 1971. Code of Federal Regulations Title 40 Part 50 National primary and secondary ambient air quality standards. https://www.ecfr.gov/current/title-40/chapter-I/subchapter-C/part-50. Accessed: 03/10/2023

European Commission, 2022. Proposal for a directive of the European Parliament and of the council on ambient air quality and cleaner air for Europe (recast). https://eur-lex.europa.eu/legal-content/EN/TXT/?uri=CELEX%3A52022PC0542&qid=1696327827017. Accessed: 03/10/2023

European Parliament and Council, 2008. Directive 2008/50/EC of the European Parliament and of the Council of 21 May 2008 on ambient air quality and cleaner air for Europe. Official Journal of the European Union. https://eur-lex.europa.eu/legal-content/EN/TXT/?uri=celex%3A32008L0050. Accessed: 03/10/2023

Fomba, K.W., Deabji, N., Barcha, S.E.I., Ouchen, I., Elbaramoussi, E.M., El Moursli, R.C., Harnafi, M., El Hajjaji, S., Mellouki, A., Herrmann, H., 2020. Application of TXRF in monitoring trace metals in particulate matter and cloud water. Atmos Meas Tech 13, 4773-4790. https://doi.org/10.5194/amt-13-4773-2020

Fomba, K.W., Müller, K., van Pinxteren, D., Herrmann, H., 2013. Aerosol size-resolved trace metal composition in remote northern tropical Atlantic marine environment: case study Cape Verde islands. Atmos Chem Phys 13, 4801-4814. https://doi.org/10.5194/acp-13-4801-2013

Frick, R., Muller-Edenborn, B., Schlicker, A., Rothen-Rutishauser, B., Raemy, D.O., Gunther, D., Hattendorf, B., Stark, W., Beck-Schimmer, B., 2011. Comparison of manganese oxide nanoparticles and manganese sulfate with regard to oxidative stress, uptake and apoptosis in alveolar epithelial cells. Toxicol Lett 205, 163-172. https://doi.org/10.1016/j.toxlet.2011.05.1037

Fussell, J.C., Kelly, F.J., 2021. Mechanisms underlying the health effects of desert sand dust. Environ Int 157, 106790. https://doi.org/10.1016/j.envint.2021.106790

Ghio, A.J., Devlin, R.B., 2001. Inflammatory lung injury after bronchial instillation of air pollution particles. Am J Respir Crit Care Med 164, 704-708. https://doi.org/10.1164/ajrccm.164.4.2011089

Ghio, A.J., Kennedy, T.P., Whorton, A.R., Crumbliss, A.L., Hatch, G.E., Hoidal, J.R., 1992. Role of surface complexed iron in oxidant generation and lung inflammation induced by silicates. Am J Physiol 263, L511-518. https://doi.org/10.1152/ajplung.1992.263.5.L511

Ghio, A.J., Kummarapurugu, S.T., Tong, H., Soukup, J.M., Dailey, L.A., Boykin, E., Gilmour, I.M., Ingram, P., Roggli, V.L., Goldstein, H.L., Reynolds, R.L., 2014. Biological effects of desert dust in respiratory epithelial cells and a murine model. Inhal Toxicol 26, 299-309. https://doi.org/10.3109/08958378.2014.888109

Ghozikali, M.G., Ansarin, K., Naddafi, K., Nabizadeh, R., Yaghmaeian, K., Jaafari, J., Dehghanzadeh, R., Atafar, Z., Faraji, M., Mohammadi, A., Goudarzi, G., Yunesian, M., 2022. Status of TNF-alpha and IL-6 as pro-inflammatory cytokines in exhaled breath condensate of late adolescents with asthma and healthy in the dust storm and non-dust storm conditions. Sci Total Environ 838, 155536. https://doi.org/10.1016/j.scitotenv.2022.155536

Gilmour, P.S., Brown, D.M., Lindsay, T.G., Beswick, P.H., MacNee, W., Donaldson, K., 1996. Adverse health effects of PM10 particles: involvement of iron in generation of hydroxyl radical. Occup Environ Med 53, 817-822. https://doi.org/10.1136/oem.53.12.817

Ginoux, P., Prospero, J.M., Gill, T.E., Hsu, N.C., Zhao, M., 2012. Global-scale attribution of anthropogenic and natural dust sources and their emission rates based on MODIS Deep Blue aerosol products. Rev Geophys 50, https://doi.org/10.1029/2012rg000388

Grailer, J.J., Canning, B.A., Kalbitz, M., Haggadone, M.D., Dhond, R.M., Andjelkovic, A.V., Zetoune, F.S., Ward, P.A., 2014. Critical role for the NLRP3 inflammasome during acute lung injury. J Immunol 192, 5974-5983. https://doi.org/10.4049/jimmunol.1400368

Grytting, V.S., Refsnes, M., Lag, M., Erichsen, E., Rohr, T.S., Snilsberg, B., White, R.A., Ovrevik, J., 2022. The importance of mineralogical composition for the cytotoxic and pro-inflammatory effects of mineral dust. Part Fibre Toxicol 19, 46. https://doi.org/10.1186/s12989-022-00486-7

Guastadisegni, C., Kelly, F.J., Cassee, F.R., Gerlofs-Nijland, M.E., Janssen, N.A., Pozzi, R., Brunekreef, B., Sandstrom, T., Mudway, I., 2010. Determinants of the proinflammatory action of ambient particulate matter in immortalized murine macrophages. Environ Health Perspect 118, 1728-1734. https://doi.org/10.1289/ehp.1002105

Gutierrez, M.P., Zuidema, P., Mirsaeidi, M., Campos, M., Kumar, N., 2020. Association between African Dust Transport and Acute Exacerbations of COPD in Miami. J Clin Med 9, 2496. https://doi.org/10.3390/jcm9082496

HaMai, D., Bondy, S.C., 2004. Oxidative basis of manganese neurotoxicity. Ann N Y Acad Sci 1012, 129-141. https://doi.org/10.1196/annals.1306.010

He, M., Ichinose, T., Song, Y., Yoshida, Y., Bekki, K., Arashidani, K., Yoshida, S., Nishikawa, M., Takano, H., Shibamoto, T., Sun, G., 2016. Desert dust induces TLR signaling to trigger Th2-dominant lung allergic inflammation via a MyD88-dependent signaling pathway. Toxicol Appl Pharmacol 296, 61-72. https://doi.org/10.1016/j.taap.2016.02.011

He, M., Ichinose, T., Yoshida, S., Nishikawa, M., Mori, I., Yanagisawa, R., Takano, H., Inoue, K., Sun, G., Shibamoto, T., 2010. Airborne Asian sand dust enhances murine lung eosinophilia. Inhal Toxicol 22, 1012-1025. https://doi.org/10.3109/08958378.2010.510151

He, M., Ichinose, T., Yoshida, S., Nishikawa, M., Sun, G., Shibamoto, T., 2019. Role of iron and oxidative stress in the exacerbation of allergic inflammation in murine lungs caused by urban particulate matter <2.5 µm and desert dust. J Appl Toxicol 39, 855-867. https://doi.org/10.1002/jat.3773

Hiyoshi, K., Ichinose, T., Sadakane, K., Takano, H., Nishikawa, M., Mori, I., Yanagisawa, R., Yoshida, S., Kumagai, Y., Tomura, S., Shibamoto, T., 2005. Asian sand dust enhances ovalbumin-induced eosinophil recruitment in the alveoli and airway of mice. Environ Res 99, 361-368. https://doi.org/10.1016/j.envres.2005.03.008

Ho, K.F., Wu, K.C., Niu, X., Wu, Y., Zhu, C.S., Wu, F., Cao, J.J., Shen, Z.X., Hsiao, T.C., Chuang, K.J., Chuang, H.C., 2019. Contributions of local pollution emissions to particle bioreactivity in downwind cities in China during Asian dust periods. Environ Pollut 245, 675-683. https://doi.org/10.1016/j.envpol.2018.11.035

Honda, A., Matsuda, Y., Murayama, R., Tsuji, K., Nishikawa, M., Koike, E., Yoshida, S., Ichinose, T., Takano, H., 2014. Effects of Asian sand dust particles on the respiratory and immune system. J Appl Toxicol 34, 250-257. https://doi.org/10.1002/jat.2871

Hosoki, K., Ying, S., Corrigan, C., Qi, H., Kurosky, A., Jennings, K., Sun, Q., Boldogh, I., Sur, S., 2015. Analysis of a Panel of 48 Cytokines in BAL Fluids Specifically Identifies IL-8 Levels as the Only Cytokine that Distinguishes Controlled Asthma from Uncontrolled Asthma, and Correlates Inversely with FEV1. PLoS One 10, e0126035. https://doi.org/10.1371/journal.pone.0126035

Ichinose, T., Nishikawa, M., Takano, H., Sera, N., Sadakane, K., Mori, I., Yanagisawa, R., Oda, T., Tamura, H., Hiyoshi, K., Quan, H., Tomura, S., Shibamoto, T., 2005. Pulmonary toxicity induced by intratracheal instillation of Asian yellow dust (Kosa) in mice. Environ Toxicol Pharmacol 20, 48-56. https://doi.org/10.1016/j.etap.2004.10.009

Ichinose, T., Yoshida, S., Sadakane, K., Takano, H., Yanagisawa, R., Inoue, K., Nishikawa, M., Mori, I., Kawazato, H., Yasuda, A., Shibamoto, T., 2008. Effects of asian sand dust, Arizona sand dust, amorphous silica and aluminum oxide on allergic inflammation in the murine lung. Inhal Toxicol 20, 685-694. https://doi.org/10.1080/08958370801935133

ICRP, 1994. Human Respiratory Tract Model for Radiological Protection. ICRP Publication 66. Ann ICRP 24, 1-482.

Iinuma, Y., Engling, G., Puxbaum, H., Herrmann, H., 2009. A highly resolved anion-exchange chromatographic method for determination of saccharidic tracers for biomass combustion and primary bio-particles in atmospheric aerosol. Atmos Environ 43, 1367-1371. https://doi.org/10.1016/j.atmosenv.2008.11.020

Ikuta, N., Taniguchi, H., Kondoh, Y., Takagi, K., Hayakawa, T., 1996. Sustained high levels of circulatory interleukin-8 are associated with a poor outcome in patients with adult respiratory distress syndrome. Intern Med 35, 855-860. https://doi.org/10.2169/internalmedicine.35.855

Jalava, P.I., Salonen, R.O., Pennanen, A.S., Happo, M.S., Penttinen, P., Halinen, A.I., Sillanpaa, M., Hillamo, R., Hirvonen, M.R., 2008. Effects of solubility of urban air fine and coarse particles on

cytotoxic and inflammatory responses in RAW 264.7 macrophage cell line. Toxicol Appl Pharmacol 229, 146-160. https://doi.org/10.1016/j.taap.2008.01.006

Jarjour, N.N., Busse, W.W., 1995. Cytokines in bronchoalveolar lavage fluid of patients with nocturnal asthma. Am J Respir Crit Care Med 152, 1474-1477. https://doi.org/10.1164/ajrccm.152.5.7582279

Kashima, S., Yorifuji, T., Bae, S., Honda, Y., Lim, Y.-H., Hong, Y.-C., 2016. Asian dust effect on cause-specific mortality in five cities across South Korea and Japan. Atmos Environ 128, 20-27. https://doi.org/10.1016/j.atmosenv.2015.12.063

Kikuchi, S., Kikuchi, I., Takaku, Y., Kobayashi, T., Hagiwara, K., Kanazawa, M., Nagata, M., 2009. Neutrophilic inflammation and CXC chemokines in patients with refractory asthma. Int Arch Allergy Immunol 149 Suppl 1, 87-93. https://doi.org/10.1159/000211379

Kim, K., Kim, S.-D., Shin, T.-H., Bae, C.-S., Ahn, T., Shin, S.-S., Kim, H.-J., Lee, C.-M., Suh, G.-H., 2021. Respiratory and Systemic Toxicity of Inhaled Artificial Asian Sand Dust in Pigs. Life 11, https://doi.org/10.3390/life11010025

Lappalainen, U., Whitsett, J.A., Wert, S.E., Tichelaar, J.W., Bry, K., 2005. Interleukin-1beta causes pulmonary inflammation, emphysema, and airway remodeling in the adult murine lung. Am J Respir Cell Mol Biol 32, 311-318. https://doi.org/10.1165/rcmb.2004-0309OC

Lei, Y.C., Chan, C.C., Wang, P.Y., Lee, C.T., Cheng, T.J., 2004. Effects of Asian dust event particles on inflammation markers in peripheral blood and bronchoalveolar lavage in pulmonary hypertensive rats. Environ Res 95, 71-76. https://doi.org/10.1016/S0013-9351(03)00136-1

Lwin, K.S., Tobias, A., Chua, P.L., Yuan, L., Thawonmas, R., Ith, S., Htay, Z.W., Yu, L.S., Yamasaki, L., Roque, M., Querol, X., Fussell, J.C., Nadeau, K.C., Stafoggia, M., Saliba, N.A., Sheng Ng, C.F., Hashizume, M., 2023. Effects of Desert Dust and Sandstorms on Human Health: A Scoping Review. Geohealth 7, e2022GH000728. https://doi.org/10.1029/2022GH000728

Mallone, S., Stafoggia, M., Faustini, A., Gobbi, G.P., Marconi, A., Forastiere, F., 2011. Saharan dust and associations between particulate matter and daily mortality in Rome, Italy. Environ Health Perspect 119, 1409-1414. https://doi.org/10.1289/ehp.1003026

Manzano-León, N., Serrano-Lomelin, J., Sánchez, B.N., Quintana-Belmares, R., Vega, E., Vázquez-Lopez, I., Rojas-Bracho, L., López-Villegas, M.T., Vadillo-Ortega, F., De Vizcaya-Ruiz, A., Perez, I.R., O'Neill, M.S., Osornio-Vargas, A.R., 2016. TNFalpha and IL-6 Responses to Particulate Matter in Vitro: Variation According to PM Size, Season, and Polycyclic Aromatic Hydrocarbon and Soil Content. Environ Health Perspect 124, 406-412. https://doi.org/10.1289/ehp.1409287

Martinon, F., Burns, K., Tschopp, J., 2002. The inflammasome: a molecular platform triggering activation of inflammatory caspases and processing of proIL-beta. Mol Cell 10, 417-426. https://doi.org/10.1016/s1097-2765(02)00599-3

Middleton, N.J., 2017. Desert dust hazards: A global review. Aeolian Res 24, 53-63. https://doi.org/10.1016/j.aeolia.2016.12.001

Miyabara, Y., Yanagisawa, R., Shimojo, N., Takano, H., Lim, H.B., Ichinose, T., Sagai, M., 1998. Murine strain differences in airway inflammation caused by diesel exhaust particles. Eur Respir J 11, 291-298. https://doi.org/10.1183/09031936.98.11020291

Monn, C., Becker, S., 1999. Cytotoxicity and induction of proinflammatory cytokines from human monocytes exposed to fine (PM2.5) and coarse particles (PM10-2.5) in outdoor and indoor air. Toxicol Appl Pharmacol 155, 245-252. https://doi.org/10.1006/taap.1998.8591

Nordenhäll, C., Pourazar, J., Blomberg, A., Levin, J.O., Sandström, T., Ädelroth, E., 2000. Airway inflammation following exposure to diesel exhaust: a study of time kinetics using induced sputum. Eur Respir J 15, 1046-1051. https://doi.org/10.1034/j.1399-3003.2000.01512.x

Okada, S., Inoue, H., Yamauchi, K., Iijima, H., Ohkawara, Y., Takishima, T., Shirato, K., 1995. Potential role of interleukin-1 in allergen-induced late asthmatic reactions in guinea pigs: suppressive effect of

interleukin-1 receptor antagonist on late asthmatic reaction. J Allergy Clin Immunol 95, 1236-1245. https://doi.org/10.1016/s0091-6749(95)70081-1

Pardo, M., Katra, I., Schaeur, J.J., Rudich, Y., 2017. Mitochondria-mediated oxidative stress induced by desert dust in rat alveolar macrophages. Geohealth 1, 4-16. https://doi.org/10.1002/2016GH000017

Pascal, L.E., Tessier, D.M., 2004. Cytotoxicity of chromium and manganese to lung epithelial cells in vitro. Toxicol Lett 147, 143-151. https://doi.org/10.1016/j.toxlet.2003.11.004

Pease, J.E., Sabroe, I., 2002. The role of interleukin-8 and its receptors in inflammatory lung disease: implications for therapy. Am J Respir Med 1, 19-25. https://doi.org/10.1007/BF03257159

Peveri, P., Walz, A., Dewald, B., Baggiolini, M., 1988. A novel neutrophil-activating factor produced by human mononuclear phagocytes. J Exp Med 167, 1547-1559. https://doi.org/10.1084/jem.167.5.1547

Piguet, P.F., Collart, M.A., Grau, G.E., Sappino, A.P., Vassalli, P., 1990. Requirement of tumour necrosis factor for development of silica-induced pulmonary fibrosis. Nature 344, 245-247. https://doi.org/10.1038/344245a0

R Core Team. R: A Language and Environment for Statistical Computing. R Foundation for Statistical Computing, Vienna, Austria; 2023

Rodriguez-Cotto, R.I., Ortiz-Martinez, M.G., Jimenez-Velez, B.D., 2015. Organic extracts from African dust storms stimulate oxidative stress and induce inflammatory responses in human lung cells through Nrf2 but not NF-kappaB. Environ Toxicol Pharmacol 39, 845-856. https://doi.org/10.1016/j.etap.2015.02.015

Rodríguez-Cotto, R.I., Ortiz-Martínez, M.G., Rivera-Ramírez, E., Méndez, L.B., Dávila, J.C., Jiménez-Vélez, B.D., 2013. African Dust Storms Reaching Puerto Rican Coast Stimulate the Secretion of IL-6 and IL-8 and Cause Cytotoxicity to Human Bronchial Epithelial Cells (BEAS-2B). Health 5, 14-28. https://doi.org/10.4236/health.2013.510A2003

Rodriguez-Navarro, C., di Lorenzo, F., Elert, K., 2018. Mineralogy and physicochemical features of Saharan dust wet deposited in the Iberian Peninsula during an extreme red rain event. Atmos Chem Phys 18, 10089-10122. https://doi.org/10.5194/acp-18-10089-2018

Schaumann, F., Borm, P.J., Herbrich, A., Knoch, J., Pitz, M., Schins, R.P., Luettig, B., Hohlfeld, J.M., Heinrich, J., Krug, N., 2004. Metal-rich ambient particles (particulate matter 2.5) cause airway inflammation in healthy subjects. Am J Respir Crit Care Med 170, 898-903. https://doi.org/10.1164/rccm.200403-423OC

Schins, R.P., Lightbody, J.H., Borm, P.J., Shi, T., Donaldson, K., Stone, V., 2004. Inflammatory effects of coarse and fine particulate matter in relation to chemical and biological constituents. Toxicol Appl Pharmacol 195, 1-11. https://doi.org/10.1016/j.taap.2003.10.002

Schröder, J.M., Mrowietz, U., Morita, E., Christophers, E., 1987. Purification and partial biochemical characterization of a human monocyte-derived, neutrophil-activating peptide that lacks interleukin 1 activity. J Immunol 139, 3474-3483. https://doi.org/10.4049/jimmunol.139.10.3474

Shin, S.H., Ye, M.K., Hwang, Y.J., Kim, S.T., 2013. The effect of Asian sand dust-activated respiratory epithelial cells on activation and migration of eosinophils. Inhal Toxicol 25, 633-639. https://doi.org/10.3109/08958378.2013.826755

Skuland, T., Grytting, V.S., Lag, M., Jorgensen, R.B., Snilsberg, B., Leseman, D., Kubatova, A., Emond, J., Cassee, F.R., Holme, J.A., Ovrevik, J., Refsnes, M., 2022. Road tunnel-derived coarse, fine and ultrafine particulate matter: physical and chemical characterization and pro-inflammatory responses in human bronchial epithelial cells. Part Fibre Toxicol 19, 45. https://doi.org/10.1186/s12989-022-00488-5

Stafoggia, M., Zauli-Sajani, S., Pey, J., Samoli, E., Alessandrini, E., Basagana, X., Cernigliaro, A., Chiusolo, M., Demaria, M., Diaz, J., Faustini, A., Katsouyanni, K., Kelessis, A.G., Linares, C., Marchesi, S., Medina, S., Pandolfi, P., Perez, N., Querol, X., Randi, G., Ranzi, A., Tobias, A., Forastiere, F.,

Group, M.-P.S., 2016. Desert Dust Outbreaks in Southern Europe: Contribution to Daily PM(1)(0) Concentrations and Short-Term Associations with Mortality and Hospital Admissions. Environ Health Perspect 124, 413-419. https://doi.org/10.1289/ehp.1409164

Steerenberg, P.A., van Amelsvoort, L., Lovik, M., Hetland, R.B., Alberg, T., Halatek, T., Bloemen, H.J., Rydzynski, K., Swaen, G., Schwarze, P., Dybing, E., Cassee, F.R., 2006. Relation between sources of particulate air pollution and biological effect parameters in samples from four European cities: an exploratory study. Inhal Toxicol 18, 333-346. https://doi.org/10.1080/08958370500515913

Stephens, K.E., Ishizaka, A., Larrick, J.W., Raffin, T.A., 1988. Tumor necrosis factor causes increased pulmonary permeability and edema. Comparison to septic acute lung injury. Am Rev Respir Dis 137, 1364-1370. https://doi.org/10.1164/ajrccm/137.6.1364

Stern, R.A., Mahmoudi, N., Buckee, C.O., Schartup, A.T., Koutrakis, P., Ferguson, S.T., Wolfson, J.M., Wofsy, S.C., Daube, B.C., Sunderland, E.M., 2021. The Microbiome of Size-Fractionated Airborne Particles from the Sahara Region. Environ Sci Technol 55, 1487-1496. https://doi.org/10.1021/acs.est.0c06332

Sun, H., Shamy, M., Kluz, T., Munoz, A.B., Zhong, M., Laulicht, F., Alghamdi, M.A., Khoder, M.I., Chen, L.C., Costa, M., 2012. Gene expression profiling and pathway analysis of human bronchial epithelial cells exposed to airborne particulate matter collected from Saudi Arabia. Toxicol Appl Pharmacol 265, 147-157. https://doi.org/10.1016/j.taap.2012.10.008

Taylor, K., Foster, M.L., Law, J.M., Centeno, J.A., Fornero, E., Henderson, M.S., Trager, S.A., Stockelman, M.G., Dorman, D.C., 2013. Assessment of geographical variation in the respiratory toxicity of desert dust particles. Inhal Toxicol 25, 405-416. https://doi.org/10.3109/08958378.2013.797524

Thornberry, N.A., Bull, H.G., Calaycay, J.R., Chapman, K.T., Howard, A.D., Kostura, M.J., Miller, D.K., Molineaux, S.M., Weidner, J.R., Aunins, J., et al., 1992. A novel heterodimeric cysteine protease is required for interleukin-1 beta processing in monocytes. Nature 356, 768-774. https://doi.org/10.1038/356768a0

Val, S., Liousse, C., Doumbia el, H.T., Galy-Lacaux, C., Cachier, H., Marchand, N., Badel, A., Gardrat, E., Sylvestre, A., Baeza-Squiban, A., 2013. Physico-chemical characterization of African urban aerosols (Bamako in Mali and Dakar in Senegal) and their toxic effects in human bronchial epithelial cells: description of a worrying situation. Part Fibre Toxicol 10, 10. https://doi.org/10.1186/1743-8977-10-10

Washington, R., Todd, M., Middleton, N.J., Goudie, A.S., 2003. Dust-Storm Source Areas Determined by the Total Ozone Monitoring Spectrometer and Surface Observations. Ann Assoc Am Geogr 93, 297-313. https://doi.org/10.1111/1467-8306.9302003

Wessels, A., Birmili, W., Albrecht, C., Hellack, B., Jermann, E., Wick, G., Harrison, R.M., Schins, R.P., 2010. Oxidant generation and toxicity of size-fractionated ambient particles in human lung epithelial cells. Environ Sci Technol 44, 3539-3545. https://doi.org/10.1021/es9036226

World Health Organization (WHO), 2022. Ambient (outdoor) air pollution. https://www.who.int/news-room/fact-sheets/detail/ambient-(outdoor)-air-quality-and-health. Accessed: 03/10/2023

Yanagisawa, R., Takano, H., Ichinose, T., Mizushima, K., Nishikawa, M., Mori, I., Inoue, K., Sadakane, K., Yoshikawa, T., 2007. Gene expression analysis of murine lungs following pulmonary exposure to Asian sand dust particles. Exp Biol Med 232, 1109-1118. https://doi.org/10.3181/0612-RM-311

Yang, L., Li, F., Yan, M., Su, X., 2014. Association of the CYP1A1 MspI and TNFalpha-308 polymorphisms with chronic obstructive pulmonary disease in Inner Mongolia. Genet Mol Res 13, 3209-3217. https://doi.org/10.4238/2014.April.25.6

Zhang, Y., Li, X., Grailer, J.J., Wang, N., Wang, M., Yao, J., Zhong, R., Gao, G.F., Ward, P.A., Tan, D.X., Li, X., 2016b. Melatonin alleviates acute lung injury through inhibiting the NLRP3 inflammasome. J Pineal Res 60, 405-414. https://doi.org/10.1111/jpi.12322

Zou, Y., Chen, X., Liu, J., Zhou, D.B., Kuang, X., Xiao, J., Yu, Q., Lu, X., Li, W., Xie, B., Chen, Q., 2017. Serum IL-1beta and IL-17 levels in patients with COPD: associations with clinical parameters. Int J Chron Obstruct Pulmon Dis 12, 1247-1254. https://doi.org/10.2147/COPD.S131877

3.8 Supplemental material

Table S3.1. Reagents and resources.

Reagent or resource	Source	Catalog no.	Lot/Batch no.
Materials for dust collection			
Ahlstrom micro-quartz fiber filters MK 360	VWR	#BINZ420013	#3614, #3693
Materials for the quantification of water-soluble ions			
Ammonium standard	Sigma/Merck	#59755	
Calcium standard	VWR	#84958180	
Chloride standard	Sigma/Merck	#39883	
Dionex EGC 500 MSA Cartridge	Thermo Fisher	#75779	
Dionex EGC 500 KOH Cartridge	Thermo Fisher	#75778	
Dionex IonPac AG18 guard columns	Thermo Fisher	#60555	
Dionex IonPac AS18 columns	Thermo Fisher	#60553	
Dionex IonPac CG16 guard columns	Thermo Fisher	#88583	
Dionex IonPac CS16 columns	Thermo Fisher	#88582	
Fluoride standard	Sigma/Merck	#77365	
Magnesium standard	VWR	#84975180	
Methansulfonate standard	Sigma/Merck	#42735	
Nitrate standard	Sigma/Merck	#74246	
Oxalate standard	Sigma/Merck	#73139	
Phosphate standard	Sigma/Merck	#90071	
Potassium standard	Sigma/Merck	#53337	
Sodium standard	Sigma/Merck	#43492	
Materials for the quantification of elements			
Cobalt standard solution	Sigma/Merck	#1.19785	#HC55212185
Hydrochloric acid	Roth	#HN53.3	#4121060
Nitric acid	Roth	#HN50.3	#1120080
Scandium standard solution	Roth	#2459.1	#822293
Materials for dust extraction and preparation for *in vitro* cell exposure			
Butyl injection stoppers 20 mm	Faust	#7060433	#8000040077
Cell strainer 20 µm	neoLab	#C-8226	Was not provided
Cell strainer 40 µm	Corning	#431750	#210409
Crimp caps 20 mm	Sigma/Merck	#508500	#149167, #153504
Endotoxin-free water	Sigma/Merck	#TMS-011-A	#3597009, #3808165
Glass vials 20 mL	Fisher Scientific	#10600173	#0000029142
Cell culture materials			
A549 cells	ATCC	#TIB-202	Was not provided
Accutase	Sigma/Merck	#A6964	#SLCH7391, #SLCK9646
Alveolar macrophages	Epithelix Sárl	#EP81AM-1	#MØ0905
Bovine serum albumin (BSA)	Sigma/Merck	#A7906	#SLCH8448

Culture medium for alveolar macrophages	Epithelix Sárl	#EP12AM	Was not provided
D-(+)-Glucose solution	Sigma/Merck	#G8769	#RNBK2839, #RNBK0711
Dulbecco's phosphate buffered saline (PBS)	Sigma/Merck	#D8537	#RNBK6345, #RNBL0127
Fetal calf serum (FCS)	Sigma/Merck	#F7524	#BCCD0778
Hank's Balanced Salt Solution containing $MgCl_2$ and $CaCl_2$	Thermo Fisher	#14025	#2192641
Lipopolysaccharides from E. coli	Sigma/Merck	#L4391	#0000110081, #0000140462
2-Mercaptoethanol	Thermo Fisher	#31350	#2368887
MucilAir culture medium	Epithelix Sárl	#EP05MM	Was not provided
MycoStrip tests	InvivoGen	#rep-mys	#10440-4411
Penicillin-Streptomycin	Sigma/Merck	#P0781	#0000182653
12-phorbol 13-myristate acetate (PMA)	Sigma/Merck	#P1585	#SLCD3659, #SLCL5743
RPMI medium 1640 with HEPES	Thermo Fisher	#52400	#2661119
Sodium pyruvate solution	Thermo Fisher	#11360	#2340203, #2492879
Triton X-100	Sigma/Merck	#T8532	#123K0112
LDH assays materials			
Beta-Nicotinamide adenine dinucleotide (NAD)	Sigma/Merck	#N0632	#SLCG5629
H_2SO_4	Roth	X944.1	#249282395
Iodonitrotetrazolium chloride	Sigma/Merck	#I8377	#SLBZ5575
Lithium L-Lactate	Sigma/Merck	#L2250	#SLCC1372
Multiwell plates, 96-wells	Sigma/Merck	#M4936	#MKCO9390
Phenazine methosulfate	Sigma/Merck	#P9625	#0000116989
TRIS base	Roth	#4855.2	#082320427
TRIS hydrochloride	Sigma/Merck	#T-3253	#69H5424
ELISA materials			
Dulbecco's phosphate buffered saline (PBS), 10x	Sigma/Merck	#D1408	#RNBL0778
H_2SO_4	Roth	X944.1	#249282395
Human IL-1 beta DuoSet ELISA kit	R&D Systems	#DY201	#P218283, #P233743, #P263217, #P275844
Human IL-8 beta DuoSet ELISA kit	R&D Systems	#DY208	#P241644, #P338671, #P348910
Human TNF-alpha beta DuoSet ELISA kit	R&D Systems	#DY210	#P220748, #P266270
Multiwell immuno plates, 96-well	Thermo Fisher	#442404	#177118
$NaHCO_3$	Roth	#HN01.1	#328261885
TMB Peroxidase EIA Substrate Kit	BioRad	#1721067	#64408421, #64477831, #64445745
Tween-20	Sigma/Merck	#P1379	#SLBV2781

Materials for endotoxin quantification			
Acetic acid	Sigma/Merck	#1.00063	#K21620363507
Pierce Chromogenic Endotoxin Quant Kit	Thermo Fisher	#A39552	#0D33D30700

Table S3.2. Interference of dusts with enzyme-linked immune-sorbent assays (ELISAs).

Sampling Day	Concentration	Sampling station	Cytokine recovery in % of negative control					
			$PM_{2.5}$			PM_{10}		
			IL-1β	IL-8	TNFα	IL-1β	IL-8	TNFα
RP D1 26-27/01/2022	100 L/cm²	Station 3	102	100	104	98	102	100
		Station 4	106	98	101	97	98	108
	5 µg/cm²	Station 1	94	95	103	101	99	104
		Station 2	98	96	101	104	100	100
		Station 3	94	96	99	96	99	102
		Station 4	103	105	103	97	93	99
RP D2 27-28/01/2022	100 L/cm²	Station 3	110	105	109	95	99	100
		Station 4	114	106	117	93	100	98
	5 µg/cm²	Station 1	90	107	98	106	107	98
		Station 2	96	99	99	105	108	97
		Station 3	97	105	101	97	108	98
		Station 4	103	110	109	94	101	98
RP D3 28-29/01/2022	100 L/cm²	Station 3	101	106	111	97	103	110
		Station 4	107	102	115	90	99	105
	5 µg/cm²	Station 1	94	95	106	111	100	112
		Station 2	98	99	104	104	104	103
		Station 3	98	97	107	97	99	107
		Station 4	107	102	114	94	97	102
RP D4 29-30/01/2022	100 L/cm²	Station 3	117	108	109	104	102	109
		Station 4	115	106	110	102	104	108
	5 µg/cm²	Station 1	103	86	99	114	91	112
		Station 2	101	81	104	108	95	103
		Station 3	107	85	104	103	99	103
		Station 4	107	83	111	103	82	104
DE1 D1 10-11/02/2022	5 µg/cm²	Station 1	98	95	96	102	89	100
		Station 2	103	93	92	102	90	95

		Station 3	98	73	79	100	95	96
		Station 4	97	97	85	100	101	96
DE1 D2 11-12/02/2022	5 µg/cm²	Station 1	98	78	99	101	99	103
		Station 2	101	90	99	99	74	99
		Station 3	100	88	92	101	71	101
		Station 4	105	92	91	100	82	102
DE1 D3 12-13/02/2022	5 µg/cm²	Station 1	91	87	98	94	88	103
		Station 2	102	106	106	95	88	103
		Station 3	100	90	97	96	87	103
		Station 4	97	90	91	93	90	104
DE2 D1 17-18/02/2022	100 L/cm²	Station 3	83	74	101	78	29	97
		Station 4	86	78	99	73	30	94
	5 µg/cm²	Station 3	95	85	98	115	88	107
		Station 4	91	84	95	104	81	101
DE2 D2 18-19/02/2022	100 L/cm²	Station 3	81	82	100	83	80	99
		Station 4	89	90	99	83	73	97
	5 µg/cm²	Station 3	83	78	98	97	88	98
		Station 4	91	83	100	97	90	96
29/12/2016-06/01/2017	5 µg/cm²	Station 3				92	77	97

Abbreviations: D, Day; DE, Dust Event; IL, interleukin; PM, particulate matter; RP, Reference Period; TNF, tumor necrosis factor. Dates: DD/MM/YYYY.

Table S3.3. Dusts' contents of elements and ions in mg/g.

		$PM_{2.5}$			PM_{10}		
		RP	**DE1**	**DE2**	**RP**	**DE1**	**DE2**
Elements	K	82.7	22.3	13.3	15.7	16.5	9.7
	Ca	74.2	55.1	41.9	36.8	43.4	25.3
	Zn	53.4	7.5	8.1	7.5	1.6	1.0
	Fe	17.6	34.4	13.7	13.2	36.8	25.9
	P	11.8	2.2	1.4	1.9	1.3	0.74
	Mg	8.7	8.7	10.7	11.1	8.5	6.1
	Ba	3.1	0.77	0.20	0.06	0.54	0.43
	Ti	2.8	1.8	0.7	1.3	1.8	1.0
	Mn	0.52	0.70	0.30	0.28	0.65	0.32
	Cr	0.28	0.090	0.037	0.059	0.091	0.052
	Cu	0.26	0.042	0.027	0.016	0.015	0.001
	V	0.24	0.050	0.024	0.023	0.054	0.036
	Ni	0.23	0.15	0.070	0.050	0.022	0.000
	Sr	0.18	0.27	0.13	0.15	0.37	0.15
	Rb	0.045	0.043	0.028	0.013	0.047	0.030
Ions	Cl^-	70.8	19.9	24.3	145.6	49.6	46.2
	SO_4^{2-}	54.5	20.5	23.2	39.8	24.8	18.7
	Na^+	51.1	12.7	16.8	87.2	29.3	27.3
	NO_3^-	19.3	10.7	9.5	24.7	14.6	9.5
	NH_4^+	10.7	3.5	7.2	3.4	3.3	6.1
	Ca^{2+}	3.6	14.4	18.5	12.6	24.4	12.3
	Mg^{2+}	3.6	1.7	2.3	9.4	3.9	3.5
	Oxalate	2.5	1.1	1.0	1.6	0.94	0.70
	PO_4^{3-}	0.50	0.57	0.33	0.59	0.37	0.15
	K^+	0.42	1.2	2.3	3.8	2.4	2.3
	MSA^-	0.12	0.27	0.13	0.18	0.19	0.016
	F^-	0.001	0.045	0.041	0.017	0.040	0.027

The elemental composition was analyzed by total reflection X-rays fluorescence (TXRF). The ionic composition was analyzed by ion chromatography. Abbreviations: MSA^-, methanesulfonic acid; PM, particulate matter.

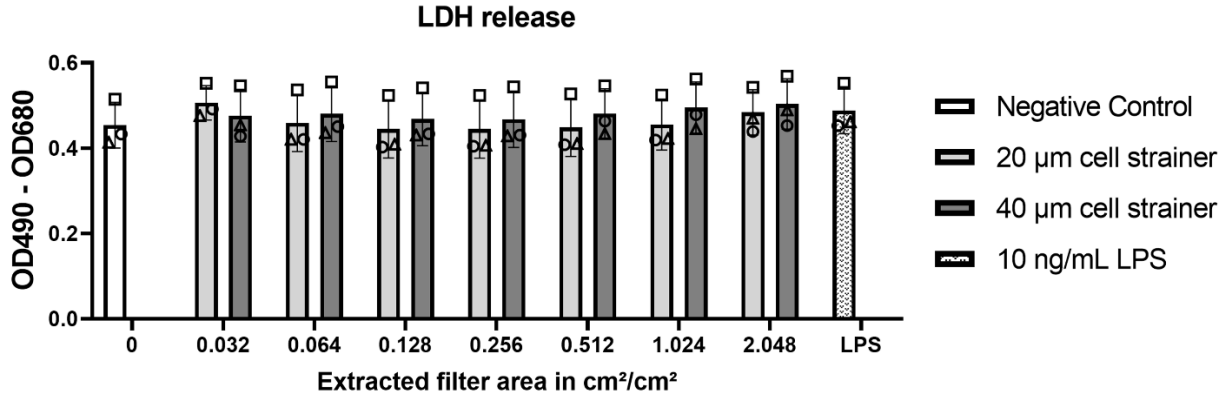

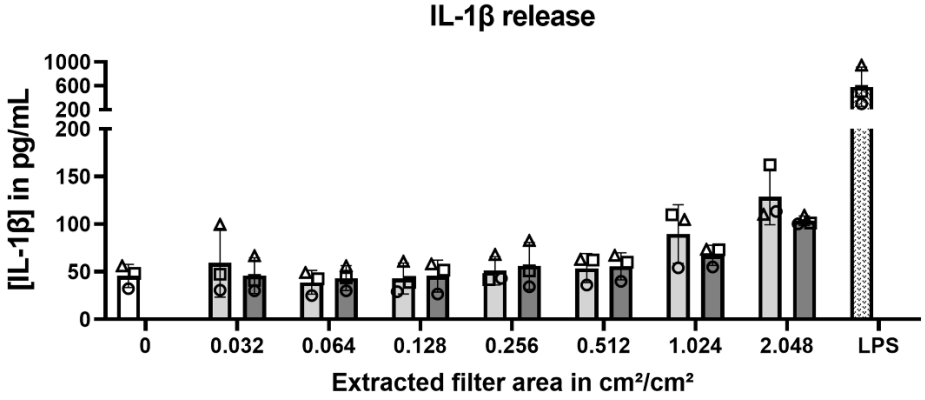

	0.032	0.064	0.128	0.256	0.512	1.024	2.048
20 µm	0.89	0.88	1	0.98	0.90	0.014	0.0003
40 µm	1	1	1	0.63	0.46	0.030	<0.0001

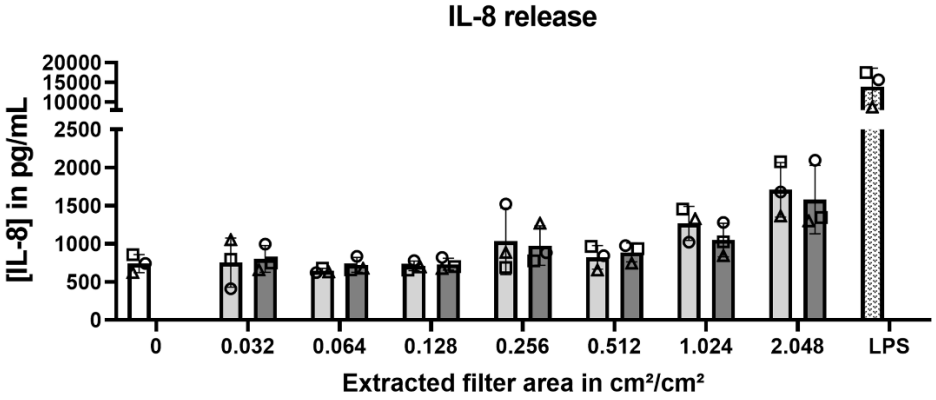

	0.032	0.064	0.128	0.256	0.512	1.024	2.048
20 µm	1	0.98	1	0.65	1	0.12	0.0090
40 µm	0.99	1	1	0.29	0.63	0.10	0.0004

Figure S3.1. Cytotoxicity and cytokine release upon blank filter extract exposure. Blank filters were subjected to the same extraction procedure as filters loaded with dust and passed through cell strainers with pore sizes of 20 µm and 40 µm. THP-1 cells were exposed to filter material corresponding to 0-2.048 cm² extracted filter area per cm² well surface and 10 ng/mL lipopolysaccharides (LPS) as a positive control for cytokine release. The lactate dehydrogenase (LDH) assay was performed on the supernatants.

The releases of IL-1β and IL-8 into the supernatants were assessed via ELISA. Presented are mean values with standard deviations of $N = 3$ independent experiments. Shapes of the data points represent the independent experiments. IL-1β and IL-8 releases upon filter extract exposure were stratified for the pore size of the cell strainer and compared to the unexposed negative control using mixed-effects models with Dunnett's post hoc tests. Exposure was applied as fixed factor and the independent experiment number as random factor. *p*-values are shown in the tables underneath the graphs. Abbreviations: IL, interleukin; LDH, lactate dehydrogenase; LPS, lipopolysaccharides; OD, optical density; SD, Saharan dust.

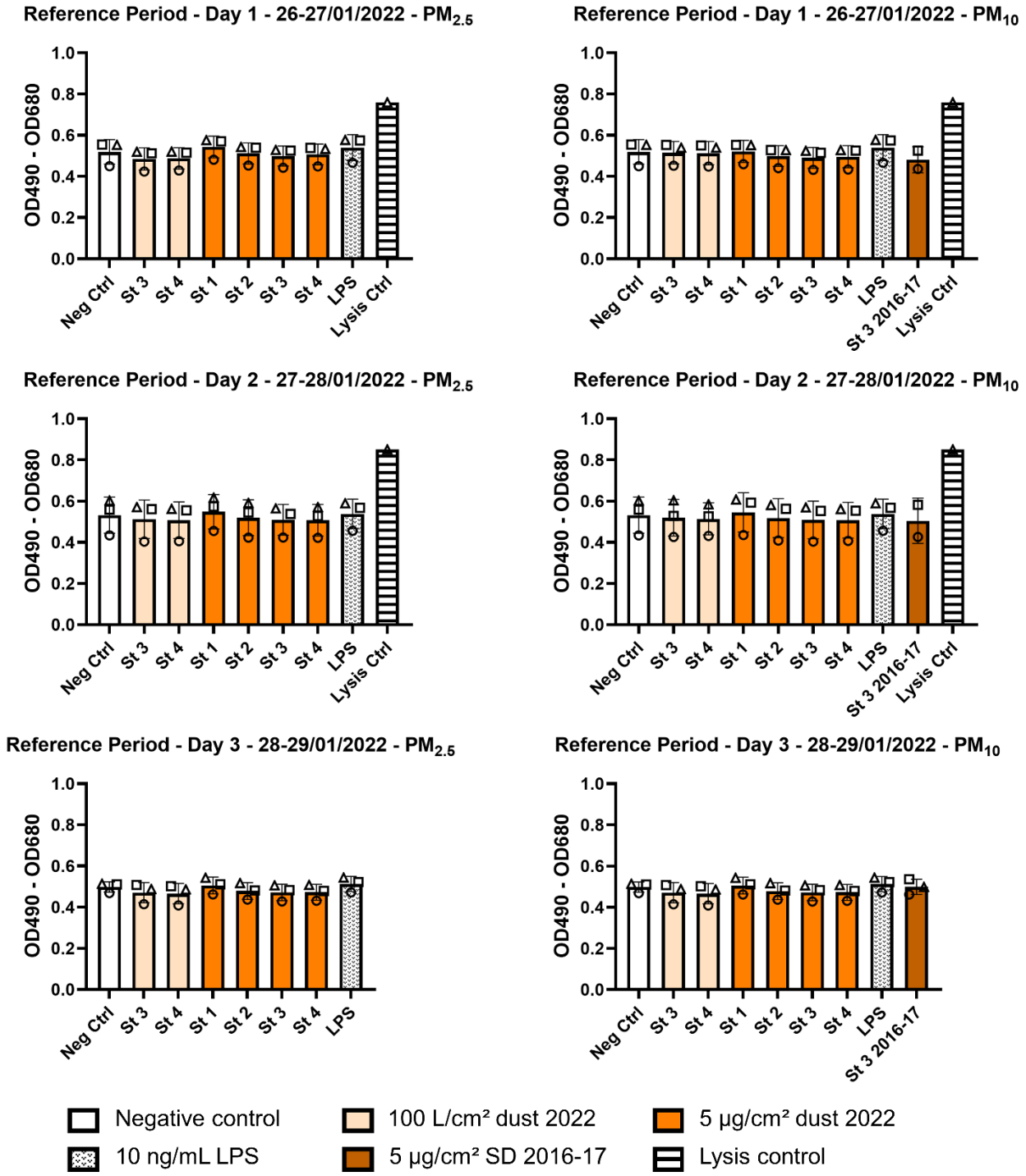

Figure S3.2 continues on the next page.

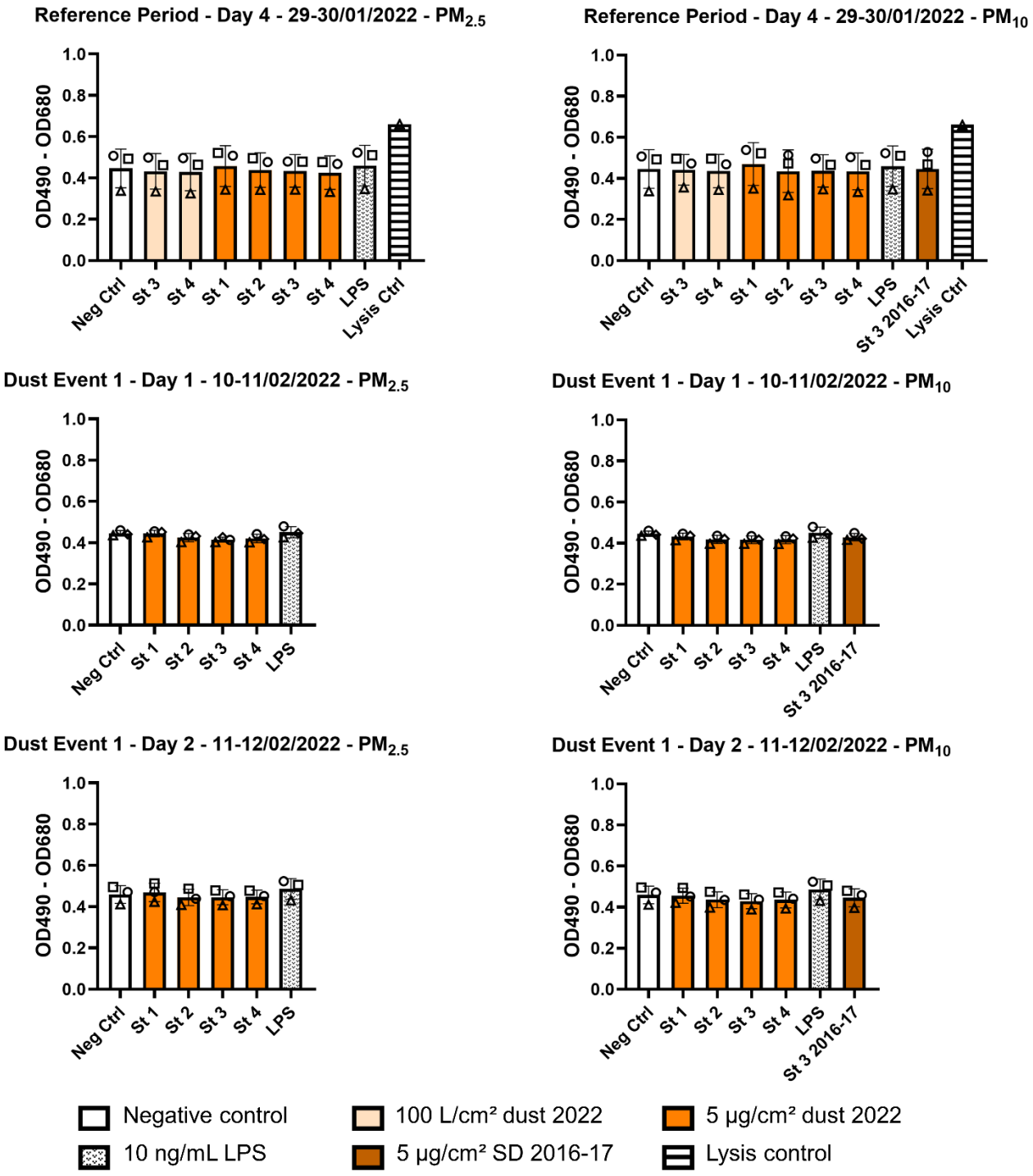

Figure S3.2 continues on the next page.

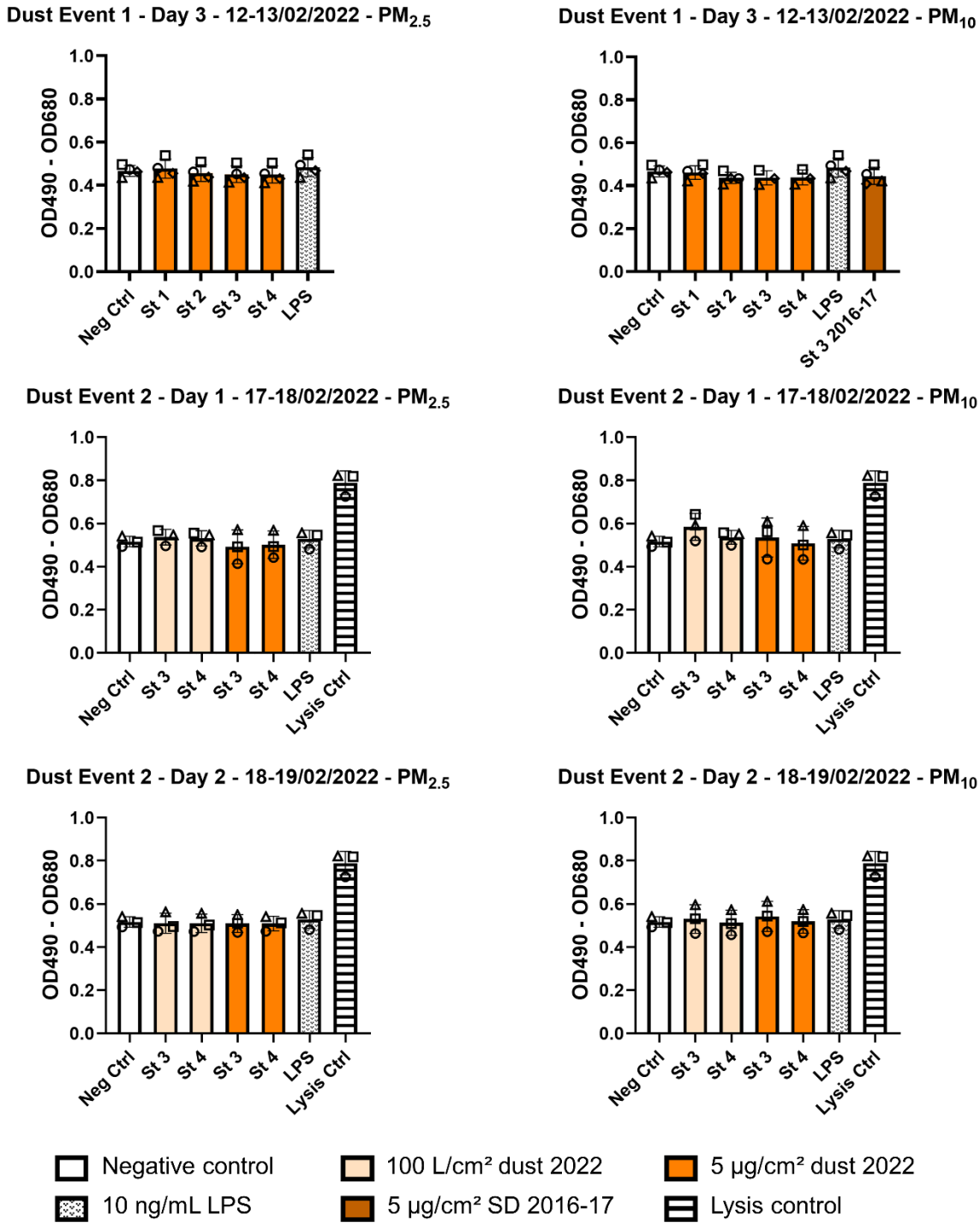

Figure S3.2. Cytotoxicity of dusts according to the lactate dehydrogenase (LDH) assay. THP-1 cells were exposed for 24 h to exposure medium as negative control, 10 ng/mL lipopolysaccharide (LPS), $PM_{2.5}$ and PM_{10} collected 2022 at 5 µg/cm², and 100 L/cm² (the latter concentration only for samples from stations 3 and 4 obtained during the reference period and dust event 2) and 5 µg/cm² SD collected 2016-17. As lysis control, 0.5% Triton X-100 was added 30 min before the end of exposure. Plotted are mean values with standard deviations of *N* = 3-4 independent experiments. Within each plot, points with the same shape belong to the same independent experiment. Abbreviations: LPS, lipopolysaccharides; Neg Ctrl., negative control; OD, optical density; PM, particulate matter; SD, Saharan dust; St, sampling station.

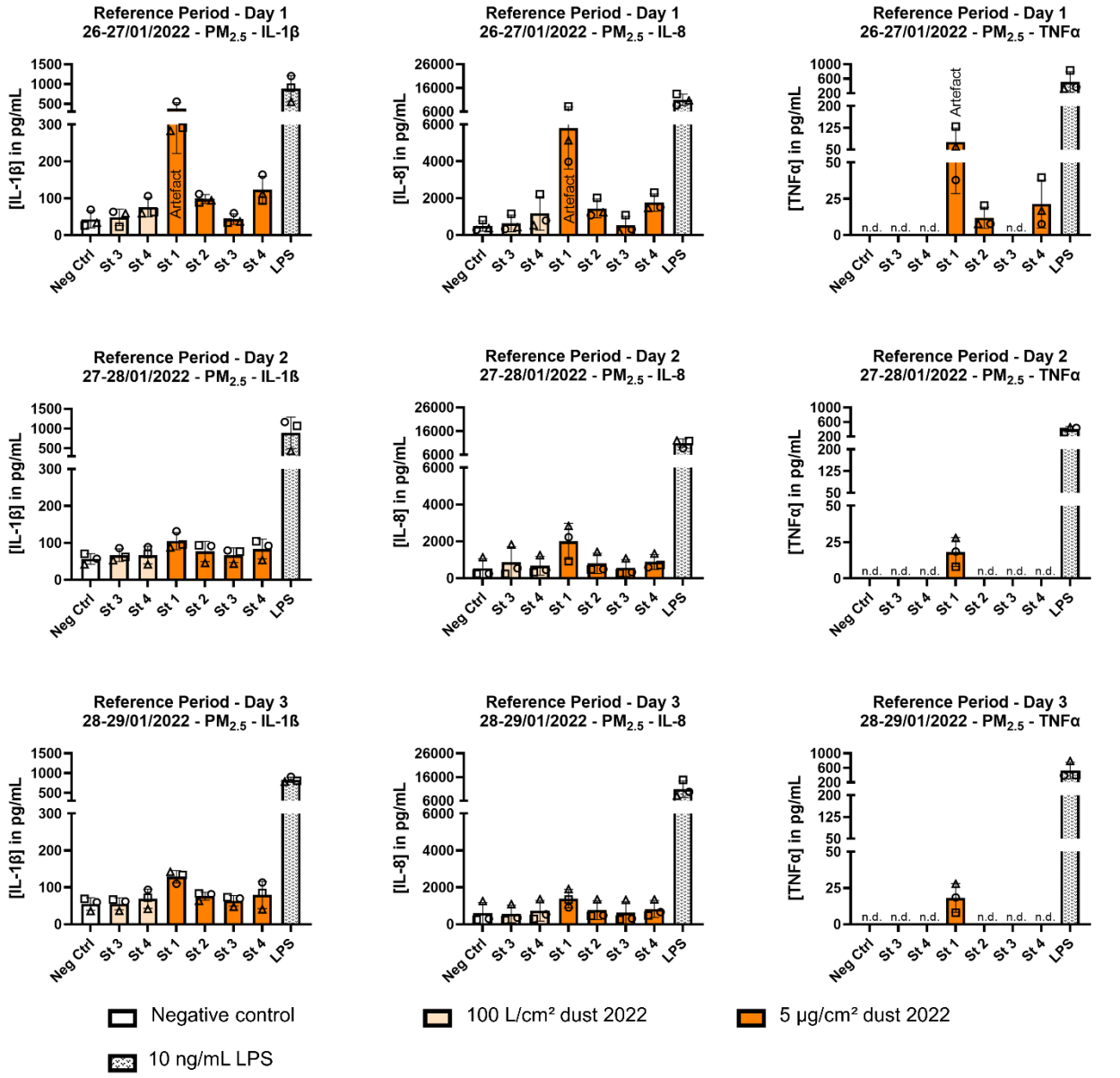

Figure S3.3 continues on the next page.

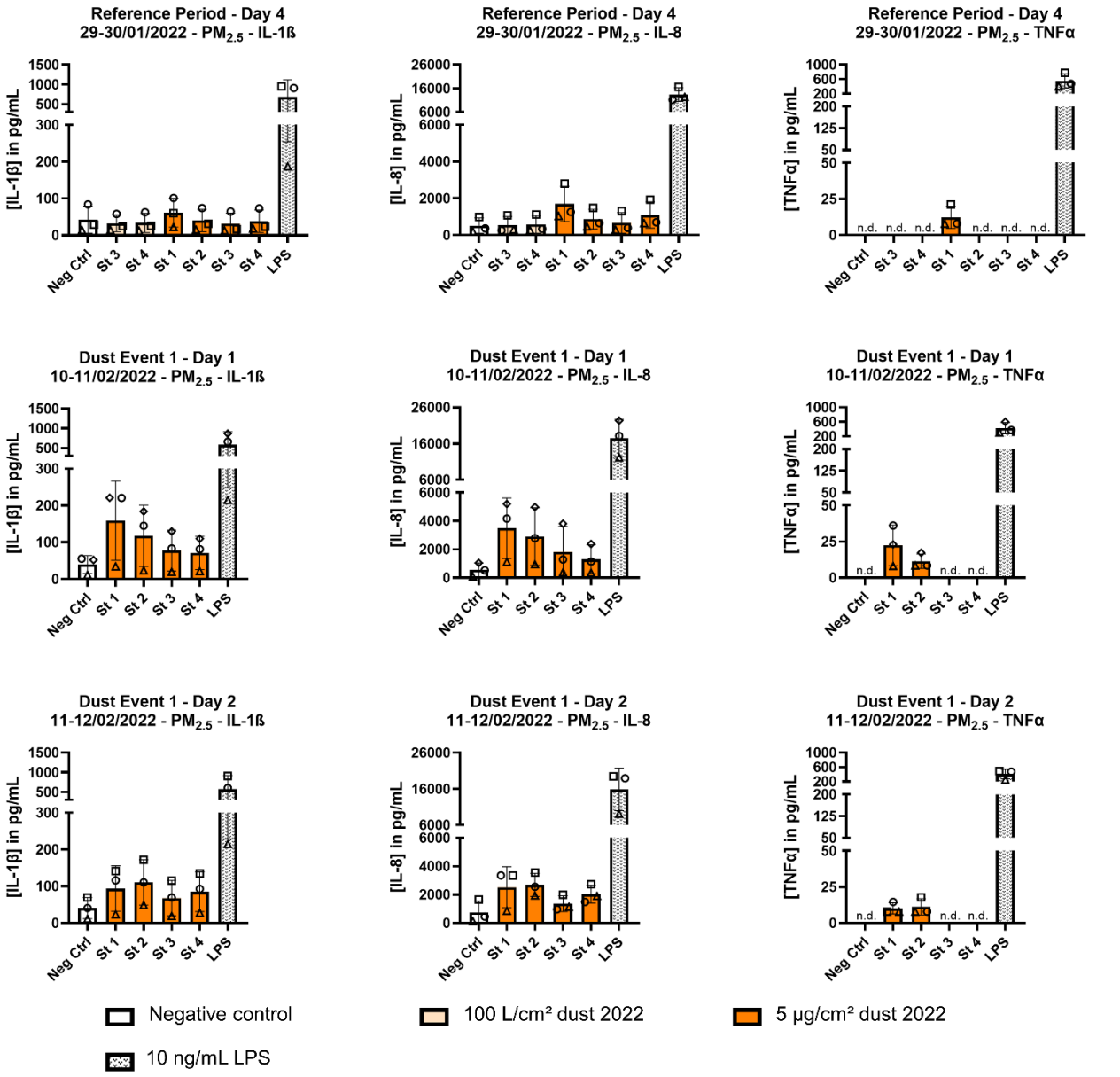

Figure S3.3 continues on the next page.

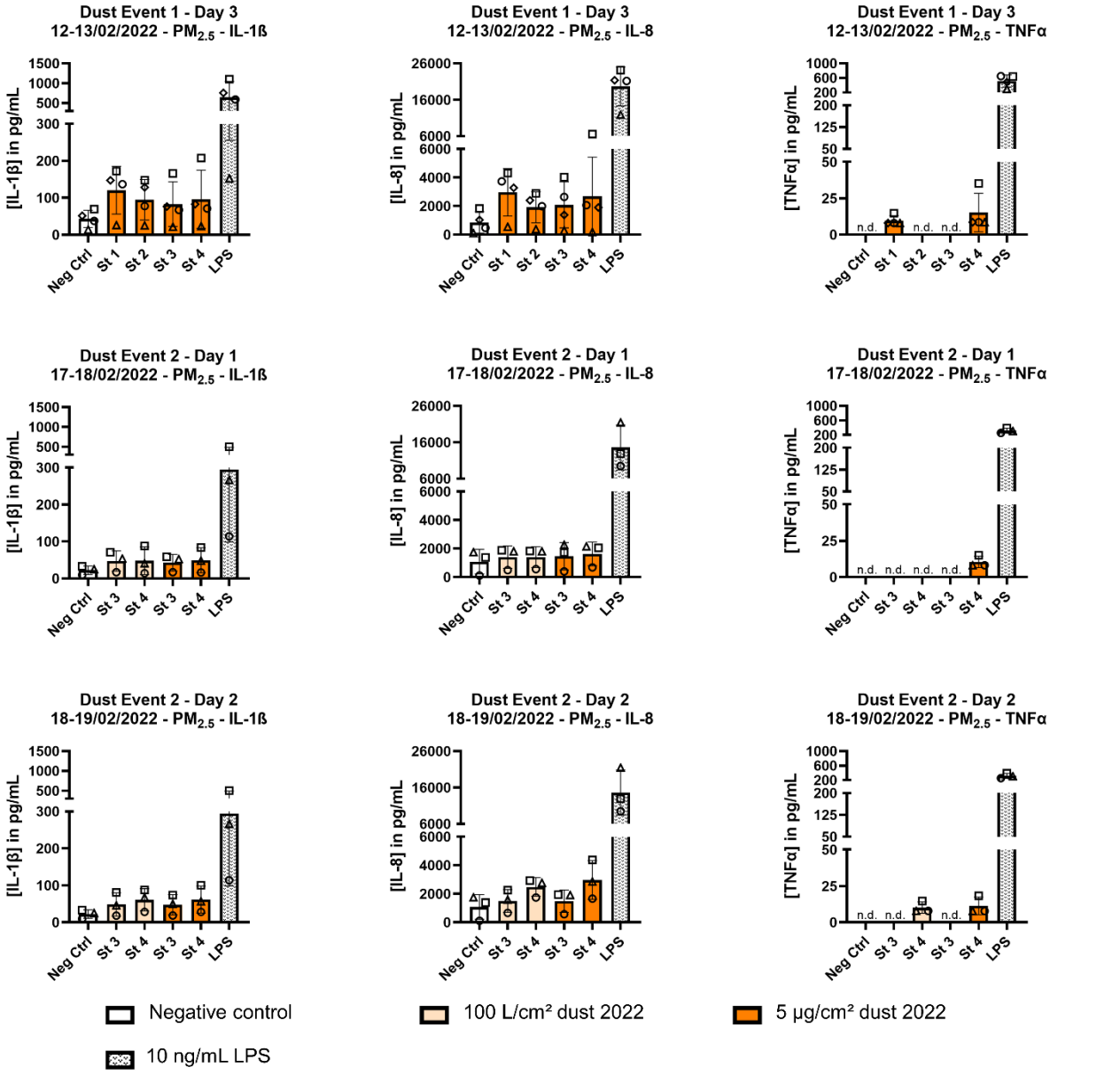

Figure S3.3 continues on the next page.

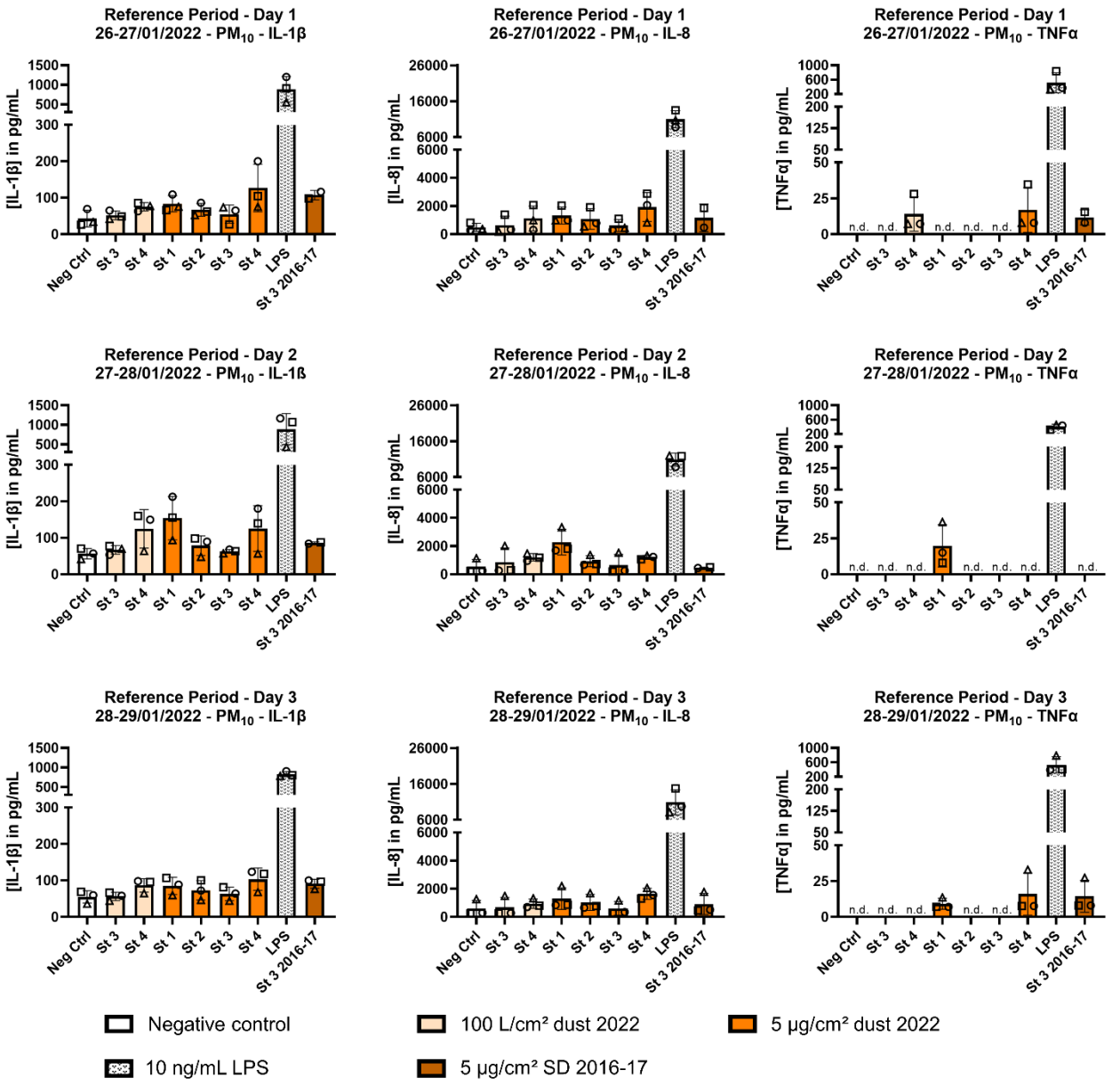

Figure S3.3 continues on the next page.

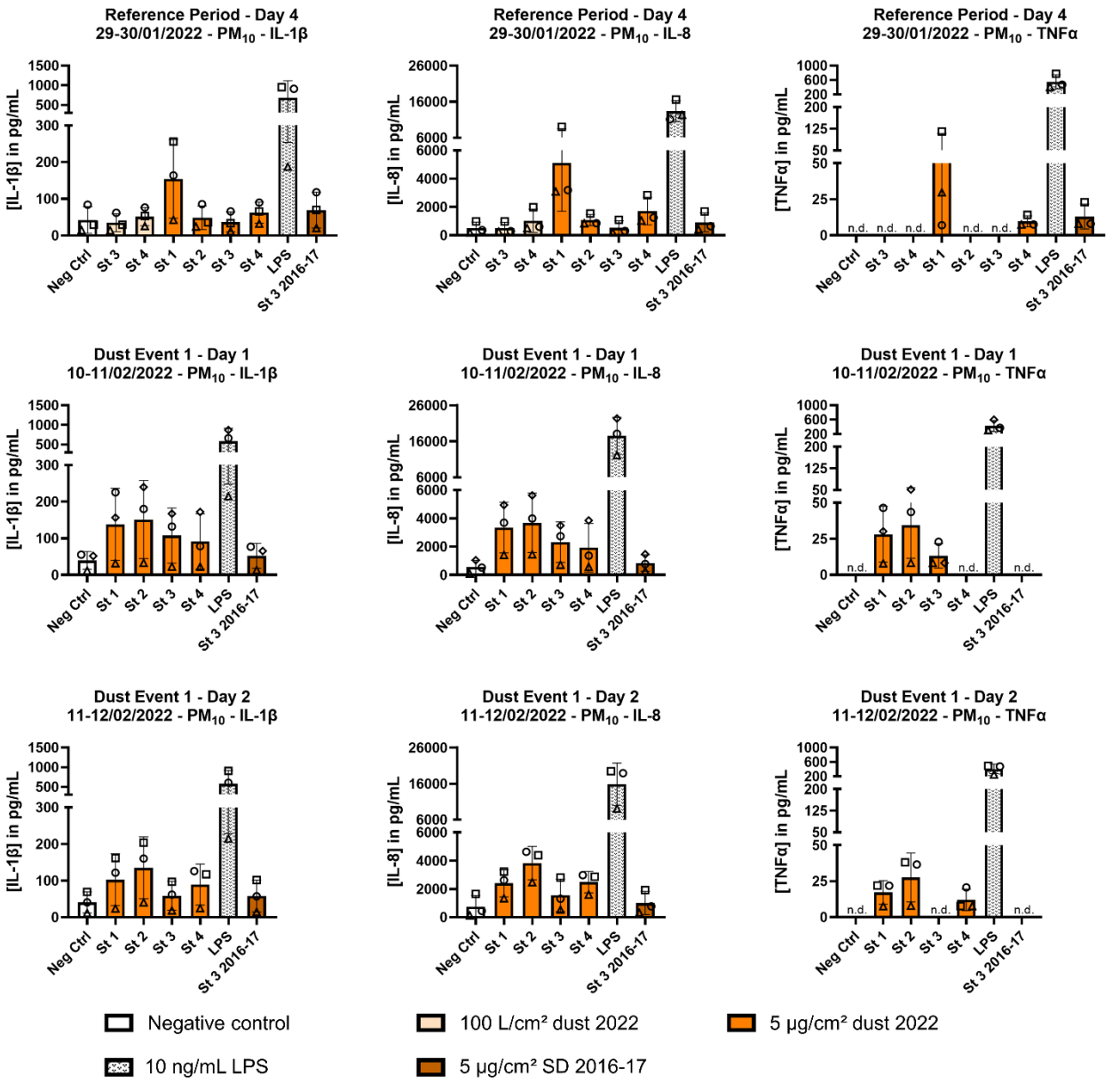

Figure S3.3 continues on the next page.

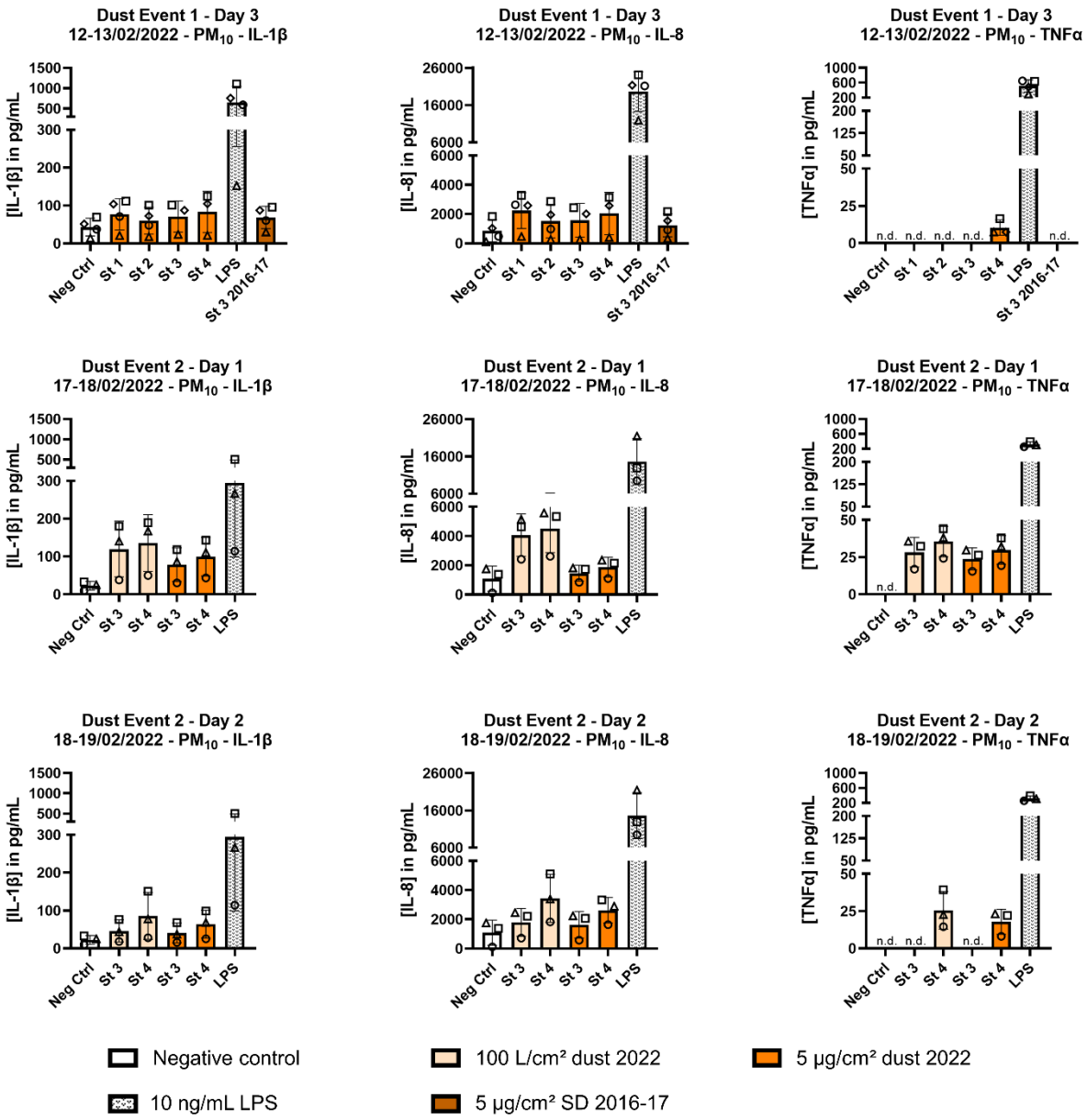

Figure S3.3. IL-1β, IL-8, and TNFα release in response to $PM_{2.5}$ and PM_{10} dust exposure. THP-1 cells were exposed for 24 h to exposure medium as negative control, 10 ng/mL LPS as positive control, $PM_{2.5}$ and PM_{10} dust collected 2022 at 5 µg/cm², and 100 L/cm² (the latter concentration only for samples from stations 3 and 4 obtained during the reference period and dust event 2) and 5 µg/cm² SD collected 2016-17. Cytokine concentrations in the supernatants were measured by ELISA. Plotted are mean values with standard deviations of *N* = 3-4 independent experiments. Within each plot, points with the same shape belong to the same independent experiment. The $PM_{2.5}$ sample collected at station 1 during day 1 of the reference period was regarded an artefact and excluded from analyses and interpretations. Abbreviations: IL, interleukin; LPS, lipopolysaccharides; Neg Ctrl, negative control; PM, particulate matter; SD, Saharan dust; St, sampling station; TNF, tumor necrosis factor. Dates: DD/MM/YYYY.

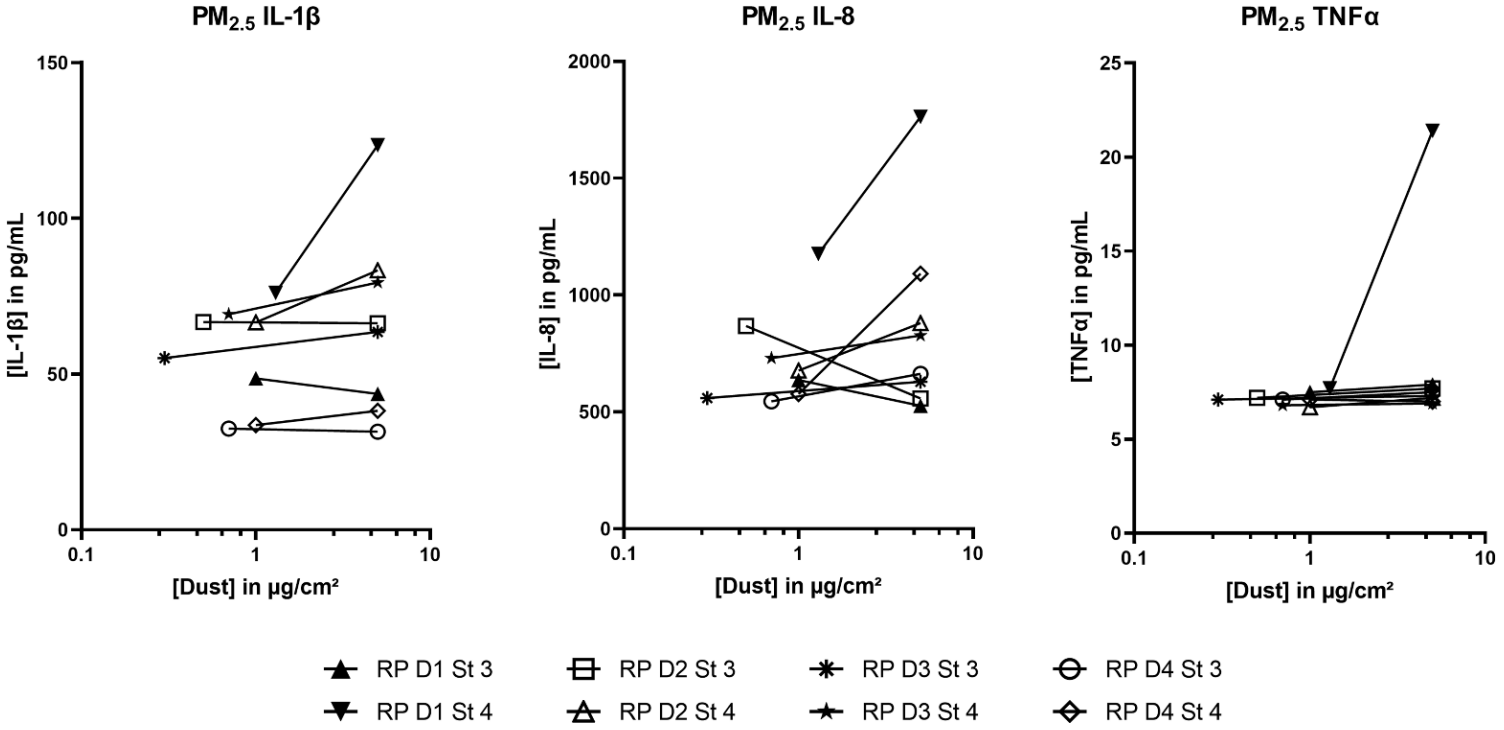

Figure S3.4 continues on the next page.

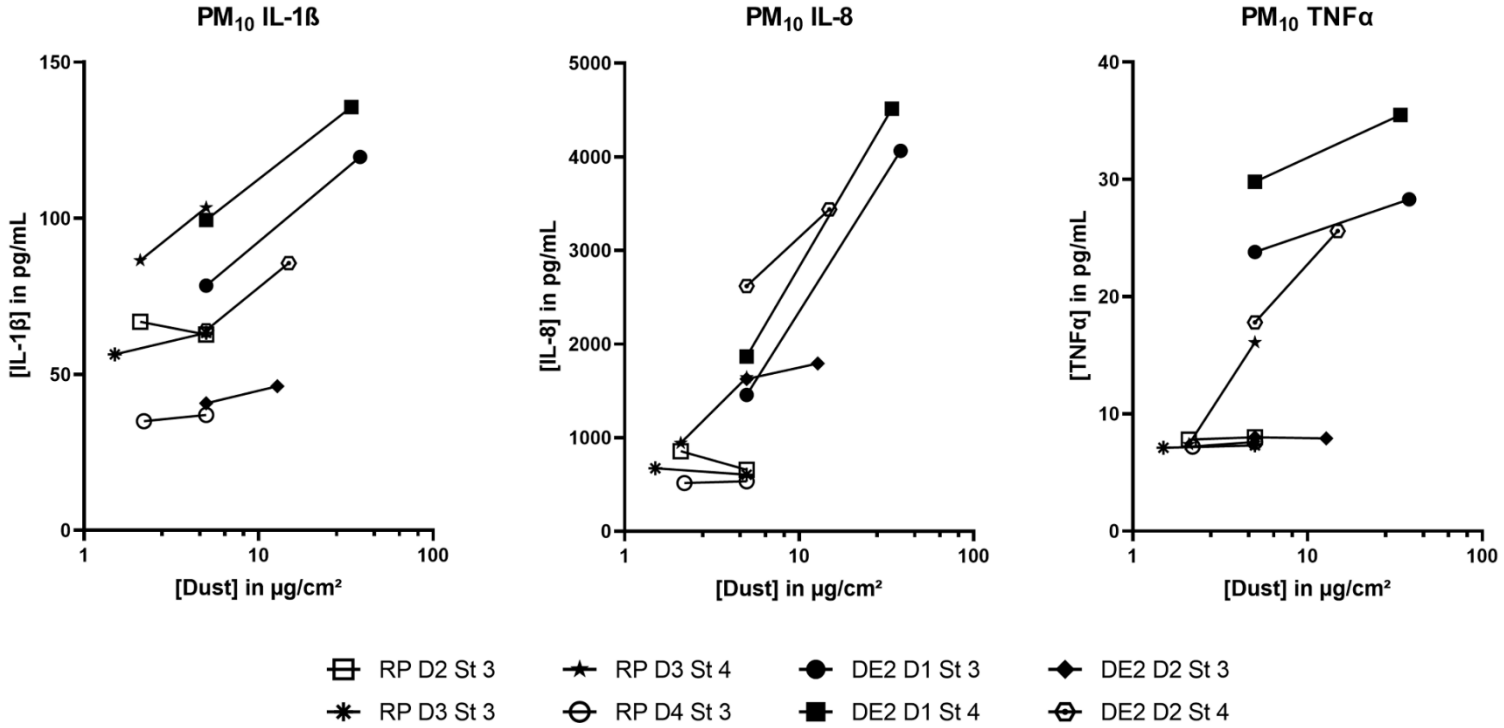

Figure S3.4. Concentration-response relationships upon $PM_{2.5}$ and PM_{10} exposure. $PM_{2.5}$ and PM_{10} dust samples are depicted of which the two tested concentrations differed by at least factor two. THP-1 cells were exposed to dust samples for 24 h before supernatants were collected and IL-1β, IL-8, and TNFα concentrations were determined by ELISA. The plotted cytokine releases are mean values of $N = 3$-4 independent experiments. Abbreviations: D, day; DE, dust event; IL, interleukin; PM, particulate matter; RP, reference period; TNF, tumor necrosis factor.

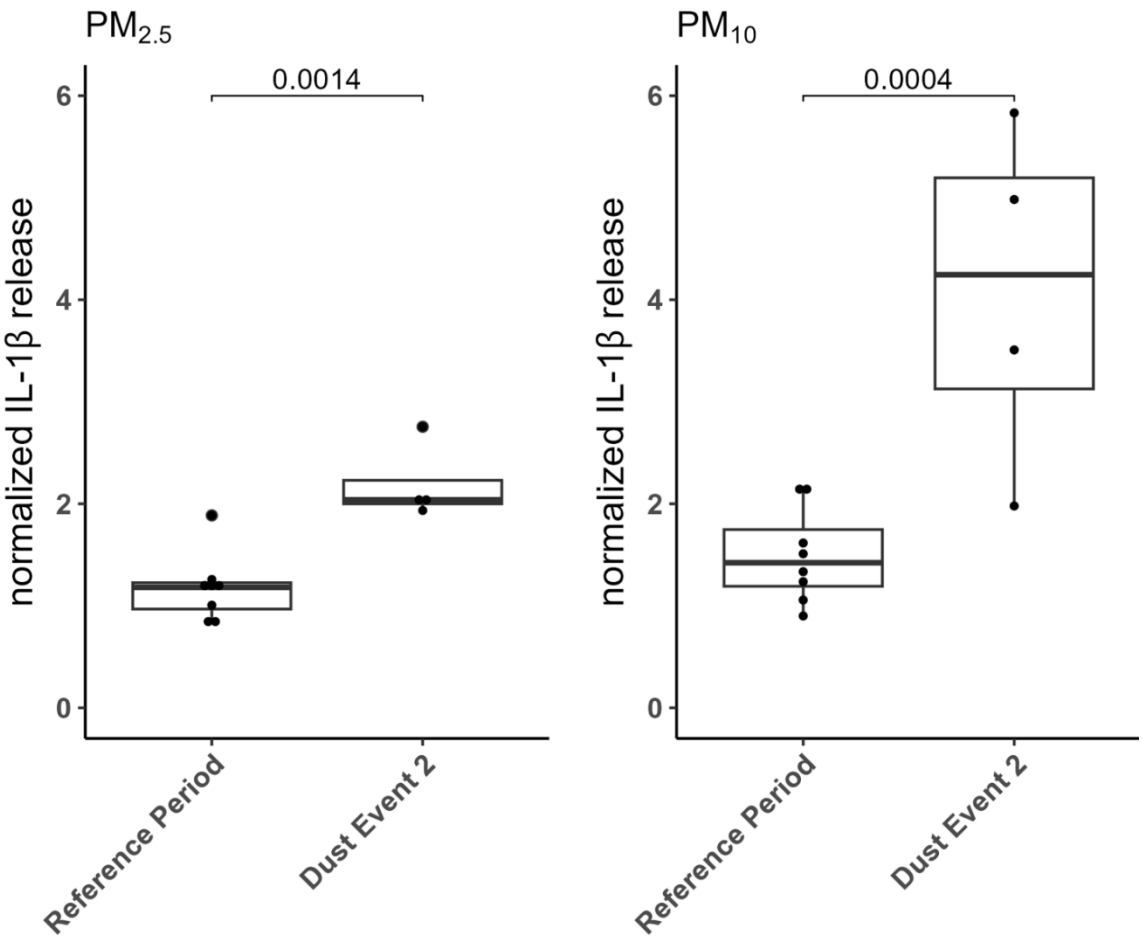

Figure S3.5. Dust event dependent IL-1β release at 100 L/cm². THP-1 cells were exposed to $PM_{2.5}$ and PM_{10} dust concentrations corresponding to 100 L/cm² for 24 h. IL-1β concentrations in the supernatants were measured by ELISA and normalized to unexposed negative controls. Each point represents the mean normalized IL-1β releases of $N = 3$ independent experiments per sampling day and sampling station. *p*-values for the differences between the reference period and dust event 2 are shown in the graphs and were calculated by applying linear models to the natural logarithm of the mean normalized IL-1β releases. The linear models with event as predictor were adjusted for the sampling station. Abbreviations: IL, interleukin; PM, particulate matter.

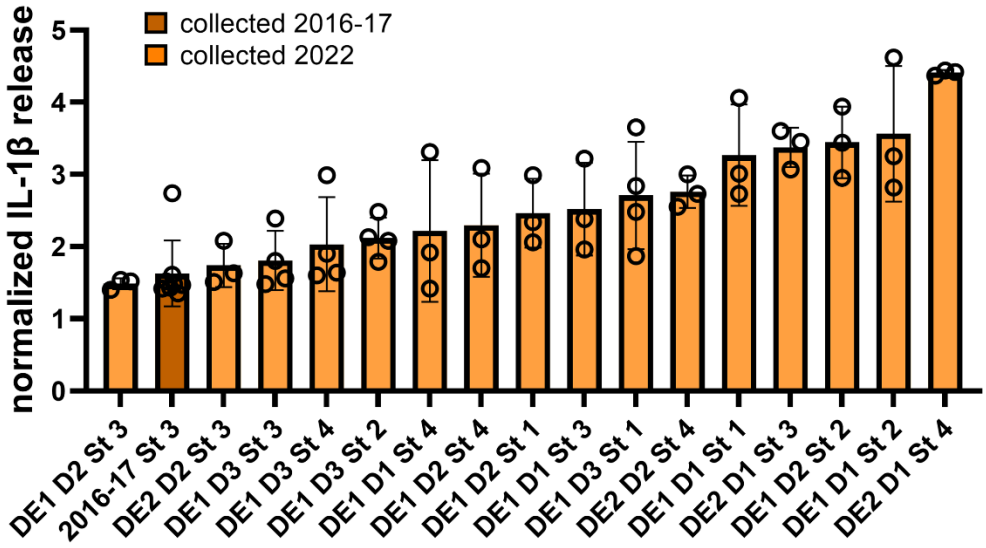

Figure S3.6. PM_{10}-induced IL-1β releases compared to a Saharan dust sample collected 2016-17. THP-1 cells were exposed to 5 µg/cm² of PM_{10} or reference Saharan dust (SD) for 24 h. IL-1β concentrations in the supernatants were measured by ELISA and normalized to unexposed negative controls. *N* = 3-4 independent experiments per sampling day and sampling station were performed for PM_{10} samples collected in 2022 and *N* = 8 independent experiments for the SD sample collected at station 3 from December 29, 2016 to January 6, 2017. Plotted are individual experiments (circles), mean values, and standard deviations. Abbreviations: D, day; DE, dust event; IL, interleukin; St, sampling station.

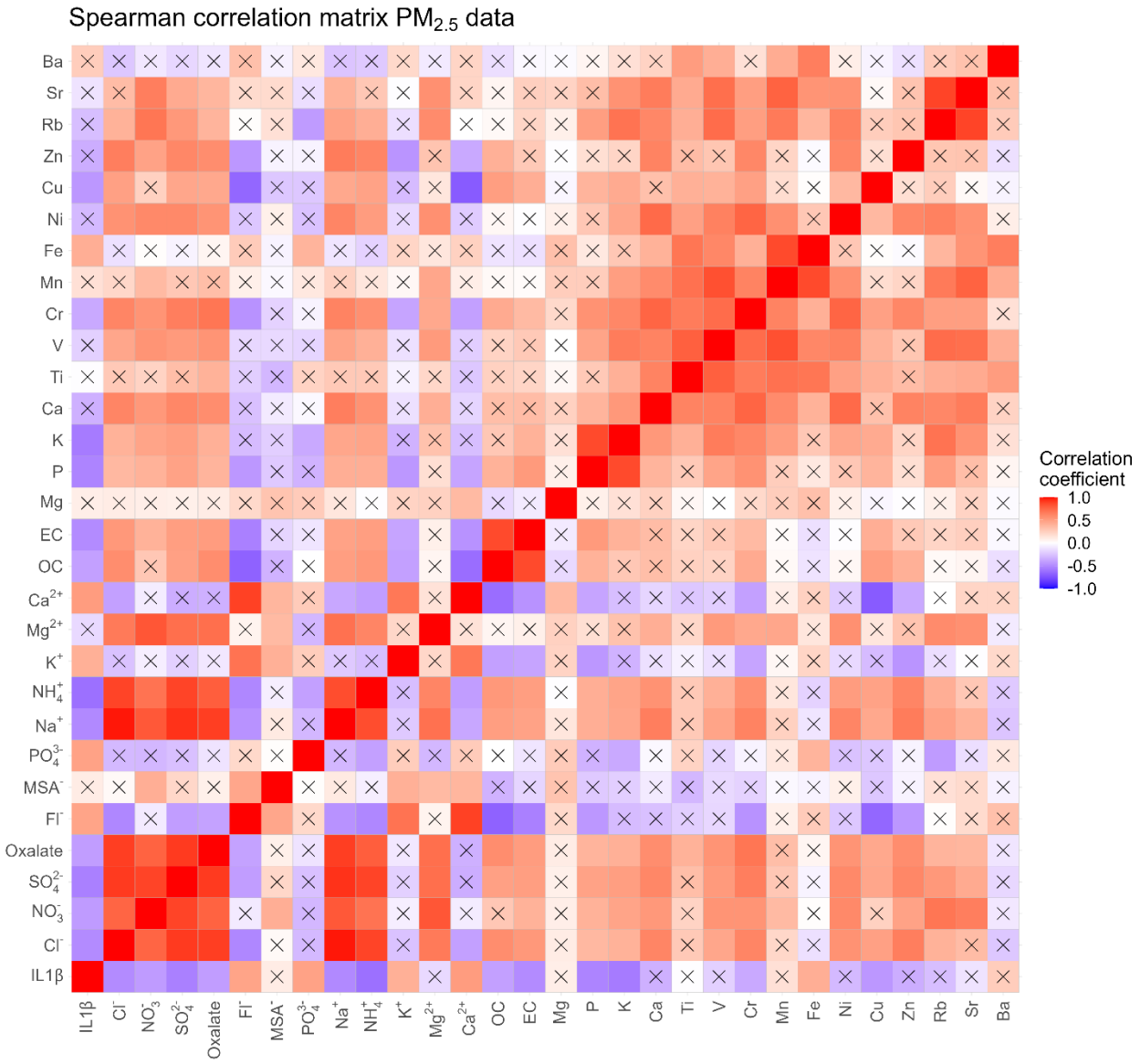

Figure S3.7 continues on the next page.

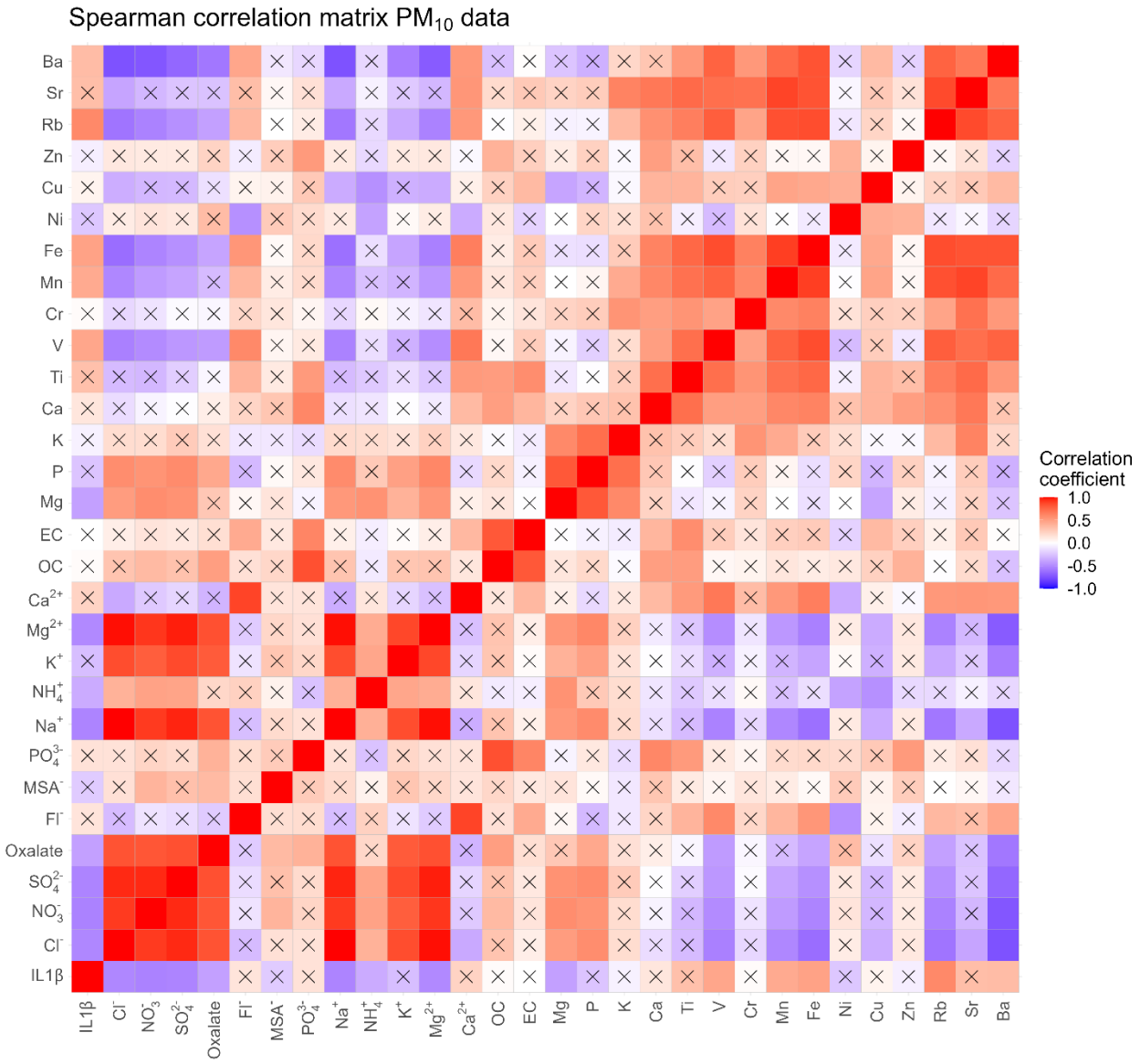

Figure S3.7. Spearman correlations between IL-1β release and PM constituents. THP-1 cells were exposed to 5 µg/cm² $PM_{2.5}$ and PM_{10} for 24 h in *N* = 3-4 independent experiments. IL-1β concentrations in the supernatants were measured by ELISA and normalized to unexposed negative controls. The contents of water-soluble ions, carbonaceous constituents, and elements were measured by ion chromatography, thermal desorption techniques, and total reflection X-ray fluorescence respectively. Spearman correlations were calculated separately for $PM_{2.5}$ and PM_{10}. Correlations with *p*-values ≤ 0.05 were considered statistically significant. Non-significant correlations are marked with an x in the depicted matrices. Abbreviations: EC, elemental carbon; IL, interleukin; MSA^-, methanesulfonic acid; OC, organic carbon; PM, particulate matter.

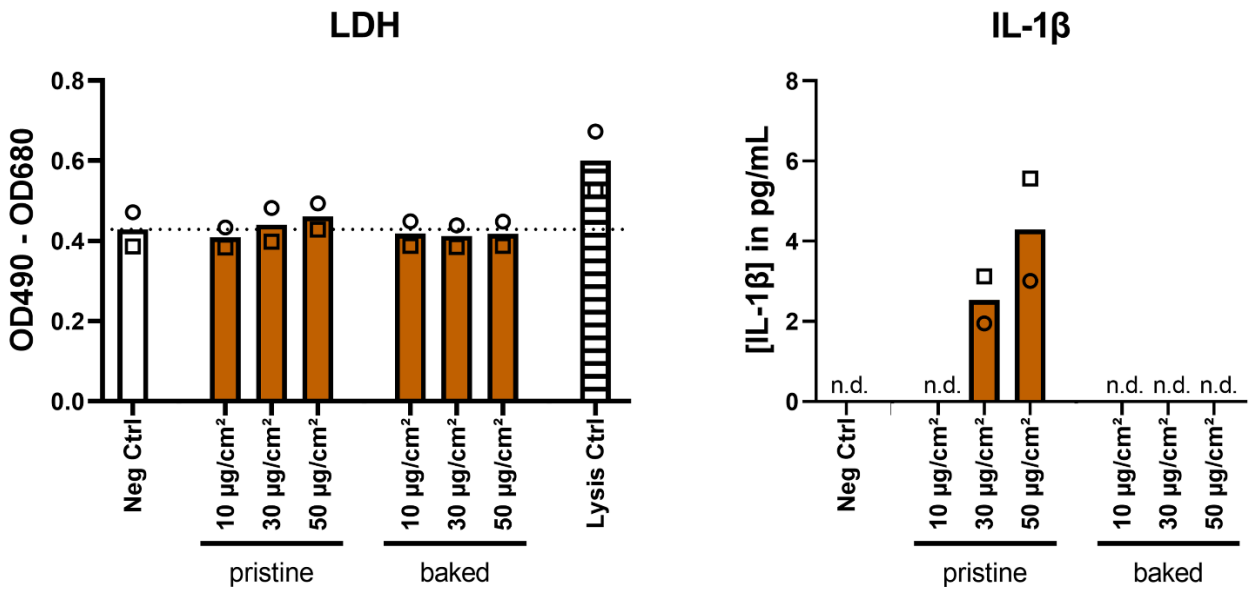

Figure S3.8. LDH and IL-1β release from primary human alveolar macrophages. The macrophages were exposed to pristine and baked (220°C, overnight) SD collected at station 3 from December 29, 2016 to January 6, 2017. As lysis control, 0.5% Triton X-100 was added 30 min before the end of exposure. LDH and IL-1β concentrations in the supernatants after exposure for 24 h were measured by LDH assay and ELISA, respectively. Plotted are mean values of *N* = 2 independent experiments. Points with the same shape belong to the same independent experiment. Abbreviations: Ctrl, control; LDH, lactate dehydrogenase; IL, interleukin; n.d., not detected; Neg Ctrl, negative control; OD, optical density.

4 Saharan dust induces NLRP3-dependent inflammatory cytokines in an alveolar air-liquid interface co-culture model

Gerrit Bredeck,[a] Jochen Dobner,[a] Burkhard Stahlmecke,[b] Khanneh Wadinga Fomba,[c] Hartmut Herrmann,[c] Andrea Rossi,[a] Roel P. F. Schins[a]

[a]*IUF – Leibniz Research Institute for Environmental Medicine, Düsseldorf, Germany*

[b]*Institut für Umwelt & Energie, Technik & Analytik e.V. (IUTA), Duisburg, Germany*

[c]*Atmospheric Chemistry Department (ACD), Leibniz-Institute for Tropospheric Research (TROPOS), Leipzig, Germany*

Particle and Fibre Toxicology (2023) 20:39

Doi: 10.1186/s12989-023-00550-w

Author contribution: The author of this thesis planned and performed *in vitro* experiments, prepared the graphs, interpreted and discussed the results, and wrote the manuscript. Relative contribution: about 75%.

Bredeck *et al. Particle and Fibre Toxicology* (2023) 20:39
https://doi.org/10.1186/s12989-023-00550-w

Particle and Fibre Toxicology

RESEARCH Open Access

Saharan dust induces NLRP3-dependent inflammatory cytokines in an alveolar air-liquid interface co-culture model

Gerrit Bredeck[1*], Jochen Dobner[1], Burkhard Stahlmecke[2], Khanneh Wadinga Fomba[3], Hartmut Herrmann[3], Andrea Rossi[1] and Roel P. F. Schins[1]

Abstract

Background Epidemiological studies have related desert dust events to increased respiratory morbidity and mortality. Although the Sahara is the largest source of desert dust, Saharan dust (SD) has been barely examined in toxicological studies. Here, we aimed to assess the NLRP3 inflammasome-caspase-1-pathway-dependent pro-inflammatory potency of SD in comparison to crystalline silica (DQ12 quartz) in an advanced air-liquid interface (ALI) co-culture model. Therefore, we exposed ALI co-cultures of alveolar epithelial A549 cells and macrophage-like differentiated THP-1 cells to 10, 21, and 31 µg/cm² SD and DQ12 for 24 h using a Vitrocell Cloud system. Additionally, we exposed ALI co-cultures containing *caspase* (*CASP*)*1*$^{-/-}$ and *NLRP3*$^{-/-}$ THP-1 cells to SD.

Results Characterization of nebulized DQ12 and SD revealed that over 90% of agglomerates of both dusts were smaller than 2.5 µm. Characterization of the ALI co-culture model revealed that it produced surfactant protein C and that THP-1 cells remained viable at the ALI. Moreover, wild type, *CASP1*$^{-/-}$, and *NLRP3*$^{-/-}$ THP-1 cells had comparable levels of the surface receptors cluster of differentiation 14 (CD14), toll-like receptor 2 (TLR2), and TLR4. Exposing ALI co-cultures to non-cytotoxic doses of DQ12 and SD did not induce oxidative stress marker gene expression. SD but not DQ12 upregulated gene expressions of interleukin 1 Beta (*IL1B*), *IL6*, and *IL8* as well as releases of IL-1β, IL-6, IL-8, and tumor necrosis factor α (TNFα). Exposing wild type, *CASP1*$^{-/-}$, and *NLRP3*$^{-/-}$ co-cultures to SD induced *IL1B* gene expression in all co-cultures whereas IL-1β release was only induced in wild type co-cultures. In *CASP1*$^{-/-}$ and *NLRP3*$^{-/-}$ co-cultures, IL-6, IL-8, and TNFα releases were also reduced.

Conclusions Since surfactants can decrease the toxicity of poorly soluble particles, the higher potency of SD than DQ12 in this surfactant-producing ALI model emphasizes the importance of readily soluble SD components such as microbial compounds. The higher potency of SD than DQ12 also renders SD a potential alternative particulate positive control for studies addressing acute inflammatory effects. The high pro-inflammatory potency depending on NLRP3, CASP-1, and IL-1β suggests that SD causes acute lung injury which may explain desert dust event-related increased respiratory morbidity and mortality.

Keywords African dust, Lung inflammation, Alveolar epithelium, In vitro, Endotoxin

*Correspondence:
Gerrit Bredeck
gerrit.bredeck@iuf-duesseldorf.de
[1]IUF – Leibniz Research Institute for Environmental Medicine, 40225 Düsseldorf, Germany
[2]Institut für Umwelt & Energie, Technik & Analytik e. V. (IUTA), 47229 Duisburg, Germany
[3]Atmospheric Chemistry Department (ACD), Leibniz Institute for Tropospheric Research (TROPOS), 04318 Leipzig, Germany

Background

Epidemiological studies have revealed that desert dust exposure increases respiratory morbidity and mortality [1–5]. In toxicological studies, desert dusts from different regions have been demonstrated to induce oxidative stress and inflammatory signaling. Especially Asian sand dust [6, 7], Middle East desert dust [8, 9], and Northern American desert dust [10, 11] have been tested in animal models as well as in cell culture models of epithelial cells and macrophages. Studies comparing desert dusts from different sources or different dust events reported variations in toxic potencies related to their heterogeneous composition [7, 9, 12, 13]. Desert dusts are mixtures containing amongst others inorganic particles, metals, and ions as well as organic carbon compounds, microbial components such as fungal β-glucans and bacterial endotoxins, and even viable microbes [7, 9, 14, 15].

Although Saharan dust (SD) accounts for over 50% of the global desert dust emission [16], few studies have addressed its toxicity: Organic extracts from SD collected in Puerto Rico [17–19] and SD containing urban pollutants from Mali [20] were shown to trigger oxidative stress and inflammation using in vitro models of bronchial epithelial cells. Furthermore, we could recently demonstrate that SD collected on the Cape Verde islands induced oxidative stress and inflammatory cytokines in alveolar epithelial A549 cells as well as pro-inflammatory cytokine secretion from macrophage-like THP-1 cells [21]. The latter was strongly dependent on the NACHT, LRR, and PYD domains-containing protein 3 (NLRP3) inflammasome.

Activation of the NLRP3 inflammasome is a two-step process that leads to the secretion of the pro-inflammatory cytokine interleukin (IL)-1β from innate immune cells such as macrophages. The first, or priming, step can be mediated by toll-like receptor (TLR) signaling which is triggered by microbial danger signals, e.g. lipopolysaccharides [22, 23]. Upon priming the expressions of NLRP3 and pro-IL-1β are upregulated [22, 23]. The second, or activation, step can be mediated by multiple stimuli, including bacterial pathogens and their components, and particles such as quartz (extensively reviewed in [24]). In the activation step, the NLRP3 inflammasome is assembled, leading to the activation of caspase (CASP)-1, which in turn cleaves pro-IL-1β to mature IL-1β [25, 26]. Mature IL-1β induces further cytokines such as IL-6 and IL-8 [27–29]. The NLRP3-mediated production of IL-1β has a critical role in acute lung injury [30–32] and is crucial in the development of particle-induced lung inflammation and fibrosis, i.e. silicosis [33, 34]. Apart from IL-1β, the NLRP3 inflammasome-CASP-1 pathway also leads to the release of IL-18 from macrophages [33, 35]. The role of IL-18 in silicosis is less well established than of IL-1β [36–38]. Besides IL-1β, tumor necrosis factor α (TNFα) is the other critical early pro-inflammatory cytokine for the development of acute lung injury [39] and silicosis [40].

In this study, we analyzed the effects of SD in an air-liquid interface (ALI) co-culture model of A549 and differentiated THP-1 cells combining two major advantages. Firstly, the culture at the ALI enables more realistic exposure conditions and causes more realistic properties, e.g. production of surfactant and a lower surface tension through higher amounts of lipids [41–43]. Secondly, the co-culture of both cell types enables their cross-talk. Cytokines released from macrophages can substantially enhance the cytokine response of epithelial cells [44, 45]. The other way around, contact with epithelial cells shapes the activity of alveolar macrophages [46–49]. For instance, surfactant proteins A and C have been reported to attenuate the activations of TLR2 [48], TLR4 [49], and cluster of differentiation (CD)14 [50] through microbial components. Moreover, the surfactant lining can facilitate the uptake of particles by macrophages and epithelial cells [51]. Also, surfactants can decrease the cytotoxicity towards alveolar macrophages and the pro-inflammatory activity of quartz dust [52–54]. While desert dust represents one of the main sources of global non-anthropogenic air pollution, to the best of our knowledge, to date, desert dust has neither been tested in a co-culture of epithelial cells and macrophages nor in an ALI co-culture model.

Using this advanced ALI co-culture model, we aimed to compare the potencies of SD and DQ12 quartz dust to induce oxidative and pro-inflammatory signaling. In addition, we sought to analyze the role of the NLRP3 inflammasome regarding potential pro-inflammatory effects in this ALI co-culture model.

Results

Size distribution of nebulized dusts

To assess the size distribution of DQ12 and SD deposited on the ALI co-cultures, we examined nebulized dust by scanning electron microscopy (SEM) (Fig. 1; Fig. S1, Additional File 1). Since a particle can consist of smaller (primary) particles that agglomerated to a bigger compact particle which is considered to be relevant for exposure, we did not assess the primary particle size distribution but the agglomerate size distribution. The sizes of agglomerates (including single particles) were log-normally distributed with mode diameters of 223 nm (variance of $\sigma=2.18$) and 176 nm (variance of $\sigma=1.55$) for DQ12 and SD, respectively. Nebulized DQ12 consisted of larger agglomerates than SD. About 93% and 97% of DQ12 and SD agglomerates were smaller than 1.0 µm, respectively. More than 99% of agglomerates of both dusts were smaller than 2.5 µm.

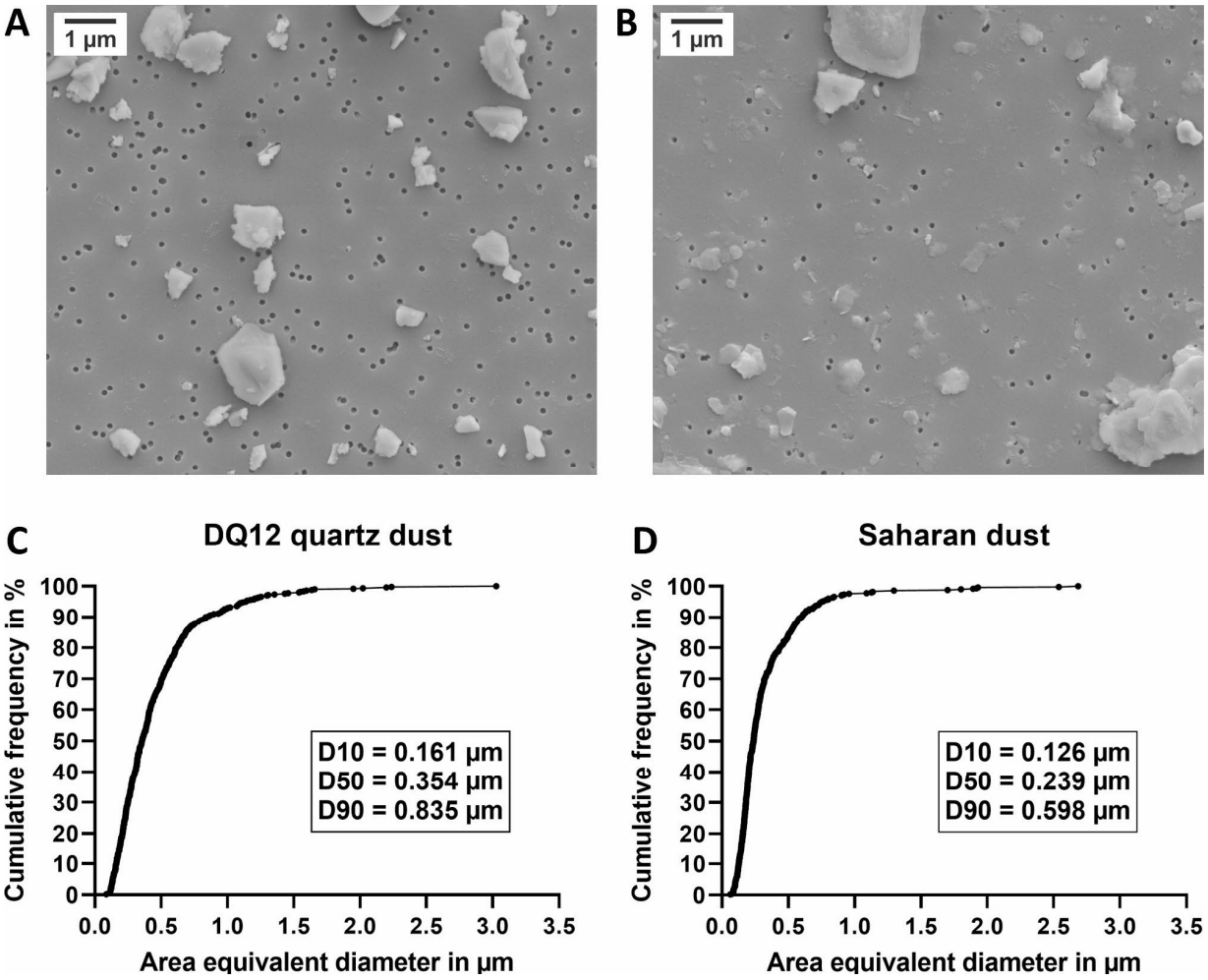

Fig. 1 Cumulative agglomerate size distributions of area equivalent diameters. Suspensions of DQ12 quartz dust (**A**, **C**) and Saharan dust (**B**, **D**) in endotoxin-free H_2O containing 1.25% PBS were sonicated and nebulized onto 0.1 µm pore-size nucleopore filters. SEM images were obtained at a nominal magnification of 5,000 x (pixel size: 6.2 nm). Images **A** and **B** show excerpts from images used for size determination. For 500 agglomerates, the area equivalent diameter was determined based on $Feret_{max}$ and $Feret_{min}$ diameters (**C**, **D**)

Characterization of the in vitro model

To analyze whether the surface levels of the receptors CD14, TLR2, and TLR4 were different between differentiated wild type, *CASP1*$^{-/-}$, and *NLRP3*$^{-/-}$ THP-1 cells, we performed immuno-staining and assessed the cells via flow cytometry (Fig. 2; Fig. S2, Additional File 2). We did not observe significant differences in surface levels between the genotypes for any of the investigated receptors. These results indicate that wild type, *CASP1*$^{-/-}$, and *NLRP3*$^{-/-}$ THP-1 cells can be used to assess the role of the NLRP3 inflammasome-CASP-1 pathway without confounding through differential surface levels of upstream receptors.

We analyzed the capacity of co-cultures of A549 cells with wild type, *CASP1*$^{-/-}$, and *NLRP3*$^{-/-}$ THP-1 cells and A549 mono-cultures to produce surfactant protein C (SP-C) by immuno-staining and visualization by fluorescence microscopy (Fig. 3). Simultaneously, we examined the presence of differentiated THP-1 cells after 48 h of ALI culture via staining of CD45. We observed slightly stronger staining of SP-C for the co-cultures than for A549 mono-cultures. The genotype of the THP-1 cells did not influence the intensity of SP-C staining. CD45 staining indicated that THP-1 cells of all genotypes were still present after 48 h of ALI culture. The correct genotypes of THP-1 cells were confirmed by submerged lipopolysaccharide (LPS) exposure of THP-1 cell mono-cultures in parallel to ALI co-culture experiments and comparison of the IL-1β release to the results from a previous study (Fig. S3, Additional File 3) [55].

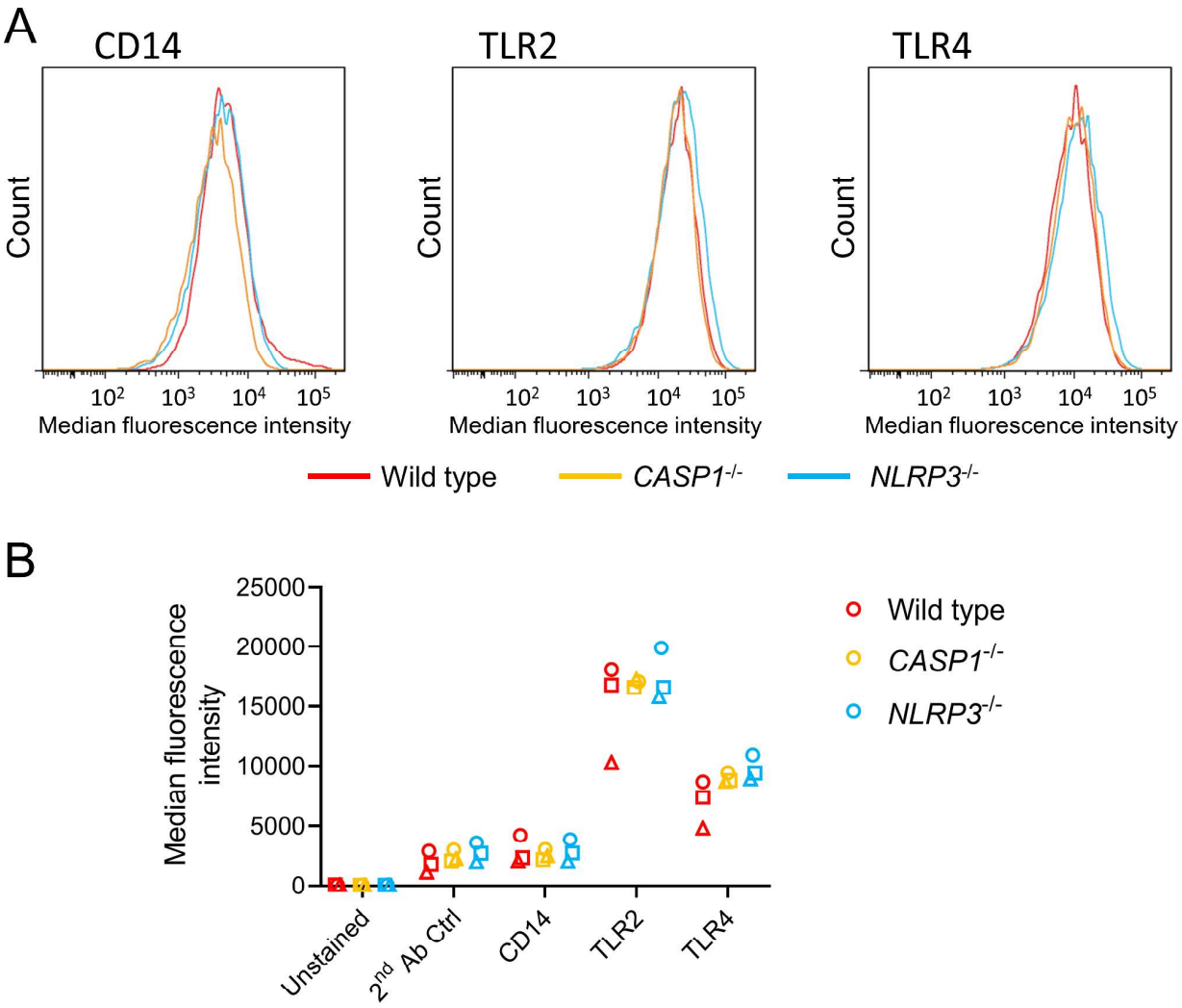

Fig. 2 Surface receptor levels of CD14, TLR2, and TLR4 of differentiated THP-1 cells. Differentiated wild type, *CASP1*$^{-/-}$, and *NLRP3*$^{-/-}$ THP-1 cells were immuno-stained for surface CD14, TLR2, or TLR4. Fluorescence intensities were measured by flow cytometry. Representative histograms are shown in **A**. The median fluorescence intensities from $N=3$ independent experiments are plotted in **B** (one biological replicate per group). A two-way ANOVA with Tukey's post hoc test was calculated (no significant differences between genotypes obtained; different shapes represent experimental runs)

Toxicities of DQ12 quartz dust and Saharan dust at the air-liquid interface

We exposed the co-cultures to DQ12 and SD at the ALI, using a Vitrocell Cloud 12α. To verify exposure to the dusts and visualize the morphology of the nebulized dusts, transmission electron microscopy (TEM) grids were loaded in parallel to the ALI co-cultures and were subsequently assessed via SEM (Fig. S4, Additional File 4). Due to surface tension, the dusts on the TEM grids agglomerated during drying. The agglomerates of both dusts were of a rather compact shape. DQ12 appeared to have sharper edges than SD. The deposited doses were quantified via quartz crystal microbalance (sQCM) (Table S1, Additional File 5).

Absence of cytotoxicity. To monitor the cytotoxicity of DQ12, SD, and LPS in the ALI co-cultures, we examined the release of adenylate kinase (AK) (Fig. 4). Neither DQ12 nor SD induced cytotoxicity at the tested doses. The release of AK into the basolateral compartment was relatively high, compared to the lysis control. This could be due to the short incubation time of 15 min with Triton X-100 which was not sufficient to allow diffusion of AK to the basolateral compartment.

Absence of oxidative stress. To analyze oxidative stress, we assessed the mRNA levels of the marker genes heme oxygenase 1 (*HMOX1*), apurinic-apyrimidinic endonuclease 1/redox factor 1 (*APE1/REF1*), gamma-glutamylcysteine synthetase (*GGCS*), and NAD(P)H quinone dehydrogenase (*NQO1*) via quantitative reverse

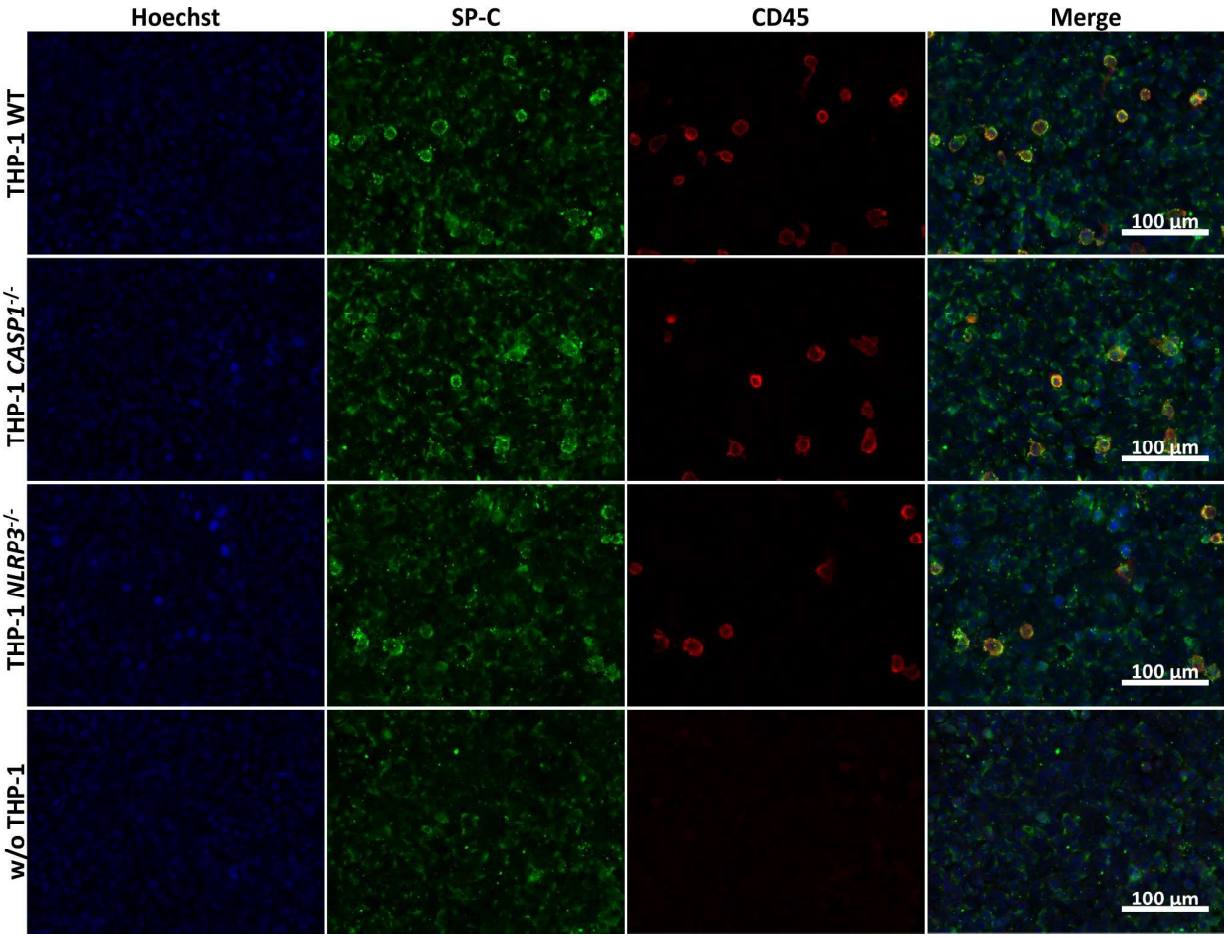

Fig. 3 Surfactant production and macrophage viability at the air-liquid interface (ALI). Co-cultures of A549 cells with wild type (WT), *CASP1*$^{-/-}$, and *NLRP3*$^{-/-}$ THP-1 cells as well as A549 mono-cultures were fixed after 48 h of cultivation at the ALI. Nuclei were stained with Hoechst 33342. Immunostaining of surfactant protein C (SP-C) and CD45 was performed. Representative images were obtained at 100 x magnification

transcription polymerase chain reaction (qRT-PCR) (Fig. 5). None of the investigated marker genes was dysregulated upon 24 h of exposure to DQ12 or SD. The positive control for inflammatory effects, LPS, was tested in parallel. LPS did not induce the oxidative stress marker genes either.

Pro-inflammatory effects of SD. To analyze pro-inflammatory effects, we examined the gene expressions of *IL1B*, *IL6*, *IL8*, *TNFA*, and *IL18* and cytokine releases of IL-1β, IL-6, IL-8, TNFα, and IL-18 (Fig. 6). Surprisingly, DQ12 did not affect any of these cytokines. On the other hand, SD significantly enhanced cytokine gene expression and release. The highest tested dose of 31 µg/cm² SD upregulated *IL1B* and *IL6* gene expression as well as IL-1β and IL-6 release about three to five-fold. At the same dose, *IL8* gene expression and IL-8 release were upregulated about two-fold. *TNFA* gene expression was not significantly upregulated. TNFα release was induced at all tested SD doses whereas only at the medium dose statistical significance was reached. *IL18* gene expression was not affected by SD exposure. The concentrations of released IL-18 remained below the limit of detection for controls and all SD doses. The increases in the expressions of *IL1B*, *IL6*, and *IL8* as well as release of IL-1β and IL-6 showed a dose-dependent trend. The lack of this trend for IL-8 release might be due to increasing interference with the IL-8 ELISA with increasing SD dose (see Fig. S5, Additional File 6). As expected, the positive control LPS strongly induced the gene expression of *IL1B*, *IL6*, *IL8*, and *TNFA* and the release of all investigated cytokines. LPS did not affect the gene expression of *IL18*. In summary, SD was a more potent inducer of pro-inflammatory cytokines than DQ12.

NLRP3 inflammasome dependence of cytokine releases. To address the role of the NLRP3 inflammasome, we exposed ALI co-cultures with THP-1 wild type and CRISPR/Cas9-generated THP-1 *CASP1*$^{-/-}$ and *NLRP3*$^{-/-}$ cells (hereinafter "wild type co-cultures",

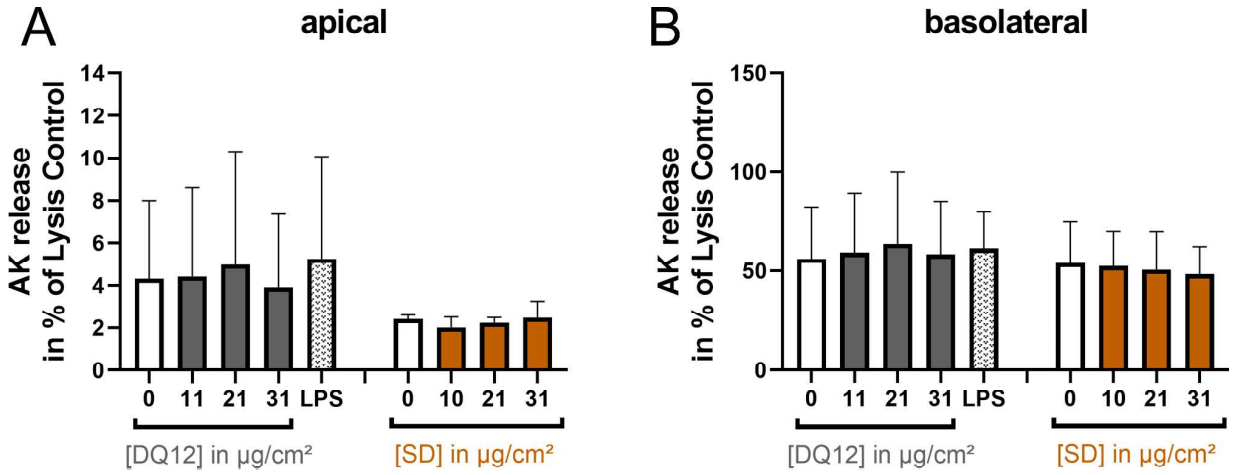

Fig. 4 DQ12 quartz dust and Saharan dust were not cytotoxic. Air-liquid interface (ALI) co-cultures were exposed to DQ12 and Saharan dust (SD) at doses in the range of 0–31 µg/cm² for 24 h or to 250 ± 60 ng/cm² LPS for 21 h. The apical (**A**) and basolateral (**B**) release of adenylate kinase (AK) was examined as a marker of cytotoxicity using the ToxiLight assay. ALI cultures treated with 0.5% Triton X-100 served as lysis control. The values are plotted as means ± standard deviation of $N = 4$ independent experiments (Controls and LPS: one or two biological replicates; DQ12 and SD; duplicates per concentration). A mixed-effects model with Šidák's post hoc test was calculated (no significant differences obtained)

"*CASP1*$^{-/-}$ co-cultures", and "*NLRP3*$^{-/-}$ co-cultures") to 31 µg/cm² SD or the positive control LPS (see sQCM-measured doses in Table S2, Additional File 7). SD upregulated *IL1B* gene expression irrespective of the THP-1 cells' genotype (Fig. 7). SD exposure only induced the release of IL-1β from wild type co-cultures. In contrast, for *CASP1*$^{-/-}$ and *NLRP3*$^{-/-}$ co-cultures, no IL-1β could be detected in the basolateral supernatant, not even after stimulation with LPS.

As in wild-type co-cultures, SD exposure enhanced the gene expression of *IL6* in *CASP1*$^{-/-}$ and *NLRP3*$^{-/-}$ co-cultures, though statistical significance was not reached ($p = 0.067$ and $p = 0.052$, respectively). The IL-6 concentration in the basolateral supernatants from SD-exposed *CASP1*$^{-/-}$ co-cultures was below the limit of detection, whereas augmented IL-6 release from SD-exposed *NLRP3*$^{-/-}$ co-cultures was detected.

SD exposure upregulated the gene expression of *IL8* by about 1.5 to two-fold irrespective of the genotype. We observed an increase of IL-8 release in wild type and *NLRP3*$^{-/-}$ but not in *CASP1*$^{-/-}$ co-cultures. Yet, interference of SD with the IL-8 ELISA could have masked an upregulation in *CASP1*$^{-/-}$ co-cultures (see Fig. S5, Additional File 6).

SD exposure did not lead to enhanced gene expression of *TNFA* for any of the investigated genotypes. TNFα release was only stimulated in wild type co-cultures, while the TNFα concentrations were below the limit of detection for SD-exposed *CASP1*$^{-/-}$ and *NLRP3*$^{-/-}$ co-cultures.

For all genotypes, LPS exposure strongly induced the gene expressions and releases of *IL6*/IL-6, *IL8*/IL-8, and *TNFA*/TNFα. Within each exposure group, the released concentrations of IL-6, IL-8, and TNFα from the co-cultures followed the order wild type > *NLRP3*$^{-/-}$ > *CASP1*$^{-/-}$. We confirmed the correct genotypes of THP-1 cells by submerged LPS exposure of THP-1 cell mono-cultures in parallel to ALI co-culture experiments and comparison of the IL-1β release to the results from a previous study (Fig. S3, Additional File 3) [55].

In summary, deficiencies of CASP-1 and NLRP3 abrogated the SD-induced secretion of IL-1β. In addition, deficiencies of CASP-1 and NLRP3 reduced the gene expressions and releases of *IL6*/IL-6, *IL8*/IL-8, and *TNFA*/TNFα across all exposure groups.

Discussion

In this study, we tested Saharan dust (SD) toxicity in an advanced ALI co-culture model. This model produces surfactant and includes the crosstalk between epithelial and macrophage-like cells. In our exposure system, the SD deposited on the ALI co-cultures was in a respirable size range. In the ALI co-culture model, SD had a higher pro-inflammatory potency than DQ12 quartz dust (DQ12). SD but not DQ12 induced IL-1β, IL-6, IL-8, and TNFα. Further, our data show that the NLRP3 inflammasome-CASP-1 pathway is essential to boost the inflammatory response to SD exposure. In *CASP1*$^{-/-}$ and *NLRP3*$^{-/-}$ co-cultures, SD did not trigger IL-1β secretion, and the releases of IL-6, IL-8, and TNFα were substantially lower than in wild type co-cultures.

Advantages of the air-liquid interface co-culture model

Here, we applied an advanced in vitro ALI co-culture model comprising alveolar epithelial A549 cells and macrophage-like differentiated THP-1 cells. This enabled

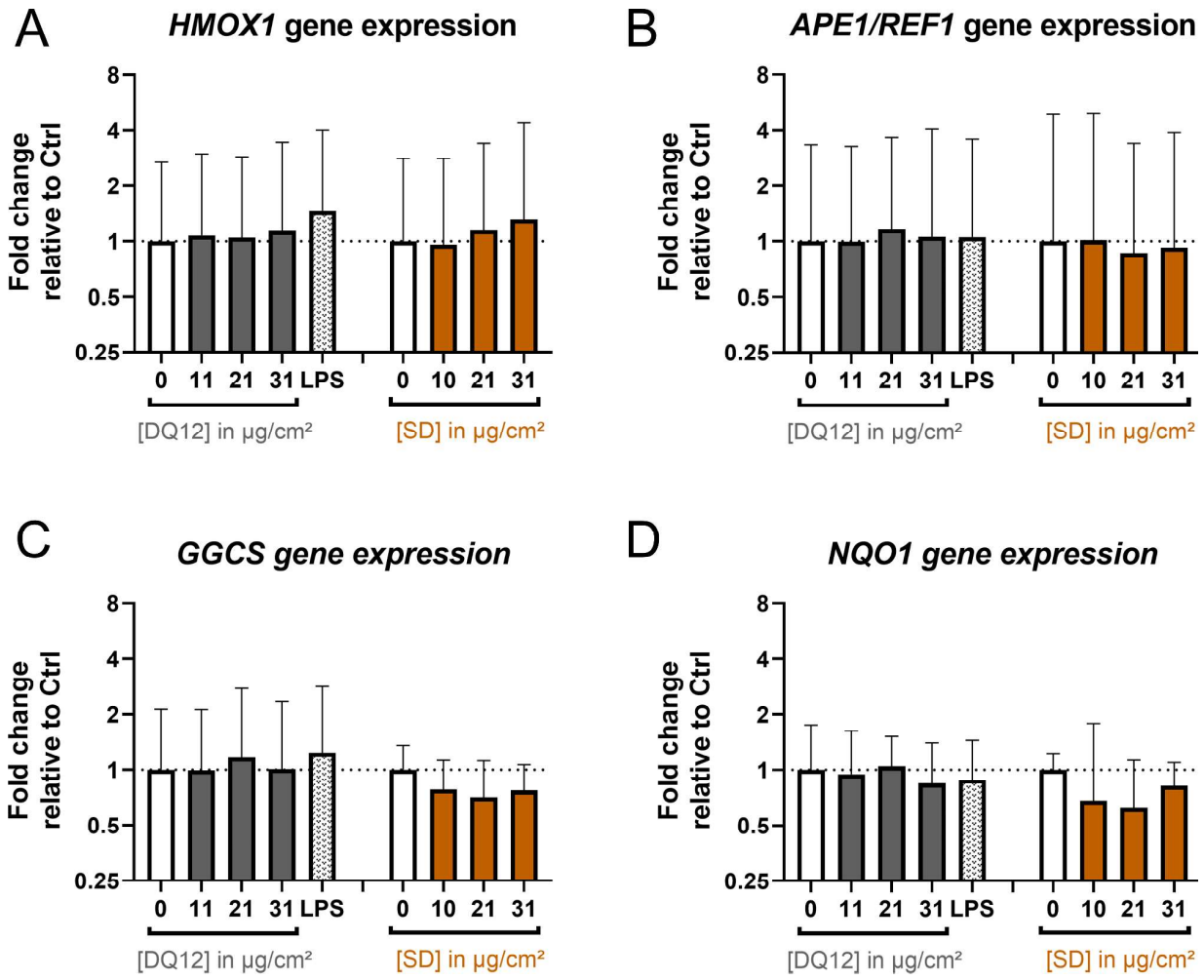

Fig. 5 DQ12 quartz dust and Saharan dust did not induce oxidative stress marker gene expression. Air-liquid interface co-cultures were exposed to DQ12 and Saharan dust (SD) at doses in the range of 0–31 µg/cm² for 24 h or 250 ± 60 ng/cm² LPS for 21 h. The relative gene expression of *HMOX1* (**A**), *APE1/REF1* (**B**), *GGCS* (**C**), and *NQO1* (**D**) was assessed by qRT-PCR. The results were normalized to control ALI cultures as well as to the reference genes *ACTB* and *GAPDH*. The depicted fold changes with standard deviations were derived from the means of the $\Delta\Delta C_T$ values and standard deviations of the ΔC_T values of $N = 4$ independent experiments (Controls and LPS: one or two biological replicates; DQ12 and SD: duplicates per concentration). A mixed-effects model with Šidák's post hoc test was calculated based on the ΔC_T values (no significant differences obtained)

us to test desert dust toxicity in a more advanced model than traditional submerged monocultures. The ALI co-culture model produces surfactant which can modify the toxicity of particles [51, 56, 57] and microbial compounds [50, 58, 59]. The ALI co-culture model also includes the important crosstalk between epithelial cells and macrophages [44–49]. Furthermore, the ALI co-culture model allows us to do mechanistic research by using specific knock-out models. Here, we could specifically address the role of the NLRP3 inflammasome-CASP-1 pathway in macrophages. We could confirm by flow cytometry that the deficiencies of NLRP3 and CASP-1 did not affect the levels of relevant surface receptors upstream of NLRP3 inflammasome activation, i.e., CD14, TLR2, and TLR4 [22, 60]. In addition, this ALI co-culture model offers the opportunity to selectively introduce further genetic modifications to epithelial cells or macrophages. Therefore, this in vitro model could be used instead of conditional mutant animals.

Using the ALI co-culture model, we could test SD in comparison to well-investigated DQ12 quartz dust. In our Vitrocell Cloud exposure system, the size range of the deposited agglomerates matches the respirable particle size range [61]. The doses tested in our study correspond to concentrations of quartz dust that were necessary to cause oxidative stress and inflammatory cytokine upregulation in previous in vitro studies by us and others [62–64]. Testing of SD concentrations that are at least as high as quartz concentrations is supported by the expected doses in acute exposure scenarios: Quartz

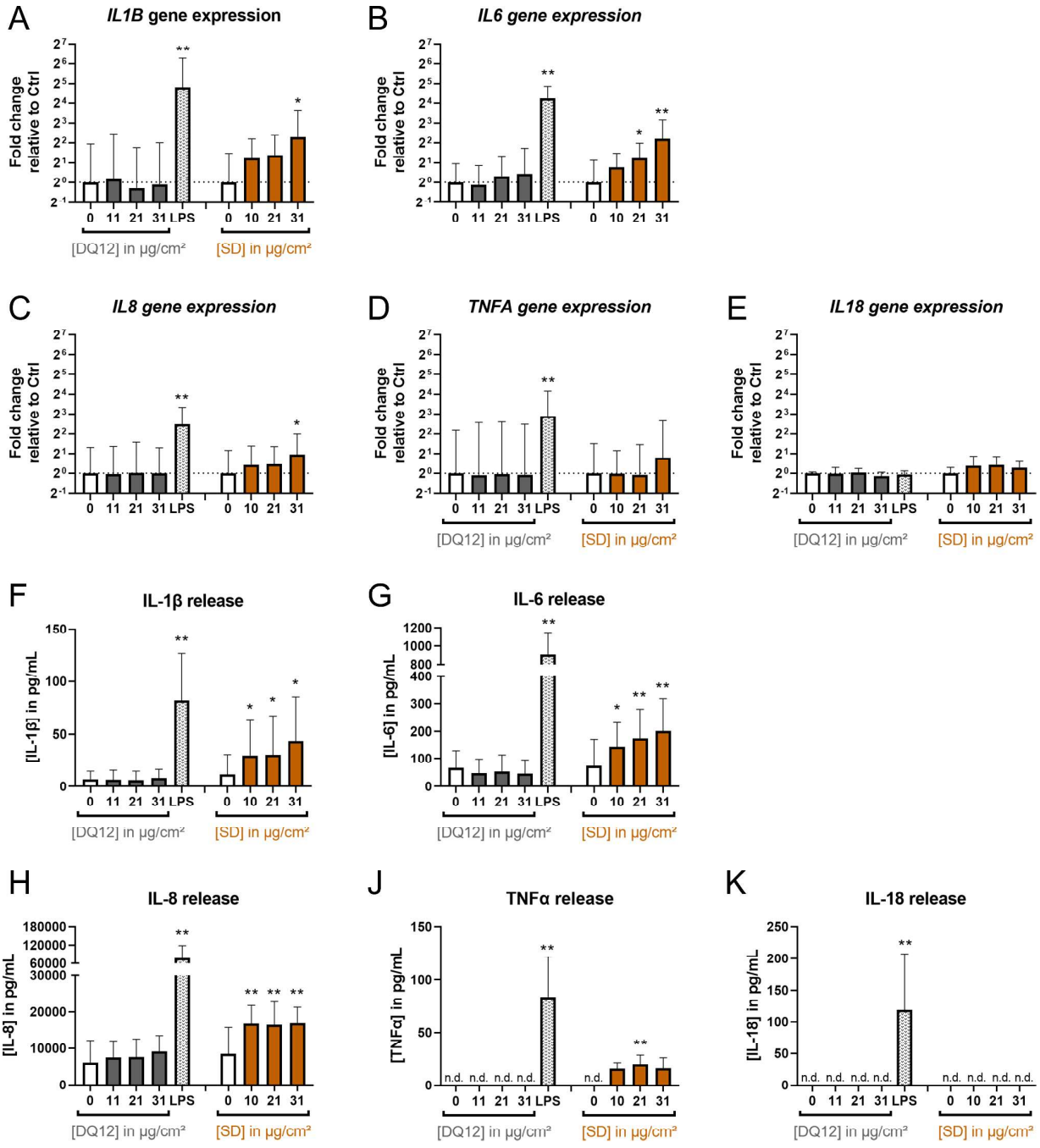

Fig. 6 Saharan dust but not DQ12 quartz dust induced cytokine gene expression and release. Air-liquid interface co-cultures were exposed to DQ12 and Saharan dust (SD) at doses in the range of 0–31 µg/cm² for 24 h or 250 ± 60 ng/cm² LPS for 21 h. The relative gene expressions of *IL1B* (**A**), *IL6* (**B**), *IL8* (**C**), *TNFA* (**D**), and *IL18* (**E**) as well as basolateral cytokine releases of IL-1β (**F**), IL-6 (**G**), IL-8 (**H**), TNFα (**J**), and IL-18 (**K**) were assessed by qRT-PCR and ELISA, respectively. The gene expression results were normalized to control ALI cultures as well as to the reference genes *ACTB* and *GAPDH*. Fold changes were derived from the means of $\Delta\Delta C_T$ values and standard deviations of ΔC_T values. Depicted are mean values with standard deviations. Mixed-effects models with Šidák's post hoc test were calculated based on the ΔC_T values and absolute cytokine concentrations for qRT-PCR and ELISA data, respectively. $N = 4$ independent experiments were performed ($N = 3$ for IL-18 release; Controls and LPS: one or two biological replicates; DQ12 and SD: duplicates per concentration; $^*p \le 0.05$; $^{**}p \le 0.01$). n.d.: not detected

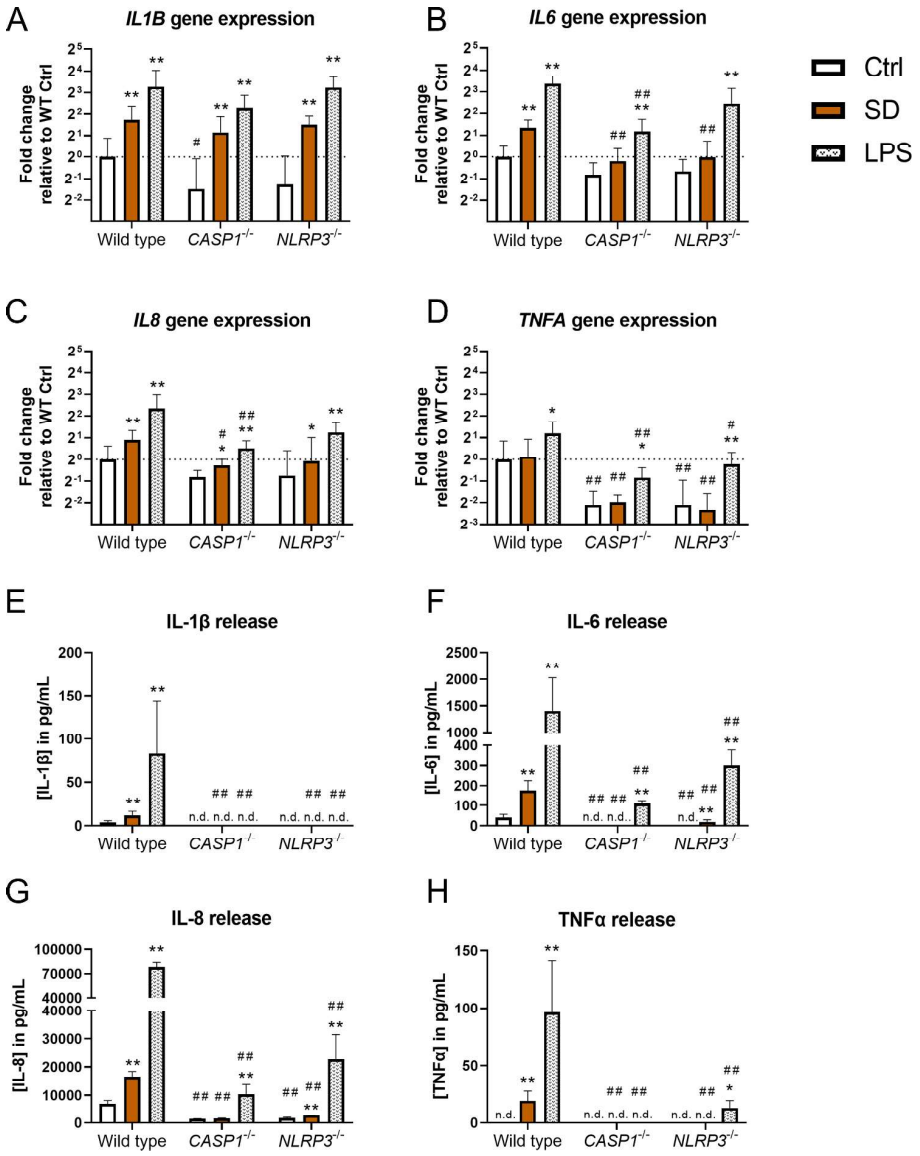

Fig. 7 Caspase-1 and NLRP3 dependent cytokine gene expression and release in response to Saharan dust. Air-liquid interface co-cultures with either wild type, *caspase (CASP)1*$^{-/-}$, or *NLRP3*$^{-/-}$ THP-1 cells were exposed to 31 µg/cm^2 SD for 24 h or to 260 ± 30 ng/cm^2 LPS for 21 h. The relative gene expressions of *IL1B* (**A**), *IL6* (**B**), *IL8* (**C**), and *TNFA* (**D**) as well as basolateral cytokine releases of IL-1β (**E**), IL-6 (**F**), IL-8 (**G**), and TNFα (**H**) were assessed by qRT-PCR and ELISA, respectively. The gene expression results were normalized to wild type control ALI cultures as well as to the reference genes *ACTB* and *GAPDH*. Fold changes were derived from the means of $\Delta\Delta C_T$ values and standard deviations of ΔC_T values. Depicted are mean values with standard deviations. Mixed-effects models with Šidák's post hoc test were calculated based on the ΔC_T values and absolute cytokine concentrations for qRT-PCR and ELISA data, respectively. $N = 4$ independent experiments were performed (Control and LPS: one biological replicate per genotype; SD: duplicates; Comparisons to the non-exposed controls of the respective genotype: $^{*}p \leq 0.05$; $^{**}p \leq 0.01$; Comparisons to equally exposed wild type co-cultures: $^{\#}p \leq 0.05$; $^{\#\#}p \leq 0.01$) n.d.: not detected

dust is an occupational pollutant and maximum air concentrations are regulated. In contrast, concentrations of the environmental pollutant SD cannot be regulated. During dust events, SD concentrations can even exceed the maximum occupational concentrations of respirable quartz of 50 µg/m^3 and 100 µg/m^3 in the USA [65] and the European Union [66], respectively [67, 68].

So far, alveolar epithelial ALI co-culture models have especially been applied to toxicity testing of nanomaterials [69–71]. Moreover, such models have been used to assess environmental pollutants [72, 73] and crystalline silica [62, 71]. Here, to the best of our knowledge, for the first time, an ALI co-culture model is applied to assess desert dust toxicity. Overall, the use of this advanced

in vitro model for the assessment of the toxicity of SD agrees with the replacement of animal studies as an essential part of the 3 Rs by Russell and Burch [74], particularly considering the high animal numbers required for in vivo knock-out models.

Higher acute pro-inflammatory potency of Saharan dust than DQ12 quartz dust

Notably, in this advanced ALI co-culture model, SD but not DQ12 induced the gene expression and release of pro-inflammatory cytokines. Because of its known potential to trigger NLRP3-dependent cytokine production, DQ12 had originally been included as a positive control [34]. The higher inflammatory potency of SD compared to DQ12 contrasts existing studies which compared desert and quartz dusts. These contrasts may be explained by different potencies amongst different desert dusts and by the use of different models. The pro-inflammatory potency of SD widely agrees with the existing literature on desert dust toxicity both in in vivo [6, 8, 11, 75–77] and in vitro [10, 12, 17, 19, 21] studies.

Contrasting our results, Ghio et al. [10] found pro-inflammatory cytokine releases which were similar or stronger upon quartz dust exposure compared to desert dust exposure. They exposed mice and human bronchial epithelial BEAS-2B cells to Arizona surface dust and quartz dust. Similarly, Kim et al. [78] exposed rat lung alveolar epithelial RLE-6TN cells to Asian yellow sand dust and quartz dust and observed comparable potencies to induce TNFα secretion. A possible explanation for the different inflammatory potencies between the desert dust sample from our study and other studies may be the different sampling locations [9, 10, 13]. In particular, the microbial composition could be the factor that distinguishes our Saharan dust sample and dust samples from other deserts, considering that even at the same sampling location there can already be substantial daily variability in microbial composition [79]. Furthermore, as we reported previously [21], our Saharan dust sample contains iron, aluminum, trace metals, sulfate, diatomaceous earth, and organic and elemental carbon; constituents that are absent or barely contained in quartz dust, that can vary between desert dust samples and that potentially contribute to toxicity.

Contrasts between our and other studies may also be due to varying toxic potencies in different in vitro models. For instance, in the in vitro models of the aforementioned studies by Ghio et al. [10] and Kim et al. [78] no macrophages were included. Macrophages could potentiate the pro-inflammatory cytokine response to microbial components that are contained in SD but not DQ12 [21]. Additionally, differences between in vitro models are reflected by the huge range of quartz dust concentrations needed in different studies to obtain inflammatory effects in vitro, reaching from 0.23 µg/cm² [80] to 320 µg/cm² [81]. The use of different models must also explain the higher inflammatory potency of SD than DQ12 and the low inflammatory potency of DQ12 in the present study compared to our previous study [21]. In the previous study, we tested the same SD and DQ12 samples in submerged mono-cultures of A549 and differentiated THP-1 cells: In A549 cells, DQ12 induced *IL8* expression even more potently than SD after 24 h of exposure. In differentiated TPH-1 cells, SD and DQ12 induced IL-1β release with similarly strong potencies. The higher relative potency of SD compared to DQ12 may be explained by the surfactant produced by the ALI co-culture model. Surfactant can decrease the toxicity of poorly soluble particles [52–54]. The stronger effects of poorly soluble particles in submerged than ALI co-culture models are in line with studies directly comparing the sensitivities of submerged versus ALI models [62, 73, 82]. Accordingly, in our more realistic ALI co-culture model, readily soluble components such as microbial compounds that are only contained in SD but not in DQ12 would become more important and drive SD-triggered inflammatory signaling.

In the ALI co-culture model, we did not observe oxidative stress in response to SD or DQ12 although oxidative stress after desert dust exposure [10, 21, 83] and quartz dust exposure [21, 63, 84] was reported in previous studies using submerged models. This difference between submerged models and the ALI co-culture model may again be explained by the lower potency of poorly soluble particles in ALI models. Moreover, the absence of oxidative stress in our study suggests that the inflammatory potency of SD is oxidative stress independent. This agrees with our previous study of SD in submerged A549 cells. In the A549 cells, SD upregulated *IL6* and *IL8* expression at 4 h but not at 24 h whereas oxidative stress was only induced at the later time point [21].

In contrast to acute effects, persistent inflammatory effects could not be addressed using our ALI co-culture model since at extended cultivation times the cells overgrow. Still, due to the failure of clearance, persistent inflammation, which can lead to fibrosis, is especially relevant for poorly soluble particles such as quartz dust [85, 86]. In studies on camels, desert dust exposure has been correlated with persistent inflammation and lung fibrosis as well [87, 88]. To investigate these potential chronic effects of desert dust in vitro, more sophisticated models will be required such as primary cell tissues or organoids.

NLRP3 inflammasome and caspase-1 dependence

Our results suggest that SD can mediate the priming step of the NLRP3 inflammasome-CASP-1 pathway and that SD-triggered IL-1β release strongly depends on the NLRP3 inflammasome and CASP-1. The transcriptional

upregulation of *IL1B* gene expression suggests SD-induced priming of the NLRP3 inflammasome-CASP-1 pathway. Especially, the upregulation of *IL1B* gene expression in *CASP1*$^{-/-}$ and *NLRP3*$^{-/-}$ co-cultures supports the ability of SD to induce the priming step as in these co-cultures *IL1B* gene expression cannot have been upregulated by autocrine IL-1β signaling. In concordance with our results, He et al. [6] found increased expression of *NLRP3* and *IL1B* in Asian sand dust (ASD)-exposed murine macrophage-like cells. That desert dust can prime the NLRP3 inflammasome-CASP-1 pathway is not surprising, considering its content of microbial components [79]. The dependence of SD-induced IL-1β secretion on the NLRP3 inflammasome-CASP-1 pathway agrees with the findings from our previous study of SD in wild type and *NLRP3*$^{-/-}$ THP-1 mono-cultures [21]. Also, we found that SD did not induce the NLRP3 inflammasome-CASP-1 pathway-dependent cytokine IL-18. The difference between IL-1β and IL-18 induction aligns well with a study by Midtbö et al. [89]. Their study also agrees with our findings regarding the incapacity of LPS to induce *IL18* gene expression in THP-1 cells. Which components of SD drive the specificity for IL-1β over IL-18 induction remains to be determined.

Additionally, our results show that beyond the direct downstream cytokine IL-1β, the functional NLRP3 inflammasome boosts the secretion of the pro-inflammatory cytokines IL-6, IL-8, and TNFα upon SD exposure. The dependence of IL-8 secretion on IL-1β concentrations has also been described by other authors [44, 45]. For the inductions of IL-6 and IL-8 secretion, we found the same dependences on exposure and genotype. IL-6 and IL-8 have in common that the NFκB pathway contributes to their regulation [27, 28]. Further supporting the boost of secondary cytokines through the NLRP3 inflammasome-CASP-1 pathway, CASP-1 has been demonstrated to activate the transcription factor NF-κB via caspase-7 activation, so without the necessity of IL-1β activation [90]. Furthermore, IL-1β has been suggested to induce TNFα via the NFκB pathway, though the exact mechanism is still being discussed [91]. Further studies are required to unravel the involvement of the NFκB pathway in the inflammatory effects of SD.

Besides NLRP3, further inflammasomes may play a role in SD-induced inflammatory signaling, as well. The involvement of further inflammasomes could explain the higher IL-6 and IL-8 secretion from *NLRP3*$^{-/-}$ co-cultures than from *CASP1*$^{-/-}$ co-cultures. Amongst others, the NLRP1 [92], NLRC4 (or IPAF) [93], AIM2 [94], and NLRP6 (or PYPAF5) [95] inflammasomes have been reported to activate caspase-1. The potential dependence of SD toxicity on the listed inflammasomes is emphasized by the fact that they can be induced by different microbial components (reviewed by [96, 97]) and that the bacterial endotoxin LPS also had stronger effects on *NLRP3*$^{-/-}$ co-cultures than on *CASP1*$^{-/-}$ co-cultures. Our ALI co-culture model is suitable to address the role of these inflammasomes in future studies using similar genetic-targeting approaches as used in the current study.

Conclusion

In conclusion, in an advanced air-liquid interface co-culture model, only Saharan dust but not DQ12 quartz dust upregulated pro-inflammatory cytokines. As discussed in our previous study, a main difference between Saharan and quartz dust is the presence of readily soluble components, especially microbial compounds [21]. Here we suggest that in the more realistic ALI co-culture model, the soluble components are more relevant for toxicity. Which soluble and especially which microbial compounds contribute to Saharan dust's toxicity needs to be addressed in further studies.

Moreover, considering the higher potency of Saharan dust and the absence of quartz dust toxicity which has also been observed in other studies [98, 99], we suggest using Saharan dust as an alternative particulate positive control. A well-characterized and stored batch of Saharan dust could be used in studies addressing acute inflammatory effects.

Furthermore, the pro-inflammatory effects of Saharan dust in the absence of quartz dust-induced effects and the association with the NLRP3-caspase-1-IL-1β axis strongly underline its hazardousness. To understand the roles of the NLRP3 inflammasome-caspase-1 pathway's priming and activation step more closely, the expression of NLRP3 and the cleavage of CASP-1 should be addressed in further studies. Considering the importance of the NLRP3 inflammasome in acute lung injury [30–32], it could mechanistically link desert dust events to the epidemiologically observed increases in respiratory morbidity and mortality [1–5]. In future studies, the involvement of the NLRP3 inflammasome-caspase-1 pathway could be addressed by analyzing the susceptibility towards desert dust-mediated morbidities depending on single nucleotide polymorphisms in the NLRP3 gene. In addition to the NLRP3 inflammasome-caspase-1 pathway, further mechanisms must be involved in desert dust toxicity as indicated by the residual Saharan dust-induced pro-inflammatory effects in *CASP1*$^{-/-}$ and *NLRP3*$^{-/-}$ co-culture. Given the stronger effects in *NLRP3*$^{-/-}$ than in *CASP1*$^{-/-}$ co-cultures, other inflammasomes should be assessed. Future studies should unravel these mechanisms.

Materials and methods

Chemicals and reagents

RPMI-1640 media, 2-mercaptoethanol (ME), Hank's Balanced Salt Solution containing $MgCl_2$ and $CaCl_2$ (HBSS),

sodium pyruvate, and TRIzol® reagent were purchased from Thermo Fisher Scientific. Fetal calf serum (FCS), bovine serum albumin (BSA), Penicillin/Streptomycin (P/S), D-glucose, trypsin, accutase, phorbol 12-myristate-13-acetate (PMA), LPS, endotoxin-free H_2O, phosphate-buffered saline (PBS), 4-(2-hydroxyethyl)-1-piperazineethanesulfonic acid (HEPES), 2-propanol, and the amplification grade DNase I Kit were purchased from Sigma-Aldrich/Merck. The ToxiLight assay kit was purchased from Lonza. Ethanol and sulfuric acid were purchased from Roth. Nuclease-free water was purchased from Qiagen. The iScript™ cDNA Synthesis Kit and the iQ™ SYBR® Green Supermix were purchased from Bio-Rad. Primers for qPCR were purchased from Eurofins. The Human IL-1β, IL-6, IL-8, and TNFα DuoSet ELISA Kits were purchased from R&D Systems.

Dusts

The collection and characterization of the SD sample have been described previously [21]. Dörentrup Quartz (DQ12) was used. To ensure DQ12 was free of biological contaminants, it was baked at 220 °C overnight before application to cells.

Scanning electron microscopy

To assess the agglomerate size distribution applied to the co-cultures, dusts were suspended to 4 mg/mL in endotoxin-free H_2O containing 1.25% PBS. The suspensions were probe sonicated at 6.9 W for 17 min to reach a total delivered acoustic energy of 7056 J using a Branson Sonifier 450 at 20% amplitude. A nucleopore filter (0.1 µm pore size) was placed on the moistened frit of a vacuum filtration unit and a vacuum was applied. Above the nucleopore filter, 75 µL of dust suspension was nebulized using a Vitrocell 9–12 µm nebulizer to which a 600 Hz square signal was applied using a Velleman PCSU200 Oscilloscope. Due to the vacuum, the liquid was drawn through the filter pores leaving the agglomerates on top of the filter without altering their sizes through the surface tension, which would lead to further agglomeration during drying. A layer of 5 nm gold was applied onto the filters by sputter coating (Quantum Design Q150V ES Plus) to render them conductive for SEM imaging. SEM images were obtained at a nominal magnification of 5.000 x (pixel size of 6.2 nm) and the $Feret_{max}$ and $Feret_{min}$ diameters of 500 particles/agglomerates were assessed using ImageJ (version 1.51f, https://imagej.nih.gov/ij). The area equivalent diameter of the particles/agglomerates was then calculated based on the Feret diameters.

To assess agglomerate deposition and morphology during ALI co-culture exposure, TEM grids were loaded with dusts during ALI exposure of co-cultures and assessed via SEM. Different from the filter samples no gold coating was applied since the TEM grids are conductive. Images of the TEM grids were obtained at different magnifications, starting with an overview of the complete grids up to high-resolution images of single agglomerates.

Generation of *CASP1*$^{-/-}$ and *NLRP3*$^{-/-}$ THP-1 cells

CASP1$^{-/-}$ and *NLRP3*$^{-/-}$ THP-1 cells were generated as previously described [100]. Briefly, gRNAs were designed using the CRISPR design tool CHOPCHOP (http://chopchop.cbu.uib.no/) and cloned into a modified PX458 plasmid (Addgene #48138). The resulting bicistronic vector encoded the respective gRNA, Cas9 nuclease, and a GFP selection marker. gRNA efficiency was assessed using High-Resolution Melt Analysis (HRMA). A gRNA targeting *CASP1* exon 5 (5'-TAATGAGAGCAAGACGTGTG-3') and *NLRP3* exon 2 (5'-GCTAATGATCGACTTCAATG-3') was chosen for further experiments (HRMA primers, *CASP1*: Fwd 5'-CACCGTAATGAGAGCAAGACGTGTG-3', Rev 5'-AAACCACACGTCTTGCTCTCATTAC-3'; *NLRP3*: Fwd 5'-CAGACCATGTGGATCTAGCC-3', Rev 5'-TGTTGATCGCAGCGAAGAT-3'). THP-1 cells were electroporated using a Neon transfection system (Thermo Fisher Scientific) according to the manufacturer's instructions. After 48 h, cells were FACS sorted and plated as single cells into 96-well plates. Cells were duplicated into maintenance and lysis plates after a week. Clones were then lysed with proteinase K and genotyped by PCR followed by deep sequencing using a miSeq Illumina sequencer and a V2 Nano cassette.

Cell culture procedure

We worked with the cell lines A549 and THP-1 that are widely used in particle toxicology [21, 41, 42, 45, 62, 64, 70–72, 81, 82, 98]. A549 (ATCC) cells were stored in liquid nitrogen at passage nine and cultured in RPMI-1640 (containing L-glutamine) substituted with 10% FCS and 1% P/S, hereinafter A549 medium. Cells were detached with trypsin for subcultivation upon reaching about 80% confluence every third or fourth day and reseeded in 75 cm^2 flasks (Greiner) at densities of $5*10^5$ or $2.5*10^5$ cells, respectively. A549 cells were used at passages 2–20 after thawing. THP-1 (ATCC) cells were stored in liquid nitrogen at passage nine and cultured in RPMI-1640 (containing L-glutamine and 25 mM HEPES) substituted with 10% FCS, 1% P/S, 1 mM sodium pyruvate, 0.7% D-glucose and 50 nM ME, hereinafter THP-1 medium. THP-1 cells were maintained at densities between $2*10^5$ and $8*10^5$ cells/ml. THP-1 cells were used at passages 5–15 after thawing. Cell cultures were incubated at 37 °C, 5% CO_2, and saturated humidity. The absence of mycoplasma was confirmed using the InvivoGen MycoStrip™ assay according to the manufacturer's instructions.

For co-culture preparation, on day 1, $1.12*10^5$ A549 cells in 0.5 mL A549 medium, corresponding to $1*10^5$ cells/cm², were seeded on the apical side of a transwell filter (Corning, #3460) (Fig. S6, Additional File 8). To the basolateral side, 1.0 mL A549 medium was added. On day 2, the apical and basolateral A549 medium was changed. In parallel, $3*10^6$ THP-1 cells at passages 5–15 after thawing were differentiated with 100 nM PMA in 25 cm² flasks (Greiner) for 24 h. On day 3, the basolateral A549 medium was changed and the apical A549 was removed. The differentiated THP-1 cells were detached with accutase. Immediately after removing the apical A549 medium, $4.4*10^4$ differentiated THP-1 cells in 0.5 mL THP-1 medium without ME were seeded on the apical side of the confluent A549 cell layer. After attachment for 2 h, the apical THP-1 medium was removed and the co-cultures were lifted to the ALI. The co-culture was maintained in contact with air for 22–26 h until exposure on day 4. On day 5, after 24 h of exposure, supernatants and cells were harvested. The cell numbers were chosen to obtain a ratio of about 10:1 of A549 cells to differentiated THP-1 cells when starting the co-cultivation of both cell lines [62, 70, 73].

When wild type, *CASP1*$^{-/-}$, and *NLRP3*$^{-/-}$ THP-1 cells were used for ALI experiments, THP-1 cells were additionally exposed to LPS under submerged conditions to confirm the genotype via IL-1β ELISA. A total of $1.2*10^5$ THP-1 cells/well in 1.0 mL THP-1 medium without ME was seeded into 24-well plates (Greiner). After attachment for 1 h, the medium was removed and cells were exposed to 0 ng/mL and 10 ng/mL LPS in THP-1 medium without ME containing 1% FCS. After exposure for 24 h, the supernatants were collected.

Flow cytometry

For analysis of macrophage-specific basal surface receptor levels, differentiated THP-1 wild type, *CASP1*$^{-/-}$, and *NLRP3*$^{-/-}$ cells were harvested, placed on ice, washed once each with cold PBS and FACS buffer (PBS containing 2 mM EDTA and 0.5% FCS), and resuspended in cold FACS buffer at 1×10^5 cells per staining condition. Cells were then individually stained with antibodies for CD14 (1:1000, Thermo Fisher Scientific, #14-0149-82), TLR2 (1:250, Thermo Fisher Scientific, #14-9922-82), or TLR4 (1:500, Thermo Fisher Scientific, #14-9917-82) for 25 min on ice in the dark. Unstained and secondary antibody-only controls were each resuspended in cold FACS buffer. Afterwards, cells were washed twice with cold FACS buffer and incubated with an anti-mouse Alexa647-conjugated donkey-anti-mouse (1:250; Dianova) secondary antibody for 25 min on ice in the dark. Unstained controls were resuspended in cold FACS buffer and incubated likewise. Afterwards, cells were washed twice with cold FACS buffer, resuspended in FACS buffer, and analyzed with FACS Aria III (BD Bioscience). Gates were set to remove debris and select single cells (Fig. S2, Additional File 2). Median fluorescence intensities were analyzed to obtain relative surface receptor levels. Post-measurement analysis was performed with FlowJo™ version 10.8.1 (BD Life Sciences).

Immunocytochemistry

To determine the presence of SP-C and the survival of differentiated THP-1 cells at the ALI, immunocytochemical staining and fluorescence microscopy were used. A549 cells in co-culture with wild type, *CASP1*$^{-/-}$, or *NLRP3*$^{-/-}$ THP-1 cells or without THP-1 cells were cultivated at the ALI for 48 h. Subsequently the cultures were fixed with 4% paraformaldehyde in PBS. After blocking with 10% normal goat serum (NGS) and 3% BSA in PBS, the co-cultures were incubated with SP-C (1:40; Thermo Fisher Scientific, #PA5-71680) and CD45 (1:500; BD Biosciences, #561863) primary antibodies in blocking solution overnight at 4 °C. After rinsing 5x with 3% BSA in PBS, the co-cultures were incubated with Alexa488 goat-anti-rabbit and Alexa596 goat-anti-mouse (both 6.7 µg/mL; Thermo Fisher Scientific) secondary antibodies and Hoechst 33342 (0.5 µg/mL) in blocking solution for 1 h at room temperature. After rinsing 5x with 3% BSA in PBS, 1x with PBS, and 1x with dH_2O, the co-cultures were placed into a drop of Prolong Gold Antifade Mountant (Thermo Fisher Scientific) on a microscopy glass slide. Fluorescence images were acquired at 100 x magnification using a Zeiss Axio Imager.M2 fluorescence microscope. Simultaneously, images of autofluorescent plastic slides (Chroma) were acquired for flat field correction. Flat field corrections for each channel, for CD45 rolling ball background subtractions with a radius of 40, and merging of images were done with ImageJ (version 1.53t) macros (Supplementary Material 1, Additional File 9). Simultaneously, control stainings without first antibodies or without secondary antibodies were performed (Fig. S7, Additional File 10).

Air-liquid interface exposure procedure

Dusts were suspended and sonicated as described above. As a negative control, endotoxin-free H_2O containing 1.25% PBS was sonicated under the same conditions. The suspensions were warmed to 37 °C and vortexed vigorously before use. For exposure at the ALI, the Vitrocell Cloud 12α system was used. Dust suspensions were nebulized using a Vitrocell 9–12 µm nebulizer to which a 600 Hz square signal was applied using a Velleman PCSU200 Oscilloscope. Through preliminary experiments using suspensions spiked with fluorescein, the uniform deposition in all used wells could be confirmed. Controls and LPS were nebulized using 4–6 µm nebulizers.

The Cloud system was loaded as exemplified in Fig. S8A, Additional File 11. The bigger exposure chamber consisted of nine wells and the smaller control chamber of three wells. The top-left well of the exposure chamber was equipped with a Vitrocell sQCM for online dosimetry. To the middle well and one other well of the exposure chamber, 3 mL PBS was added. The middle well was left empty. To analyze the deposited dusts via SEM, a TEM grid was placed into a stainless-steel insert which was placed onto PBS. To the residual six wells of the exposure chamber and the three wells of the control chamber, 3 mL A549 medium containing 25 mM HEPES was added and inserts with co-cultures were placed on top. For each dose or genotype, one corner well and one side well were used.

After loading, exposure was performed as illustrated in Fig. S8B, Additional File 11. The aerosol chamber was mounted and humidity in the aerosol chamber was allowed to saturate for 30 min. Subsequently, 500 µL of an SD or DQ12 suspension corresponding to a deposited concentration of about 10 µg/cm² was nebulized in the exposure chamber. Simultaneously, 236 µL control solution was nebulized in the control chamber. The sedimentation process was observed based on the sQCM signal. When sedimentation was completed after about 30 min, the aerosol chamber was dismounted and the sQCM signal was allowed to stabilize. Optionally, to test different doses, transwell inserts were transferred back from the Cloud system to 12-well plates with 1.2 mL fresh A549 medium. Per two exposed co-cultures, one control co-culture was removed from the Cloud system. Then the procedure was repeated twice more to reach doses of about 20 µg/cm² and about 30 µg/cm². To expose co-cultures to LPS as a positive control directly afterwards, the aerosol chamber was cleaned and the required wells of the exposure chamber were rinsed and filled with fresh A549 medium containing 25 mM HEPES. The aerosol chamber was mounted and humidity in the aerosol chamber was allowed to saturate for 30 min. Subsequently, 200 µL of 262 µg/mL LPS in endotoxin-free H_2O containing 1.25% PBS corresponding to a deposited LPS concentration of about 250 ng/cm² was nebulized in the exposure chamber. Sedimentation was observed based on the sQCM signal, the aerosol chamber was removed, the sQCM signal was allowed to stabilize, and co-cultures were transferred back to 12-well plates with 1.2 mL fresh A549 medium.

A volume of 600 µL of 12% BSA in HBSS containing $CaCl_2$ and $MgCl_2$ was added to the apical side of each co-culture 30 min before the end of exposure time. BSA served to inhibit interferences with ELISAs caused by the absorbance of cytokines on the particle surfaces. Exposure was terminated 24 h after the first nebulization of SD or DQ12. Of the apical and basolateral supernatants, 2×20 µL were collected for the ToxiLight assay. The residual supernatants were stored at -20 °C for ELISAs. The inserts with cells were rinsed with PBS twice, lysed in TRIzol reagent, and stored at -80 °C for RNA isolation.

To assess the interference of SD with cytokine ELISAs, instead of transwell inserts with cells, stainless steel inserts filled with a mixture of recombinant cytokines were used. Each stainless steel insert was filled with 200 µL of A549 medium substituted with 750 pg/mL IL-1β, 600 pg/mL IL-6, 1920 pg/mL IL-8, and 960 pg/mL TNFα. In the exposure chamber and control chamber, an SD suspension and control solution were nebulized onto the cytokine mixtures, respectively, following the procedure described above. After incubation for 23.5 h, 1.0 mL of 14% BSA in HBSS containing $CaCl_2$ and $MgCl_2$ was added to each insert. After a further 30 min, the mixtures were collected and the cytokine concentrations were analyzed via ELISA.

ToxiLight cytotoxicity assay

To assess cytotoxicity, the Lonza ToxiLight assay measuring adenylate kinase release was performed according to the supplier's instructions. Briefly, 2×20 µL of apical and basolateral supernatants were transferred to white 96-well plates. To each well, 100 µL adenylate kinase detection reagent mix was added. Following incubation for 15–30 min, luminescence was measured using a TECAN Spark or TECAN Infinite 200 Pro reader. As positive control, 15 min before the end of exposure, 120 µL and 60 µL of 5% Triton X-100 were added to the basolateral and apical side of each transwell, respectively.

Gene expression analysis

The expressions of *HMOX1*, *APE1/REF1*, *GGCS*, *NQO1*, *IL1B*, *IL6*, *IL8*, *TNFA*, and *IL18* were assessed by qRT-PCR. RNA was isolated from TRIzol lysates as described previously [21]. RNA quantification, DNase I digestion, reverse transcription, and qRT-PCR were performed as described previously [101]. Briefly, the optical density of RNA was measured at 260 and 280 nm to determine the concentration. A total of 1.5 µg RNA per sample was treated with amplification grade DNase I. Of this RNA, 2×0.5 µg was reverse transcribed using the iScript™ cDNA synthesis kit. A no reverse transcriptase control (nRTc) with 0.5 µg RNA was performed in parallel to control for residual DNA. The cDNA and nRTc were diluted in nuclease-free H_2O by factor 15. When less RNA was available, the amount of RNA and the dilution factor were decreased proportionally. The primers listed in Table S3, Additional File 12, were used. Actin beta (*ACTB*) and glyceraldehyde 3phosphate dehydrogenase (*GAPDH*) were analyzed as reference genes. C_T values were determined using the Bio-Rad iQ5 software

(v2.1) or QuantStudio™ Design & Analysis Software and corrected for primer efficiencies. Exposure-dependent changes in the gene expression were calculated using the $\Delta\Delta C_T$ method [102]. Relatively large standard deviations can be explained by variability of the constitutive gene expression between the independent experiments. This did not affect the statistical analysis since the experimental run was included as a random factor in the mixed-effects models (see Statistics).

Cytokine quantification by ELISA

The concentrations of IL-1β, IL-6, IL-8, TNFα, and IL-18 in apical and basolateral supernatants were analyzed using R&D systems DuoSet ELISA kits as described previously [103]. Briefly, high-protein-binding 96-well plates were coated with primary antibody, blocked with BSA, and incubated with 100 µL sample. Consecutively, detection antibody, horseradish peroxidase, and BioRad TMB Peroxidase EIA Substrate were incubated. The color reaction was stopped with H_2SO_4 and absorbance was measured at 450 and 540 nm. The standard curve was plotted using a four-parameter log fit. In case the measured concentrations were below the limit of detection (LOD), half the LODs, i.e. 1.95 pg/mL, 4.69 pg/mL, 15.63 pg/mL, 7.81 pg/mL, and 5.86 pg/mL for IL-1β, IL-6, IL-8, TNFα, and IL-18, respectively, were used for calculations and statistics. Relatively large standard deviations can be explained by variability of the constitutive cytokine releases between the independent experiments. This did not affect the statistical analysis since the experimental run was included as a random factor in the mixed-effects models (see Statistics).

Statistics

Histograms of fluorescence intensities from flow cytometry were created with FlowJo™ version 10.8.1. For all other data, GraphPad Prism version 9.1.0 was used for the visualization of means and standard deviation. Microsoft Excel was used to calculate ΔC_T values, $\Delta\Delta C_T$ values, fold changes, mean values, and standard deviations. Firstly, for each independent experiment, mean values were calculated from the biological replicates. These mean values from at least three independent experiments were then used for further calculations. For the gene expression analyses, ΔC_T values were used for statistics. For visualization, mean values from $\Delta\Delta C_T$ values with standard deviations from ΔC_T values were converted into fold changes. To test statistical significance of the flow cytometry data, a two-way ANOVA with Tukey's post hoc test was calculated in GraphPad Prism. For all other data, mixed-effects models with Šídák's post hoc test were applied in R version 4.1.2 to test statistical significance. In the mixed-effects models, exposure and, where applicable genotype, were applied as fixed factors. The experimental run was applied as random factor. *p*-values of ≤ 0.05 were considered statistically significant.

Supplementary Information

The online version contains supplementary material available at https://doi.org/10.1186/s12989-023-00550-w.

Additional file 1: "Fig. S1.jpg". Representative images of nebulized DQ12 and Saharan dust used for size determination. Suspensions of DQ12 quartz dust (**A**, **B**) and Saharan dust (**C**, **D**) in endotoxin-free H_2O containing 1.25% PBS were sonicated and nebulized onto 0.1 µm pore-size nucleopore filters. Images were obtained at a nominal magnification of 5,000 x (pixel size: 6.2 nm). Images **A** and **C** show excerpts from images used for size determination. Images **B** and **D** show the same areas after size determination using ImageJ.

Additional file 2: "Fig. S2.jpg". Gating strategy of flow cytometry analysis. The first gate (SSC-A vs. FSC-A) was set to remove debris. Then doublets were discriminated (linear FSC-H vs. FSC-A) and median fluorescence intensity was determined in the APC-A channel. A representative dot plot is shown for differentiated unstained THP-1 wild type cells. The gating strategy is identical for all samples. SSC: side scatter, FSC: forward scatter, APC: allophycocyanin, A: area, H: height.

Additional file 3: "Fig. S3.tif". IL-1β release from THP-1 cells submerged. In parallel to ALI co-culture experiments (Figs. 3 and 7), the same wild type, *CASP1*$^{-/-}$, and *NLRP3*$^{-/-}$ THP-1 cells were seeded in 24-well plates and exposed to 10 ng/mL LPS submerged for 24 h. In each experiment, one biological replicated was tested per group. The IL-1β concentrations in the supernatants were measured via ELISA. These submerged experiments were performed to confirm the genotypes of the THP-1 cells via comparison of the results to data from a previous study [55]. Depicted are means and standard deviations of $N = 4$ independent experiments. n.d.: not detected.

Additional file 4: "Fig. S4.jpg". Exemplary scanning electron microscopy images of Saharan dust and DQ12 quartz dust deposited on transmission electron microscopy grids during air-liquid interface exposure of co-cultures. A stainless steel insert with a TEM grid was placed into the Vitrocell Cloud 12α in parallel to ALI co-cultures and loaded with Saharan dust or DQ12, which were nebulized and deposited onto the inserts. Deposited doses of 10.9 µg/cm² SD (**A**-**C**), 10.4 µg/cm² DQ12 (**D**-**F**), 30.8 µg/cm² SD (**G**-**J**), and 30.1 µg/cm² DQ12 (**K**-**M**) were measured via quartz crystal microbalance. Images were obtained at nominal magnifications of 61 x (pixel size: 1.02 µm) (**A**, **D**, **G**, **K**), 2.5 kx (pixel size: 24.8 nm) (**B**, **E**, **H**, **L**), and 10 kx (pixel size: 6.2 nm) (**C**, **F**, **J**, **M**).

Additional file 5: "Table S1.docx". Depositions of DQ12, LPS, and SD in µg/cm² measured with Vitrocell sQCM. (belonging to Figs. 4, 5, and 6). Depositions from single experiments are presented with their means and standard deviations (St. dev.). For DQ12 and SD, accumulative doses after first (1x), second (2x), and third (3x) nebulization are shown.

Additional file 6: "Fig. S5.tif". Interference with cytokine ELISAs. In a previous study, we found that SD but not DQ12 interfered with enzyme-linked immuno-sorbent assays (ELISAs) [21]. To assess the interaction of nebulized SD with IL-1β, IL-6, IL-8, and TNFα ELISAs, we nebulized and deposited SD on mixtures of recombinant cytokines ($N = 1$). The control was tested in triplicate, and each dust concentration in duplicates. Cytokine concentrations were determined after incubation for 24 h. SD weakly decreased the recovery of IL-6 by about 15% at the highest tested concentration of 27.8 µg/cm². SD concentrations of 9.2–27.8 µg/cm² decreased the recovery of IL-8 more strongly and dose-dependently by about 45–75%. SD barely affected the recovery of TNFα. For IL-1β, the interference could not be analyzed. Even in the negative control, IL-1β could not be detected after incubation in stainless steel inserts for 24 h. Considering the much lower interference of SD with IL-1β than with IL-8 in submerged experiments [21], at most a weak interference of SD with IL-1β is expected. In addition, in the interference experiment, SD was nebulized into a simulated apical compartment whereas basolateral supernatants were analyzed for cytokine release. Thus, even lower interferences in the ALI co-culture exposures than in this simulation are expected.

Additional file 7: "Table S2.docx". Depositions of SD and LPS in µg/cm² measured with Vitrocell sQCM (belonging to Fig. 7). Depositions from single experiments are presented with their means and standard deviations (St. dev.). For SD, the accumulative doses after the third (3x) nebulization are shown.

Additional file 8: "Fig. S6.tif". Air-liquid interface co-culture preparation. On day 1, A549 cells are seeded on the apical side of transwell inserts. On day 2, after incubation for 24 h, apical and basolateral medium are changed. Simultaneously, THP-1 cells are differentiated to macrophage-like cells through incubation with phorbol 12-myristate-13-acetate (PMA) for 24 h. On day 3, the differentiated THP-1 cells are detached with accutase and seeded on the apical side of the confluent A549 layer. Following attachment for 2 h, the apical medium is removed to initiate air-liquid interface (ALI) culture. On day 4, following 22–26 h of culture at the ALI, co-cultures are exposed at the ALI using a Vitrocell Cloud 12α. Co-cultures are exposed for 24 h.

Additional file 9: "Supplementary material 1.docx". ImageJ macro codes. Codes used to perform flat field corrections (**A**-**D**), rolling ball background subtraction (**C**, **D**), and merging (**D**) for images depicted in Fig. 3 and Fig. S7.

Additional file 10: "Fig. S7.tif". Control staining for surfactant protein C (SP-C) and CD45. Co-cultures of A549 cells with wild type THP-1 cells were fixed after 48 h of cultivation at the ALI. Nuclei were stained with Hoechst 33342. Immunostaining of SP-C and CD45 was performed using either primary and secondary antibodies, primary antibodies only, or secondary antibodies only. Representative images were obtained at 100 x magnification.

Additional file 11: "Fig. S8.tif". Exemplary loading pattern and procedure of Vitrocell Cloud 12α experiments. **A**: The bigger exposure chamber consists of nine wells and the smaller control chamber of three wells. The Vitrocell quartz crystal microbalance (sQCM) was installed in the top-left well. The middle well and the left-middle well of the exposure chamber were filled with 3 mL PBS. Optionally, a stainless-steel insert with a transmission electron microscopy (TEM) grid was placed into the middle-left position. The other wells were filled with 3 mL A549 medium containing 25 mM HEPES and co-culture inserts were placed on top. For each dose, one corner and one middle well were used. **B**: After each nebulization of SD or DQ12, sedimentation took about 30 min. The aerosol chamber was dismounted and optionally co-cultures could be removed from the Cloud system to obtain different doses. Subsequently, the aerosol chamber was mounted again and humidity was allowed to saturate for 30 min. This procedure was repeated twice. Directly after the third sedimentation of DQ12 and removing exposed co-cultures, the aerosol chamber and required wells for exposure to lipopolysaccharide (LPS) were cleaned and loaded. LPS was nebulized. All co-cultures were incubated until 24 h after the first nebulization of particles had passed.

Additional file 12: "Table S3.docx". qPCR primer pairs. Sequences and concentrations of the used qPCR primers and amplicon lengths and efficiencies of the used qPCR Primer pairs on both used devices.

Acknowledgements
We would like to thank Keld Alstrup Jensen from The National Research Centre for the Working Environment (NFA), Denmark, for the information on the probe sonication methodology. Also, we would like to thank Haribaskar Ramachandran from IUF for his support in establishing the caspase-1 and NLRP3-deficient THP-1 cells. Furthermore, we are grateful to Luis Neves from the National Institute of Meteorology of Cape Verde (INMG) for assistance in the sample collection.

Authors' contributions
GB concepted and designed the study, performed and analyzed, the air-liquid interface experiments, interpreted the data, and wrote the original manuscript draft. JD performed and analyzed the flow cytometry experiments and revised the manuscript. BS performed and analyzed the electron microscopical evaluation and revised the manuscript. KWF concepted the study, collected the Saharan dust sample, and revised the manuscript. HH concepted the study and revised the manuscript. AR supported with the genetic engineering of the THP-1 cells and revised the manuscript. RS concepted and designed the study, interpreted the data, and revised the manuscript. All authors read and approved the final manuscript.

Funding
This work has received funding from the Leibniz Association in the framework of the Leibniz Collaborative Excellence Programme project DUSTRISK under grant agreement number K225/2019.
Open Access funding enabled and organized by Projekt DEAL.

Data Availability
The datasets generated and/or analyzed during the current study are available in the Mendeley Data repository, doi: https://doi.org/10.17632/znd6v266cx.2.

Declarations

Ethics approval and consent to participate
Not applicable.

Consent for publication
Not applicable.

Competing interests
The authors declare no competing interests.

Received: 8 May 2023 / Accepted: 9 October 2023
Published online: 20 October 2023

References

1. Kotsyfakis M, Zarogiannis SG, Patelarou E. The health impact of Saharan dust exposure. Int J Occup Med Environ Health. 2019;32 6:749–60. https://doi.org/10.13075/ijomeh.1896.01466.
2. Stafoggia M, Zauli-Sajani S, Pey J, Samoli E, Alessandrini E, Basagana X, et al. Desert Dust outbreaks in Southern Europe: contribution to Daily PM(1)(0) concentrations and short-term associations with Mortality and Hospital admissions. Environ Health Perspect. 2016;124 4:413–9. https://doi.org/10.1289/ehp.1409164.
3. Trianti SM, Samoli E, Rodopoulou S, Katsouyanni K, Papiris SA, Karakatsani A. Desert dust outbreaks and respiratory morbidity in Athens, Greece. Environ Health. 2017;16(1):72. https://doi.org/10.1186/s12940-017-0281-x.
4. Johnston F, Hanigan I, Henderson S, Morgan G, Bowman D. Extreme air pollution events from bushfires and dust Storms and their association with mortality in Sydney, Australia 1994–2007. Environ Res. 2011;111 6:811–6. https://doi.org/10.1016/j.envres.2011.05.007.
5. Kashima S, Yorifuji T, Bae S, Honda Y, Lim Y-H, Hong Y-C. Asian dust effect on cause-specific mortality in five cities across South Korea and Japan. Atmos Environ. 2016;128:20–7. https://doi.org/10.1016/j.atmosenv.2015.12.063.
6. He M, Ichinose T, Yoshida S, Nishikawa M, Mori I, Yanagisawa R, et al. Airborne Asian sand dust enhances murine lung eosinophilia. Inhal Toxicol. 2010;22 12:1012–25. https://doi.org/10.3109/08958378.2010.510151.
7. Ichinose T, Nishikawa M, Takano H, Sera N, Sadakane K, Mori I, et al. Pulmonary toxicity induced by intratracheal instillation of Asian yellow dust (Kosa) in mice. Environ Toxicol Pharmacol. 2005;20(1):48–56. https://doi.org/10.1016/j.etap.2004.10.009.
8. Wilfong ER, Lyles M, Rietcheck RL, Arfsten DP, Boeckman HJ, Johnson EW, et al. The acute and long-term effects of Middle East sand particles on the rat airway following a single intratracheal instillation. J Toxicol Env Heal a. 2011;74 20:1351–65. https://doi.org/10.1080/15287394.2010.516239.
9. Taylor K, Foster ML, Law JM, Centeno JA, Fornero E, Henderson MS, et al. Assessment of geographical variation in the respiratory toxicity of desert dust particles. Inhal Toxicol. 2013;25 7:405–16. https://doi.org/10.3109/08958378.2013.797524.
10. Ghio AJ, Kummarapurugu ST, Tong H, Soukup JM, Dailey LA, Boykin E, et al. Biological effects of desert dust in respiratory epithelial cells and a murine model. Inhal Toxicol. 2014;26 5:299–309. https://doi.org/10.3109/08958378.2014.888109.
11. Keil DE, Buck B, Goossens D, McLaurin B, Murphy L, Leetham-Spencer M, et al. Nevada desert dust with heavy metals suppresses IgM antibody production. Toxicol Rep. 2018;5:258–69. https://doi.org/10.1016/j.toxrep.2018.01.006.

12. Shin SH, Ye MK, Hwang YJ, Kim ST. The effect of Asian sand dust-activated respiratory epithelial cells on activation and migration of eosinophils. Inhal Toxicol. 2013;25 11:633–9. https://doi.org/10.3109/08958378.2013.826755.
13. He M, Ichinose T, Song Y, Yoshida Y, Arashidani K, Yoshida S, et al. Effects of two Asian sand dusts transported from the dust source regions of Inner Mongolia and northeast China on murine lung eosinophilia. Toxicol Appl Pharmacol. 2013;272 3:647–55. https://doi.org/10.1016/j.taap.2013.07.010.
14. Rodriguez-Navarro C, di Lorenzo F, Elert K. Mineralogy and physicochemical features of Saharan dust wet deposited in the Iberian Peninsula during an extreme red rain event. Atmos Chem Phys. 2018;18 13:10089–122. https://doi.org/10.5194/acp-18-10089-2018.
15. Schlesinger P, Mamane Y, Grishkan I. Transport of microorganisms to Israel during Saharan dust events. Aerobiologia. 2006;22 4:259–73. https://doi.org/10.1007/s10453-006-9038-7.
16. Ginoux P, Prospero JM, Gill TE, Hsu NC, Zhao M. Global-scale attribution of anthropogenic and natural dust sources and their emission rates based on MODIS Deep Blue aerosol products. Rev Geophys. 2012;50(3). https://doi.org/10.1029/2012rg000388.
17. Ortiz-Martinez MG, Rodriguez-Cotto RI, Ortiz-Rivera MA, Pluguez-Turull CW, Jimenez-Velez BD. Linking endotoxins, African dust PM10 and Asthma in an Urban and Rural Environment of Puerto Rico. Mediat Inflamm. 2015;2015:784212. https://doi.org/10.1155/2015/784212.
18. Rodriguez-Cotto RI, Ortiz-Martinez MG, Jimenez-Velez BD. Organic extracts from African dust Storms stimulate oxidative stress and induce inflammatory responses in human lung cells through Nrf2 but not NF-kappaB. Environ Toxicol Pharmacol. 2015;39(2):845–56. https://doi.org/10.1016/j.etap.2015.02.015.
19. Rodriguez-Cotto RI, Ortiz-Martinez MG, Rivera-Ramirez E, Mendez LB, Davila JC, Jimenez-Velez BD. African dust Storms reaching Puerto Rican Coast stimulate the secretion of IL-6 and IL-8 and cause cytotoxicity to human bronchial epithelial cells (BEAS-2B). Health (Irvine Calif). 2013;5 10B:14–28. https://doi.org/10.4236/health.2013.510A2003.
20. Val S, Liousse C, Doumbia el HT, Galy-Lacaux C, Cachier H, Marchand N, et al. Physico-chemical characterization of African urban aerosols (Bamako in Mali and Dakar in Senegal) and their toxic effects in human bronchial epithelial cells: description of a worrying situation. Part Fibre Toxicol. 2013;10:10. https://doi.org/10.1186/1743-8977-10-10.
21. Bredeck G, Busch M, Rossi A, Stahlmecke B, Fomba KW, Herrmann H, et al. Inhalable saharan dust induces oxidative stress, NLRP3 inflammasome activation, and inflammatory cytokine release. Environ Int. 2023;172:107732. https://doi.org/10.1016/j.envint.2023.107732.
22. Bauernfeind FG, Horvath G, Stutz A, Alnemri ES, MacDonald K, Speert D, et al. Cutting edge: NF-kappaB activating pattern recognition and cytokine receptors license NLRP3 inflammasome activation by regulating NLRP3 expression. J Immunol. 2009;183(2):787–91. https://doi.org/10.4049/jimmunol.0901363.
23. Kahlenberg JM, Lundberg KC, Kertesy SB, Qu Y, Dubyak GR. Potentiation of caspase-1 activation by the P2X7 receptor is dependent on TLR signals and requires NF-kappaB-driven protein synthesis. J Immunol. 2005;175 11:7611–22. https://doi.org/10.4049/jimmunol.175.11.7611.
24. Jo EK, Kim JK, Shin DM, Sasakawa C. Molecular mechanisms regulating NLRP3 inflammasome activation. Cell Mol Immunol. 2016;13 2:148–59. https://doi.org/10.1038/cmi.2015.95.
25. Thornberry NA, Bull HG, Calaycay JR, Chapman KT, Howard AD, Kostura MJ, et al. A novel heterodimeric cysteine protease is required for interleukin-1 beta processing in monocytes. Nature. 1992;356 6372:768–74. https://doi.org/10.1038/356768a0.
26. Martinon F, Burns K, Tschopp J. The inflammasome: a molecular platform triggering activation of inflammatory caspases and processing of proIL-beta. Mol Cell. 2002;10 2:417–26. https://doi.org/10.1016/s1097-2765(02)00599-3.
27. Jobin C, Haskill S, Mayer L, Panja A, Sartor RB. Evidence for altered regulation of I kappa B alpha degradation in human colonic epithelial cells. J Immunol. 1997;158(1):226–34. https://doi.org/10.4049/jimmunol.158.1.226.
28. Parikh AA, Salzman AL, Kane CD, Fischer JE, Hasselgren PO. IL-6 production in human intestinal epithelial cells following stimulation with IL-1 beta is associated with activation of the transcription factor NF-kappa B. J Surg Res. 1997;69(1):139–44. https://doi.org/10.1006/jsre.1997.5061.
29. Bonizzi G, Piette J, Merville MP, Bours V. Distinct signal transduction pathways mediate nuclear factor-kappab induction by IL-1beta in epithelial and lymphoid cells. J Immunol. 1997;159 11:5264–72. https://doi.org/10.4049/jimmunol.159.11.5264.
30. Grailer JJ, Canning BA, Kalbitz M, Haggadone MD, Dhond RM, Andjelkovic AV, et al. Critical role for the NLRP3 inflammasome during acute lung injury. J Immunol. 2014;192 12:5974–83. https://doi.org/10.4049/jimmunol.1400368.
31. Yang HH, Duan JX, Liu SK, Xiong JB, Guan XX, Zhong WJ, et al. A COX-2/sEH dual inhibitor PTUPB alleviates lipopolysaccharide-induced acute lung injury in mice by inhibiting NLRP3 inflammasome activation. Theranostics. 2020;10 11:4749–61. https://doi.org/10.7150/thno.43108.
32. Zhang Y, Li X, Grailer JJ, Wang N, Wang M, Yao J, et al. Melatonin alleviates acute lung injury through inhibiting the NLRP3 inflammasome. J Pineal Res. 2016;60(4):405–14. https://doi.org/10.1111/jpi.12322.
33. Cassel SL, Eisenbarth SC, Iyer SS, Sadler JJ, Colegio OR, Tephly LA, et al. The Nalp3 inflammasome is essential for the development of silicosis. Proc Natl Acad Sci U S A. 2008;105 26:9035–40. https://doi.org/10.1073/pnas.0803933105.
34. Dostert C, Petrilli V, Van Bruggen R, Steele C, Mossman BT, Tschopp J. Innate immune activation through Nalp3 inflammasome sensing of asbestos and silica. Science. 2008;320 5876:674–7. https://doi.org/10.1126/science.1156995.
35. Ghayur T, Banerjee S, Hugunin M, Butler D, Herzog L, Carter A, et al. Caspase-1 processes IFN-gamma-inducing factor and regulates LPS-induced IFN-gamma production. Nature. 1997;386 6625:619–23. https://doi.org/10.1038/386619a0.
36. Davis GS, Pfeiffer LM, Hemenway DR, Rincon M. Interleukin-12 is not essential for silicosis in mice. Part Fibre Toxicol. 2006;3:2. https://doi.org/10.1186/1743-8977-3-2.
37. Mohebbi I, Rad IA, Bagheri M. Interleukin-18, interleukin-8, and CXCR2 and the risk of silicosis. Toxicol Ind Health. 2013;29 9:830–7. https://doi.org/10.1177/0748233712445048.
38. Jessop F, Hamilton RF, Rhoderick JF, Shaw PK, Holian A. Autophagy deficiency in macrophages enhances NLRP3 inflammasome activity and chronic lung Disease following silica exposure. Toxicol Appl Pharmacol. 2016;309:101–10. https://doi.org/10.1016/j.taap.2016.08.029.
39. Stephens KE, Ishizaka A, Larrick JW, Raffin TA. Tumor necrosis factor causes increased pulmonary permeability and edema. Comparison to septic acute lung injury. Am Rev Respir Dis. 1988;137 6:1364–70. https://doi.org/10.1164/ajrccm/137.6.1364.
40. Piguet PF, Collart MA, Grau GE, Sappino AP, Vassalli P. Requirement of tumour necrosis factor for development of silica-induced pulmonary fibrosis. Nature. 1990;344 6263:245–7. https://doi.org/10.1038/344245a0.
41. Ohlinger K, Kolesnik T, Meindl C, Galle B, Absenger-Novak M, Kolb-Lenz D, et al. Air-liquid interface culture changes surface properties of A549 cells. Toxicol in Vitro. 2019;60:369–82. https://doi.org/10.1016/j.tiv.2019.06.014.
42. Blank F, Rothen-Rutishauser BM, Schurch S, Gehr P. An optimized in vitro model of the respiratory tract wall to study particle cell interactions. J Aerosol Med. 2006;19 3:392–405. https://doi.org/10.1089/jam.2006.19.392.
43. Wu J, Wang Y, Liu G, Jia Y, Yang J, Shi J, et al. Characterization of air-liquid interface culture of A549 alveolar epithelial cells. Braz J Med Biol Res. 2017;51(2):e6950. https://doi.org/10.1590/1414-431X20176950.
44. Herseth JI, Volden V, Schwarze PE, Lag M, Refsnes M. IL-1beta differently involved in IL-8 and FGF-2 release in crystalline silica-treated lung cell co-cultures. Part Fibre Toxicol. 2008;5:16. https://doi.org/10.1186/1743-8977-5-16.
45. Standiford TJ, Kunkel SL, Basha MA, Chensue SW, Lynch JP 3rd, Toews GB, et al. Interleukin-8 gene expression by a pulmonary epithelial cell line. A model for cytokine networks in the lung. J Clin Invest. 1990;86 6:1945–53. https://doi.org/10.1172/JCI114928.
46. Li S, Sun Z, Chen T, Pan J, Shen Y, Chen X, et al. The role of mir-431-5p in regulating pulmonary surfactant expression in vitro. Cell Mol Biol Lett. 2019;24:25. https://doi.org/10.1186/s11658-019-0150-4.
47. Hussell T, Bell TJ. Alveolar macrophages: plasticity in a tissue-specific context. Nat Rev Immunol. 2014;14 2:81–93. https://doi.org/10.1038/nri3600.
48. Murakami S, Iwaki D, Mitsuzawa H, Sano H, Takahashi H, Voelker DR, et al. Surfactant protein A inhibits peptidoglycan-induced Tumor necrosis factor-alpha secretion in U937 cells and alveolar macrophages by direct interaction with toll-like receptor 2. J Biol Chem. 2002;277 9:6830–7. https://doi.org/10.1074/jbc.M106671200.
49. Yamada C, Sano H, Shimizu T, Mitsuzawa H, Nishitani C, Himi T, et al. Surfactant protein A directly interacts with TLR4 and MD-2 and regulates inflammatory cellular response. Importance of supratrimeric oligomerization. J Biol Chem. 2006;281 31:21771–80. https://doi.org/10.1074/jbc.M513041200.
50. Augusto LA, Synguelakis M, Espinassous Q, Lepoivre M, Johansson J, Chaby R. Cellular antiendotoxin activities of lung surfactant protein C in lipid vesicles. Am J Resp Crit Care. 2003;168(3):335–41. https://doi.org/10.1164/rccm.200212-1440OC.

51. Gehr P, Green FH, Geiser M, Im Hof V, Lee MM, Schurch S. Airway surfactant, a primary defense barrier: mechanical and immunological aspects. J Aerosol Med. 1996;9(2):163–81. https://doi.org/10.1089/jam.1996.9.163.
52. Wallace WE, Keane MJ, Mike PS, Hill CA, Vallyathan V, Regad ED. Contrasting respirable quartz and kaolin retention of lecithin surfactant and expression of membranolytic activity following phospholipase A2 digestion. J Toxicol Environ Health. 1992;37 3:391–409. https://doi.org/10.1080/15287399209531679.
53. Emerson RJ, Davis GS. Effect of alveolar lining material-coated silica on rat alveolar macrophages. Environ Health Perspect. 1983;51:81–4. https://doi.org/10.1289/ehp.835181.
54. Pavan C, Rabolli V, Tomatis M, Fubini B, Lison D. Why does the hemolytic activity of silica predict its pro-inflammatory activity? Part Fibre Toxicol. 2014;11:76. https://doi.org/10.1186/s12989-014-0076-y.
55. Busch M, Ramachandran H, Wahle T, Rossi A, Schins RPF. Investigating the role of the NLRP3 inflammasome pathway in Acute Intestinal inflammation: use of THP-1 knockout cell lines in an Advanced Triple Culture Model. Front Immunol. 2022;13:898039. https://doi.org/10.3389/fimmu.2022.898039.
56. Thomassen MJ, Antal JM, Connors MJ, Meeker DP, Wiedemann HP. Characterization of exosurf (surfactant)-mediated suppression of stimulated human alveolar macrophage cytokine responses. Am J Respir Cell Mol Biol. 1994;10 4:399–404. https://doi.org/10.1165/ajrcmb.10.4.8136155.
57. Kanj RS, Kang JL, Castranova V. Interaction between primary alveolar macrophages and primary alveolar type II cells under basal conditions and after lipopolysaccharide or quartz exposure. J Toxicol Environ Health A. 2006;69 11:1097–116. https://doi.org/10.1080/14736480500360504.
58. Kuan SF, Rust K, Crouch E. Interactions of surfactant protein D with bacterial lipopolysaccharides. Surfactant protein D is an Escherichia coli-binding protein in bronchoalveolar lavage. J Clin Invest. 1992;90 1:97–106. https://doi.org/10.1172/JCI115861.
59. McNeely TB, Coonrod JD. Comparison of the opsonic activity of human surfactant protein A for Staphylococcus aureus and Streptococcus pneumoniae with rabbit and human macrophages. J Infect Dis. 1993;167(1):91–7. https://doi.org/10.1093/infdis/167.1.91.
60. Chow JC, Young DW, Golenbock DT, Christ WJ, Gusovsky F. Toll-like receptor-4 mediates lipopolysaccharide-induced signal transduction. J Biol Chem. 1999;274 16:10689–92. https://doi.org/10.1074/jbc.274.16.10689.
61. International Commission on Radiological Protection (ICRP). Human respiratory tract model for Radiological Protection. ICRP publication 66. Ann ICRP. 1994;24:1–3.
62. Friesen A, Fritsch-Decker S, Hufnagel M, Mulhopt S, Stapf D, Hartwig A, et al. Comparing alpha-quartz-Induced cytotoxicity and Interleukin-8 release in Pulmonary Mono- and co-cultures exposed under submerged and air-liquid interface conditions. Int J Mol Sci. 2022;23:12. https://doi.org/10.3390/ijms23126412.
63. van Berlo D, Knaapen AM, van Schooten FJ, Schins RP, Albrecht C. NF-kappaB dependent and Independent mechanisms of quartz-induced proinflammatory activation of lung epithelial cells. Part Fibre Toxicol. 2010;7:13. https://doi.org/10.1186/1743-8977-7-13.
64. Schins RP, McAlinden A, MacNee W, Jimenez LA, Ross JA, Guy K, et al. Persistent depletion of I kappa B alpha and interleukin-8 expression in human pulmonary epithelial cells exposed to quartz particles. Toxicol Appl Pharmacol. 2000;167(2):107–17. https://doi.org/10.1006/taap.2000.8982.
65. United States Department of Labor Occupational Safety and Health Administration. 1910.1053 - Respirable crystalline silica.https://www.osha.gov/laws-regs/regulations/standardnumber/1910/1910.1053. Accessed 10 Apr 2023.
66. European Parliament. Directive (EU) 2017/2398 of the European Parliament and of the Council of 12 December 2017 amending Directive 2004/37/EC on the protection of workers from the risks related to exposure to carcinogens or mutagens at work (Text with EEA relevance).2017. https://eur-lex.europa.eu/eli/dir/2017/2398/oj. Accessed 12 Apr 2023.
67. Gama C, Tchepel O, Baldasano JM, Basart S, Ferreira J, Pio C, et al. Seasonal patterns of Saharan dust over Cape Verde – a combined approach using observations and modelling. Tellus B. 2015;67:1. https://doi.org/10.3402/tellusb.v67.24410.
68. Garrison VH, Majewski MS, Konde L, Wolf RE, Otto RD, Tsuneoka Y. Inhalable desert dust, urban emissions, and potentially biotoxic metals in urban saharan–sahelian air. Sci Total Environ. 2014;500–1. https://doi.org/10.1016/j.scitotenv.2014.08.106.
69. Bitterle E, Karg E, Schroeppel A, Kreyling WG, Tippe A, Ferron GA, et al. Dose-controlled exposure of A549 epithelial cells at the air-liquid interface to airborne ultrafine carbonaceous particles. Chemosphere. 2006;65 10:1784–90. https://doi.org/10.1016/j.chemosphere.2006.04.035.
70. Loret T, Peyret E, Dubreuil M, Aguerre-Chariol O, Bressot C, le Bihan O, et al. Air-liquid interface exposure to aerosols of poorly soluble nanomaterials induces different biological activation levels compared to exposure to suspensions. Part Fibre Toxicol. 2016;13(1):58. https://doi.org/10.1186/s12989-016-0171-3.
71. Skuland T, Lag M, Gutleb AC, Brinchmann BC, Serchi T, Ovrevik J, et al. Pro-inflammatory effects of crystalline- and nano-sized non-crystalline silica particles in a 3D alveolar model. Part Fibre Toxicol. 2020;17(1:13). https://doi.org/10.1186/s12989-020-00345-3.
72. Alfaro-Moreno E, Nawrot TS, Vanaudenaerde BM, Hoylaerts MF, Vanoirbeek JA, Nemery B, et al. Co-cultures of multiple cell types mimic pulmonary cell communication in response to urban PM10. Eur Respir J. 2008;32 5:1184–94. https://doi.org/10.1183/09031936.00044008.
73. Wang G, Zhang X, Liu X, Zheng J. Co-culture of human alveolar epithelial (A549) and macrophage (THP-1) cells to study the potential toxicity of ambient PM2.5: a comparison of growth under ALI and submerged conditions. Toxicol Res (Camb). 2020;9 5:636–51. https://doi.org/10.1093/toxres/tfaa072.
74. Russell WMS, Burch RL. The principles of Humane experimental technique. Methuen; 1959.
75. Naota M, Mukaiyama T, Shimada A, Yoshida A, Okajima M, Morita T, et al. Pathological study of acute pulmonary toxicity induced by intratracheally instilled Asian sand dust (kosa). Toxicol Pathol. 2010;38 7:1099–110. https://doi.org/10.1177/0192623310385143.
76. Ren Y, Ichinose T, He M, Song Y, Yoshida Y, Yoshida S, et al. Enhancement of OVA-induced murine lung eosinophilia by co-exposure to contamination levels of LPS in Asian sand dust and heated dust. Allergy Asthma Cl Im. 2014;10(1):30. https://doi.org/10.1186/1710-1492-10-30.
77. Kim K, Kim S-D, Shin T-H, Bae C-S, Ahn T, Shin S-S, et al. Respiratory and systemic toxicity of Inhaled Artificial Asian Sand Dust in pigs. Life. 2021;11:1. https://doi.org/10.3390/life11010025.
78. Kim YH, Kim KS, Kwak NJ, Lee KH, Kweon SA, Lim Y. Cytotoxicity of yellow sand in lung epithelial cells. J Biosci. 2003;28 1:77–81. https://doi.org/10.1007/BF02970135.
79. Stern RA, Mahmoudi N, Buckee CO, Schartup AT, Koutrakis P, Ferguson ST, et al. The Microbiome of size-fractionated Airborne particles from the Sahara Region. Environ Sci Technol. 2021;55 3:1487–96. https://doi.org/10.1021/acs.est.0c06332.
80. Endes C, Schmid O, Kinnear C, Mueller S, Camarero-Espinosa S, Vanhecke D, et al. An in vitro testing strategy towards mimicking the inhalation of high aspect ratio nanoparticles. Part Fibre Toxicol. 2014;11:40. https://doi.org/10.1186/s12989-014-0040-x.
81. Ovrevik J, Refsnes M, Schwarze P, Lag M. The ability of oxidative stress to mimic quartz-induced chemokine responses is lung cell line-dependent. Toxicol Lett. 2008;181 2:75–80. https://doi.org/10.1016/j.toxlet.2008.07.001.
82. Panas A, Comouth A, Saathoff H, Leisner T, Al-Rawi M, Simon M, et al. Silica nanoparticles are less toxic to human lung cells when deposited at the air-liquid interface compared to conventional submerged exposure. Beilstein J Nanotech. 2014;5:1590–602. https://doi.org/10.3762/bjnano.5.171.
83. Geng H, Meng Z, Zhang Q. Effects of blowing sand fine particles on plasma membrane permeability and fluidity, and intracellular calcium levels of rat alveolar macrophages. Toxicol Lett. 2005;157(2):129–37. https://doi.org/10.1016/j.toxlet.2005.01.010.
84. Ghiazza M, Scherbart AM, Fenoglio I, Grendene F, Turci F, Martra G, et al. Surface iron inhibits quartz-induced cytotoxic and inflammatory responses in alveolar macrophages. Chem Res Toxicol. 2011;24 1:99–110. https://doi.org/10.1021/tx1003003.
85. Albrecht C, Schins RP, Hohr D, Becker A, Shi T, Knaapen AM, et al. Inflammatory time course after quartz instillation: role of Tumor necrosis factor-alpha and particle surface. Am J Respir Cell Mol Biol. 2004;31 3:292–301. https://doi.org/10.1165/rcmb.2003-0300OC.
86. Nakano-Narusawa Y, Yokohira M, Yamakawa K, Saoo K, Imaida K, Matsuda Y. Single Intratracheal Quartz Instillation Induced chronic inflammation and tumourigenesis in rat lungs. Sci Rep. 2020;10(1):6647. https://doi.org/10.1038/s41598-020-63667-4.
87. Goodarzi M, Azizi S, Koupaei MJ, Moshkelani S. Pathologic findings of Anthraco-silicosis in the lungs of one Humped camels (Camelus dromedarius) and its role in the occurrence of Pneumonia. Kafkas Univ Vet Fak. 2014. https://doi.org/10.9775/kvfd.2013.9564.
88. Hansen HJ, Jama FM, Nilsson C, Norrgren L, Abdurahman OS. Silicate pneumoconiosis in camels (Camelus dromedarius L). J Vet Med A. 1989;36 10:789–96. https://doi.org/10.1111/j.1439-0442.1989.tb00793.x.

89. Midtbo K, Eklund D, Sarndahl E, Persson A. Molecularly distinct NLRP3 inducers mediate diverse ratios of Interleukin-1beta and Interleukin-18 from human monocytes. Mediators Inflamm. 2020;2020:4651090. https://doi.org/10.1155/2020/4651090.
90. Erener S, Petrilli V, Kassner I, Minotti R, Castillo R, Santoro R, et al. Inflammasome-activated caspase 7 cleaves PARP1 to enhance the expression of a subset of NF-kappaB target genes. Mol Cell. 2012;46(2):200–11. https://doi.org/10.1016/j.molcel.2012.02.016.
91. Falvo JV, Tsytsykova AV, Goldfeld AE. Transcriptional control of the TNF gene. Curr Dir Autoimmun. 2010;11:27–60. https://doi.org/10.1159/000289196.
92. Martinon F, Burns K, Tschopp J. The Inflammasome. Mol Cell. 2002;10 2:417–26. https://doi.org/10.1016/s1097-2765(02)00599-3.
93. Poyet JL, Srinivasula SM, Tnani M, Razmara M, Fernandes-Alnemri T, Alnemri ES. Identification of Ipaf, a human caspase-1-activating protein related to Apaf-1. J Biol Chem. 2001;276 30:28309–13. https://doi.org/10.1074/jbc.C100250200.
94. Burckstummer T, Baumann C, Bluml S, Dixit E, Durnberger G, Jahn H, et al. An orthogonal proteomic-genomic screen identifies AIM2 as a cytoplasmic DNA sensor for the inflammasome. Nat Immunol. 2009;10(3):266–72. https://doi.org/10.1038/ni.1702.
95. Grenier JM, Wang L, Manji GA, Huang WJ, Al-Garawi A, Kelly R, et al. Functional screening of five PYPAF family members identifies PYPAF5 as a novel regulator of NF-kappaB and caspase-1. FEBS Lett. 2002;530(1–3):73–8. https://doi.org/10.1016/s0014-5793(02)03416-6.
96. Case CL. Regulating caspase-1 during Infection: roles of NLRs, AIM2, and ASC. Yale J Biol Med. 2011;84:4333–43.
97. Sollberger G, Strittmatter GE, Garstkiewicz M, Sand J, Beer HD. Caspase-1: the inflammasome and beyond. Innate Immun. 2014;20(2):115–25. https://doi.org/10.1177/1753425913484374.
98. Barosova H, Karakocak BB, Septiadi D, Petri-Fink A, Stone V, Rothen-Rutishauser B. An in Vitro Lung System to assess the Proinflammatory Hazard of Carbon Nanotube Aerosols. Int J Mol Sci. 2020;21 15:5335. https://doi.org/10.3390/ijms21155335.
99. Braakhuis HM, He R, Vandebriel RJ, Gremmer ER, Zwart E, Vermeulen JP, et al. An air-liquid interface bronchial epithelial model for realistic, repeated Inhalation exposure to Airborne particles for toxicity testing. J Vis Exp. 2020;159. https://doi.org/10.3791/61210.
100. Ramachandran H, Martins S, Kontarakis Z, Krutmann J, Rossi A. Fast but not furious: a streamlined selection method for genome-edited cells. Life Sci Alliance. 2021;4 6:e202101051. https://doi.org/10.26508/lsa.202101051.
101. Kampfer AAM, Busch M, Buttner V, Bredeck G, Stahlmecke B, Hellack B, et al. Model complexity as determining factor for in Vitro Nanosafety studies: effects of Silver and Titanium Dioxide nanomaterials in Intestinal models. Small. 2021;17 15:e2004223. https://doi.org/10.1002/smll.202004223.
102. Livak KJ, Schmittgen TD. Analysis of relative gene expression data using real-time quantitative PCR and the ΔΔCT method. Methods. 2001;25 4:402–8. https://doi.org/10.1006/meth.2001.1262.
103. Busch M, Bredeck G, Kampfer AAM, Schins RPF. Investigations of acute effects of polystyrene and polyvinyl chloride micro- and nanoplastics in an advanced in vitro triple culture model of the healthy and inflamed intestine. Environ Res. 2021;193:110536. https://doi.org/10.1016/j.envres.2020.110536.

Publisher's Note

4.8 Supplemental material

Material 1. ImageJ macro codes. Codes used to perform flat field corrections (A-D), rolling ball background subtraction (C, D), and merging (D) for images depicted in Fig. 3 and Fig. S7.

A: Hoechst 33342 staining

```
run("Clear Results");
extension = "czi";
inputDirectory = getDirectory("Select a directory containing one or several ."+extension+" files.");
fileList = getFileList(inputDirectory);

for (i = 0; i < fileList.length; i++)
{
run("Bio-Formats Importer", "open=" + inputDirectory+fileList[3*(i)] + " color_mode=Default
view=Hyperstack stack_order=XYCZT");
MyImage = substring(getTitle(), 0, lengthOf(getTitle())-13);

run("Bio-Formats Importer", "open=" + inputDirectory+fileList[3*(i)+1] + " color_mode=Default
view=Hyperstack stack_order=XYCZT");
run("Bio-Formats Importer", "open=" + inputDirectory+"221227_Background_Hoechst.czi
color_mode=Default view=Hyperstack stack_order=XYCZT"); //open Background for Flat field correction
run("Measure");
mean = getResult("Mean", "row=nResults-1");

//run actual flat field correction
run("Select None");
run("Select None");
run("Calculator Plus", "i1="+fileList[3*(i)+1]+" i2=221227_Background_Hoechst.czi operation=[Divide: i2 =
(i1/i2) x k1 + k2] k1="+mean+" k2=0 create");
rename("HoechstFFcorr");

run("Set Scale...", "distance=1.5477 known=1 unit=micron");
run("RGB Color");
run("Make Composite");
run("Split Channels");
selectWindow("C3-HoechstFFcorr");
run("Scale Bar...", "width=100 height=100 thickness=10 font=30 color=White background=None
location=[Lower Right] horizontal bold overlay");
saveAs("tiff", inputDirectory+MyImage+ "_Hoechst.tiff");
close("*");
}
```

B: Immunostaining for surfactant protein C (SP-C)

```
run("Clear Results");
extension = "czi";
inputDirectory = getDirectory("Select a directory containing one or several ."+extension+" files.");
fileList = getFileList(inputDirectory);

for (i = 0; i < fileList.length; i++)
```

```
{
run("Bio-Formats Importer", "open=" + inputDirectory+fileList[3*(i)] + " color_mode=Default
view=Hyperstack stack_order=XYCZT");
MyImage = substring(getTitle(), 0, lengthOf(getTitle())-13);

run("Bio-Formats Importer", "open=" + inputDirectory+fileList[3*(i)+2] + " color_mode=Default
view=Hyperstack stack_order=XYCZT");
run("Bio-Formats Importer", "open=" + inputDirectory+"221227_Background_SFTPC.czi
color_mode=Default view=Hyperstack stack_order=XYCZT"); //open Background for Flat field correction
run("Measure");
mean = getResult("Mean", "row=nResults-1");

//run actual flat field correction
run("Select None");
run("Select None");
run("Calculator Plus", "i1="+fileList[3*(i)+2]+" i2=221227_Background_SFTPC.czi operation=[Divide: i2 =
(i1/i2) x k1 + k2] k1="+mean+" k2=0 create");
rename("SFTPCFFcorr");

run("Set Scale...", "distance=1.5477 known=1 unit=micron");
run("RGB Color");
run("Make Composite");
run("Split Channels");
selectWindow("C2-SFTPCFFcorr");
run("Scale Bar...", "width=100 height=100 thickness=10 font=30 color=White background=None
location=[Lower Right] horizontal bold overlay");
saveAs("tiff", inputDirectory+MyImage+ "_SFTPC.tiff");
close("*");
}
```

C: Immunostaining for CD45

```
run("Clear Results");
extension = "czi";
inputDirectory = getDirectory("Select a directory containing one or several ."+extension+" files.");
fileList = getFileList(inputDirectory);


for (i = 0; i < fileList.length; i++)
{
run("Bio-Formats Importer", "open=" + inputDirectory+fileList[3*(i)] + " color_mode=Default
view=Hyperstack stack_order=XYCZT");
MyImage = substring(getTitle(), 0, lengthOf(getTitle())-13);

run("Bio-Formats Importer", "open=" + inputDirectory+"221227_Background_CD45.czi
color_mode=Default view=Hyperstack stack_order=XYCZT"); //open Background for Flat field correction
run("Measure");
mean = getResult("Mean", "row=nResults-1");

//run actual flat field correction
run("Select None");
run("Select None");
```

```
run("Calculator Plus", "i1="+fileList[3*(i)]+" i2=221227_Background_CD45.czi operation=[Divide: i2 =
(i1/i2) x k1 + k2] k1="+mean+" k2=0 create");
rename("CD45FFcorr");
//run rolling ball background subtraction
run("Subtract Background...", "rolling=40");

run("Set Scale...", "distance=1.5477 known=1 unit=micron");
run("RGB Color");
run("Make Composite");
run("Split Channels");
selectWindow("C1-CD45FFcorr");
run("Scale Bar...", "width=100 height=100 thickness=10 font=30 color=White background=None
location=[Lower Right] horizontal bold overlay");
saveAs("tiff", inputDirectory+MyImage+ "_merge.tiff");
close("*");
}
```

D: Merged image

```
run("Clear Results");
extension = "czi";
inputDirectory = getDirectory("Select a directory containing one or several ."+extension+" files.");
fileList = getFileList(inputDirectory);

for (i = 0; i < fileList.length; i++)
{
run("Bio-Formats Importer", "open=" + inputDirectory+fileList[3*(i)] + " color_mode=Default
view=Hyperstack stack_order=XYCZT");
MyImage = substring(getTitle(), 0, lengthOf(getTitle())-13);

run("Bio-Formats Importer", "open=" + inputDirectory+"221227_Background_CD45.czi
color_mode=Default view=Hyperstack stack_order=XYCZT"); //open Background for Flat field correction
run("Measure");
mean = getResult("Mean", "row=nResults-1");

//run actual flat field correction
run("Select None");
run("Select None");
run("Calculator Plus", "i1="+fileList[3*(i)]+" i2=221227_Background_CD45.czi operation=[Divide: i2 =
(i1/i2) x k1 + k2] k1="+mean+" k2=0 create");
rename("CD45FFcorr");
//run rolling ball background subtraction
run("Subtract Background...", "rolling=40");

run("Bio-Formats Importer", "open=" + inputDirectory+fileList[3*(i)+1] + " color_mode=Default
view=Hyperstack stack_order=XYCZT");
run("Bio-Formats Importer", "open=" + inputDirectory+"221227_Background_Hoechst.czi
color_mode=Default view=Hyperstack stack_order=XYCZT"); //open Background for Flat field correction
run("Measure");
mean = getResult("Mean", "row=nResults-1");

//run actual flat field correction
```

```
run("Select None");
run("Select None");
run("Calculator Plus", "i1="+fileList[3*(i)+1]+" i2=221227_Background_Hoechst.czi operation=[Divide: i2 =
(i1/i2) x k1 + k2] k1="+mean+" k2=0 create");
rename("HoechstFFcorr");


run("Bio-Formats Importer", "open=" + inputDirectory+fileList[3*(i)+2] + " color_mode=Default
view=Hyperstack stack_order=XYCZT");
run("Bio-Formats Importer", "open=" + inputDirectory+"221227_Background_SFTPC.czi
color_mode=Default view=Hyperstack stack_order=XYCZT"); //open Background for Flat field correction
run("Measure");
mean = getResult("Mean", "row=nResults-1");

//run actual flat field correction
run("Select None");
run("Select None");
run("Calculator Plus", "i1="+fileList[3*(i)+2]+" i2=221227_Background_SFTPC.czi operation=[Divide: i2 =
(i1/i2) x k1 + k2] k1="+mean+" k2=0 create");
rename("SFTPCFFcorr");


run("Merge Channels...", "c1=CD45FFcorr c2=SFTPCFFcorr c3=HoechstFFcorr create"); //1 red, 2 green,
3 blue
run("Set Scale...", "distance=1.5477 known=1 unit=micron");
run("RGB Color");
run("Scale Bar...", "width=100 height=100 thickness=10 font=30 color=White background=None
location=[Lower Right] horizontal bold overlay");
saveAs("png", inputDirectory+MyImage+ "_merge.png"); //for scale bar
saveAs("tiff", inputDirectory+MyImage+ "_merge.tiff"); //for quality
close("*");
}
```

Table S1. Depositions of DQ12, LPS, and SD in µg/cm² measured with Vitrocell sQCM.

	1x DQ12	2x DQ12	3x DQ12	LPS	1x SD	2x SD	3x SD
Exp. 1	10.4	21.3	31.1	0.25	10.9	21.8	32.4
Exp. 2	10.9	21.2	31.1	0.33	9.94	20.0	30.1
Exp. 3	11.0	20.3	30.1	0.16	10.2	20.4	30.8
Exp. 4	10.6	20.6	30.5	0.27	10.0	19.7	29.8
Mean	10.7	20.9	30.7	0.25	10.2	20.5	30.8
St. dev.	0.2	0.4	0.4	0.06	0.4	0.8	1.0

These depositions belong to Figs. 4, 5, and 6. Depositions from single experiments are presented with their means and standard deviations (St. dev.). For DQ12 and SD, accumulative doses after first (1x), second (2x), and third (3x) nebulization are shown.

Table S2. Depositions of SD and LPS in µg/cm² measured with Vitrocell sQCM.

	3x SD	LPS
Exp. 1	30.8	0.26
Exp. 2	30.7	0.29
Exp. 3	N/A[1]	N/A[1]
Exp. 4	30.9	0.22
Mean	30.8	0.26
St. dev.	0.1	0.03

[1]The deposition could not be assessed, because the sQCM signal was interrupted during the experiment.

These depositions belong to Fig. 7. Depositions from single experiments are presented with their means and standard deviations (St. dev.). For SD, the accumulative doses after the third (3x) nebulization are shown.

Table S3. qPCR primer pairs.

Gene		Sequence (5′ → 3′)	Working conc. (nM)		Amplicon length (bp)	Primer efficiency (%)	
			MyiQ	QS3		MyiQ	QS3
ACTB	fw	CCTGGCACCCAGCACAAT	60	200	70	90.3	81.2
	rv	GCCGATCCACACGGAGTACT	60	200			
GAPDH	fw	CCCCCACCACACTGAATCTC	37.5	200	65	105.4	90.3
	rv	GCCCCTCCCCTCTTCAAG	37.5	200			
IL1B	fw	GCCAGTGAAATGATGGCTTATT	50	50	82	94.0	81.7
	rv	AGGAGCACTTCATCTGTTTAGG	50	50			
IL6	fw	TCATCACTGGTCTTTTGGAG	200	200	161	92.3	80.2
	rv	GTCAGGGGTGGTTATTGC	200	200			
IL8	fw	ACTCCAAACCTTTCCACCC	60	200	168	91.2	83.7
	rv	CCCTCTTCAAAAACTTCTCCAC	60	200			
TNFA	fw	ACTTTGGAGTGATCGGCC	200	200	139	102.4	94.4
	rv	GCTTGAGGGTTTGCTACAAC	200	200			
IL18	fw	TCTTCATTGACCAAGGAAATCGG		200	75		93.3
	rv	TCCGGGGTGCATTATCTCTAC		200			
HMOX1	fw	ATGACACCAAGGACCAGAGCC	200	200	151	91.6	86.9
	rv	GTAAGGACCCATCGGAGAAGC	200	200			
APE1/REF1	fw	CTGCCTGGACTCTCTCATCAATAC	200	200	118	92.3	94.6
	rv	CCTCATCGCCTATGCCGTAAG	200	200			
GGCS	fw	TTGCAGGAAGGCATTGATCA	200	200	101	103.0	89.3
	rv	GCATCATCCAGGTGTATTTTCTCTT	200	200			
NQO1	fw	AACCACGAGCCCAGCCAAT		200	177		96.3
	rv	TGGCATAGAGGTCCGACTCC		200			

Sequences and concentrations of the used qPCR primers and amplicon lengths and efficiencies of the used qPCR Primer pairs on both used devices. MyiQ: MyiQTM cycler (Bio-Rad), QS3TM: QuantStudio 3 device (Thermo Fisher Scientific).

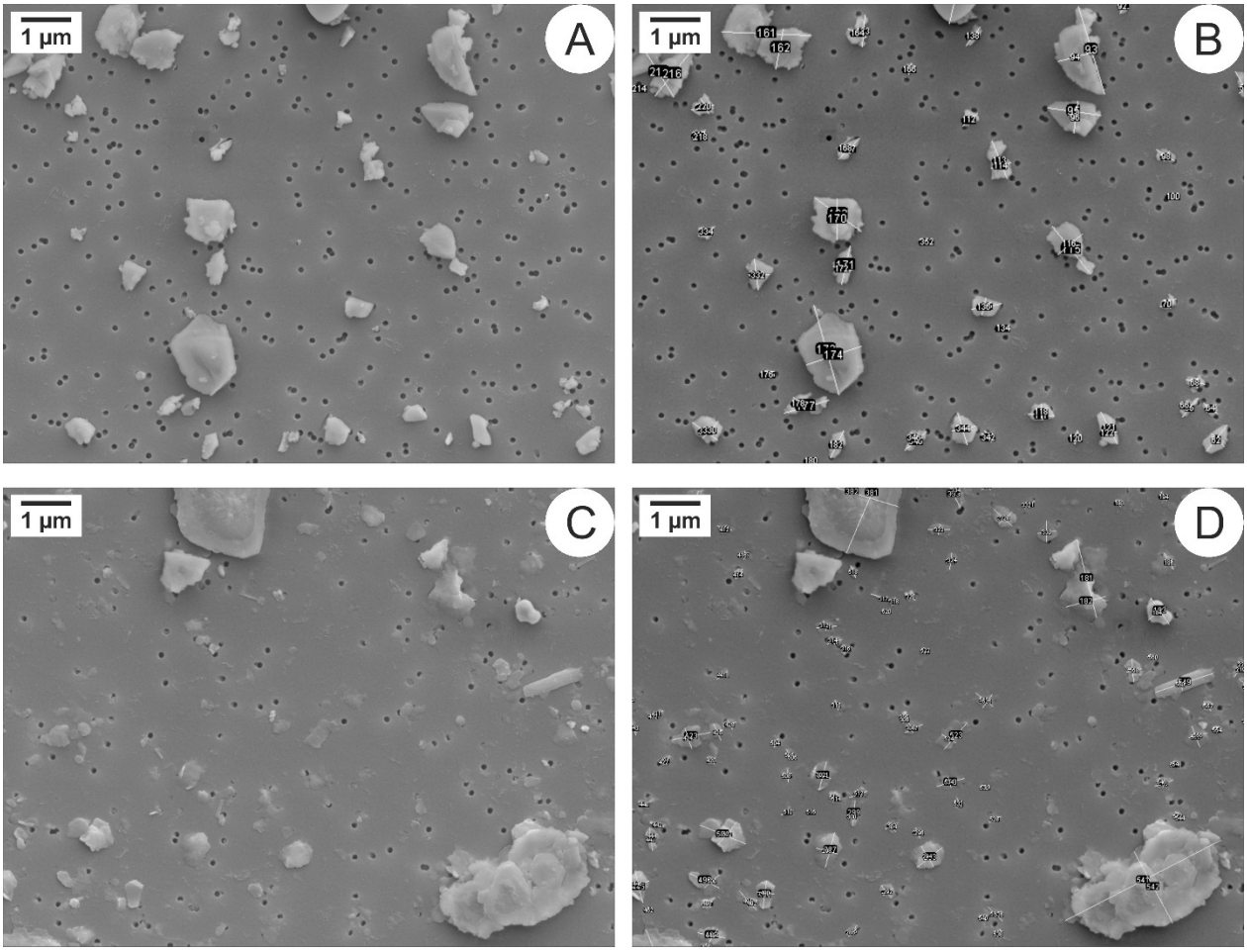

Fig. S1. Representative images of nebulized DQ12 and Saharan dust used for size determination. Suspensions of DQ12 quartz dust (A, B) and Saharan dust (C, D) in endotoxin-free H2O containing 1.25% PBS were sonicated and nebulized onto 0.1 µm pore-size nucleopore filters. Images were obtained at a nominal magnification of 5,000 x (pixel size: 6.2 nm). Images A and C show excerpts from images used for size determination. Images B and D show the same areas after size determination using ImageJ.

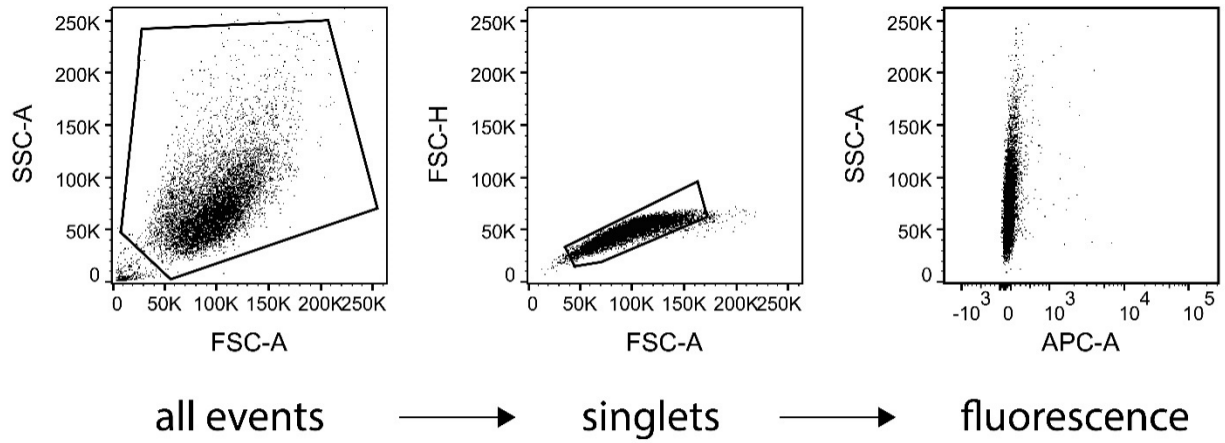

Fig. S2. Gating strategy of flow cytometry analysis. The first gate (SSC-A vs. FSC-A) was set to remove debris. Then doublets were discriminated (linear FSC-H vs. FSC-A) and median fluorescence intensity was determined in the APC-A channel. A representative dot plot is shown for differentiated unstained THP-1 wild type cells. The gating strategy is identical for all samples. SSC: side scatter, FSC: forward scatter, APC: allophycocyanin, A: area, H: height.

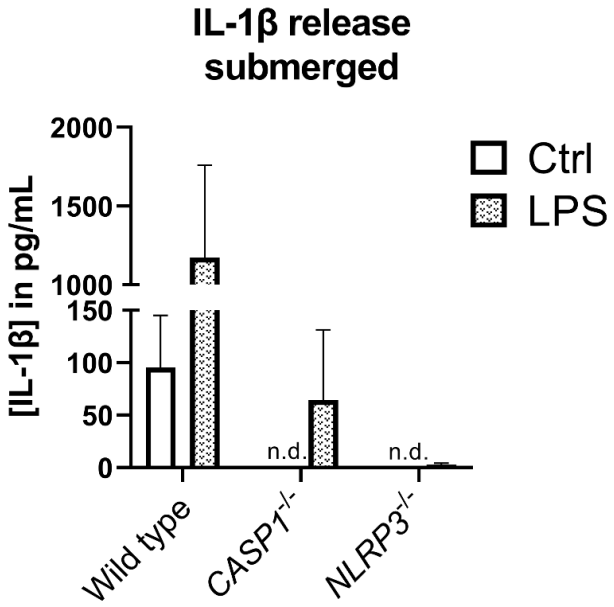

Fig. S3. IL-1β release from THP-1 cells submerged. In parallel to ALI co-culture experiments (Figs. 3 and 7), the same wild type, *CASP1*$^{-/-}$, and *NLRP3*$^{-/-}$ THP-1 cells were seeded in 24-well plates and exposed to 10 ng/mL LPS submerged for 24 h. In each experiment, one biological replicated was tested per group. The IL-1β concentrations in the supernatants were measured via ELISA. These submerged experiments were performed to confirm the genotypes of the THP-1 cells via comparison of the results to data from a previous study[i]. Depicted are means and standard deviations of $N = 4$ independent experiments. n.d.: not detected.

[i] Busch M, Ramachandran H, Wahle T, Rossi A, Schins RPF. Investigating the role of the NLRP3 inflammasome pathway in Acute Intestinal inflammation: use of THP-1 knockout cell lines in an Advanced Triple Culture Model. Front Immunol. 2022;13:898039. https://doi.org/10.3389/fimmu.2022.898039.

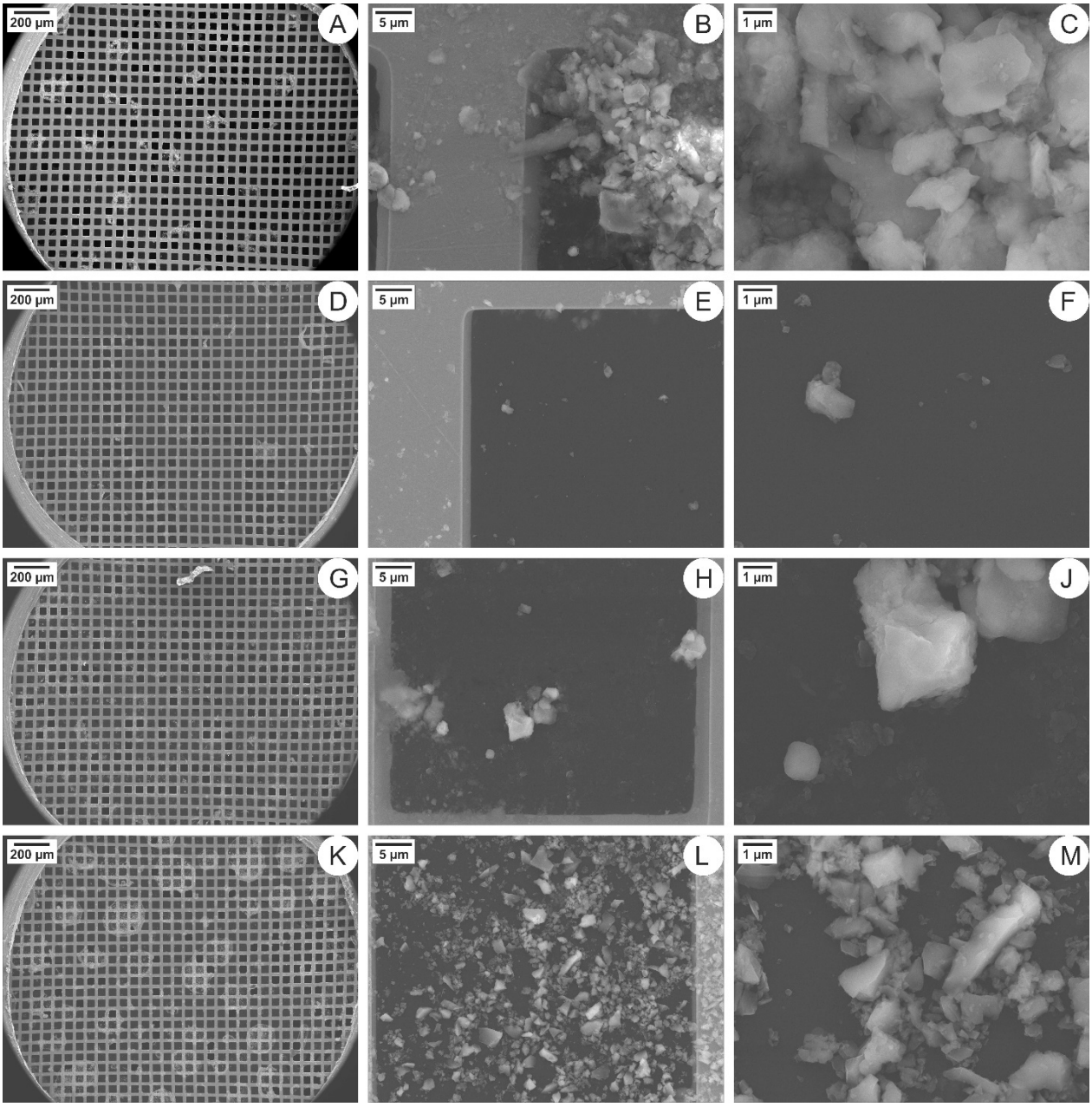

Fig. S4. Exemplary scanning electron microscopy images of Saharan dust and DQ12 quartz dust deposited on transmission electron microscopy grids during air-liquid interface (ALI) exposure of co-cultures. A stainless steel insert with a TEM grid was placed into the Vitrocell Cloud 12α in parallel to ALI co-cultures and loaded with Saharan dust (SD) or DQ12, which were nebulized and deposited onto the inserts. Deposited doses of 10.9 µg/cm² SD (A-C), 10.4 µg/cm² DQ12 (D-F), 30.8 µg/ cm² SD (G-J), and 30.1 µg/cm² DQ12 (K-M) were measured via quartz crystal microbalance. Images were obtained at nominal magnifications of 61 x (pixel size: 1.02 µm) (A, D, G, K), 2.5 kx (pixel size: 24.8 nm) (B, E, H, L), and 10 kx (pixel size: 6.2 nm) (C, F, J, M).

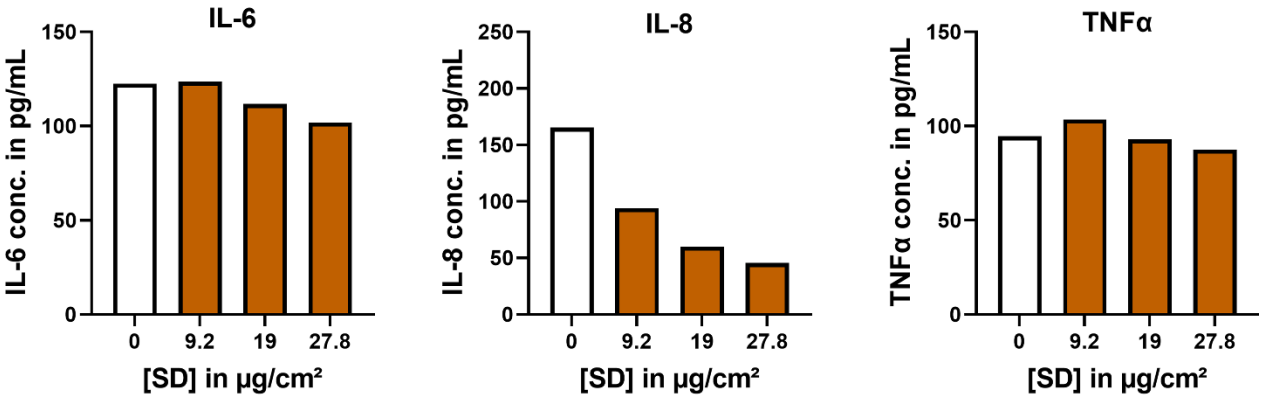

Fig. S5. Interference with cytokine ELISAs. In a previous study, we found that Saharan dust (SD) but not DQ12 interfered with enzyme-linked immuno-sorbent assays (ELISAs).[i] To assess the interaction of nebulized SD with IL-1β, IL-6, IL-8, and TNFα ELISAs, we nebulized and deposited SD on mixtures of recombinant cytokines (*N* = 1). The control was tested in triplicate, and each dust concentration in duplicates. Cytokine concentrations were determined after incubation for 24 h. SD weakly decreased the recovery of IL-6 by about 15% at the highest tested concentration of 27.8 µg/cm². SD concentrations of 9.2–27.8 µg/ cm² decreased the recovery of IL-8 more strongly and dose-dependently by about 45–75%. SD barely affected the recovery of TNFα. For IL-1β, the interference could not be analyzed. Even in the negative control, IL-1β could not be detected after incubation in stainless steel inserts for 24 h. Considering the much lower interference of SD with IL-1β than with IL-8 in submerged experiments,[i] at most a weak interference of SD with IL-1β is expected. In addition, in the interference experiment, SD was nebulized into a simulated apical compartment whereas basolateral supernatants were analyzed for cytokine release. Thus, even lower interferences in the ALI co-culture exposures than in this simulation are expected.

[i] Bredeck G, Busch M, Rossi A, Stahlmecke B, Fomba KW, Herrmann H, et al. Inhalable Saharan dust induces oxidative stress, NLRP3 inflammasome activation, and inflammatory cytokine release. Environ Int. 2023;172:107732. https://doi.org/10.1016/j.envint.2023.107732.

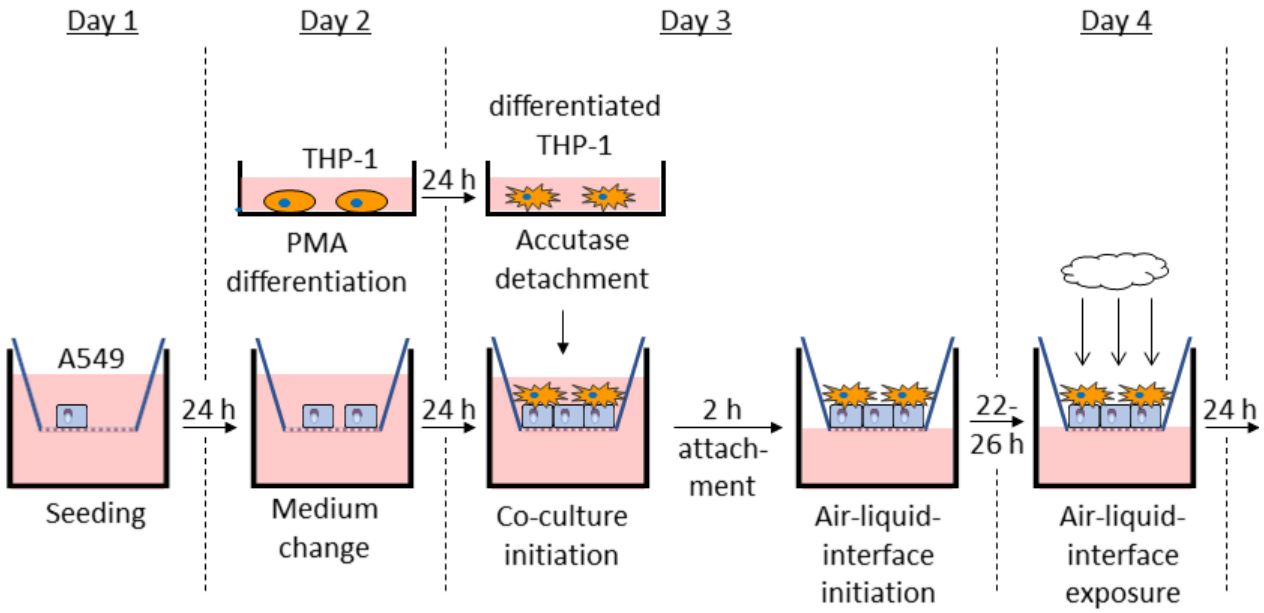

Fig. S6. Air-liquid interface co-culture preparation. On day 1, A549 cells are seeded on the apical side of transwell inserts. On day 2, after incubation for 24 h, apical and basolateral medium are changed. Simultaneously, THP-1 cells are differentiated to macrophage-like cells through incubation with phorbol 12-myristate-13-acetate (PMA) for 24 h. On day 3, the differentiated THP-1 cells are detached with accutase and seeded on the apical side of the confluent A549 layer. Following attachment for 2 h, the apical medium is removed to initiate air-liquid interface (ALI) culture. On day 4, following 22–26 h of culture at the ALI, co-cultures are exposed at the ALI using a Vitrocell Cloud 12α. Co-cultures are exposed for 24 h.

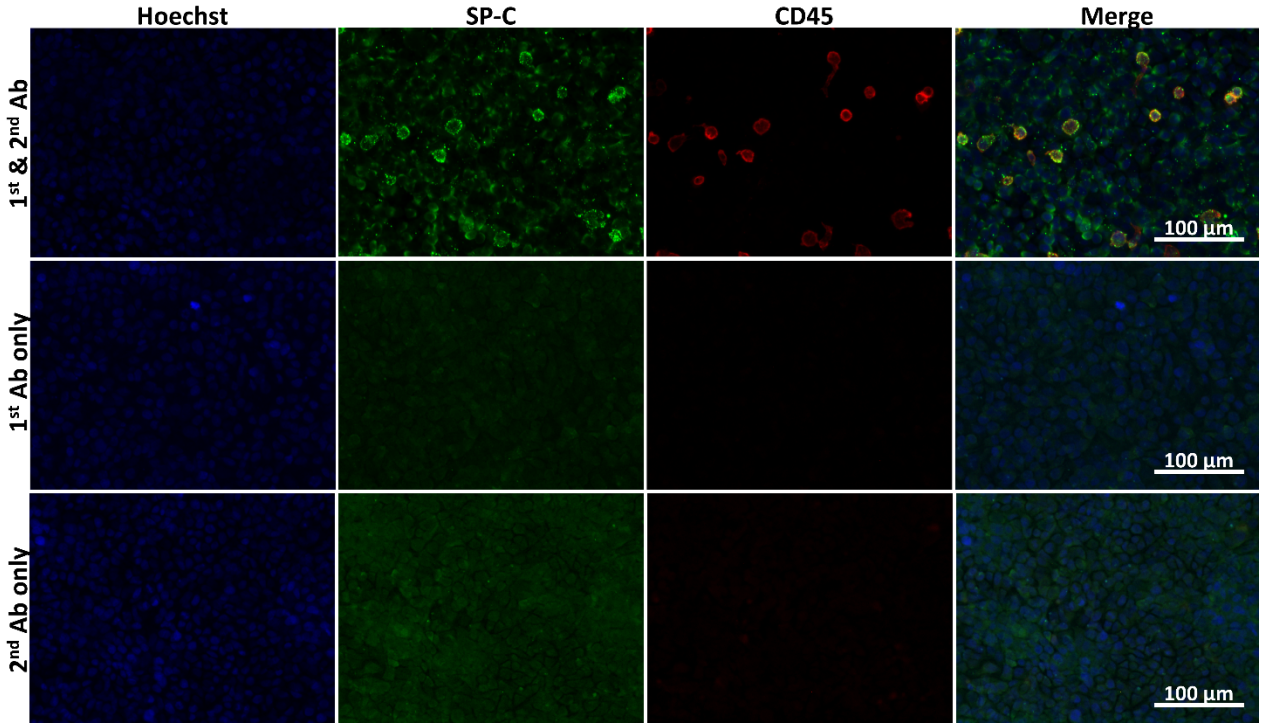

Fig. S7. Control staining for surfactant protein C (SP-C) and CD45. Co-cultures of A549 cells with wild type THP-1 cells were fixed after 48 h of cultivation at the ALI. Nuclei were stained with Hoechst 33342. Immunostaining of SP-C and CD45 was performed using either primary and secondary antibodies, primary antibodies only, or secondary antibodies only. Representative images were obtained at 100 x magnification.

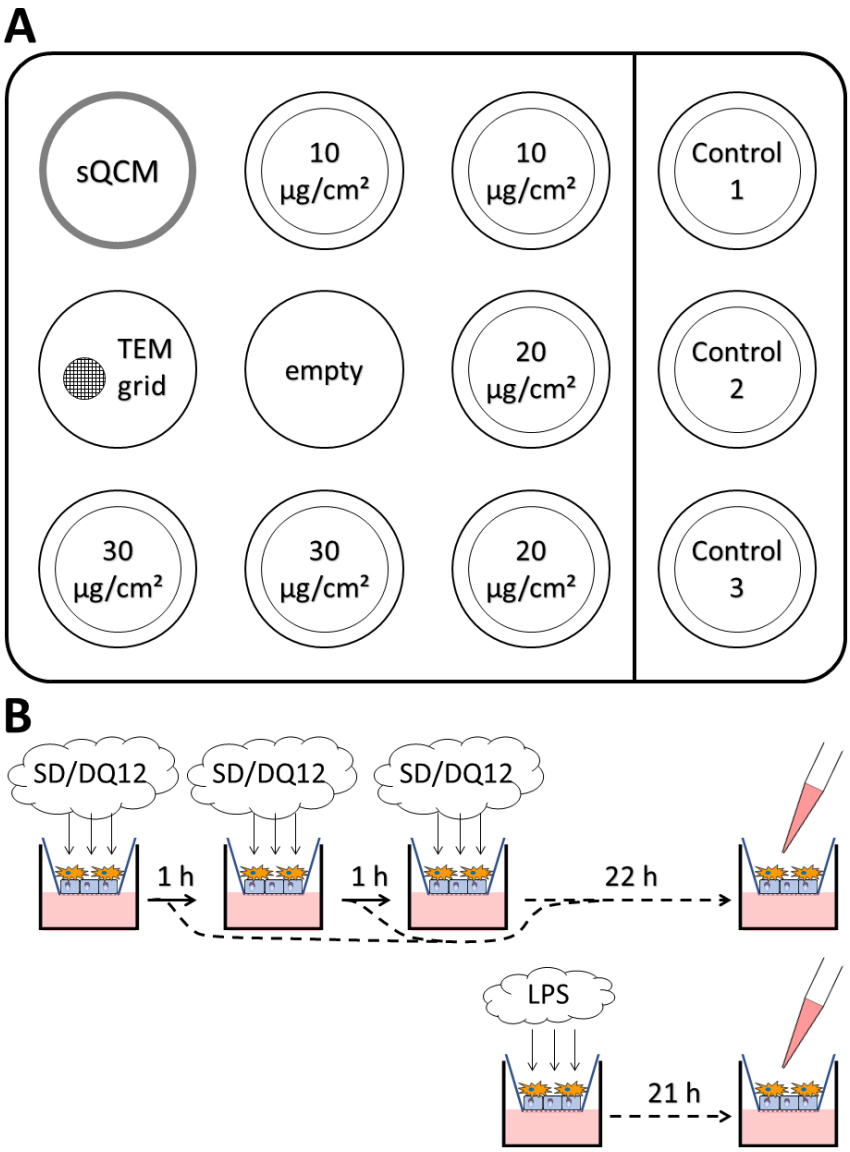

Fig. S8. Exemplary loading pattern and procedure of Vitrocell Cloud 12α experiments. A: The bigger exposure chamber consists of nine wells and the smaller control chamber of three wells. The Vitrocell quartz crystal microbalance (sQCM) was installed in the top-left well. The middle well and the left-middle well of the exposure chamber were filled with 3 mL PBS. Optionally, a stainless-steel insert with a transmission electron microscopy (TEM) grid was placed into the middle-left position. The other wells were filled with 3 mL A549 medium containing 25 mM HEPES and co-culture inserts were placed on top. For each dose, one corner and one middle well were used. B: After each nebulization of Saharan dust (SD) or DQ12, sedimentation took about 30 min. The aerosol chamber was dismounted and optionally co-cultures could be removed from the Cloud system to obtain different doses. Subsequently, the aerosol chamber was mounted again and humidity was allowed to saturate for 30 min. This procedure was repeated twice. Directly after the third sedimentation of DQ12 and removing exposed co-cultures, the aerosol chamber and required wells for exposure to lipopolysaccharide (LPS) were cleaned and loaded. LPS was nebulized. All co-cultures were incubated until 24 h after the first nebulization of particles had passed.

5 Saharan dust induces the lung disease-related cytokines granulocyte-macrophage colony-stimulating factor and granulocyte colony-stimulating factor

Gerrit Bredeck,[a] Jochen Dobner,[a] Andrea Rossi,[a] Roel P. F. Schins[a]

[a]*IUF – Leibniz Research Institute for Environmental Medicine, Düsseldorf, Germany*

Manuscript submitted to Environmental Science & Technology

Author contribution: The author of this thesis planned and performed *in vitro* experiments, prepared the graphs, interpreted and discussed the results, and wrote the manuscript. Relative contribution: about 70%.

5.1 Abstract

Desert dust exposure is associated with increased respiratory mortality and morbidities such as asthma. Desert dusts are complex pollutant mixtures that include respirable crystalline and amorphous particles, metals, and microbial constituents. Considering the health effects of desert dusts and their heterogeneity, not yet identified harmful biological pathways may be triggered. Therefore, we exposed human *in vitro* air-liquid interface co-cultures of alveolar epithelial A549 cells and macrophage-like differentiated THP-1 cells to Saharan dust (SD). For comparison, we used the known pulmonary toxicant DQ12 quartz dust. Via RNA sequencing, we identified that SD increased the gene expression of granulocyte-macrophage colony-stimulating factor (*GMCSF*) and granulocyte colony-stimulating factor (*GCSF*). According to gene set enrichment analysis, SD mainly upregulated inflammation-related gene sets which contained *GMCSF* and *GCSF*. We confirmed the SD but not DQ12-mediated enhanced gene expression of *GMCSF* and *GCSF* by quantitative reverse transcriptase PCR. Furthermore, we observed that SD triggered the releases of GM-CSF and G-CSF. GM-CSF and G-CSF have previously been associated with lung diseases such as asthma and fibrosis. Hence, we present two cytokines that may contribute to the adverse health effects of desert dusts and might serve as drug targets for this globally relevant non-anthropogenic air pollutant.

5.2 Introduction

Epidemiological studies have shown that desert dust events increase respiratory morbidity and mortality (Bener et al., 1996; Gyan et al., 2005; Johnston et al., 2011; Kashima et al., 2016; Lwin et al., 2023; Zauli Sajani et al., 2011; Zhang et al., 2016a). Adverse respiratory effects have already been reported in more than 120 epidemiological studies covering desert dust exposures on five continents (Lwin et al., 2023; Zhang et al., 2016a). Hence, the need to understand the underlying molecular mechanisms is of major importance.

So far, studies have especially addressed inflammation and exacerbation of allergic reactions, as extensively reviewed by Fussell and Kelly (2021). Desert dust exposure has been shown to promote the secretion of pro-inflammatory cytokines like interleukin (IL)-6 and tumor necrosis factor α (TNFα), and the migration of leukocytes, particularly neutrophils, into the lung (Ghio et al., 2014; He et al., 2010; Ichinose et al., 2005; Naota et al., 2010). The inflammatory potency of desert dusts has been related to toll-like receptor (TLR) and myeloid differentiation primary response 88 (MyD88) signaling (He et al., 2013; He et al., 2016), and activation of the NLRP3 inflammasome-caspase-1 pathway (Bredeck et al., 2023a; Bredeck et al., 2023b; He et al., 2010). Desert dusts

have also been described to induce oxidative stress (Bredeck et al., 2023a; Geng et al., 2005; Ghio et al., 2014) and the expression of mucus (Choi et al., 2015; Kim et al., 2011).

However, due to the plethora of molecular pathways discussed in the field of pulmonary particle toxicology, it is likely that further not yet investigated effects are triggered by desert dust exposure. Components of desert dusts include crystalline and amorphous particles, diverse microbial constituents, metals, and further anthropogenic pollutants (Bredeck et al., 2023a; Ghio et al., 2014; Ichinose et al., 2005; Rodriguez-Navarro et al., 2018; Stern et al., 2021; Val et al., 2013). Each of these components has been discussed to potentially dysregulate multiple molecular pathways (Barnes et al., 2019; Castranova, 2004; Kelly and Fussell, 2011; Napierska et al., 2010; Schweitzer et al., 2018; Sengul and Asmatulu, 2020). Thus, a holistic approach to detecting molecular pathways that are affected by desert dust exposure is required.

Such a holistic approach is offered by RNA sequencing and screening for differentially expressed genes (DEGs). To the best of our knowledge, only Yanagisawa et al. (2007) and Sun et al. (2012) have used RNA sequencing analysis to assess desert dust toxicity. Yanagisawa et al. (2007) applied Asian sand dust to mice by intratracheal instillation, analyzed transcriptomes of the lung, and found that especially chemokine and cytokine gene expression was induced. Specifically, they confirmed the upregulations of the chemokines C-X-C motif chemokine ligand 1 (*CXCL1*), *CXCL2*, *CXCL3*, and *CXCL10* by quantitative reverse transcriptase PCR (qRT-PCR) and enzyme-linked immunosorbent assay (ELISA). Drawbacks of the aforementioned study are possible artifacts caused by the mode of application and species differences: Particle instillation can cause artificially strong responses compared to inhalation (Osier and Oberdorster, 1997). Studies comparing transcriptomic studies on inflammatory diseases in humans and mouse models revealed that only a minority of genes differentially expressed in humans were reflected in mice (Seok et al., 2013; Warren et al., 2015). Sun et al. (2012) exposed submerged human bronchial epithelial BEAS-2B cells to urban and desert dust from Saudi Arabia. They observed that both dusts particularly induced oxidative stress and drug metabolism-related DEGs after one day, and cell metabolism-related DEGs after four days. Other relevant DEGs and molecular pathways can likely be identified by applying the RNA sequencing approach to a human *in vitro* air-liquid interface (ALI) model including both epithelial and innate immune cells.

Here, we used an ALI co-culture model of alveolar A549 cells and macrophage-like differentiated THP-1 cells. The ALI culture provides more realistic properties than traditional submerged models such as the formation of surfactant and a lower surface tension due to the secretion of lipids (Blank et al., 2006; Ohlinger et al., 2019; Wu et al., 2017). The surfactant lining can increase the uptake (Gehr et al., 1996), and decrease the cytotoxicity and pro-inflammatory potency of dust (Emerson

and Davis, 1983; Pavan et al., 2014; Wallace et al., 1992). Moreover, the ALI co-culture model includes the cross-talk between epithelial and innate immune cells which can substantially shape each other's activity (Herseth et al., 2008; Hussell and Bell, 2014; Murakami et al., 2002; Standiford et al., 1990).

This study aimed to identify lung-disease-relevant pathways involved in the health effects of desert dusts. Therefore, we exposed the ALI co-culture model to Saharan dust (SD), identified DEGs by RNA sequencing, and confirmed the upregulations by qRT-PCR and ELISA.

5.3 Material and methods

5.3.1 Chemicals and reagents

RPMI-1640 media, 2-mercaptoethanol (ME), Hank's Balanced Salt Solution containing $MgCl_2$ and $CaCl_2$ (HBSS), RNase OUT, Maxima H Minus Reverse Transcriptase, Qubit HS dsDNA kit, sodium pyruvate, and TRIzol® reagent were purchased from Thermo Fisher Scientific. Fetal calf serum, bovine serum albumin (BSA), Penicillin/Streptomycin (P/S), D-glucose, trypsin, accutase, phorbol 12-myristate-13-acetate (PMA), lipopolysaccharide (LPS), endotoxin-free H_2O, phosphate-buffered saline (PBS), 4-(2-hydroxyethyl)-1-piperazineethanesulfonic acid (HEPES), 2-propanol, and the amplification grade DNase I Kit were purchased from Sigma-Aldrich/Merck. The ToxiLight assay kit was purchased from Lonza, ethanol and sulfuric acid from Roth, nuclease-free water from Qiagen, the iScript™ cDNA Synthesis Kit, and the iQ™ SYBR® Green Supermix from Bio-Rad, primers for qPCR from Eurofins, and the Human GM-CSF and G-CSF DuoSet ELISA Kits from R&D Systems. Sequencing library preparation and MinION (R9.4.1) flow cell kits were purchased from Oxford Nanopore Technologies. Deoxyribonucleotide triphosphates were purchased from Vazyme, LongAmp Taq Master Mix and Exonuclease I from New England Biolabs, ScreenTape devices and assays from Agilent, and AMPure XP beads from Beckman Coulter.

5.3.2 Dust samples

The collection and characterization of the SD sample from the Cape Verdean island São Vicente has been described previously (Bredeck et al., 2023a). As a crystalline silica sample, Dörentrup Quartz DQ12 was used. DQ12 was baked at 220°C overnight before application to *in vitro* models to ensure it was free of biological contaminants.

5.3.3 Cell culture procedure

We used the cell lines A549 and THP-1 as they are frequently applied in particle toxicology (Alfaro-Moreno et al., 2008; Blank et al., 2006; Bredeck et al., 2023a; Friesen et al., 2022; Loret et al., 2016; Ohlinger et al., 2019; Standiford et al., 1990; Wang et al., 2020a). The cell culture media and procedure were as described previously (Bredeck et al., 2023a). Briefly, A549 (ATCC) cells were maintained at up to 80% confluence and were used at passages 2–20 after thawing. THP-1 (ATCC) cells were kept between $2*10^5$ and $8*10^5$ cells/mL and used at passages 5–15 after thawing. For differentiation, $3*10^6$ THP-1 cells were incubated with 100 nM PMA in 25 cm² flasks (Greiner) for 24 h. Cell cultures were kept at 37°C, 5% CO_2, and saturated humidity. Using the InvivoGen MycoStrip™ assay, the absence of mycoplasma was confirmed

Co-cultures were prepared as described previously (Bredeck et al., 2023b). Briefly, $1.12*10^5$ A549 cells were seeded on the apical side of a transwell filter (Corning, #3460). After two days, when a confluent monolayer had formed, $4.4*10^4$ differentiated THP-1 cells were seeded on the apical side of the A549 cell monolayer to obtain a ratio of about 10:1 of A549 cells to differentiated THP-1 cells when starting the co-cultivation of both cell lines (Friesen et al., 2022; Loret et al., 2016; Wang et al., 2020a). After attachment for 2 h, by removing the apical THP-1 medium the co-cultures were lifted to the ALI. The co-culture was maintained in contact with air for 22–26 h before exposure. After 24 h of exposure, supernatants and cells were harvested.

5.3.4 Air-liquid interface exposure procedure

Co-cultures were exposed at the ALI as described previously (Bredeck et al., 2023b). Briefly, dusts were suspended to 4 mg/mL in endotoxin-free H_2O containing 1.25% PBS. The suspensions were probe sonicated at 6.9 W for 17 min to reach a total delivered acoustic energy of 7056 J using a Branson Sonifier 450 at 20% amplitude. The suspensions were warmed to 37°C and vortexed vigorously immediately before use. For exposure at the ALI, the Vitrocell Cloud 12α system was used. Dust suspensions were nebulized using a Vitrocell 9-12 µm nebulizer to which a 600 Hz square signal was applied using a Velleman PCSU200 Oscilloscope. Controls and LPS were nebulized using 4-6 µm nebulizers. A Vitrocell quartz crystal microbalance (sQCM) was used for online dosimetry. In the Cloud system, the co-cultures were placed on A549 medium containing 25 mM HEPES. The aerosol chamber was mounted and humidity in the aerosol chamber was allowed to saturate for 30 min. Subsequently, 500 µL of an SD suspension, corresponding to a deposited concentration of 10.2±0.4 µg/cm², was nebulized in the exposure chamber. Simultaneously, 236 µL control solution was nebulized in the control chamber. Sedimentation was observed based on the sQCM signal. When sedimentation was completed, the aerosol chamber was dismounted. To test different doses, one control and two exposed co-cultures were moved

from the Cloud system to a 12-well plate with 1.2 mL A549 medium. Then the procedure was repeated twice more to reach doses of 20.5±0.8 µg/cm² and 30.8±1.0 µg/cm². To expose co-cultures to 10.7±0.2 µg/cm², 20.9±0.4 µg/cm², and 30.7±0.4 µg/cm² DQ12, the same procedure as for SD was followed. To expose co-cultures to LPS as a positive control directly afterwards, the aerosol chamber was cleaned and the required wells of the exposure chamber were rinsed and filled with fresh A549 medium containing 25 mM HEPES. The aerosol chamber was mounted and humidity in the aerosol chamber was allowed to saturate for 30 min. Subsequently, 200 µL of 262 µg/mL LPS in endotoxin-free H_2O containing 1.25% PBS, corresponding to a deposited LPS concentration of 250±60 ng/cm², was nebulized in the exposure chamber.

A volume of 600 µL of 12% BSA in HBSS containing $CaCl_2$ and $MgCl_2$ was added to the apical side of each co-culture 30 min before the end of exposure time. BSA served to inhibit interferences with ELISAs caused by the absorbance of cytokines on the particle surfaces (Bredeck et al., 2023a). Exposure was terminated 24 h after the first nebulization of SD or DQ12. The supernatants were stored at -20°C for ELISAs. The inserts with cells were rinsed with PBS twice, lysed in TRIzol reagent, and stored at -80°C for RNA isolation.

5.3.5 RNA sequencing analysis

To screen for DEGs, RNA sequencing was performed for co-cultures exposed to the highest concentration of 31 µg/cm² SD and DQ12 and the respective controls. RNA was isolated from TRIzol lysates as described previously (Bredeck et al., 2023a). RNA quantification and DNase I digestion were performed as described previously (Kampfer et al., 2021). Briefly, the optical density of RNA was measured at 260 nm and 280 nm to determine the concentration. A total of 1.1 µg RNA per sample was treated with amplification grade DNase I.

RNA quality was assessed using the High Sensitivity RNA ScreenTape assay and RNAs with an RNA integrity number equivalent of at least 7 were subjected to library preparation. Libraries were prepared using the PCR cDNA Barcoding (SQK-PCB109) kit according to the protocol version PCB_9092_v109_revD_10Oct2019 according to update 13/09/2021. Briefly, 50 ng total RNA per sample was reverse transcribed into cDNA and barcoded by PCR using 14 cycles. Subsequently, barcoded samples were cleaned up, pooled to a total of 100 fmol. The library size was analyzed with the D1000 ScreenTape assay. The samples were loaded onto a MinION flow cell, and subjected to a 72 h sequencing run. Subsequently, raw signals were basecalled using Guppy (v5.0.16), and sequences were mapped to the Human reference transcriptome (GRCh38) using Minimap2 (v2.19). Transcripts were counted using Rsubread (v2.12.3) and differential gene expression analysis was performed using edgeR (v3.40.2). Gene set enrichment analysis (GSEA)

was performed using clusterProfiler (v4.6.2) with an unadjusted *p*-value cutoff of 0.05. Genes with an absolute log2 fold change > 1.5 were considered. The final list of enriched gene sets was created by taking the mean of ten resamplings of the analysis and ranking by absolute values of normalized enrichment score accounting for differences in gene set size and representing the degree of overrepresentation of a given gene set in the dataset. The data were visualized using ggplot2 (v3.4.3).

5.3.6 Analysis of cytokine release by protein array

To screen for cytokine release, basolateral supernatants from control, SD-exposed, and LPS-exposed co-cultures were analyzed using the Proteome Profiler Human XL Cytokine Array Kit (R&D Systems) according to the manufacturer's instructions. Briefly, array membranes were blocked with antibodies for one hour. Basolateral supernatants were centrifugated at 14,000 g and 4°C for 5 min and 0.7 mL of supernatant, diluted with array buffer to 1.5 mL, was added per membrane and incubated under agitation overnight at 4°C. The following day, the detection antibody cocktail, streptavidin-HRP, and luminescence reagent were applied to the membranes for 1 h, 30 min, and 1 min, respectively. Images were acquired using the Imager CHEMI Premium (VWR) device. Luminescence intensity was quantified using the HLImage++ software (Western Vision Software) and normalized to the reference spots. Fold changes were calculated using R (v4.3.0).

5.3.7 Targeted gene expression analysis by quantitative reverse transcriptase PCR

GMCSF, *GCSF*, and *SLC39A8* gene expressions were analyzed by qRT-PCR. RNA quantification, DNase I digestion, reverse transcription, and qPCR were performed as described previously (Kampfer et al., 2021). Briefly, measuring the light absorbance at 260 nm and 280 nm RNA concentrations were determined. Per sample, 1.5 µg RNA was treated with amplification grade DNase I. Using the iScript™ cDNA synthesis kit, 2x 0.5 µg was reverse transcribed. In parallel a no reverse transcriptase control (nRTc) was performed with 0.5 µg RNA to control for residual DNA. The primer pairs in Table S5.1 were used. As reference genes, Actin beta (*ACTB*) and glyceraldehyde 3-phosphate dehydrogenase (*GAPDH*) were assessed. C_T values were determined using the QuantStudio™ Design & Analysis Software and corrected for primer efficiencies. Using the $\Delta\Delta C_T$ method (Livak and Schmittgen, 2001), effects on the gene expression were calculated.

5.3.8 Targeted cytokine quantification by ELISA

The concentrations of GM-CSF and G-CSF in apical and basolateral supernatants were analyzed using R&D systems DuoSet ELISA kits as described previously (Busch et al., 2021). Briefly,

96-well MaxiSorp plates were coated with primary antibody, blocked with BSA, and incubated with test samples. Detection antibody, horseradish peroxidase, and BioRad TMB Peroxidase EIA Substrate were added consecutively. The color reaction was terminated with H_2SO_4. Absorbance was measured at 450 nm and 540 nm. Using a four-parameter log fit, the standard curve was plotted and cytokine concentrations were calculated.

5.3.9 Statistics

For RNA sequencing results, DEGs were determined using edgeR (v3.40.2) with an unadjusted *p* value cutoff of 0.05 and a log2 fold change cutoff of 1.5. Microsoft Excel was used to calculate ΔC_T values, $\Delta\Delta C_T$ values, fold changes, mean values, and standard deviations from at least three independent experiments. For the qRT-PCR analyses, ΔC_T values were used for statistics. For visualization, fold changes were calculated from mean values of $\Delta\Delta C_T$ values with standard deviations of ΔC_T values. For qRT-PCR and ELISA data, GraphPad Prism (v9.1.0) was used for the visualization of means and standard deviation. For qRT-PCR and ELISA data, mixed-effects models with Šídák's post hoc test were applied in R (v4.1.2) to test statistical significance. In the mixed-effects models, exposure was applied as fixed factor. The experimental run was applied as random factor. *p*-values of ≤ 0.05 were considered statistically significant.

5.4 Results and discussion

We applied an RNA sequencing approach to an air-liquid interface (ALI) co-culture model of epithelial cells and macrophages, to determine factors involved in the health effects of Saharan dust (SD). To compare to a well-studied particulate toxicant, we assessed DQ12 quartz dust in parallel. As we previously discussed (Bredeck et al., 2023b), we used SD and DQ12 quartz dust doses relevant for *in vitro* testing.

5.4.1 Genes differentially expressed in response to Saharan dust exposure

Based on the RNA sequencing data we determined DEGs for SD and DQ12 compared to their negative controls (Figure 5.1). SD caused significant differential expression of 147 genes of which 91 and 56 were upregulated and downregulated, respectively (Figure 5.1A). In contrast to SD, DQ12 only caused significant differential expression of 55 genes of which 29 and 26 were upregulated and downregulated, respectively (Figure 5.1B). The DEG most strongly upregulated by SD was granulocyte-macrophage colony-stimulating factor (*GMCSF*), also known as *CSF2*, with a fold change of about 17, whereas DQ12 upregulated *GMCSF* by about 3-fold and not statistically significantly ($p = 0.134$). Further genes strongly upregulated by SD were zinc finger protein 419 (*ZNF419*), C-C motif chemokine ligand 3 like 1 (*CCL3L1*), granulocyte colony-

stimulating factor (*GCSF*), also known as *CSF3*, and *IL6* with fold changes between 8 and 11. The upregulation of *GCSF* did not reach statistical significance (p = 0.051). Of the ten genes most strongly upregulated through SD, none were significantly affected by DQ12. Of the ten genes most strongly upregulated through DQ12, merely HECT and RLD domain containing E3 ubiquitin protein ligase 5 (*HERC5*) was also upregulated by SD. Of the ten genes most strongly downregulated through SD, none was significantly affected by DQ12 and vice versa.

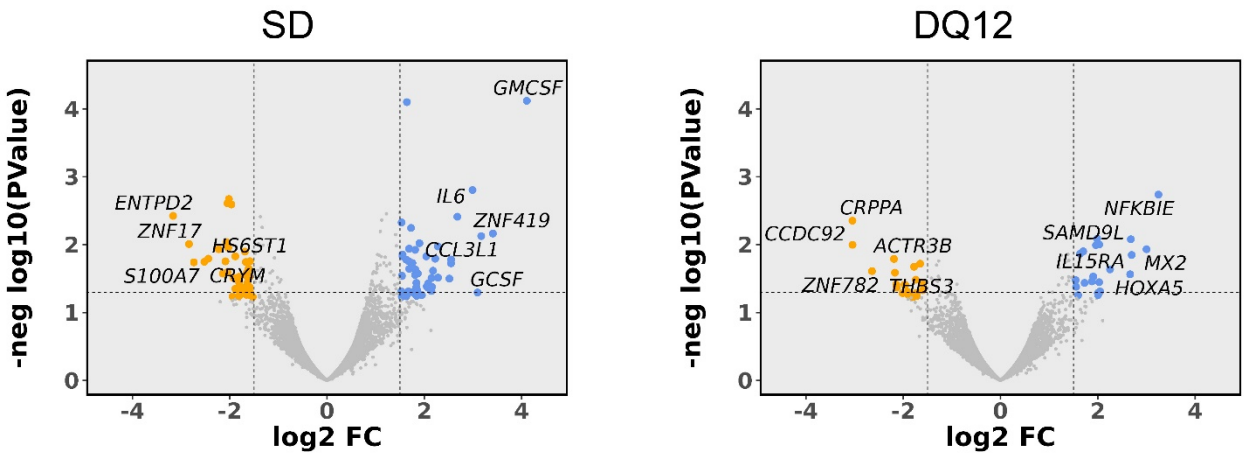

Figure 5.1. Differentially expressed genes upon exposure to SD and DQ12. RNA sequencing was performed for ALI co-cultures exposed to 31 µg/cm² SD (**A**) or DQ12 (**B**) and corresponding negative controls (N = 3 independent experiments; Controls: one or two replicates; DQ12 and SD: duplicates). Raw gene expression counts were normalized to counts per million. DEGs of SD- or DQ12-exposed ALI co-cultures were determined using edgeR and visualized using ggplot2. Volcano plots show color-coded DEGs (orange: downregulated; blue: upregulated) with a p-value threshold of 0.05 (for labels: 0.06) and an absolute log2 fold change threshold of 1.5.

5.4.2 Gene set enrichment analysis

To obtain an overview of the biological processes, molecular functions, and cellular components affected by SD and DQ12, we performed gene set enrichment analysis. For SD, a total of 85 enriched gene sets were found of which 74 were upregulated and 11 were downregulated (Table 5.1). The top 10 gene sets are displayed in Figure 5.2. All of the top 10 and the majority of all gene sets upregulated through SD can be related to immune responses, inflammation, and inflammatory signaling. Interestingly, among all upregulated gene sets, 11 specifically concerned the response to other organisms or their components, e.g. “response to biotic stimulus” or “response to lipopolysaccharide”. The DEG *GMCSF* was contained in 72 of the 74 upregulated gene sets. Further DEGs contained in at least 25 of the upregulated gene sets were *IL6* (69 sets), *GCSF* (61 sets), cluster of differentiation 74 (*CD74*) (58 sets), TNF receptor superfamily member 1B (*TNFRSF1B*) (44 sets), and *CCL3L1* (27 sets). The majority of gene sets downregulated by SD were related to cellular components. For DQ12, only 12 enriched gene sets

were found of which 3 were upregulated and 9 were downregulated (Figure 5.2, Table 5.1). The 3 gene sets upregulated by DQ12 were also upregulated by SD and were related to the responses to other organisms. Similar to SD, the gene sets downregulated by DQ12 were related to cellular components.

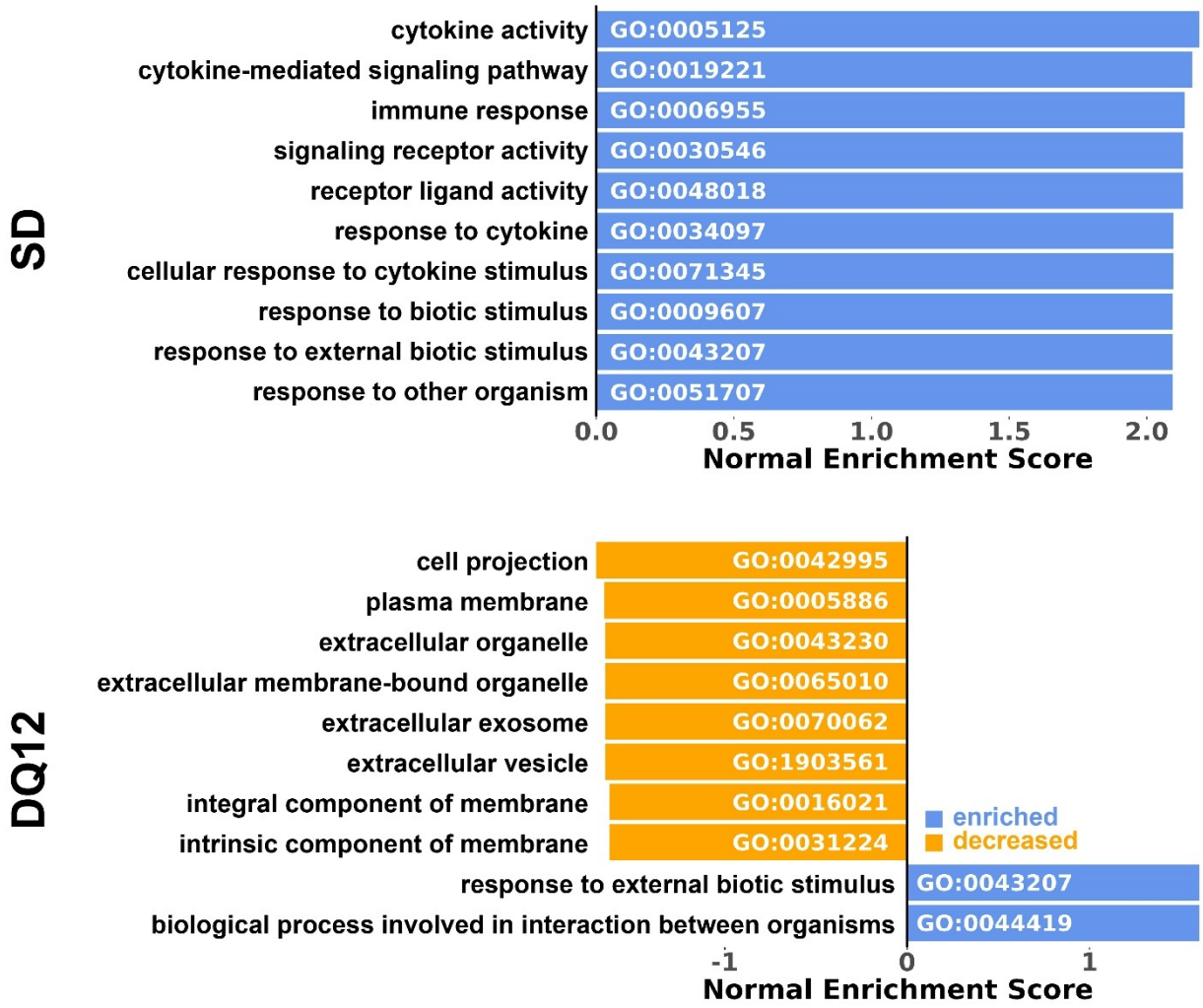

Figure 5.2. Gene set enrichment analysis. RNA sequencing was performed for ALI co-cultures exposed to 31 µg/cm² SD or DQ12 and corresponding negative controls (*N* = 3 independent experiments; Controls: one or two replicates; DQ12 and SD: duplicates). DEGs were identified using edgeR. For gene set enrichment analysis (GSEA), genes with an absolute log2 fold change ≥ 1.5 were considered. GSEA was performed using clusterProfiler with an unadjusted *p*-value cutoff of 0.05 and resampled ten times. The final result is based on the mean of normal(ized) enrichment scores. The top 10 enriched gene sets are represented and color-coded based on whether a gene set was found to be increased (blue) or decreased (orange).

Table 5.1. Number of gene sets enriched and decreased per ontology in response to exposure to SD and DQ12.

	SD enriched/decreased	DQ12 enriched/decreased	Shared enriched/decreased
All	74/11	3/9	3/3
Biological process	63/0	3/0	3/0
Molecular function	7/5	0/0	0/0
Cellular Component	4/6	0/9	0/3

RNA sequencing was performed for ALI co-cultures exposed to 31 µg/cm² SD or DQ12 and corresponding negative controls (*N* = 3 independent experiments; Controls: one or two replicates; DQ12 and SD: duplicates). DEGs were identified using edgeR. For gene set enrichment analysis (GSEA), genes with an absolute log2 fold change ≥ 1.5 were considered. GSEA was performed using clusterProfiler with an unadjusted *p*-value cutoff of 0.05 and resampled ten times. The final result is based on the mean of normal(ized) enrichment scores.

5.4.3 Released cytokines induced by Saharan dust exposure

Because SD particularly induced inflammation-related genes, we tested the release of 105 cytokines into the basolateral compartment of the ALI co-cultures using a protein array. SD exposure increased the concentrations of 16 of these cytokines by at least 1.5-fold (Table S5.2). We observed the strongest upregulation of about 3.7-fold for IL-16. GM-CSF and G-CSF were upregulated by about 2.3 and 1.5-fold, respectively. The positive control LPS upregulated 51 of the cytokines by at least 1.5-fold.

5.4.4 Confirmation of *GMCSF* and *GCSF* upregulation

Summarizing the results so far, SD particularly induced the expression of inflammatory genes and gene sets. Amongst these, *GMCSF* and *GCSF* were two of the four genes most potently upregulated through SD exposure whereas DQ12 exposure did not affect their expression. Protein array analysis suggested that GM-CSF and G-CSF were also induced at the protein level. For three reasons, we chose to follow up on *GMCSF* and *GCSF*: Firstly, physiologically, GM-CSF and G-CSF are important factors in immune cell differentiation and recruitment. GM-CSF is crucial for the development of alveolar macrophages (Paine et al., 2001; Piccoli et al., 2015; Suzuki et al., 2008). G-CSF contributes to the development of neutrophil granulocytes (Lieschke et al., 1994). Excessive concentrations of either cytokine have been associated with inflammatory pulmonary diseases, especially allergy and asthma as well as fibrosis (Lee et al., 2022; Ouyang et al., 2020; Patel et al., 2019; Stampfli et al., 1998; Suzuki et al., 2020; Wang et al., 2021; Willart et al., 2012; Yamashita et al., 2002; Zhou et al., 2014). Secondly, GM-CSF and G-CSF have not received any

substantial attention in the investigation of desert dust toxicity. Thirdly, they have recently emerged as promising drug targets. Neutralizing antibodies (Behrens et al., 2015; Taylor et al., 2019; Temesgen et al., 2022) and antagonists (Gamell et al., 2023) are already being developed for other fields of indication.

We confirmed the upregulation of *GMCSF* and *GCSF* gene expressions in the ALI co-cultures via qRT-PCR (Figure 5.3A&B). Importantly, the SD-induced upregulation of both genes was dose-dependent. At the medium dose, SD caused an about 3-fold increased expression of both genes while at the high dose, SD upregulated the expressions of *GMCSF* and *GCSF* by about 7 and 9-fold, respectively. In agreement with the RNA sequencing data, at the high dose, DQ12 upregulated *GMCSF* expression to a lesser extent by about 2-fold while again statistical significance was not reached ($p = 0.170$). Besides, DQ12 did not have a significant effect on *GCSF* expression. LPS strongly induced the expressions of *GMCSF* and *GCSF*.

Subsequently, we assessed the releases of both cytokines upon exposure to SD via ELISA (Figure 5.3C&D). At all tested concentrations, we found significantly induced releases of both GM-CSF and G-CSF by about 2-fold. DQ12 did not affect the release of G-CSF (Figure S5.1). LPS induced strong releases of GM-CSF and G-CSF. Overall, the results from gene expression and cytokine release analysis were in good agreement with the RNA sequencing and protein array data.

The increases in *GMCSF* and *GCSF* gene expression and GM-CSF and G-CSF release are mainly in concordance with the literature on pulmonary exposure to particulate matter. In agreement with our data, *GMCSF* expression (Yanagisawa et al., 2007) and GM-CSF secretion (Kim et al., 2011) have been reported to be enhanced in mice and human nasal polyp cells, respectively, exposed to Asian sand dust. Val et al. (2013) found elevated *GMCSF* expression and GM-CSF secretion from human bronchial epithelial 16HBE14o$^-$ cells exposed to urban dust containing SD. Further studies have reported increased concentrations of GM-CSF (Baulig et al., 2004; Fujii et al., 2002) and G-CSF (Alfaro-Moreno et al., 2008; Phillippi et al., 2022; Son et al., 2022; Wen et al., 2022) in 16HBE14o$^-$ cells human bronchial epithelial BEAS-2B cells, a co-culture of primary bronchial epithelial cells and alveolar macrophages, a tetra-culture of A549 cells, THP-1 cells, HMC-1 mast cells, and endothelial EAHY926 cells, mice, and humans in response to urban dust and diesel exhaust particles. That there was no effect of DQ12 quartz dust on G-CSF agrees with the minimal increase of G-CSF release reported for murine RAW264.7 macrophages exposed to 100 µg/ml quartz dust (Beyerle et al., 2009).

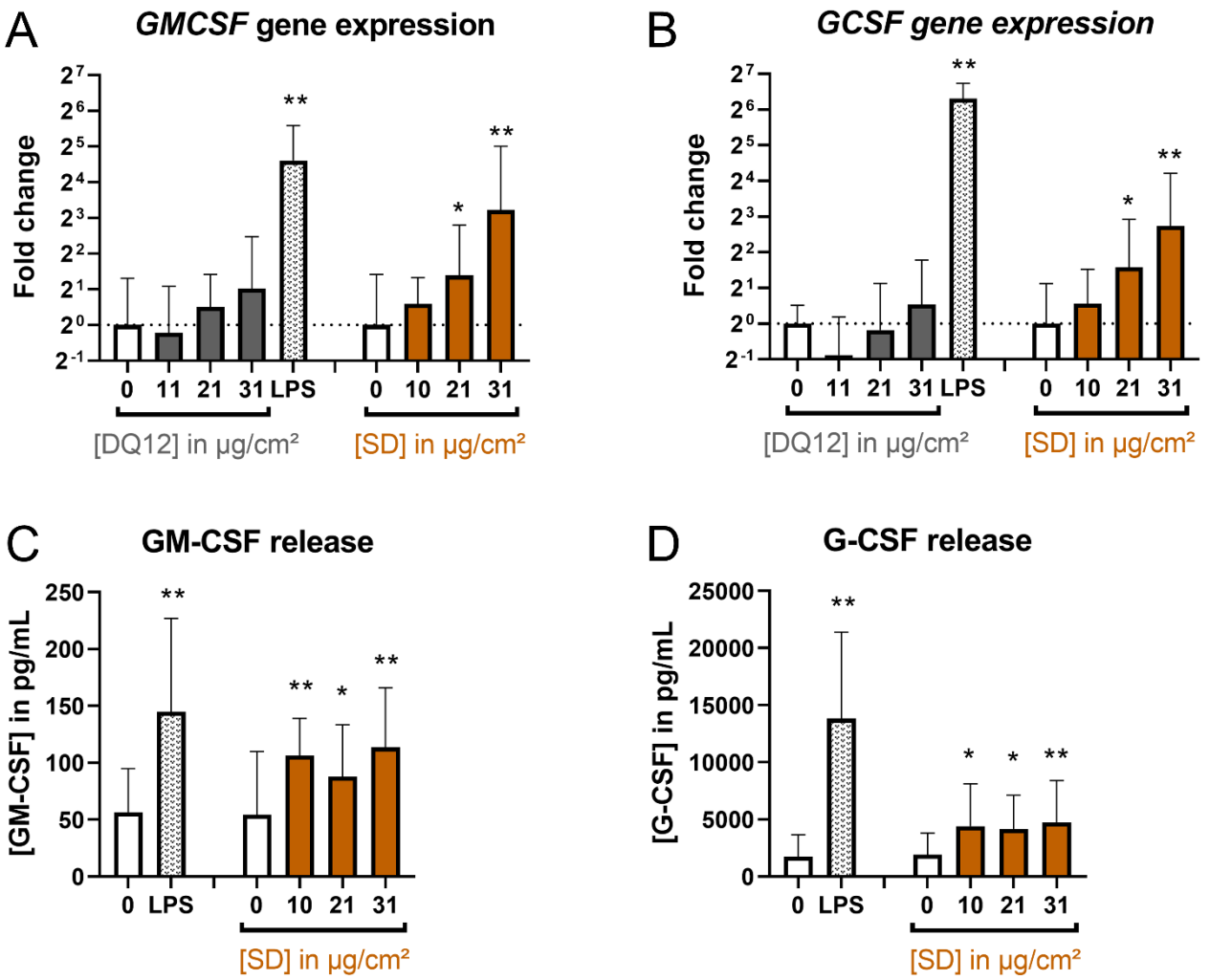

Figure 5.3. **Confirmation of SD-induced upregulation of GMCSF and GCSF gene expression and GM-CSF and G-CSF release.** ALI co-cultures were exposed to 0-31 µg/cm² DQ12 and SD for 24 h or 250 ± 60 ng/cm² LPS for 21 h. The relative gene expressions of *GMCSF* (**A**) and *GCSF* (**B**) as well as basolateral cytokine releases of GM-CSF (**C**) and G-CSF (**D**) were measured by qRT-PCR and ELISA, respectively. The gene expression data were normalized to control ALI cultures and to the reference genes *ACTB* and *GAPDH*. Shown are mean values with standard deviations. Fold changes were calculated with the means of $\Delta\Delta C_T$ values and standard deviations of ΔC_T values. Shown are mean values with standard deviations. For qRT-PCR and ELISA data, mixed-effects models with Šidák's post hoc test were calculated based on the ΔC_T values and absolute cytokine concentrations, respectively. *N* = 3-4 independent experiments were performed (Controls and LPS: one or two replicates; DQ12 and SD: duplicates per concentration; $*p \leq 0.05$; $**p \leq 0.01$).

5.4.5 Desert dust, GM-CSF, G-CSF, allergy, and asthma

The SD-mediated increases in GM-CSF and G-CSF may be especially relevant to allergic sensitization and asthma. Several epidemiological studies have found a link between desert dust exposure and asthma (Bener et al., 1996; Gyan et al., 2005; Samoli et al., 2011; Yang et al., 2005). Moreover, multiple studies demonstrated that Asian sand dust could exacerbate allergic

inflammatory reactions and suggested an Asian sand dust-mediated development of asthma (He et al., 2010; Ren et al., 2014a; Ren et al., 2014b; Ren et al., 2019). Allergy and asthma are accompanied by elevated concentrations of GM-CSF (Broide and Firestein, 1991; Saha et al., 2009) and G-CSF (Kim et al., 2020) in sputum and bronchioalveolar lavages. GM-CSF is essential in airway hyperresponsiveness in allergic asthma (Stampfli et al., 1998; Willart et al., 2012; Yamashita et al., 2002; Zhou et al., 2014) and the development of chronic asthma (Nobs et al., 2021). Thus, the GM-CSF-mediated adjuvant effect of air pollutants previously described for diesel exhaust particles may also apply to desert dusts (Bleck et al., 2006; Ohta et al., 1999). GM-CSF especially contributes to eosinophilic allergic inflammation (Stampfli et al., 1998; Willart et al., 2012; Yamashita et al., 2002; Zhou et al., 2014). Nevertheless, studies demonstrating the exacerbation of eosinophilia through Asian sand dust did not assess GM-CSF while they found increased concentrations of eosinophil-stimulating IL-5 (He et al., 2010; Ren et al., 2014a; Ren et al., 2014b; Ren et al., 2019). According to our cytokine array results (Table S5.2), SD also induced IL-5 in our ALI co-culture model.

G-CSF has been demonstrated to promote allergen sensitization (Patel et al., 2019) and allergic asthma (Wang et al., 2021). Ouyang et al. (2020) causally associated increased *GCSF* expression with allergen-induced neutrophilic inflammation in a mouse model of asthma. Kim et al. (2020) demonstrated that neutrophilic asthma is driven by G-CSF. The connection between desert dust exposure, GM-CSF, G-CSF, allergy, and asthma, should be confirmed in future studies: For example, GM-CSF and G-CSF neutralizing antibodies could be tested on models of allergy and asthma exposed to SD. Additionally, known single nucleotide polymorphisms of *GMCSF* and *GCSF* could be mapped against the susceptibility towards desert dust-induced asthma (He et al., 2008).

A pathway that should be explored in future studies on the exacerbation of allergy and asthma after desert dust exposure, is the induction of TNFα and IL-17A which then synergistically trigger the production of the neutrophil-attracting and stimulating CXCL1, CXCL2, and G-CSF (Kim et al., 2020; Ouyang et al., 2020). TNFα production in response to desert dusts has previously been reported by others (Ghio et al., 2014; Kim et al., 2003; Naota et al., 2010) as well as ourselves using the same ALI model and SD sample (Bredeck et al., 2023b). Studies on Asian desert dusts demonstrated the induction of CXCL1 and CXCL2 (He et al., 2012; Ichinose et al., 2005; Yanagisawa et al., 2007) which also agrees with our RNA sequencing data (Table S5.2). In the current study, we show that SD triggers G-CSF secretion (Figure 5.3D, Table S5.2).

5.4.6 Desert dust, GM-CSF, G-CSF, and fibrosis

Besides allergy and asthma, SD-mediated upregulations of GM-CSF and G-CSF may be involved in lung fibrosis. Whether these cytokines are deleterious or protective towards fibrosis is unclear considering the contradictory literature: In rats, overexpression of GM-CSF led to lung fibrosis (Xing et al., 1996) and application of G-CSF deteriorated bleomycin-induced fibrosis (Adach et al., 2002; Azoulay et al., 2003). Enhanced G-CSF concentrations have been found in lung lavages of patients with fibrosis (Ashitani et al., 1999; Lee et al., 2022). Amongst fibrosis patients higher G-CSF levels have been associated with lower survival rates (Lee et al., 2022). Contrarily, in mice GM-CSF (Hu et al., 2020; Piguet et al., 1993) and G-CSF (Zhang et al., 2011; Zhao et al., 2020) ameliorated fibrosis. Also, Suzuki et al. (2020) described a mouse model chronically overexpressing GM-CSF in the lung that developed no or minimal fibrosis.

That SD may promote fibrosis agrees with Dominguez-Rodriguez et al. (2020b) who reported increased levels of the pro-fibrotic transforming growth factor (TGF)-β1 and the fibrosis marker hydroxyproline in the sputum of SD-exposed ischemic heart disease patients. Moreover, SD exposure has been related to lung fibrosis in camels (Goodarzi et al., 2014; Hansen et al., 1989). In our ALI co-culture model, DQ12 quartz, which is known to cause fibrosis (Cassel et al., 2008; Dostert et al., 2008), did not affect *GMCSF* or *GCSF* (Figure 5.3A&B). In a previous study using the same model (Bredeck et al., 2023b), we also observed that DQ12 quartz neither induced IL-1β nor TNFα which are critical in particle-mediated lung fibrosis (Cassel et al., 2008; Dostert et al., 2008; Piguet et al., 1990). Contrarily, SD did induce IL-1β and TNFα. As discussed previously (Bredeck et al., 2023b), the stronger effects of SD than of DQ12 may be due to soluble constituents such as microbial components that are contained in SD but not DQ12 (Bredeck et al., 2023a). Overall, further investigations on the possible roles of GM-CSF and G-CSF in SD-induced fibrosis using more sophisticated human models such as organoids that include fibroblasts are necessary.

5.4.7 Further implications for health effects of desert dusts

If a causality between desert dust-induced GM-CSF and G-CSF secretion and lung disease can be confirmed in future studies, these cytokines could serve as potential drug targets. Recent studies have indicated a promising role for GM-CSF neutralization in COVID-19 patients (Temesgen et al., 2022) and rheumatoid arthritis (Behrens et al., 2015; Taylor et al., 2019). A G-CSF receptor antagonist has successfully been tested in a phase I intervention study (Gamell et al., 2023).

Our current findings may also be used to identify further factors relevant to the health effects of desert dusts. For example, we observed upregulation of solute carrier family 39 member 8

(*SLC39A8*) (Figure S5.2). *SLC39A8* codes for the zinc transporter ZIP8 which has been implicated in the defense against pathogens (Liu et al., 2013; Pyle et al., 2017) and epithelia renewal in the context of lung fibrosis (Foster et al., 2022). The induction of *SLC39A8* through microbial components aligns with *in vitro* and mouse studies testing LPS (Liu et al., 2013; Pyle et al., 2017). *CCL3L1* (Figure 5.1) and IL-16 (Table S5.2) are other factors that may be followed up on. *CCL3L1* gene deletions have been reported to be more frequent in asthmatics and the chemokine CCL3L1 has been shown to stimulate the secretion of anti-inflammatory IL-10 (Lee et al., 2011). IL-16 has been reported to be inversely correlated with lung emphysema (Bowler et al., 2013).

Finally, with our *in vitro* co-culture model we could unravel factors involved in the health effects of SD without the need to perform animal experiments. Thus, we adhered to replacing animal testing as a pivotal part of the 3Rs by Russell and Burch (1959). We identified GM-CSF and G-CSF as two cytokines prominently enhanced through SD. Further research is warranted on the role of these cytokines in lung diseases caused by exposure to desert dusts which affects hundreds of millions of people across five continents (Lwin et al., 2023; Zhang et al., 2016a).

Funding

This work has received funding from the Leibniz Association in the framework of the Leibniz Collaborative Excellence Programme project DUSTRISK under grant agreement number K225/2019. The IUF is funded by the federal and state governments - the Ministry of Culture and Science of North Rhine-Westphalia (MKW) and the Federal Ministry of Education and Research (BMBF).

Acknowledgments

We would like to thank Khanneh Wadinga Fomba and Hartmut Herrmann from the Leibniz Institute for Tropospheric Research (TROPOS), Germany, as well as Luis Neves from the National Institute of Meteorology of Cape Verde (INMG) for collecting and providing the Saharan dust sample. Furthermore, we are grateful to Keld Alstrup Jensen from The National Research Centre for the Working Environment (NFA), Denmark, for the information on the probe sonication methodology.

5.5 References

Adach, K., Suzuki, M., Sugimoto, T., Suzuki, S., Niki, R., Oyama, A., Uetsuka, K., Nakamaya, H., Doi, K., 2002. Granulocyte colony-stimulating factor exacerbates the acute lung injury and pulmonary fibrosis induced by intratracheal administration of bleomycin in rats. Exp Toxicol Pathol 53, 501-510. https://doi.org/10.1078/0940-2993-00218

Alfaro-Moreno, E., Nawrot, T.S., Vanaudenaerde, B.M., Hoylaerts, M.F., Vanoirbeek, J.A., Nemery, B., Hoet, P.H., 2008. Co-cultures of multiple cell types mimic pulmonary cell communication in

response to urban PM10. Eur Respir J 32, 1184-1194. https://doi.org/10.1183/09031936.00044008

Ashitani, J., Mukae, H., Taniguchi, H., Ihi, T., Kadota, J., Kohno, S., Matsukura, S., 1999. Granulocyte-colony stimulating factor levels in bronchoalveolar lavage fluid from patients with idiopathic pulmonary fibrosis. Thorax 54, 1015-1020. https://doi.org/10.1136/thx.54.11.1015

Azoulay, E., Herigault, S., Levame, M., Brochard, L., Schlemmer, B., Harf, A., Delclaux, C., 2003. Effect of granulocyte colony-stimulating factor on bleomycin-induced acute lung injury and pulmonary fibrosis. Crit Care Med 31, 1442-1448. https://doi.org/10.1097/01.CCM.0000050453.28177.33

Barnes, H., Goh, N.S.L., Leong, T.L., Hoy, R., 2019. Silica-associated lung disease: An old-world exposure in modern industries. Respirology 24, 1165-1175. https://doi.org/10.1111/resp.13695

Baulig, A., Poirault, J.J., Ausset, P., Schins, R., Shi, T., Baralle, D., Dorlhene, P., Meyer, M., Lefevre, R., Baeza-Squiban, A., Marano, F., 2004. Physicochemical characteristics and biological activities of seasonal atmospheric particulate matter sampling in two locations of Paris. Environ Sci Technol 38, 5985-5992. https://doi.org/10.1021/es049476z

Behrens, F., Tak, P.P., Ostergaard, M., Stoilov, R., Wiland, P., Huizinga, T.W., Berenfus, V.Y., Vladeva, S., Rech, J., Rubbert-Roth, A., Korkosz, M., Rekalov, D., Zupanets, I.A., Ejbjerg, B.J., Geiseler, J., Fresenius, J., Korolkiewicz, R.P., Schottelius, A.J., Burkhardt, H., 2015. MOR103, a human monoclonal antibody to granulocyte-macrophage colony-stimulating factor, in the treatment of patients with moderate rheumatoid arthritis: results of a phase Ib/IIa randomised, double-blind, placebo-controlled, dose-escalation trial. Ann Rheum Dis 74, 1058-1064. https://doi.org/10.1136/annrheumdis-2013-204816

Bener, A., Abdulrazzaq, Y.M., Al-Mutawwa, J., Debuse, P., 1996. Genetic and environmental factors associated with asthma. Hum Biol 68, 405-414.

Beyerle, A., Hobel, S., Czubayko, F., Schulz, H., Kissel, T., Aigner, A., Stoeger, T., 2009. In vitro cytotoxic and immunomodulatory profiling of low molecular weight polyethylenimines for pulmonary application. Toxicol In Vitro 23, 500-508. https://doi.org/10.1016/j.tiv.2009.01.001

Blank, F., Rothen-Rutishauser, B.M., Schurch, S., Gehr, P., 2006. An optimized in vitro model of the respiratory tract wall to study particle cell interactions. J Aerosol Med 19, 392-405. https://doi.org/10.1089/jam.2006.19.392

Bleck, B., Tse, D.B., Jaspers, I., Curotto de Lafaille, M.A., Reibman, J., 2006. Diesel exhaust particle-exposed human bronchial epithelial cells induce dendritic cell maturation. J Immunol 176, 7431-7437. https://doi.org/10.4049/jimmunol.176.12.7431

Bowler, R.P., Bahr, T.M., Hughes, G., Lutz, S., Kim, Y.I., Coldren, C.D., Reisdorph, N., Kechris, K.J., 2013. Integrative omics approach identifies interleukin-16 as a biomarker of emphysema. OMICS 17, 619-626. https://doi.org/10.1089/omi.2013.0038

Bredeck, G., Busch, M., Rossi, A., Stahlmecke, B., Fomba, K.W., Herrmann, H., Schins, R.P.F., 2023a. Inhalable Saharan dust induces oxidative stress, NLRP3 inflammasome activation, and inflammatory cytokine release. Environ Int 172, 107732. https://doi.org/10.1016/j.envint.2023.107732

Bredeck, G., Dobner, J., Stahlmecke, B., Fomba, K.W., Herrmann, H., Rossi, A., Schins, R.P.F., 2023b. Saharan dust induces NLRP3-dependent inflammatory cytokines in an alveolar air-liquid interface co-culture model. Part Fibre Toxicol 20, https://doi.org/10.1186/s12989-023-00550-w

Broide, D.H., Firestein, G.S., 1991. Endobronchial allergen challenge in asthma. Demonstration of cellular source of granulocyte macrophage colony-stimulating factor by in situ hybridization. J Clin Invest 88, 1048-1053. https://doi.org/10.1172/JCI115366

Busch, M., Bredeck, G., Kampfer, A.A.M., Schins, R.P.F., 2021. Investigations of acute effects of polystyrene and polyvinyl chloride micro- and nanoplastics in an advanced in vitro triple culture model of the healthy and inflamed intestine. Environ Res 193, 110536. https://doi.org/10.1016/j.envres.2020.110536

Cassel, S.L., Eisenbarth, S.C., Iyer, S.S., Sadler, J.J., Colegio, O.R., Tephly, L.A., Carter, A.B., Rothman, P.B., Flavell, R.A., Sutterwala, F.S., 2008. The Nalp3 inflammasome is essential for the development of silicosis. Proc Natl Acad Sci U S A 105, 9035-9040. https://doi.org/10.1073/pnas.0803933105

Castranova, V., 2004. Signaling pathways controlling the production of inflammatory mediators in response to crystalline silica exposure: role of reactive oxygen/nitrogen species. Free Radic Biol Med 37, 916-925. https://doi.org/10.1016/j.freeradbiomed.2004.05.032

Choi, Y.S., Bae, C.H., Song, S.Y., Kim, Y.D., 2015. Asian sand dust increases MUC8 and MUC5B expressions via TLR4-dependent ERK2 and p38 MAPK in human airway epithelial cells. Am J Rhinol Allergy 29, 161-165. https://doi.org/10.2500/ajra.2015.29.4162

Dominguez-Rodriguez, A., Rodriguez, S., Baez-Ferrer, N., Abreu-Gonzalez, P., Abreu-Gonzalez, J., Avanzas, P., Carnero, M., Moris, C., Lopez-Darias, J., Hernandez-Vaquero, D., 2020b. Impact of Saharan dust exposure on airway inflammation in patients with ischemic heart disease. Transl Res 224, 16-25. https://doi.org/10.1016/j.trsl.2020.05.011

Dostert, C., Petrilli, V., Van Bruggen, R., Steele, C., Mossman, B.T., Tschopp, J., 2008. Innate immune activation through Nalp3 inflammasome sensing of asbestos and silica. Science 320, 674-677. https://doi.org/10.1126/science.1156995

Emerson, R.J., Davis, G.S., 1983. Effect of alveolar lining material-coated silica on rat alveolar macrophages. Environ Health Perspect 51, 81-84. https://doi.org/10.1289/ehp.835181

Foster, S.P., Tay, H.L., Oliver, B.G., 2022. Deficiency in the zinc transporter ZIP8 impairs epithelia renewal and enhances lung fibrosis. J Clin Invest 132, https://doi.org/10.1172/JCI160595

Friesen, A., Fritsch-Decker, S., Hufnagel, M., Mulhopt, S., Stapf, D., Hartwig, A., Weiss, C., 2022. Comparing alpha-Quartz-Induced Cytotoxicity and Interleukin-8 Release in Pulmonary Mono- and Co-Cultures Exposed under Submerged and Air-Liquid Interface Conditions. Int J Mol Sci 23, https://doi.org/10.3390/ijms23126412

Fujii, T., Hayashi, S., Hogg, J.C., Mukae, H., Suwa, T., Goto, Y., Vincent, R., van Eeden, S.F., 2002. Interaction of alveolar macrophages and airway epithelial cells following exposure to particulate matter produces mediators that stimulate the bone marrow. Am J Respir Cell Mol Biol 27, 34-41. https://doi.org/10.1165/ajrcmb.27.1.4787

Fussell, J.C., Kelly, F.J., 2021. Mechanisms underlying the health effects of desert sand dust. Environ Int 157, 106790. https://doi.org/10.1016/j.envint.2021.106790

Gamell, C., Bankovacki, A., Scalzo-Inguanti, K., Sedgmen, B., Alhamdoosh, M., Gail, E., Turkovic, L., Millar, C., Johnson, L., Wahlsten, M., Richter, J., Schuster, J., Dyson, A., Nicolopoulos, J., Varigos, G., Ng, M., Wilson, N., Field, J., Kern, J.S., Lindqvist, L.M., 2023. CSL324, a granulocyte colony-stimulating factor receptor antagonist, blocks neutrophil migration markers that are upregulated in hidradenitis suppurativa. Br J Dermatol 188, 636-648. https://doi.org/10.1093/bjd/ljad013

Gehr, P., Green, F.H., Geiser, M., Im Hof, V., Lee, M.M., Schurch, S., 1996. Airway surfactant, a primary defense barrier: mechanical and immunological aspects. J Aerosol Med 9, 163-181. https://doi.org/10.1089/jam.1996.9.163

Geng, H., Meng, Z., Zhang, Q., 2005. Effects of blowing sand fine particles on plasma membrane permeability and fluidity, and intracellular calcium levels of rat alveolar macrophages. Toxicol Lett 157, 129-137. https://doi.org/10.1016/j.toxlet.2005.01.010

Ghio, A.J., Kummarapurugu, S.T., Tong, H., Soukup, J.M., Dailey, L.A., Boykin, E., Gilmour, I.M., Ingram, P., Roggli, V.L., Goldstein, H.L., Reynolds, R.L., 2014. Biological effects of desert dust in respiratory epithelial cells and a murine model. Inhal Toxicol 26, 299-309. https://doi.org/10.3109/08958378.2014.888109

Goodarzi, M., Azizi, S., Koupaei, M.J., Moshkelani, S., 2014. Pathologic Findings of Anthraco-silicosis in the Lungs of One Humped Camels (Camelus dromedarius) and Its Role in the Occurrence of Pneumonia. Kafkas Univ Vet Fak, https://doi.org/10.9775/kvfd.2013.9564

Gyan, K., Henry, W., Lacaille, S., Laloo, A., Lamsee-Ebanks, C., McKay, S., Antoine, R.M., Monteil, M.A., 2005. African dust clouds are associated with increased paediatric asthma accident and emergency admissions on the Caribbean island of Trinidad. Int J Biometeorol 49, 371-376. https://doi.org/10.1007/s00484-005-0257-3

Hansen, H.J., Jama, F.M., Nilsson, C., Norrgren, L., Abdurahman, O.S., 1989. Silicate pneumoconiosis in camels (Camelus dromedarius L.). J Vet Med A 36, 789-796. https://doi.org/10.1111/j.1439-0442.1989.tb00793.x

He, J.Q., Shumansky, K., Connett, J.E., Anthonisen, N.R., Pare, P.D., Sandford, A.J., 2008. Association of genetic variations in the CSF2 and CSF3 genes with lung function in smoking-induced COPD. Eur Respir J 32, 25-34. https://doi.org/10.1183/09031936.00040307

He, M., Ichinose, T., Song, Y., Yoshida, Y., Arashidani, K., Yoshida, S., Liu, B., Nishikawa, M., Takano, H., Sun, G., 2013. Effects of two Asian sand dusts transported from the dust source regions of Inner Mongolia and northeast China on murine lung eosinophilia. Toxicol Appl Pharmacol 272, 647-655. https://doi.org/10.1016/j.taap.2013.07.010

He, M., Ichinose, T., Song, Y., Yoshida, Y., Bekki, K., Arashidani, K., Yoshida, S., Nishikawa, M., Takano, H., Shibamoto, T., Sun, G., 2016. Desert dust induces TLR signaling to trigger Th2-dominant lung allergic inflammation via a MyD88-dependent signaling pathway. Toxicol Appl Pharmacol 296, 61-72. https://doi.org/10.1016/j.taap.2016.02.011

He, M., Ichinose, T., Yoshida, S., Nishikawa, M., Mori, I., Yanagisawa, R., Takano, H., Inoue, K., Sun, G., Shibamoto, T., 2010. Airborne Asian sand dust enhances murine lung eosinophilia. Inhal Toxicol 22, 1012-1025. https://doi.org/10.3109/08958378.2010.510151

He, M., Ichinose, T., Yoshida, S., Yamamoto, S., Inoue, K., Takano, H., Yanagisawa, R., Nishikawa, M., Mori, I., Sun, G., Shibamoto, T., 2012. Asian sand dust enhances murine lung inflammation caused by Klebsiella pneumoniae. Toxicol Appl Pharmacol 258, 237-247. https://doi.org/10.1016/j.taap.2011.11.003

Herseth, J.I., Volden, V., Schwarze, P.E., Lag, M., Refsnes, M., 2008. IL-1beta differently involved in IL-8 and FGF-2 release in crystalline silica-treated lung cell co-cultures. Part Fibre Toxicol 5, 16. https://doi.org/10.1186/1743-8977-5-16

Hu, D., Zhang, Y., Cao, R., Hao, Y., Yang, X., Tian, T., Zhang, J., 2020. The protective effects of granulocyte-macrophage colony-stimulating factor against radiation-induced lung injury. Transl Lung Cancer Res 9, 2440-2459. https://doi.org/10.21037/tlcr-20-1272

Hussell, T., Bell, T.J., 2014. Alveolar macrophages: plasticity in a tissue-specific context. Nat Rev Immunol 14, 81-93. https://doi.org/10.1038/nri3600

Ichinose, T., Nishikawa, M., Takano, H., Sera, N., Sadakane, K., Mori, I., Yanagisawa, R., Oda, T., Tamura, H., Hiyoshi, K., Quan, H., Tomura, S., Shibamoto, T., 2005. Pulmonary toxicity induced by intratracheal instillation of Asian yellow dust (Kosa) in mice. Environ Toxicol Pharmacol 20, 48-56. https://doi.org/10.1016/j.etap.2004.10.009

Johnston, F., Hanigan, I., Henderson, S., Morgan, G., Bowman, D., 2011. Extreme air pollution events from bushfires and dust storms and their association with mortality in Sydney, Australia 1994-2007. Environ Res 111, 811-816. https://doi.org/10.1016/j.envres.2011.05.007

Kampfer, A.A.M., Busch, M., Buttner, V., Bredeck, G., Stahlmecke, B., Hellack, B., Masson, I., Sofranko, A., Albrecht, C., Schins, R.P.F., 2021. Model Complexity as Determining Factor for In Vitro Nanosafety Studies: Effects of Silver and Titanium Dioxide Nanomaterials in Intestinal Models. Small 17, e2004223. https://doi.org/10.1002/smll.202004223

Kashima, S., Yorifuji, T., Bae, S., Honda, Y., Lim, Y.-H., Hong, Y.-C., 2016. Asian dust effect on cause-specific mortality in five cities across South Korea and Japan. Atmos Environ 128, 20-27. https://doi.org/10.1016/j.atmosenv.2015.12.063

Kelly, F.J., Fussell, J.C., 2011. Air pollution and airway disease. Clin Exp Allergy 41, 1059-1071. https://doi.org/10.1111/j.1365-2222.2011.03776.x

Kim, S.T., Ye, M.K., Shin, S.H., 2011. Effects of Asian sand dust on mucin gene expression and activation of nasal polyp epithelial cells. Am J Rhinol Allergy 25, 303-306. https://doi.org/10.2500/ajra.2011.25.3627

Kim, Y.H., Kim, K.S., Kwak, N.J., Lee, K.H., Kweon, S.A., Lim, Y., 2003. Cytotoxicity of yellow sand in lung epithelial cells. J Biosci 28, 77-81. https://doi.org/10.1007/BF02970135

Kim, Y.M., Kim, H., Lee, S., Kim, S., Lee, J.U., Choi, Y., Park, H.W., You, G., Kang, H., Lee, S., Park, J.S., Park, Y., Park, H.S., Park, C.S., Lee, S.W., 2020. Airway G-CSF identifies neutrophilic inflammation and contributes to asthma progression. Eur Respir J 55, https://doi.org/10.1183/13993003.00827-2019

Lee, H., Bae, S., Choi, B.W., Choi, J.C., Yoon, Y., 2011. Copy number variation of CCL3L1 influences asthma risk by modulating IL-10 expression. Clin Chim Acta 412, 2100-2104. https://doi.org/10.1016/j.cca.2011.07.017

Lee, J.U., Choi, J.S., Kim, M.K., Min, S.A., Park, J.S., Park, C.S., 2022. Granulocyte colony-stimulating factor in bronchoalveolar lavage fluid is a potential biomarker for prognostic prediction of idiopathic pulmonary fibrosis. Korean J Intern Med 37, 979-988. https://doi.org/10.3904/kjim.2021.442

Lieschke, G.J., Grail, D., Hodgson, G., Metcalf, D., Stanley, E., Cheers, C., Fowler, K.J., Basu, S., Zhan, Y.F., Dunn, A.R., 1994. Mice lacking granulocyte colony-stimulating factor have chronic neutropenia, granulocyte and macrophage progenitor cell deficiency, and impaired neutrophil mobilization. Blood 84, 1737-1746. https://doi.org/10.1182/blood.V84.6.1737.1737

Liu, M.J., Bao, S., Galvez-Peralta, M., Pyle, C.J., Rudawsky, A.C., Pavlovicz, R.E., Killilea, D.W., Li, C., Nebert, D.W., Wewers, M.D., Knoell, D.L., 2013. ZIP8 regulates host defense through zinc-mediated inhibition of NF-kappaB. Cell Rep 3, 386-400. https://doi.org/10.1016/j.celrep.2013.01.009

Livak, K.J., Schmittgen, T.D., 2001. Analysis of Relative Gene Expression Data Using Real-Time Quantitative PCR and the ΔΔCT Method. Methods 25, 402-408. https://doi.org/10.1006/meth.2001.1262

Loret, T., Peyret, E., Dubreuil, M., Aguerre-Chariol, O., Bressot, C., le Bihan, O., Amodeo, T., Trouiller, B., Braun, A., Egles, C., Lacroix, G., 2016. Air-liquid interface exposure to aerosols of poorly soluble nanomaterials induces different biological activation levels compared to exposure to suspensions. Part Fibre Toxicol 13, 58. https://doi.org/10.1186/s12989-016-0171-3

Lwin, K.S., Tobias, A., Chua, P.L., Yuan, L., Thawonmas, R., Ith, S., Htay, Z.W., Yu, L.S., Yamasaki, L., Roque, M., Querol, X., Fussell, J.C., Nadeau, K.C., Stafoggia, M., Saliba, N.A., Sheng Ng, C.F., Hashizume, M., 2023. Effects of Desert Dust and Sandstorms on Human Health: A Scoping Review. Geohealth 7, e2022GH000728. https://doi.org/10.1029/2022GH000728

Murakami, S., Iwaki, D., Mitsuzawa, H., Sano, H., Takahashi, H., Voelker, D.R., Akino, T., Kuroki, Y., 2002. Surfactant protein A inhibits peptidoglycan-induced tumor necrosis factor-alpha secretion in U937 cells and alveolar macrophages by direct interaction with toll-like receptor 2. J Biol Chem 277, 6830-6837. https://doi.org/10.1074/jbc.M106671200

Naota, M., Mukaiyama, T., Shimada, A., Yoshida, A., Okajima, M., Morita, T., Inoue, K., Takano, H., 2010. Pathological study of acute pulmonary toxicity induced by intratracheally instilled Asian sand dust (kosa). Toxicol Pathol 38, 1099-1110. https://doi.org/10.1177/0192623310385143

Napierska, D., Thomassen, L.C., Lison, D., Martens, J.A., Hoet, P.H., 2010. The nanosilica hazard: another variable entity. Part Fibre Toxicol 7, 39. https://doi.org/10.1186/1743-8977-7-39

Nobs, S.P., Pohlmeier, L., Li, F., Kayhan, M., Becher, B., Kopf, M., 2021. GM-CSF instigates a dendritic cell-T-cell inflammatory circuit that drives chronic asthma development. J Allergy Clin Immunol 147, 2118-2133 e2113. https://doi.org/10.1016/j.jaci.2020.12.638

Ohlinger, K., Kolesnik, T., Meindl, C., Galle, B., Absenger-Novak, M., Kolb-Lenz, D., Frohlich, E., 2019. Air-liquid interface culture changes surface properties of A549 cells. Toxicol In Vitro 60, 369-382. https://doi.org/10.1016/j.tiv.2019.06.014

Ohta, K., Yamashita, N., Tajima, M., Miyasaka, T., Nakano, J., Nakajima, M., Ishii, A., Horiuchi, T., Mano, K., Miyamoto, T., 1999. Diesel exhaust particulate induces airway hyperresponsiveness in a murine model: essential role of GM-CSF. J Allergy Clin Immunol 104, 1024-1030. https://doi.org/10.1016/s0091-6749(99)70084-9

Osier, M., Oberdorster, G., 1997. Intratracheal inhalation vs intratracheal instillation: differences in particle effects. Fundam Appl Toxicol 40, 220-227. https://doi.org/10.1006/faat.1997.2390

Ouyang, S., Liu, C., Xiao, J., Chen, X., Lui, A.C., Li, X., 2020. Targeting IL-17A/glucocorticoid synergy to CSF3 expression in neutrophilic airway diseases. JCI Insight 5, https://doi.org/10.1172/jci.insight.132836

Paine, R., 3rd, Morris, S.B., Jin, H., Wilcoxen, S.E., Phare, S.M., Moore, B.B., Coffey, M.J., Toews, G.B., 2001. Impaired functional activity of alveolar macrophages from GM-CSF-deficient mice. Am J Physiol Lung Cell Mol Physiol 281, L1210-1218. https://doi.org/10.1152/ajplung.2001.281.5.L1210

Patel, D.F., Peiro, T., Bruno, N., Vuononvirta, J., Akthar, S., Puttur, F., Pyle, C.J., Suveizdyte, K., Walker, S.A., Singanayagam, A., Carlin, L.M., Gregory, L.G., Lloyd, C.M., Snelgrove, R.J., 2019. Neutrophils restrain allergic airway inflammation by limiting ILC2 function and monocyte-dendritic cell antigen presentation. Sci Immunol 4, https://doi.org/10.1126/sciimmunol.aax7006

Pavan, C., Rabolli, V., Tomatis, M., Fubini, B., Lison, D., 2014. Why does the hemolytic activity of silica predict its pro-inflammatory activity? Part Fibre Toxicol 11, 76. https://doi.org/10.1186/s12989-014-0076-y

Phillippi, D.T., Daniel, S., Pusadkar, V., Youngblood, V.L., Nguyen, K.N., Azad, R.K., McFarlin, B.K., Lund, A.K., 2022. Inhaled diesel exhaust particles result in microbiome-related systemic inflammation and altered cardiovascular disease biomarkers in C57Bl/6 male mice. Part Fibre Toxicol 19, 10. https://doi.org/10.1186/s12989-022-00452-3

Piccoli, L., Campo, I., Fregni, C.S., Rodriguez, B.M., Minola, A., Sallusto, F., Luisetti, M., Corti, D., Lanzavecchia, A., 2015. Neutralization and clearance of GM-CSF by autoantibodies in pulmonary alveolar proteinosis. Nat Commun 6, 7375. https://doi.org/10.1038/ncomms8375

Piguet, P.F., Collart, M.A., Grau, G.E., Sappino, A.P., Vassalli, P., 1990. Requirement of tumour necrosis factor for development of silica-induced pulmonary fibrosis. Nature 344, 245-247. https://doi.org/10.1038/344245a0

Piguet, P.F., Grau, G.E., de Kossodo, S., 1993. Role of granulocyte-macrophage colony-stimulating factor in pulmonary fibrosis induced in mice by bleomycin. Exp Lung Res 19, 579-587. https://doi.org/10.3109/01902149309031729

Pyle, C.J., Akhter, S., Bao, S., Dodd, C.E., Schlesinger, L.S., Knoell, D.L., 2017. Zinc Modulates Endotoxin-Induced Human Macrophage Inflammation through ZIP8 Induction and C/EBPbeta Inhibition. PLoS One 12, e0169531. https://doi.org/10.1371/journal.pone.0169531

Ren, Y., Ichinose, T., He, M., Arashidani, K., Yoshida, Y., Yoshida, S., Nishikawa, M., Takano, H., Sun, G., Shibamoto, T., 2014a. Aggravation of ovalbumin-induced murine asthma by co-exposure to desert-dust and organic chemicals: an animal model study. Environ Health 13, 83. https://doi.org/10.1186/1476-069X-13-83

Ren, Y., Ichinose, T., He, M., Song, Y., Yoshida, Y., Yoshida, S., Nishikawa, M., Takano, H., Sun, G., Shibamoto, T., 2014b. Enhancement of OVA-induced murine lung eosinophilia by co-exposure to contamination levels of LPS in Asian sand dust and heated dust. Allergy Asthma Cl Im 10, 30. https://doi.org/10.1186/1710-1492-10-30

Ren, Y., Ichinose, T., He, M., Youshida, S., Nishikawa, M., Sun, G., 2019. Co-exposure to lipopolysaccharide and desert dust causes exacerbation of ovalbumin-induced allergic lung inflammation in mice via TLR4/MyD88-dependent and -independent pathways. Allergy Asthma Clin Immunol 15, 82. https://doi.org/10.1186/s13223-019-0396-4

Rodriguez-Navarro, C., di Lorenzo, F., Elert, K., 2018. Mineralogy and physicochemical features of Saharan dust wet deposited in the Iberian Peninsula during an extreme red rain event. Atmos Chem Phys 18, 10089-10122. https://doi.org/10.5194/acp-18-10089-2018

Russell, W.M.S., Burch, R.L. The Principles of Humane Experimental Technique. Methuen; 1959

Saha, S., Doe, C., Mistry, V., Siddiqui, S., Parker, D., Sleeman, M., Cohen, E.S., Brightling, C.E., 2009. Granulocyte-macrophage colony-stimulating factor expression in induced sputum and bronchial mucosa in asthma and COPD. Thorax 64, 671-676. https://doi.org/10.1136/thx.2008.108290

Samoli, E., Nastos, P.T., Paliatsos, A.G., Katsouyanni, K., Priftis, K.N., 2011. Acute effects of air pollution on pediatric asthma exacerbation: evidence of association and effect modification. Environ Res 111, 418-424. https://doi.org/10.1016/j.envres.2011.01.014

Schweitzer, M.D., Calzadilla, A.S., Salamo, O., Sharifi, A., Kumar, N., Holt, G., Campos, M., Mirsaeidi, M., 2018. Lung health in era of climate change and dust storms. Environ Res 163, 36-42. https://doi.org/10.1016/j.envres.2018.02.001

Sengul, A.B., Asmatulu, E., 2020. Toxicity of metal and metal oxide nanoparticles: a review. Environ Chem Lett 18, 1659-1683. https://doi.org/10.1007/s10311-020-01033-6

Seok, J., Warren, H.S., Cuenca, A.G., Mindrinos, M.N., Baker, H.V., Xu, W., Richards, D.R., McDonald-Smith, G.P., Gao, H., Hennessy, L., Finnerty, C.C., Lopez, C.M., Honari, S., Moore, E.E., Minei, J.P., Cuschieri, J., Bankey, P.E., Johnson, J.L., Sperry, J., Nathens, A.B., Billiar, T.R., West, M.A., Jeschke, M.G., Klein, M.B., Gamelli, R.L., Gibran, N.S., Brownstein, B.H., Miller-Graziano, C., Calvano, S.E., Mason, P.H., Cobb, J.P., Rahme, L.G., Lowry, S.F., Maier, R.V., Moldawer, L.L., Herndon, D.N., Davis, R.W., Xiao, W., Tompkins, R.G., Inflammation, Host Response to Injury, L.S.C.R.P., 2013. Genomic responses in mouse models poorly mimic human inflammatory diseases. Proc Natl Acad Sci U S A 110, 3507-3512. https://doi.org/10.1073/pnas.1222878110

Son, E.S., Ko, U.W., Jeong, H.Y., Park, S.Y., Lee, Y.E., Park, J.W., Jeong, S.H., Kim, S.H., Kyung, S.Y., 2022. miRNA-6515-5p regulates particulate matter-induced inflammatory responses by targeting CSF3 in human bronchial epithelial cells. Toxicol In Vitro 84, 105428. https://doi.org/10.1016/j.tiv.2022.105428

Stampfli, M.R., Wiley, R.E., Neigh, G.S., Gajewska, B.U., Lei, X.F., Snider, D.P., Xing, Z., Jordana, M., 1998. GM-CSF transgene expression in the airway allows aerosolized ovalbumin to induce allergic sensitization in mice. J Clin Invest 102, 1704-1714. https://doi.org/10.1172/JCI4160

Standiford, T.J., Kunkel, S.L., Basha, M.A., Chensue, S.W., Lynch, J.P., 3rd, Toews, G.B., Westwick, J., Strieter, R.M., 1990. Interleukin-8 gene expression by a pulmonary epithelial cell line. A model for cytokine networks in the lung. J Clin Invest 86, 1945-1953. https://doi.org/10.1172/JCI114928

Stern, R.A., Mahmoudi, N., Buckee, C.O., Schartup, A.T., Koutrakis, P., Ferguson, S.T., Wolfson, J.M., Wofsy, S.C., Daube, B.C., Sunderland, E.M., 2021. The Microbiome of Size-Fractionated Airborne Particles from the Sahara Region. Environ Sci Technol 55, 1487-1496. https://doi.org/10.1021/acs.est.0c06332

Sun, H., Shamy, M., Kluz, T., Munoz, A.B., Zhong, M., Laulicht, F., Alghamdi, M.A., Khoder, M.I., Chen, L.C., Costa, M., 2012. Gene expression profiling and pathway analysis of human bronchial epithelial cells exposed to airborne particulate matter collected from Saudi Arabia. Toxicol Appl Pharmacol 265, 147-157. https://doi.org/10.1016/j.taap.2012.10.008

Suzuki, T., McCarthy, C., Carey, B.C., Borchers, M., Beck, D., Wikenheiser-Brokamp, K.A., Black, D., Chalk, C., Trapnell, B.C., 2020. Increased Pulmonary GM-CSF Causes Alveolar Macrophage Accumulation. Mechanistic Implications for Desquamative Interstitial Pneumonitis. Am J Respir Cell Mol Biol 62, 87-94. https://doi.org/10.1165/rcmb.2018-0294OC

Suzuki, T., Sakagami, T., Rubin, B.K., Nogee, L.M., Wood, R.E., Zimmerman, S.L., Smolarek, T., Dishop, M.K., Wert, S.E., Whitsett, J.A., Grabowski, G., Carey, B.C., Stevens, C., van der Loo, J.C., Trapnell, B.C., 2008. Familial pulmonary alveolar proteinosis caused by mutations in CSF2RA. J Exp Med 205, 2703-2710. https://doi.org/10.1084/jem.20080990

Taylor, P.C., Saurigny, D., Vencovsky, J., Takeuchi, T., Nakamura, T., Matsievskaia, G., Hunt, B., Wagner, T., Souberbielle, B., Group, N.S., 2019. Efficacy and safety of namilumab, a human monoclonal antibody against granulocyte-macrophage colony-stimulating factor (GM-CSF) ligand in patients with rheumatoid arthritis (RA) with either an inadequate response to background methotrexate therapy or an inadequate response or intolerance to an anti-TNF (tumour necrosis factor) biologic therapy: a randomized, controlled trial. Arthritis Res Ther 21, 101. https://doi.org/10.1186/s13075-019-1879-x

Temesgen, Z., Burger, C.D., Baker, J., Polk, C., Libertin, C.R., Kelley, C.F., Marconi, V.C., Orenstein, R., Catterson, V.M., Aronstein, W.S., Durrant, C., Chappell, D., Ahmed, O., Chappell, G., Badley, A.D., Group, L.-A.S., 2022. Lenzilumab in hospitalised patients with COVID-19 pneumonia (LIVE-AIR): a phase 3, randomised, placebo-controlled trial. Lancet Respir Med 10, 237-246. https://doi.org/10.1016/S2213-2600(21)00494-X

Val, S., Liousse, C., Doumbia el, H.T., Galy-Lacaux, C., Cachier, H., Marchand, N., Badel, A., Gardrat, E., Sylvestre, A., Baeza-Squiban, A., 2013. Physico-chemical characterization of African urban aerosols (Bamako in Mali and Dakar in Senegal) and their toxic effects in human bronchial epithelial cells: description of a worrying situation. Part Fibre Toxicol 10, 10. https://doi.org/10.1186/1743-8977-10-10

Wallace, W.E., Keane, M.J., Mike, P.S., Hill, C.A., Vallyathan, V., Regad, E.D., 1992. Contrasting respirable quartz and kaolin retention of lecithin surfactant and expression of membranolytic activity following phospholipase A2 digestion. J Toxicol Environ Health 37, 391-409. https://doi.org/10.1080/15287399209531679

Wang, G., Zhang, X., Liu, X., Zheng, J., 2020a. Co-culture of human alveolar epithelial (A549) and macrophage (THP-1) cells to study the potential toxicity of ambient PM2.5: a comparison of growth under ALI and submerged conditions. Toxicol Res-UK 9, 636-651. https://doi.org/10.1093/toxres/tfaa072

Wang, H., Aloe, C., McQualter, J., Papanicolaou, A., Vlahos, R., Wilson, N., Bozinovski, S., 2021. G-CSFR antagonism reduces mucosal injury and airways fibrosis in a virus-dependent model of severe asthma. Br J Pharmacol 178, 1869-1885. https://doi.org/10.1111/bph.15415

Warren, H.S., Tompkins, R.G., Moldawer, L.L., Seok, J., Xu, W., Mindrinos, M.N., Maier, R.V., Xiao, W., Davis, R.W., 2015. Mice are not men. Proc Natl Acad Sci U S A 112, E345. https://doi.org/10.1073/pnas.1414857111

Wen, F., Huang, J., Sun, Y., Zhao, Y., Li, B., Wu, S., Zhang, L., 2022. Sensitive inflammatory biomarkers of acute fine particulate matter exposure among healthy young adults: Findings from a randomized, double-blind crossover trial on air filtration. Environ Pollut 301, 119026. https://doi.org/10.1016/j.envpol.2022.119026

Willart, M.A., Deswarte, K., Pouliot, P., Braun, H., Beyaert, R., Lambrecht, B.N., Hammad, H., 2012. Interleukin-1alpha controls allergic sensitization to inhaled house dust mite via the epithelial release of GM-CSF and IL-33. J Exp Med 209, 1505-1517. https://doi.org/10.1084/jem.20112691

Wu, J., Wang, Y., Liu, G., Jia, Y., Yang, J., Shi, J., Dong, J., Wei, J., Liu, X., 2017. Characterization of air-liquid interface culture of A549 alveolar epithelial cells. Braz J Med Biol Res 51, e6950. https://doi.org/10.1590/1414-431X20176950

Xing, Z., Ohkawara, Y., Jordana, M., Graham, F., Gauldie, J., 1996. Transfer of granulocyte-macrophage colony-stimulating factor gene to rat lung induces eosinophilia, monocytosis, and fibrotic reactions. J Clin Invest 97, 1102-1110. https://doi.org/10.1172/JCI118503

Yamashita, N., Tashimo, H., Ishida, H., Kaneko, F., Nakano, J., Kato, H., Hirai, K., Horiuchi, T., Ohta, K., 2002. Attenuation of airway hyperresponsiveness in a murine asthma model by neutralization of granulocyte-macrophage colony-stimulating factor (GM-CSF). Cell Immunol 219, 92-97. https://doi.org/10.1016/s0008-8749(02)00565-8

Yanagisawa, R., Takano, H., Ichinose, T., Mizushima, K., Nishikawa, M., Mori, I., Inoue, K., Sadakane, K., Yoshikawa, T., 2007. Gene expression analysis of murine lungs following pulmonary exposure to Asian sand dust particles. Exp Biol Med 232, 1109-1118. https://doi.org/10.3181/0612-RM-311

Yang, C.Y., Tsai, S.S., Chang, C.C., Ho, S.C., 2005. Effects of Asian dust storm events on daily admissions for asthma in Taipei, Taiwan. Inhal Toxicol 17, 817-821. https://doi.org/10.1080/08958370500241254

Zauli Sajani, S., Miglio, R., Bonasoni, P., Cristofanelli, P., Marinoni, A., Sartini, C., Goldoni, C.A., De Girolamo, G., Lauriola, P., 2011. Saharan dust and daily mortality in Emilia-Romagna (Italy). Occup Environ Med 68, 446-451. https://doi.org/10.1136/oem.2010.058156

Zhang, F., Zhang, L., Jiang, H.S., Chen, X.Y., Zhang, Y., Li, H.P., Zhang, R.X., Zheng, H., Chu, J.X., Chen, X.J., 2011. Mobilization of bone marrow cells by CSF3 protects mice from bleomycin-induced lung injury. Respiration 82, 358-368. https://doi.org/10.1159/000328762

Zhang, X., Zhao, L., Tong, D., Wu, G., Dan, M., Teng, B., 2016a. A Systematic Review of Global Desert Dust and Associated Human Health Effects. Atmosphere-Basel 7, 158. https://doi.org/10.3390/atmos7120158

Zhao, F.Y., Cheng, T.Y., Yang, L., Huang, Y.H., Li, C., Han, J.Z., Li, X.H., Fang, L.J., Feng, D.D., Tang, Y.T., Yue, S.J., Tang, S.Y., Luo, Z.Q., Liu, W., 2020. G-CSF Inhibits Pulmonary Fibrosis by Promoting BMSC Homing to the Lungs via SDF-1/CXCR4 Chemotaxis. Sci Rep 10, 10515. https://doi.org/10.1038/s41598-020-65580-2

Zhou, Q., Ho, A.W., Schlitzer, A., Tang, Y., Wong, K.H., Wong, F.H., Chua, Y.L., Angeli, V., Mortellaro, A., Ginhoux, F., Kemeny, D.M., 2014. GM-CSF-licensed CD11b+ lung dendritic cells orchestrate Th2 immunity to Blomia tropicalis. J Immunol 193, 496-509. https://doi.org/10.4049/jimmunol.1303138

5.6 Supplemental material

Table S5.1. Primer pairs used for qPCR.

Gene		Sequence (5′ → 3′)	Amplicon length (bp)	Primer efficiency (%)
ACTB	fw	CCTGGCACCCAGCACAAT	70	81.2
	rv	GCCGATCCACACGGAGTACT		
GAPDH	fw	CCCCCACCACACTGAATCTC	65	90.3
	rv	GCCCCTCCCCTCTTCAAG		
GMCSF	fw	TGAACCTGAGTAGAGACACTGC	78	105.4
	rv	GCTCCTGGAGGTCAAACATTTC		
GCSF	fw	TGGCAGCAGATGGAAGAAC	207	81.5
	rv	AGAGATAAATACATGGGATGGGG		
SLC39A8	fw	GCCAGCTGCACTTCAACCA	117	95.2
	rv	GTAAGACTGCTGGACAGATGACAG		

Table S5.2. Fold-regulation of proteins measured in cytokine array (over 3 pages).

Protein	Fold-regulation	
	SD	LPS
IL-16	3.69	5.19
IL-1ra	3.17	3.37
MIP-1alpha/MIP-1beta	2.70	23.47
G-CSF	2.28	6.20
MIP-3beta	2.18	1.39
MCP-3	1.90	2.94
ICAM-1	1.88	2.15
IL-2	1.83	2.15
IL-5	1.81	2.49
Complement Component C5/C5a	1.78	4.02
IL-3	1.65	4.18
LIF	1.62	2.60
CD30	1.61	1.72
Myeloperoxidase	1.53	1.95
GM-CSF	1.52	2.86
TNF alpha	1.51	3.05
IP-10	1.47	10.12
BAFF	1.45	2.03
IL-15	1.42	2.11
I-TAC	1.42	1.21
RBP-4	1.42	1.20
IL-18BPa	1.36	1.87
VCAM-1	1.35	1.97
MIG	1.34	3.14
Adiponectin	1.33	1.50
Resistin	1.33	2.04
IL-6	1.31	3.76
HGF	1.30	1.28
PF4	1.30	1.73
IL-17A	1.27	1.72
IL-19	1.26	1.63
Cystatin C	1.23	1.25
TIM-3	1.22	2.29
EMMPRIN	1.21	1.56
Kallikrein 3	1.20	1.50
FGF-7	1.19	1.63
M-CSF	1.18	2.08
IL-1alpha	1.18	1.35
IL-22	1.17	1.63
Leptin	1.16	1.53

Protein	Fold-regulation	
	SD	LPS
uPAR	1.16	1.12
IL-34	1.15	4.84
RAGE	1.15	1.40
IL-4	1.14	1.71
Serpin E1	1.14	1.03
IFN-gamma	1.13	1.13
IL-1beta	1.12	2.39
MMP-9	1.12	0.94
MCP-1	1.12	1.35
Relaxin-2	1.11	1.61
IL-23	1.10	1.88
Osteopontin	1.10	1.29
Angiopoietin-1	1.09	1.27
FGF-19	1.09	1.22
DPPIV	1.09	2.29
TfR	1.08	1.70
IL-27	1.07	1.66
C-Reactive Protein	1.07	1.23
Pentraxin-3	1.06	1.52
IGFBP-2	1.05	0.94
TARC	1.04	1.25
BDNF	1.03	1.61
Angiopoietin-2	1.03	1.34
Dkk-1	1.00	1.08
CD14	1.00	1.31
Thrombospondin-1	0.99	1.25
GRO-alpha	0.99	1.15
IL-13	0.99	1.31
MIP-3alpha	0.99	8.02
ENA-78	0.99	1.19
RANTES	0.98	1.42
SDF-1alpha	0.98	1.33
VEGF	0.97	1.31
Apolipoprotein A-I	0.97	1.09
Lipocalin-2	0.97	1.12
CD40 ligand	0.95	1.62
Growth Hormone	0.94	0.89
IL-31	0.93	1.31
Complement Factor D	0.93	1.10
IL-10	0.92	1.13
IL-11	0.91	1.18
IL-8	0.91	1.06

Protein	Fold-regulation	
	SD	LPS
Vitamin D BP	0.91	1.24
PDGF-AB/BB	0.90	1.84
IL-32	0.90	1.85
EGF	0.90	1.89
IL-24	0.89	1.12
CD31	0.88	1.09
Chitinase 3-like 1	0.88	1.03
TGF-alpha	0.86	1.91
SHBG	0.85	1.30
Endoglin	0.80	0.97
MIF	0.77	1.28
Cripto-1	0.75	1.17
TFF3	0.74	1.23
Flt-3 Ligand	0.73	0.94
IL-12 p70	0.73	0.97
FGF basic	0.71	0.69
IL-33	0.71	1.78
Fas Ligand	0.69	0.88
IGFBP-3	0.68	1.04
Angiogenin	0.65	1.11
ST2	0.62	1.02
GDF-15	0.57	0.81
PDGF-AA	0.55	1.11

Fold upregulation is the relative luminescence of the protein in the SD or LPS exposed ALI co-cultures compared to the control; *N* = 1 experiment. Ctrl and SD: Two replicates; LPS: Four replicates. The supernatants from replicates were pooled before using them for protein array experiments.

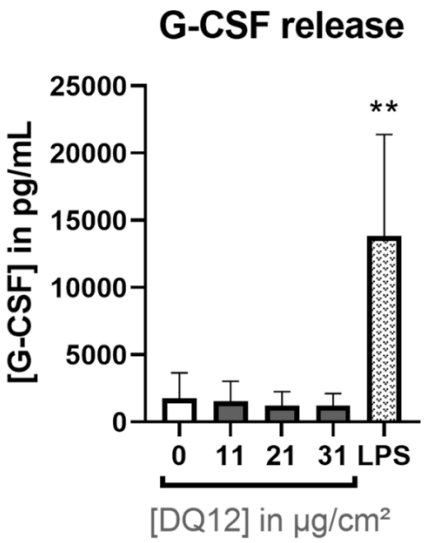

Figure S5.1. G-CSF release upon DQ12 exposure. Air-liquid interface co-cultures were exposed to DQ12 at doses in the range of 0-31 µg/cm² for 24 h or 250 ± 60 ng/cm² LPS for 21 h. The basolateral cytokine release of G-CSF was assessed by ELISA. Depicted are mean values with standard deviations. Mixed-effects models with Šidák's post hoc test were calculated based on absolute cytokine concentrations. *N* = 3-4 independent experiments were performed (Controls and LPS: one or two replicates; DQ12: duplicates per concentration; **p* ≤ 0.05; ***p* ≤ 0.01).

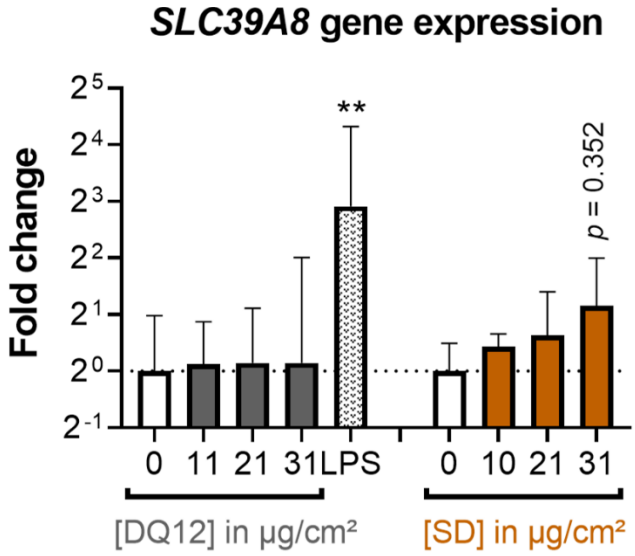

Figure S5.2. Gene expression of *SLC39A8*. Air-liquid interface co-cultures were exposed to DQ12 and Saharan dust (SD) at doses in the range of 0-31 µg/cm² for 24 h or 250 ± 60 ng/cm² LPS for 21 h. The relative gene expression *SLC39A8* was assessed by qRT-PCR. The results were normalized to control ALI cultures as well as to the reference genes *ACTB* and *GAPDH*. Shown are mean values with standard deviations. Fold changes were calculated with the means of $\Delta\Delta C_T$ values and standard deviations of ΔC_T values. Mixed-effects models with Šidák's post hoc test were calculated based on the ΔC_T values and absolute cytokine concentrations. *N* = 4 independent experiments were performed (Controls and LPS: one or two replicates; DQ12 and SD: duplicates per concentration; **p* ≤ 0.05; ***p* ≤ 0.01).

6 General discussion

6.1 Overview of study outcomes

According to the United Nations Convention to Combat Desertification (2023), “the cause-and-effect [relationship] between sand and dust in the atmosphere and health outcomes remains unclear and requires more extensive study.” The studies performed in the framework of this thesis are the first to explore the toxicity of Saharan dust (SD) samples, that are poor in urban contaminants and do not omit poorly soluble particles.

The objectives of these studies were to investigate the oxidative and inflammatory potency of SD and determine the role of its composition, with particular emphasis on microbial components. Another goal was to understand whether SD events enhance the hazardousness of local background air pollution. Furthermore, the studies aimed to determine the influence of the NLRP3 inflammasome-caspase (CASP)-1 pathway on inflammatory potency and to identify further potential mediators of toxicity using advanced pulmonary *in vitro* models.

In the first study (**Chapter 2**), the potency of SD to induce oxidative stress and inflammatory cytokines was shown using alveolar epithelial A549 cells and THP-1 macrophages. In disagreement with Ghio et al. (2014), the order of the effects indicated that oxidative stress was not the cause of inflammatory potency. The capacity to form hydroxyl radicals, as well as the contents of Fe, trace metals, sulfate, elemental carbon (EC), and diatomaceous earth were identified as properties of SD potentially contributing to toxicity. Former studies showed that the content of endotoxins contributes to desert dusts’ inflammatory potency (He et al., 2010; Rodríguez-Cotto et al., 2013). This study additionally revealed that this contribution was of a synergistic nature.

The assessment of a large panel of samples collected in Cape Verde during a reference period and two dust events (**Chapter 3**) supported the association of Fe in desert dust $PM_{2.5}$ with inflammatory potency. At the same time, despite the toxicity of other transition metals (Carter et al., 1997; Kennedy et al., 1998) and EC (Abe et al., 2000; Miyabara et al., 1998), these constituents were not related to the inflammatory potency of SD events. This could be due to the low contribution of PM from anthropogenic sources to dust events on Cape Verde (Gonçalves et al., 2014). Endotoxin content was associated with the intra but not inter-event variability of the inflammatory potency of PM_{10}. This demonstrated the importance of endotoxins and emphasized the need to identify further pro-inflammatory properties of desert dusts. Such properties could be

the mineralogical composition (Grytting et al., 2022; Rodriguez-Navarro et al., 2018) and the contents of microbial components other than endotoxins (Stern et al., 2021).

To assess the oxidative and inflammatory potency in a more realistic *in vitro* system, an air-liquid interface (ALI) co-culture model of A549 cells and THP-1 macrophages was established (**Chapter 4**). This model produced surfactant and included the crosstalk between epithelial and innate immune cells. In this ALI co-culture model Saharan but not quartz dust induced inflammatory cytokines. Because surfactant can decrease the toxicity of poorly soluble particles (Emerson and Davis, 1983; Pavan et al., 2014; Wallace et al., 1992), this finding again suggests an important role of the soluble contents of SD such as microbial endotoxins. Oxidative stress was not observed in the ALI co-culture model, indicating again the independence of SD's inflammatory from its oxidative potency.

Compared to the local background, dust events increased the inflammatory potency of $PM_{2.5}$ and PM_{10} in Cape Verde (**Chapter 3**). This stresses the hazardousness of desert dusts and warrants a revision of current health protection regulations. Current air pollution regulations exempt authorities from taking action on exceeded PM concentration if these are attributable to desert dusts (Environmental Protection Agency (EPA), 1971; European Commission, 2022; European Parliament and Council, 2008). As long as they are not complemented with risk mitigation strategies, such exemptions jeopardize the population's health.

The role of the NLRP3 inflammasome-CASP-1 axis was addressed using *NLRP3*$^{-/-}$ THP-1 macrophages in monocultures (**Chapter 2**) as well as *CASP1*$^{-/-}$ and *NLRP3*$^{-/-}$ THP-1 macrophages in ALI co-cultures (**Chapter 4**), in addition to the wild-type THP-1 macrophages. In both models, the NLRP3 inflammasome-CASP-1 axis was crucial for the release of IL-1β upon SD exposure, emphasizing the hazardousness of SD (Sayan and Mossman, 2016). *IL1B* gene expression in ALI co-cultures was upregulated independently of the genotype, indicating NLRP3 inflammasome priming through SD. Moreover, the releases of IL-6, IL-8, and TNFα from ALI co-cultures were boosted by the NLRP3 inflammasome-CASP-1 axis. At low levels, the releases of IL-6 and IL-8 were higher in ALI co-cultures with *NLRP3*$^{-/-}$ than *CASP1*$^{-/-}$ THP-1 macrophages. This suggests SD-mediated activation of CASP-1 through other inflammasomes (Burckstummer et al., 2009; Grenier et al., 2002; Martinon et al., 2002; Poyet et al., 2001) which can lead to the expression and release of NF-κB-dependent cytokines without the involvement of IL-1β (Erener et al., 2012).

Applying the ALI co-culture model in combination with RNA sequencing and protein array analysis (**Chapter 5**), SD-induced upregulation of granulocyte-macrophage colony-stimulating factor (GM-CSF) and granulocyte colony-stimulating factor (G-CSF) was identified. These upregulations

were confirmed via quantitative reverse transcriptase PCR and enzyme-linked immune-sorbent assay. Physiological concentrations of GM-CSF and G-CSF are crucial for the development of alveolar macrophages (Paine et al., 2001; Piccoli et al., 2015; Suzuki et al., 2008) and neutrophilic granulocytes (Lieschke et al., 1994), respectively, whereas elevated concentrations can promote inflammatory diseases such as allergic and chronic asthma (Kim et al., 2020; Nobs et al., 2021; Stampfli et al., 1998; Yamashita et al., 2002). Promising drugs targeting GM-CSF (Taylor et al., 2019; Temesgen et al., 2022) and G-CSF (Gamell et al., 2023) signaling are already being developed for other indications and might also remedy desert dust-mediated respiratory diseases.

6.2 Identifying dust events that pose health risks

In risk assessment, hazards need to be combined with predicted exposure concentrations and dust compositions to enable the management of foreseen health risks (Figure 6.1). This thesis contributes to the existing body of knowledge on the hazard side. Future studies should be based on this work to improve the understanding of hazardous constituents, molecular pathways, and the link between the two. On the exposure side, various forecasts of dust concentrations in different parts of the world have been developed (Querol et al., 2019). In a first effort to include the composition, the mineralogy has recently been added to a dust transport model (Gómez Maqueo Anaya et al., 2023). The ultimate goals of risk assessment must be to identify which desert dust events pose health risks and to mitigate the risks of such dust events.

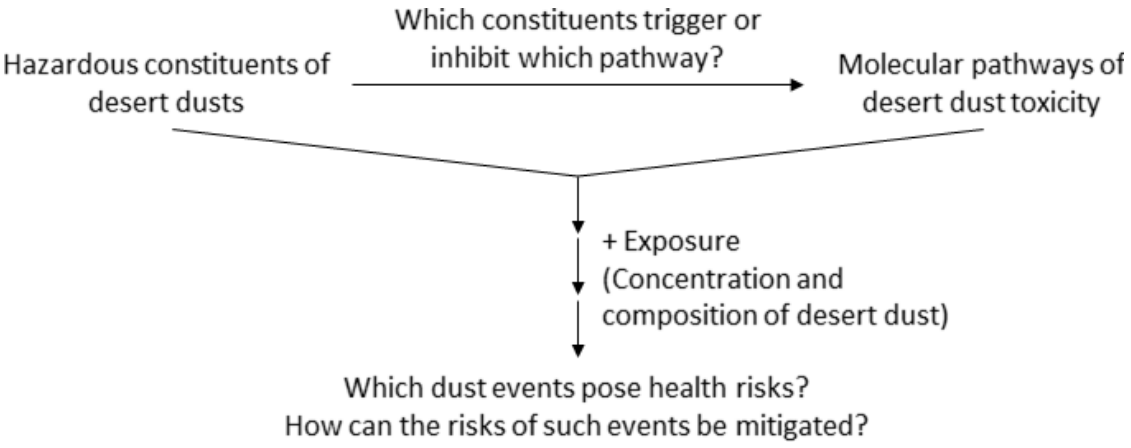

Figure 6.1. Risk assessment of desert dust events.

The question of which desert dust events pose health risks needs to be separated into sub-questions. 1) Is it necessary to distinguish dust events beyond concentration? Or in other words, can two events with the same aerosolized desert dust concentration pose different health risks?

2) At which locations do dust events pose health risks? 3) To whom do dust events pose health risks?

1) That it is necessary to distinguish dust events beyond concentration is strongly suggested by epidemiological and toxicological studies although this is not clearly reflected in the comparison between dust events presented in this thesis (Chapter 3). As reviewed by Zhang et al. (2016a), in epidemiological studies, mortalities during dust events per 10 µg/m³ differ substantially. These differences agree with toxicological studies that examined sediment desert dusts from different sources (Ghio et al., 2014; Ichinose et al., 2005; Ichinose et al., 2008; Taylor et al., 2013). In addition, He et al. (2013) and Honda et al. (2014) found distinct inflammatory potencies comparing two long-range transported Asian sand dust samples collected during two different dust events. PM_{10} but not $PM_{2.5}$ samples from the two events studied in the framework of this thesis tended to differ in inflammatory potency. Notably, variability was high amongst samples belonging to the same events which could not be connected to differences between sampling stations.

2) Nevertheless, co-exposures due to local sources of air pollution such as agriculture, the steel industry, and urban traffic may cause local differences in health risks during dust events. Agricultural activity is associated with elevated airborne endotoxin concentrations (Pavilonis et al., 2013; Roy and Thorne, 2003; Viet et al., 2001). Important sources include livestock (Thorne et al., 2009) and grain work (Schwartz et al., 1995). As reported in Chapter 2, endotoxins exacerbate the inflammatory potency of SD. Thus, co-exposure to desert dusts and agricultural pollutants could synergistically threaten pulmonary health.

Of particular relevance could also be pollutants from the steel industry that contain high shares of Fe (Ghio and Devlin, 2001; Zhang et al., 2022). Fe has been shown to contribute to the inflammatory potency of industrial PM (Smith et al., 2000). As described in Chapter 3 and in agreement with He et al. (2019), Fe is also associated with the inflammatory potency of desert dusts. Disrupted Fe homeostasis has been related to COPD and acute respiratory distress syndrome (Cloonan et al., 2017; Ghio et al., 2003). Hence, additive or synergistic effects of co-exposure to desert dusts and pollutants from the steel industry are probable.

Urban air pollution is well-known as a major cause of acute and chronic adverse health effects (Kampa and Castanas, 2008; Rajagopalan et al., 2018; Wu et al., 2012). Even though Val et al. (2013) stated that SD decreased the oxidative and inflammatory potency of urban PM on an effect-per-mass basis, the potency per inhaled volume of air can increase. Desert dusts do not replace but add to local air pollution. Hence, additive effects cannot be excluded in an urban scenario.

3) Furthermore, potentially susceptible groups, such as the elderly, individuals with pre-existing diseases, and those genetically predisposed, must be considered. Epidemiological studies have indicated that elderly people are more susceptible to the adverse health effects of desert dusts (Diaz et al., 2012; Jimenez et al., 2010; Vodonos et al., 2014; Zhang et al., 2016a).

Susceptible groups with pre-existing diseases may be identified based on the molecular mechanisms triggered by desert dust exposure. For example, SD's capacity to induce GM-CSF and G-CSF (Chapter 5) warrants consideration of the roles of these cytokines in individuals with inflammatory lung disease. Dysregulation of GM-CSF in the lung causes strong inflammatory effects: GM-CSF is required for the development of alveolar macrophages and, therefore, a lack of GM-CSF leads to pulmonary alveolar proteinosis (Huffman et al., 1996; Uchida et al., 2004). Conversely, increases in GM-CSF have been shown to provoke hyperactivity of alveolar macrophages (Suzuki et al., 2020) and hyperplasia of type 2 alveolar epithelial cells (Huffman Reed et al., 1997; Suzuki et al., 2020). Furthermore, pulmonary overexpression of GM-CSF caused the formation of granulomas consisting of macrophages and eosinophils (Xing et al., 1996) and neutralization of elevated GM-CSF concentrations has been shown to inhibit lung inflammation in mice exposed to cigarette smoke (Vlahos et al., 2010). Additionally, Aggarwal et al. (2000) found that GM-CSF and G-CSF were increased in patients suffering from acute respiratory distress syndrome in whom G-CSF levels were higher in non-survivors than survivors. G-CSF injections were shown to exacerbate ventilation-induced lung injury in mice (Karzai et al., 2005). Therefore, exacerbation of GM-CSF and G-CSF levels through desert dust exposure might severely aggravate inflammatory lung diseases.

Understanding molecular pathways can also facilitate identifying genetic predispositions of risks. For instance, various polymorphisms of the *IL1B* gene have been associated with COPD risk (Xie et al., 2014). Therefore, dust events transporting endotoxins which lead to IL-1β release via NLRP3 inflammasome-CASP-1 signaling (Chapter 2 and Bauernfeind et al. (2009)) may be of higher risk to individuals carrying those polymorphisms. Similarly, dust events transporting Fe, which was also associated with IL-1β levels (Chapter 3), may affect the same genetically pre-disposed individuals. However, translating such genetic predispositions into risk mitigation strategies is challenging because people are usually not aware of their polymorphisms.

Moreover, whether Fe in desert dusts stimulates IL-1β release via NLRP3 inflammasome-CASP-1 signaling remains uncertain and should be addressed in further studies. Nakamura et al. (2016) showed Fe^{3+} to enhance IL-1β release from THP-1 monocytes in dependence of the NLRP3 inflammasome. Liu et al. (2018) reported iron oxide nanoparticles to cause NLRP3 and CASP-1-dependent IL-1β release from murine bone marrow-derived macrophages. Speciation and

morphological characterization of Fe in desert dusts would help to understand whether it has the capacity to act through NLRP3 and CASP-1: Fe in minerals such as hematite and goethite is poorly soluble (Schwertmann, 1991). Moreover, the shape of iron oxide nanoparticles has been described to influence their NLRP3 inflammasome activating properties (Liu et al., 2018).

In summary, risk assessment based on dust concentrations, compositions, and hazards is necessary on a dust-event basis and needs to be resolved locally and by susceptible groups. Clarifying which desert dust constituents elicit which molecular pathways will enable understanding which desert dust events affect which group of people.

6.3 Mitigating the health risks of desert dust events

The question of how to mitigate the risks of identified dangerous desert dust events needs to be broken down into the following potential measures: 1) advising people to avoid exposure, 2) reducing controllable pollution, and 3) applying drugs.

1) Refraining from physical activity and staying indoors is a very effective way of preventing exposure to desert dusts. Physical activity strongly enhances the ventilation rate while the fraction of deposited PM remains constant (Bennett et al., 1985). Therefore, it can be expected to enhance the effective dose and health risks of desert dust exposure. To facilitate that people stay indoors, measures as drastic as the temporary closure of schools are taken in weeks with severe urban air pollution in New Delhi (Mollan, 2023). For desert dust events, similarly drastic measures do not necessarily need to be considered for the general population but could be effective in protecting susceptible groups. Krasnov et al. (2015) reported lower increases in indoor than outdoor PM_{10} concentrations during dust storms. Similarly, Soleimani et al. (2016) described a greater rise in microbe concentrations in outdoor settings as opposed to inside hospitals. In a more proactive approach, Achilleos et al. (2023) have shown that indoor concentrations of $PM_{2.5}$ and PM_{10} during dust events can effectively be reduced through decreased ventilation and the use of air purifiers. Such measures are urgently required considering that SD concentration has been identified as a strong predictor of in-hospital mortality of patients with heart failure (Dominguez-Rodriguez et al., 2020a). Comparing indoor and outdoor samples by screening on THP-1 macrophages, as described in Chapter 3, the effectiveness of these measures could be confirmed.

2) Reducing pollution is particularly relevant to agricultural, industrial, and urban settings in which co-exposure to desert dusts and local pollutants occurs. As suggested by Querol et al. (2019), enhanced risks due to co-exposures may be limited by abating local sources during desert dust events. Specifically, this could mean restricting agricultural and industrial activities as well as

urban traffic. However, such restrictions usually come with a cost, and eventually, political decision-makers need to find a balance between the sanitary and socioeconomic burden (Lave, 1981).

3) Desert dust exposure is frequently inevitable so that affected people could benefit from suitable drugs that are, however, still lacking. Potential drugs could be inspired by molecular mediators, e.g., IL-1β, IL-6, GM-CSF, and G-CSF, as well as hazardous desert dust constituents. To target IL-1β signaling, the recombinant IL-1 receptor antagonist anakinra has been developed. According to a case report, anakinra treatment ameliorated silicosis in a marble cave worker (Cavalli et al., 2015). Anakinra has also been shown to antagonize bleomycin-induced collagen accumulation in a mouse model of lung fibrosis (Burgy et al., 2016). Considering the involvement of the NLRP3 inflammasome in SD-mediate cytokine release and silicosis in camels from deserts (Goodarzi et al., 2014; Hansen et al., 1989), lung fibrosis may also be relevant for desert dust exposure. In COVID-19 patients with acute respiratory distress syndrome (Cavalli et al., 2020) and severe respiratory failure (Kyriazopoulou et al., 2021), complementation of medical treatment with anakinra led to clinical improvement. Therefore, anakinra might also be able to rescue acute respiratory mortality associated with desert dust events (Mallone et al., 2011). Similarly, the IL-6 receptor antagonist tocilizumab improved survival and reduced mechanical ventilation requirements in COVID-19 patients (Klopfenstein et al., 2021). However, it must be noted that the aforementioned drugs are used in COVID-19 patients to target the so-called cytokine storm, an extent of cytokine release that has not been described for desert dust exposure. Drugs that interrupt GM-CSF and G-CSF signaling could alleviate allergies and asthma. Such drugs are currently being developed for other indications (Gamell et al., 2023; Taylor et al., 2019; Temesgen et al., 2022). Another approach could be to target hazardous dust constituents such as Fe. The application of Fe chelators has been proven effective against lung damage through Fe overload in mouse models (Cloonan et al., 2017; Yatmark et al., 2015).

6.4 Conclusions

Altogether, the comparison of SD with quartz dusts stresses the substantial health hazards associated with desert dust exposure. This was seen in the SD-mediated oxidative stress (Chapter 2) and inflammatory cytokine secretion (Chapters 2-5). Among SD's various components, Fe and endotoxins stood out in their association with inflammatory potency (Chapter 3). Desert dust events were found to enhance the hazardousness of local background air pollution (Chapter 3). Furthermore, the NLRP3 inflammasome-CASP-1 pathway (Chapters 2 and 4) and the cytokines GM-CSF and G-CSF (Chapter 5), which are associated with lung diseases, were

induced upon SD exposure. In adherence with the 3 Rs (Russell and Burch, 1959), these outcomes were obtained using *in vitro* models of increasing complexity.

To enable the identification of hazardous dust events, future studies need to continue deciphering the role of specific components. Fe in desert dusts can be found in different amorphous and mineral states (Rodriguez-Navarro et al., 2018) and endotoxins are just one example of potentially toxic microbial components (Ichinose et al., 2005; Stern et al., 2021). Additionally, the mineralogical composition probably affects toxicity (Grytting et al., 2022). For this purpose, the screening approach on THP-1 macrophages presented here could be extended. This practical tool can be employed on a broader range of well-characterized desert dust samples from various events and sources.

In order to identify susceptible groups and suggest drug targets, the understanding of molecular pathways must advance. The NLRP3 inflammasome-CASP-1 pathway, IL-1β, IL-6, IL-8, TNFα, GM-CSF, and G-CSF are all crucial in inflammatory signaling. At the same time, they are parts of larger cascades and are intertwined with each other. The advanced ALI co-culture model applied in these investigations can serve as a valuable tool to unravel up- and downstream signaling as well as connections between the cytokines. Moreover, to link molecular events with pathologies, the abovementioned cytokines should be used as biomarkers in sputum or blood, and mapped against diseases occurring during desert dust events.

The *in vitro* models used in the framework of this thesis are well-suitable for future screenings and mechanistic research. Nevertheless, more realistic models such as organoids with an apical site exposable at the ALI should be developed. Such models should incorporate further cell types and allow longer exposure times. An approach to pursue could be the progression of apical-out organoids (Salahudeen et al., 2020). This will limit the need to employ animal studies while advancing research on the pulmonary toxicity of desert dusts.

Overall, these findings can serve as a strong foundation for future research on desert dusts that can ultimately be translated into effective air pollution regulations and risk mitigation strategies. In this way, toxicological research on desert dusts and the protection of human health move another step closer together.

6.5 References

Abe, S., Takizawa, H., Sugawara, I., Kudoh, S., 2000. Diesel exhaust (DE)-induced cytokine expression in human bronchial epithelial cells: a study with a new cell exposure system to freshly generated DE in vitro. Am J Respir Cell Mol Biol 22, 296-303. https://doi.org/10.1165/ajrcmb.22.3.3711

Achilleos, S., Michanikou, A., Kouis, P., Papatheodorou, S.I., Panayiotou, A.G., Kinni, P., Mihalopoulos, N., Kalivitis, N., Kouvarakis, G., Galanakis, E., Michailidi, E., Tymvios, F., Chrysanthou, A., Neophytou, M., Mouzourides, P., Savvides, C., Vasiliadou, E., Papasavvas, I., Christophides, T., Nicolaou, R., Avraamides, P., Kang, C.M., Middleton, N., Koutrakis, P., Yiallouros, P.K., 2023. Improved indoor air quality during desert dust storms: The impact of the MEDEA exposure-reduction strategies. Sci Total Environ 863, 160973. https://doi.org/10.1016/j.scitotenv.2022.160973

Aggarwal, A., Baker, C.S., Evans, T.W., Haslam, P.L., 2000. G-CSF and IL-8 but not GM-CSF correlate with severity of pulmonary neutrophilia in acute respiratory distress syndrome. Eur Respir J 15, 895-901. https://doi.org/10.1034/j.1399-3003.2000.15e14.x

Bauernfeind, F.G., Horvath, G., Stutz, A., Alnemri, E.S., MacDonald, K., Speert, D., Fernandes-Alnemri, T., Wu, J., Monks, B.G., Fitzgerald, K.A., Hornung, V., Latz, E., 2009. Cutting edge: NF-kappaB activating pattern recognition and cytokine receptors license NLRP3 inflammasome activation by regulating NLRP3 expression. J Immunol 183, 787-791. https://doi.org/10.4049/jimmunol.0901363

Bennett, W.D., Messina, M.S., Smaldone, G.C., 1985. Effect of exercise on deposition and subsequent retention of inhaled particles. J Appl Physiol (1985) 59, 1046-1054. https://doi.org/10.1152/jappl.1985.59.4.1046

Burckstummer, T., Baumann, C., Bluml, S., Dixit, E., Durnberger, G., Jahn, H., Planyavsky, M., Bilban, M., Colinge, J., Bennett, K.L., Superti-Furga, G., 2009. An orthogonal proteomic-genomic screen identifies AIM2 as a cytoplasmic DNA sensor for the inflammasome. Nat Immunol 10, 266-272. https://doi.org/10.1038/ni.1702

Burgy, O., Bellaye, P.S., Causse, S., Beltramo, G., Wettstein, G., Boutanquoi, P.M., Goirand, F., Garrido, C., Bonniaud, P., 2016. Pleural inhibition of the caspase-1/IL-1beta pathway diminishes profibrotic lung toxicity of bleomycin. Respir Res 17, 162. https://doi.org/10.1186/s12931-016-0475-8

Carter, J.D., Ghio, A.J., Samet, J.M., Devlin, R.B., 1997. Cytokine Production by Human Airway Epithelial Cells after Exposure to an Air Pollution Particle Is Metal-Dependent. Toxicol Appl Pharmacol 146, 180-188. https://doi.org/10.1006/taap.1997.8254

Cavalli, G., De Luca, G., Campochiaro, C., Della-Torre, E., Ripa, M., Canetti, D., Oltolini, C., Castiglioni, B., Tassan Din, C., Boffini, N., Tomelleri, A., Farina, N., Ruggeri, A., Rovere-Querini, P., Di Lucca, G., Martinenghi, S., Scotti, R., Tresoldi, M., Ciceri, F., Landoni, G., Zangrillo, A., Scarpellini, P., Dagna, L., 2020. Interleukin-1 blockade with high-dose anakinra in patients with COVID-19, acute respiratory distress syndrome, and hyperinflammation: a retrospective cohort study. Lancet Rheumatol 2, e325-e331. https://doi.org/10.1016/S2665-9913(20)30127-2

Cavalli, G., Fallanca, F., Dinarello, C.A., Dagna, L., 2015. Treating pulmonary silicosis by blocking interleukin 1. Am J Respir Crit Care Med 191, 596-598. https://doi.org/10.1164/rccm.201412-2150LE

Cloonan, S.M., Mumby, S., Adcock, I.M., Choi, A.M.K., Chung, K.F., Quinlan, G.J., 2017. The "Iron"-y of Iron Overload and Iron Deficiency in Chronic Obstructive Pulmonary Disease. Am J Respir Crit Care Med 196, 1103-1112. https://doi.org/10.1164/rccm.201702-0311PP

Diaz, J., Tobias, A., Linares, C., 2012. Saharan dust and association between particulate matter and case-specific mortality: a case-crossover analysis in Madrid (Spain). Environ Health 11, 11. https://doi.org/10.1186/1476-069X-11-11

Dominguez-Rodriguez, A., Baez-Ferrer, N., Rodriguez, S., Avanzas, P., Abreu-Gonzalez, P., Terradellas, E., Cuevas, E., Basart, S., Werner, E., 2020a. Saharan Dust Events in the Dust Belt -Canary Islands- and the Observed Association with in-Hospital Mortality of Patients with Heart Failure. J Clin Med 9, https://doi.org/10.3390/jcm9020376

Emerson, R.J., Davis, G.S., 1983. Effect of alveolar lining material-coated silica on rat alveolar macrophages. Environ Health Perspect 51, 81-84. https://doi.org/10.1289/ehp.835181

Environmental Protection Agency (EPA), 1971. Code of Federal Regulations Title 40 Part 50 National primary and secondary ambient air quality standards. https://www.ecfr.gov/current/title-40/chapter-I/subchapter-C/part-50. Accessed: 03/10/2023

Erener, S., Petrilli, V., Kassner, I., Minotti, R., Castillo, R., Santoro, R., Hassa, P.O., Tschopp, J., Hottiger, M.O., 2012. Inflammasome-activated caspase 7 cleaves PARP1 to enhance the expression of a subset of NF-kappaB target genes. Mol Cell 46, 200-211. https://doi.org/10.1016/j.molcel.2012.02.016

European Commission, 2022. Proposal for a directive of the European Parliament and of the council on ambient air quality and cleaner air for Europe (recast). https://eur-lex.europa.eu/legal-content/EN/TXT/?uri=CELEX%3A52022PC0542&qid=1696327827017. Accessed: 03/10/2023

European Parliament and Council, 2008. Directive 2008/50/EC of the European Parliament and of the Council of 21 May 2008 on ambient air quality and cleaner air for Europe. Official Journal of the European Union. https://eur-lex.europa.eu/legal-content/EN/TXT/?uri=celex%3A32008L0050. Accessed: 03/10/2023

Gamell, C., Bankovacki, A., Scalzo-Inguanti, K., Sedgmen, B., Alhamdoosh, M., Gail, E., Turkovic, L., Millar, C., Johnson, L., Wahlsten, M., Richter, J., Schuster, J., Dyson, A., Nicolopoulos, J., Varigos, G., Ng, M., Wilson, N., Field, J., Kern, J.S., Lindqvist, L.M., 2023. CSL324, a granulocyte colony-stimulating factor receptor antagonist, blocks neutrophil migration markers that are upregulated in hidradenitis suppurativa. Br J Dermatol 188, 636-648. https://doi.org/10.1093/bjd/ljad013

Ghio, A.J., Carter, J.D., Richards, J.H., Richer, L.D., Grissom, C.K., Elstad, M.R., 2003. Iron and iron-related proteins in the lower respiratory tract of patients with acute respiratory distress syndrome. Crit Care Med 31, 395-400. https://doi.org/10.1097/01.CCM.0000050284.35609.97

Ghio, A.J., Devlin, R.B., 2001. Inflammatory lung injury after bronchial instillation of air pollution particles. Am J Respir Crit Care Med 164, 704-708. https://doi.org/10.1164/ajrccm.164.4.2011089

Ghio, A.J., Kummarapurugu, S.T., Tong, H., Soukup, J.M., Dailey, L.A., Boykin, E., Gilmour, I.M., Ingram, P., Roggli, V.L., Goldstein, H.L., Reynolds, R.L., 2014. Biological effects of desert dust in respiratory epithelial cells and a murine model. Inhal Toxicol 26, 299-309. https://doi.org/10.3109/08958378.2014.888109

Gómez Maqueo Anaya, S., Althausen, D., Faust, M., Baars, H., Heinold, B., Hofer, J., Tegen, I., Ansmann, A., Engelmann, R., Skupin, A., Heese, B., Schepanski, K., 2023. The implementation of dust mineralogy in COSMO5.05-MUSCAT. EGUsphere preprint repository, https://doi.org/10.5194/egusphere-2023-1558

Gonçalves, C., Alves, C., Nunes, T., Rocha, S., Cardoso, J., Cerqueira, M., Pio, C., Almeida, S.M., Hillamo, R., Teinilä, K., 2014. Organic characterisation of PM10 in Cape Verde under Saharan dust influxes. Atmos Envir 89, 425-432. https://doi.org/10.1016/j.atmosenv.2014.02.025

Goodarzi, M., Azizi, S., Koupaei, M.J., Moshkelani, S., 2014. Pathologic Findings of Anthraco-silicosis in the Lungs of One Humped Camels (Camelus dromedarius) and Its Role in the Occurrence of Pneumonia. Kafkas Univ Vet Fak, https://doi.org/10.9775/kvfd.2013.9564

Grenier, J.M., Wang, L., Manji, G.A., Huang, W.J., Al-Garawi, A., Kelly, R., Carlson, A., Merriam, S., Lora, J.M., Briskin, M., DiStefano, P.S., Bertin, J., 2002. Functional screening of five PYPAF family members identifies PYPAF5 as a novel regulator of NF-kappaB and caspase-1. FEBS Lett 530, 73-78. https://doi.org/10.1016/s0014-5793(02)03416-6

Grytting, V.S., Refsnes, M., Lag, M., Erichsen, E., Rohr, T.S., Snilsberg, B., White, R.A., Ovrevik, J., 2022. The importance of mineralogical composition for the cytotoxic and pro-inflammatory effects of mineral dust. Part Fibre Toxicol 19, 46. https://doi.org/10.1186/s12989-022-00486-7

Hansen, H.J., Jama, F.M., Nilsson, C., Norrgren, L., Abdurahman, O.S., 1989. Silicate pneumoconiosis in camels (Camelus dromedarius L.). J Vet Med A 36, 789-796. https://doi.org/10.1111/j.1439-0442.1989.tb00793.x

He, M., Ichinose, T., Song, Y., Yoshida, Y., Arashidani, K., Yoshida, S., Liu, B., Nishikawa, M., Takano, H., Sun, G., 2013. Effects of two Asian sand dusts transported from the dust source regions of Inner Mongolia and northeast China on murine lung eosinophilia. Toxicol Appl Pharmacol 272, 647-655. https://doi.org/10.1016/j.taap.2013.07.010

He, M., Ichinose, T., Yoshida, S., Nishikawa, M., Mori, I., Yanagisawa, R., Takano, H., Inoue, K., Sun, G., Shibamoto, T., 2010. Airborne Asian sand dust enhances murine lung eosinophilia. Inhal Toxicol 22, 1012-1025. https://doi.org/10.3109/08958378.2010.510151

He, M., Ichinose, T., Yoshida, S., Nishikawa, M., Sun, G., Shibamoto, T., 2019. Role of iron and oxidative stress in the exacerbation of allergic inflammation in murine lungs caused by urban particulate matter <2.5 µm and desert dust. J Appl Toxicol 39, 855-867. https://doi.org/10.1002/jat.3773

Honda, A., Matsuda, Y., Murayama, R., Tsuji, K., Nishikawa, M., Koike, E., Yoshida, S., Ichinose, T., Takano, H., 2014. Effects of Asian sand dust particles on the respiratory and immune system. J Appl Toxicol 34, 250-257. https://doi.org/10.1002/jat.2871

Huffman, J.A., Hull, W.M., Dranoff, G., Mulligan, R.C., Whitsett, J.A., 1996. Pulmonary epithelial cell expression of GM-CSF corrects the alveolar proteinosis in GM-CSF-deficient mice. J Clin Invest 97, 649-655. https://doi.org/10.1172/JCI118461

Huffman Reed, J.A., Rice, W.R., Zsengeller, Z.K., Wert, S.E., Dranoff, G., Whitsett, J.A., 1997. GM-CSF enhances lung growth and causes alveolar type II epithelial cell hyperplasia in transgenic mice. Am J Physiol 273, L715-725. https://doi.org/10.1152/ajplung.1997.273.4.L715

Ichinose, T., Nishikawa, M., Takano, H., Sera, N., Sadakane, K., Mori, I., Yanagisawa, R., Oda, T., Tamura, H., Hiyoshi, K., Quan, H., Tomura, S., Shibamoto, T., 2005. Pulmonary toxicity induced by intratracheal instillation of Asian yellow dust (Kosa) in mice. Environ Toxicol Pharmacol 20, 48-56. https://doi.org/10.1016/j.etap.2004.10.009

Ichinose, T., Yoshida, S., Sadakane, K., Takano, H., Yanagisawa, R., Inoue, K., Nishikawa, M., Mori, I., Kawazato, H., Yasuda, A., Shibamoto, T., 2008. Effects of asian sand dust, Arizona sand dust, amorphous silica and aluminum oxide on allergic inflammation in the murine lung. Inhal Toxicol 20, 685-694. https://doi.org/10.1080/08958370801935133

Jimenez, E., Linares, C., Martinez, D., Diaz, J., 2010. Role of Saharan dust in the relationship between particulate matter and short-term daily mortality among the elderly in Madrid (Spain). Sci Total Environ 408, 5729-5736. https://doi.org/10.1016/j.scitotenv.2010.08.049

Kampa, M., Castanas, E., 2008. Human health effects of air pollution. Environ Pollut 151, 362-367. https://doi.org/10.1016/j.envpol.2007.06.012

Karzai, W., Cui, X., Heinicke, N., Niemann, C., Gerstenberger, E.P., Correa, R., Banks, S., Mehlhorn, B., Bloos, F., Reinhart, K., Eichacker, P.Q., 2005. Neutrophil stimulation with granulocyte colony-stimulating factor worsens ventilator-induced lung injury and mortality in rats. Anesthesiology 103, 996-1005. https://doi.org/10.1097/00000542-200511000-00014

Kennedy, T., Ghio, A.J., Reed, W., Samet, J., Zagorski, J., Quay, J., Carter, J., Dailey, L., Hoidal, J.R., Devlin, R.B., 1998. Copper-dependent Inflammation and Nuclear Factor- κ B Activation by Particulate Air Pollution. Am J Resp Cell Mol 19, 366-378. https://doi.org/10.1165/ajrcmb.19.3.3042

Kim, Y.M., Kim, H., Lee, S., Kim, S., Lee, J.U., Choi, Y., Park, H.W., You, G., Kang, H., Lee, S., Park, J.S., Park, Y., Park, H.S., Park, C.S., Lee, S.W., 2020. Airway G-CSF identifies neutrophilic inflammation and contributes to asthma progression. Eur Respir J 55, https://doi.org/10.1183/13993003.00827-2019

Klopfenstein, T., Gendrin, V., Gerazime, A., Conrozier, T., Balblanc, J.C., Royer, P.Y., Lohse, A., Mezher, C., Toko, L., Guillochon, C., Badie, J., Pierron, A., Kadiane-Oussou, N.J., Puyraveau, M., Zayet, S., team, H.N.F.H.t.m., 2021. Systematic Review and Subgroup Meta-analysis of Randomized Trials to Determine Tocilizumab's Place in COVID-19 Pneumonia. Infect Dis Ther 10, 1195-1213. https://doi.org/10.1007/s40121-021-00488-6

Krasnov, H., Katra, I., Friger, M., 2015. Insights into Indoor/Outdoor PM Concentration Ratios due to Dust Storms in an Arid Region. Atmosphere-Basel 6, 879-890. https://doi.org/10.3390/atmos6070879

Kyriazopoulou, E., Poulakou, G., Milionis, H., Metallidis, S., Adamis, G., Tsiakos, K., Fragkou, A., Rapti, A., Damoulari, C., Fantoni, M., Kalomenidis, I., Chrysos, G., Angheben, A., Kainis, I., Alexiou, Z., Castelli, F., Serino, F.S., Tsilika, M., Bakakos, P., Nicastri, E., Tzavara, V., Kostis, E., Dagna, L., Koufargyris, P., Dimakou, K., Savvanis, S., Tzatzagou, G., Chini, M., Cavalli, G., Bassetti, M., Katrini, K., Kotsis, V., Tsoukalas, G., Selmi, C., Bliziotis, I., Samarkos, M., Doumas, M., Ktena, S., Masgala, A., Papanikolaou, I., Kosmidou, M., Myrodia, D.M., Argyraki, A., Cardellino, C.S., Koliakou, K., Katsigianni, E.I., Rapti, V., Giannitsioti, E., Cingolani, A., Micha, S., Akinosoglou, K., Liatsis-Douvitsas, O., Symbardi, S., Gatselis, N., Mouktaroudi, M., Ippolito, G., Florou, E., Kotsaki, A., Netea, M.G., Eugen-Olsen, J., Kyprianou, M., Panagopoulos, P., Dalekos, G.N., Giamarellos-Bourboulis, E.J., 2021. Early treatment of COVID-19 with anakinra guided by soluble urokinase plasminogen receptor plasma levels: a double-blind, randomized controlled phase 3 trial. Nat Med 27, 1752-1760. https://doi.org/10.1038/s41591-021-01499-z

Lave, L.B., 1981. Balancing economics and health in setting environmental standards. Annu Rev Public Health 2, 183-200. https://doi.org/10.1146/annurev.pu.02.050181.001151

Lieschke, G.J., Grail, D., Hodgson, G., Metcalf, D., Stanley, E., Cheers, C., Fowler, K.J., Basu, S., Zhan, Y.F., Dunn, A.R., 1994. Mice lacking granulocyte colony-stimulating factor have chronic neutropenia, granulocyte and macrophage progenitor cell deficiency, and impaired neutrophil mobilization. Blood 84, 1737-1746. https://doi.org/10.1182/blood.V84.6.1737.1737

Liu, L., Sha, R., Yang, L., Zhao, X., Zhu, Y., Gao, J., Zhang, Y., Wen, L.-P., 2018. Impact of Morphology on Iron Oxide Nanoparticles-Induced Inflammasome Activation in Macrophages. ACS Appl Mater Inter 10, 41197-41206. https://doi.org/10.1021/acsami.8b17474

Mallone, S., Stafoggia, M., Faustini, A., Gobbi, G.P., Marconi, A., Forastiere, F., 2011. Saharan dust and associations between particulate matter and daily mortality in Rome, Italy. Environ Health Perspect 119, 1409-1414. https://doi.org/10.1289/ehp.1003026

Martinon, F., Burns, K., Tschopp, J., 2002. The inflammasome: a molecular platform triggering activation of inflammatory caspases and processing of proIL-beta. Mol Cell 10, 417-426. https://doi.org/10.1016/s1097-2765(02)00599-3

Miyabara, Y., Yanagisawa, R., Shimojo, N., Takano, H., Lim, H.B., Ichinose, T., Sagai, M., 1998. Murine strain differences in airway inflammation caused by diesel exhaust particles. Eur Respir J 11, 291-298. https://doi.org/10.1183/09031936.98.11020291

Mollan, C., 2023. Delhi pollution: No school, no play for city's children. BBC News. https://www.bbc.com/news/world-asia-india-67330016. Accessed: 23/11/2023

Nakamura, K., Kawakami, T., Yamamoto, N., Tomizawa, M., Fujiwara, T., Ishii, T., Harigae, H., Ogasawara, K., 2016. Activation of the NLRP3 inflammasome by cellular labile iron. Exp Hematol 44, 116-124. https://doi.org/10.1016/j.exphem.2015.11.002

Nobs, S.P., Pohlmeier, L., Li, F., Kayhan, M., Becher, B., Kopf, M., 2021. GM-CSF instigates a dendritic cell-T-cell inflammatory circuit that drives chronic asthma development. J Allergy Clin Immunol 147, 2118-2133 e2113. https://doi.org/10.1016/j.jaci.2020.12.638

Paine, R., 3rd, Morris, S.B., Jin, H., Wilcoxen, S.E., Phare, S.M., Moore, B.B., Coffey, M.J., Toews, G.B., 2001. Impaired functional activity of alveolar macrophages from GM-CSF-deficient mice. Am J Physiol Lung Cell Mol Physiol 281, L1210-1218. https://doi.org/10.1152/ajplung.2001.281.5.L1210

Pavan, C., Rabolli, V., Tomatis, M., Fubini, B., Lison, D., 2014. Why does the hemolytic activity of silica predict its pro-inflammatory activity? Part Fibre Toxicol 11, 76. https://doi.org/10.1186/s12989-014-0076-y

Pavilonis, B.T., Anthony, T.R., O'Shaughnessy, P.T., Humann, M.J., Merchant, J.A., Moore, G., Thorne, P.S., Weisel, C.P., Sanderson, W.T., 2013. Indoor and outdoor particulate matter and endotoxin

concentrations in an intensely agricultural county. J Expo Sci Environ Epidemiol 23, 299-305. https://doi.org/10.1038/jes.2012.123

Piccoli, L., Campo, I., Fregni, C.S., Rodriguez, B.M., Minola, A., Sallusto, F., Luisetti, M., Corti, D., Lanzavecchia, A., 2015. Neutralization and clearance of GM-CSF by autoantibodies in pulmonary alveolar proteinosis. Nat Commun 6, 7375. https://doi.org/10.1038/ncomms8375

Poyet, J.L., Srinivasula, S.M., Tnani, M., Razmara, M., Fernandes-Alnemri, T., Alnemri, E.S., 2001. Identification of Ipaf, a human caspase-1-activating protein related to Apaf-1. J Biol Chem 276, 28309-28313. https://doi.org/10.1074/jbc.C100250200

Querol, X., Tobias, A., Perez, N., Karanasiou, A., Amato, F., Stafoggia, M., Perez Garcia-Pando, C., Ginoux, P., Forastiere, F., Gumy, S., Mudu, P., Alastuey, A., 2019. Monitoring the impact of desert dust outbreaks for air quality for health studies. Environ Int 130, 104867. https://doi.org/10.1016/j.envint.2019.05.061

Rajagopalan, S., Al-Kindi, S.G., Brook, R.D., 2018. Air Pollution and Cardiovascular Disease: JACC State-of-the-Art Review. J Am Coll Cardiol 72, 2054-2070. https://doi.org/10.1016/j.jacc.2018.07.099

Rodríguez-Cotto, R.I., Ortiz-Martínez, M.G., Rivera-Ramírez, E., Méndez, L.B., Dávila, J.C., Jiménez-Vélez, B.D., 2013. African Dust Storms Reaching Puerto Rican Coast Stimulate the Secretion of IL-6 and IL-8 and Cause Cytotoxicity to Human Bronchial Epithelial Cells (BEAS-2B). Health 5, 14-28. https://doi.org/10.4236/health.2013.510A2003

Rodriguez-Navarro, C., di Lorenzo, F., Elert, K., 2018. Mineralogy and physicochemical features of Saharan dust wet deposited in the Iberian Peninsula during an extreme red rain event. Atmos Chem Phys 18, 10089-10122. https://doi.org/10.5194/acp-18-10089-2018

Roy, C.J., Thorne, P.S., 2003. Exposure to Particulates, Microorganisms, β(1–3)-Glucans, and Endotoxins During Soybean Harvesting. AIHA J 64, 487-495. https://doi.org/10.1080/15428110308984844

Russell, W.M.S., Burch, R.L. The Principles of Humane Experimental Technique. Methuen; 1959

Salahudeen, A.A., Choi, S.S., Rustagi, A., Zhu, J., van Unen, V., de la, O.S., Flynn, R.A., Margalef-Catala, M., Santos, A.J.M., Ju, J., Batish, A., Usui, T., Zheng, G.X.Y., Edwards, C.E., Wagar, L.E., Luca, V., Anchang, B., Nagendran, M., Nguyen, K., Hart, D.J., Terry, J.M., Belgrader, P., Ziraldo, S.B., Mikkelsen, T.S., Harbury, P.B., Glenn, J.S., Garcia, K.C., Davis, M.M., Baric, R.S., Sabatti, C., Amieva, M.R., Blish, C.A., Desai, T.J., Kuo, C.J., 2020. Progenitor identification and SARS-CoV-2 infection in human distal lung organoids. Nature 588, 670-675. https://doi.org/10.1038/s41586-020-3014-1

Sayan, M., Mossman, B.T., 2016. The NLRP3 inflammasome in pathogenic particle and fibre-associated lung inflammation and diseases. Part Fibre Toxicol 13, 51. https://doi.org/10.1186/s12989-016-0162-4

Schwartz, D.A., Thorne, P.S., Yagla, S.J., Burmeister, L.F., Olenchock, S.A., Watt, J.L., Quinn, T.J., 1995. The role of endotoxin in grain dust-induced lung disease. Am J Respir Crit Care Med 152, 603-608. https://doi.org/10.1164/ajrccm.152.2.7633714

Schwertmann, U., 1991. Solubility and dissolution of iron oxides. Plant Soil 130, 1-25.

Smith, K.R., Veranth, J.M., Hu, A.A., Lighty, J.S., Aust, A.E., 2000. Interleukin-8 levels in human lung epithelial cells are increased in response to coal fly ash and vary with the bioavailability of iron, as a function of particle size and source of coal. Chem Res Toxicol 13, 118-125. https://doi.org/10.1021/tx9901736

Soleimani, Z., Goudarzi, G., Sorooshian, A., Marzouni, M.B., Maleki, H., 2016. Impact of Middle Eastern dust storms on indoor and outdoor composition of bioaerosol. Atmos Environ 138, 135-143. https://doi.org/10.1016/j.atmosenv.2016.05.023

Stampfli, M.R., Wiley, R.E., Neigh, G.S., Gajewska, B.U., Lei, X.F., Snider, D.P., Xing, Z., Jordana, M., 1998. GM-CSF transgene expression in the airway allows aerosolized ovalbumin to induce allergic sensitization in mice. J Clin Invest 102, 1704-1714. https://doi.org/10.1172/JCI4160

Stern, R.A., Mahmoudi, N., Buckee, C.O., Schartup, A.T., Koutrakis, P., Ferguson, S.T., Wolfson, J.M., Wofsy, S.C., Daube, B.C., Sunderland, E.M., 2021. The Microbiome of Size-Fractionated Airborne Particles from the Sahara Region. Environ Sci Technol 55, 1487-1496. https://doi.org/10.1021/acs.est.0c06332

Suzuki, T., McCarthy, C., Carey, B.C., Borchers, M., Beck, D., Wikenheiser-Brokamp, K.A., Black, D., Chalk, C., Trapnell, B.C., 2020. Increased Pulmonary GM-CSF Causes Alveolar Macrophage Accumulation. Mechanistic Implications for Desquamative Interstitial Pneumonitis. Am J Respir Cell Mol Biol 62, 87-94. https://doi.org/10.1165/rcmb.2018-0294OC

Suzuki, T., Sakagami, T., Rubin, B.K., Nogee, L.M., Wood, R.E., Zimmerman, S.L., Smolarek, T., Dishop, M.K., Wert, S.E., Whitsett, J.A., Grabowski, G., Carey, B.C., Stevens, C., van der Loo, J.C., Trapnell, B.C., 2008. Familial pulmonary alveolar proteinosis caused by mutations in CSF2RA. J Exp Med 205, 2703-2710. https://doi.org/10.1084/jem.20080990

Taylor, K., Foster, M.L., Law, J.M., Centeno, J.A., Fornero, E., Henderson, M.S., Trager, S.A., Stockelman, M.G., Dorman, D.C., 2013. Assessment of geographical variation in the respiratory toxicity of desert dust particles. Inhal Toxicol 25, 405-416. https://doi.org/10.3109/08958378.2013.797524

Taylor, P.C., Saurigny, D., Vencovsky, J., Takeuchi, T., Nakamura, T., Matsievskaia, G., Hunt, B., Wagner, T., Souberbielle, B., Group, N.S., 2019. Efficacy and safety of namilumab, a human monoclonal antibody against granulocyte-macrophage colony-stimulating factor (GM-CSF) ligand in patients with rheumatoid arthritis (RA) with either an inadequate response to background methotrexate therapy or an inadequate response or intolerance to an anti-TNF (tumour necrosis factor) biologic therapy: a randomized, controlled trial. Arthritis Res Ther 21, 101. https://doi.org/10.1186/s13075-019-1879-x

Temesgen, Z., Burger, C.D., Baker, J., Polk, C., Libertin, C.R., Kelley, C.F., Marconi, V.C., Orenstein, R., Catterson, V.M., Aronstein, W.S., Durrant, C., Chappell, D., Ahmed, O., Chappell, G., Badley, A.D., Group, L.-A.S., 2022. Lenzilumab in hospitalised patients with COVID-19 pneumonia (LIVE-AIR): a phase 3, randomised, placebo-controlled trial. Lancet Respir Med 10, 237-246. https://doi.org/10.1016/S2213-2600(21)00494-X

Thorne, P.S., Ansley, A.C., Perry, S.S., 2009. Concentrations of bioaerosols, odors, and hydrogen sulfide inside and downwind from two types of swine livestock operations. J Occup Environ Hyg 6, 211-220. https://doi.org/10.1080/15459620902729184

Uchida, K., Nakata, K., Trapnell, B.C., Terakawa, T., Hamano, E., Mikami, A., Matsushita, I., Seymour, J.F., Oh-Eda, M., Ishige, I., Eishi, Y., Kitamura, T., Yamada, Y., Hanaoka, K., Keicho, N., 2004. High-affinity autoantibodies specifically eliminate granulocyte-macrophage colony-stimulating factor activity in the lungs of patients with idiopathic pulmonary alveolar proteinosis. Blood 103, 1089-1098. https://doi.org/10.1182/blood-2003-05-1565

United Nations Convention to Combat Desertification, 2023. Sand and dust storm frequency increasing in many world regions, UN warns. https://www.unccd.int/news-stories/press-releases/sand-and-dust-storm-frequency-increasing-many-world-regions-un-warns. Accessed: 16/11/2023

Val, S., Liousse, C., Doumbia el, H.T., Galy-Lacaux, C., Cachier, H., Marchand, N., Badel, A., Gardrat, E., Sylvestre, A., Baeza-Squiban, A., 2013. Physico-chemical characterization of African urban aerosols (Bamako in Mali and Dakar in Senegal) and their toxic effects in human bronchial epithelial cells: description of a worrying situation. Part Fibre Toxicol 10, 10. https://doi.org/10.1186/1743-8977-10-10

Viet, S.M., Buchan, R., Stallones, L., 2001. Acute respiratory effects and endotoxin exposure during wheat harvest in Northeastern Colorado. Appl Occup Environ Hyg 16, 685-697. https://doi.org/10.1080/10473220118563

Vlahos, R., Bozinovski, S., Chan, S.P., Ivanov, S., Linden, A., Hamilton, J.A., Anderson, G.P., 2010. Neutralizing granulocyte/macrophage colony-stimulating factor inhibits cigarette smoke-induced

lung inflammation. Am J Respir Crit Care Med 182, 34-40. https://doi.org/10.1164/rccm.200912-1794OC

Vodonos, A., Friger, M., Katra, I., Avnon, L., Krasnov, H., Koutrakis, P., Schwartz, J., Lior, O., Novack, V., 2014. The impact of desert dust exposures on hospitalizations due to exacerbation of chronic obstructive pulmonary disease. Air Qual Atmos Hlth 7, 433-439. https://doi.org/10.1007/s11869-014-0253-z

Wallace, W.E., Keane, M.J., Mike, P.S., Hill, C.A., Vallyathan, V., Regad, E.D., 1992. Contrasting respirable quartz and kaolin retention of lecithin surfactant and expression of membranolytic activity following phospholipase A2 digestion. J Toxicol Environ Health 37, 391-409. https://doi.org/10.1080/15287399209531679

Wu, S., Deng, F., Wei, H., Huang, J., Wang, H., Shima, M., Wang, X., Qin, Y., Zheng, C., Hao, Y., Guo, X., 2012. Chemical constituents of ambient particulate air pollution and biomarkers of inflammation, coagulation and homocysteine in healthy adults: a prospective panel study. Part Fibre Toxicol 9, 49. https://doi.org/10.1186/1743-8977-9-49

Xie, Z.K., Huang, Q.P., Huang, J., Xie, Z.F., 2014. Association between the IL1B, IL1RN polymorphisms and COPD risk: a meta-analysis. Sci Rep 4, 6202. https://doi.org/10.1038/srep06202

Xing, Z., Ohkawara, Y., Jordana, M., Graham, F., Gauldie, J., 1996. Transfer of granulocyte-macrophage colony-stimulating factor gene to rat lung induces eosinophilia, monocytosis, and fibrotic reactions. J Clin Invest 97, 1102-1110. https://doi.org/10.1172/JCI118503

Yamashita, N., Tashimo, H., Ishida, H., Kaneko, F., Nakano, J., Kato, H., Hirai, K., Horiuchi, T., Ohta, K., 2002. Attenuation of airway hyperresponsiveness in a murine asthma model by neutralization of granulocyte-macrophage colony-stimulating factor (GM-CSF). Cell Immunol 219, 92-97. https://doi.org/10.1016/s0008-8749(02)00565-8

Yatmark, P., Morales, N.P., Chaisri, U., Wichaiyo, S., Hemstapat, W., Srichairatanakool, S., Svasti, S., Fucharoen, S., 2015. Effects of Iron Chelators on Pulmonary Iron Overload and Oxidative Stress in beta-Thalassemic Mice. Pharmacology 96, 192-199. https://doi.org/10.1159/000438994

Zhang, H., Sun, W., Li, W., Wang, Y., 2022. Physical and chemical characterization of fugitive particulate matter emissions of the iron and steel industry. Atmos Pollut Res 13, https://doi.org/10.1016/j.apr.2021.101272

Zhang, X., Zhao, L., Tong, D., Wu, G., Dan, M., Teng, B., 2016a. A Systematic Review of Global Desert Dust and Associated Human Health Effects. Atmosphere-Basel 7, 158. https://doi.org/10.3390/atmos7120158

7 Publications beyond the scope of this thesis

During his doctorate, the author of this thesis contributed to additional publications which were beyond the scope of this dissertation. In this section, these additional publications are listed in chronological order.

Investigations of acute effects of polystyrene and polyvinyl chloride micro- and nanoplastics in an advanced in vitro triple culture model of the healthy and inflamed intestine

Mathias Busch,[a] Gerrit Bredeck,[a] Angela A. M. Kämpfer,[a] Roel P. F. Schins[a]

[a]*IUF – Leibniz Research Institute for Environmental Medicine, Düsseldorf, Germany*

Environmental Research 2021, 193, 110536

Doi: 10.1016/j.envres.2020.110536

Author contribution: The author of this thesis characterized the cell culture medium and the sedimentation of nanoparticles, discussed the results, and revised the manuscript.

Model Complexity as Determining Factor for In Vitro Nanosafety Studies: Effects of Silver and Titanium Dioxide Nanomaterials in Intestinal Models

Angela A. M. Kämpfer,[a] Mathias Busch,[a] Veronika Büttner,[a] Gerrit Bredeck,[a] Burkhard Stahlmecke,[b] Bryan Hellack,[b,c] Isabelle Masson,[a] Adriana Sofranko,[a] Catrin Albrecht,[a] Roel P. F. Schins[a]

[a]*IUF – Leibniz Research Institute for Environmental Medicine, Düsseldorf, Germany*

[b]*Institut für Umwelt & Energie, Technik & Analytik e.V. (IUTA), formerly: Institute for Energy and Environmental Technology e.V., Duisburg, Germany*

[c]*German Environment Agency (UBA), Langen, Germany.*

Small 2021, 17(15), 2004223

Doi: 10.1002/smll.202004223

Author contribution: The author of this thesis characterized the cell culture medium and the sedimentation of nanoparticles, analyzed RNA expression in ileal tissues, discussed the results, and revised the manuscript.

Effects of dietary exposure to the engineered nanomaterials CeO_2, SiO_2, Ag, and TiO_2 on the murine gut microbiome

Gerrit Bredeck,[a] Angela A. M. Kämpfer,[a] Adriana Sofranko,[a] Tina Wahle,[a] Dominique Lison,[b] Jérôme Ambroise,[c] Burkhard Stahlmecke,[d] Catrin Albrecht,[a] Roel P. F. Schins[a]

[a]*IUF – Leibniz Research Institute for Environmental Medicine, Düsseldorf, Germany*

[b]*Louvain Centre for Toxicology and Applied Pharmacology, Université Catholique de Louvain, Brussels, Belgium*

[c]*Centre de Technologies Moléculaires Appliquées, Institut de Recherche Expérimentale et Clinique, Université Catholique de Louvain, Brussels, Belgium*

[d]*Institut für Umwelt & Energie, Technik & Analytik e.V. (IUTA), formerly: Institute for Energy and Environmental Technology e.V., Duisburg, Germany*

Nanotoxicology 2021, 15(7), 934-50

Doi: 10.1080/17435390.2021.1940339

Author contribution: The author of this thesis isolated the DNA from feces, interpreted and discussed the results, and wrote the manuscript.

Ingested Engineered Nanomaterials Affect the Expression of Mucin Genes–An In Vitro-In Vivo Comparison

Gerrit Bredeck,[a] Angela A. M. Kämpfer,[a] Adriana Sofranko,[a] Tina Wahle,[a] Veronica Büttner,[a] Catrin Albrecht,[a] Roel P. F. Schins[a]

[a]*IUF – Leibniz Research Institute for Environmental Medicine, Düsseldorf, Germany*

Nanomaterials 2021, 11(10), 2621

Doi: 10.3390/nano11102621

Author contribution: The author of this thesis characterized the cell culture medium, nanoparticles, nanoparticle sedimentation, and *in vitro* mono-cultures, prepared and performed *in vitro* experiments, prepared the graphs, interpreted and discussed the results, and wrote the manuscript.

Tiered testing of micro- and nanoplastics using intestinal in vitro models to support hazard assessments

Gerrit Bredeck,[a,*] Blanka Halamoda-Kenzaoui,[a] Alessia Bogni,[a] Dorelia Lipsa,[a] Susanne Bremer-Hoffmann[a]

[a]*European Commission, Joint Research Centre (JRC), Ispra, Italy*

**current affiliation: IUF – Leibniz Research Institute for Environmental Medicine, Düsseldorf, Germany*

Environment International 2022, 158, 106921

Doi: 10.1016/j.envint.2021.106921

Author contribution: The author of this thesis performed the search and evaluation of the literature for the review, created graphs, wrote parts of the manuscript and revised the manuscript.

Assessing the NLRP3 Inflammasome Activating Potential of a Large Panel of Micro- and Nanoplastics in THP-1 Cells

Mathias Busch,[a] Gerrit Bredeck,[a] Friedrich Waag,[b] Khosrow Rahimi,[c] Haribaskar Ramachandran,[a] Tobias Bessel,[b] Stephan Barcikowski,[b] Andreas Herrmann,[c] Andrea Rossi,[a] Roel P. F. Schins[a]

[a]*IUF – Leibniz Research Institute for Environmental Medicine, Düsseldorf, Germany*

[b]*Technical Chemistry I, Center for Nanointegration Duisburg-Essen (CENIDE), University of Duisburg-Essen, Essen, Germany*

[c]*DWI–Leibniz Institute for Interactive Materials, Institute of Technical and Macromolecular Chemistry, RWTH Aachen University, Aachen, Germany*

Biomolecules 2022, 12(8), 1095

Doi: 10.3390/biom12081095

Author contribution: The author of this thesis prepared and performed *in vitro* experiments, interpreted and discussed the results, and revised the manuscript.

Investigating nanoplastics toxicity using advanced stem cell-based intestinal and lung *in vitro* models

Mathias Busch,[a] Hugo Brouwer,[a] Germaine Aalderink,[a] Gerrit Bredeck,[b] Angela A. M. Kämpfer,[b] Roel P. F. Schins,[b] Hans Bouwmeester[a]

[a]*Division of Toxicology, Wageningen University and Research, Wageningen, Netherlands*

[b]*IUF – Leibniz Research Institute for Environmental Medicine, Düsseldorf, Germany*

Frontiers in Toxicology 2023, 5, 1112212

Doi: 10.3389/ftox.2023.1112212

Author contribution: The author of this thesis performed the search and evaluation of literature on lung *in vitro* models, and revised the manuscript.

Eidesstattliche Erklärung

Ich versichere an Eides statt, dass die Dissertation von mir selbständig und ohne unzulässige fremde Hilfe unter Beachtung der „Grundsätze zur Sicherung guter wissenschaftlicher Praxis an der Heinrich-Heine-Universität Düsseldorf“ erstellt worden ist. Die vorliegende Dissertation habe ich selbständig verfasst und keine anderen als die angegebenen Hilfsmittel verwendet. Alle wörtlich oder inhaltlich übernommenen Stellen habe ich als solche gekennzeichnet. Außerdem versichere ich, dass diese Dissertation in der jetzigen oder einer ähnlichen Form noch keiner anderen Fakultät vorgelegt wurde und dass dies mein erster Promotionsversuch ist.

Düsseldorf, Dezember 2023

_____

Gerrit Bredeck